SYMPOSIUM PROCEEDINGS

ENGINEERING SOLUTIONS FOR CLIMATE ACTIONS, DIGITALIZATION AND GREEN INDUSTRIES

3rd International Engineering Research Symposium 2025

IERS 2025

30th October 2025, Colombo, Sri Lanka

National Engineering Research and Development Centre of Sri Lanka

Main Collaborators

Conference Proceedings of the
3rd International Engineering Research Symposium

IERS 2025

Engineering Solutions for Climate Actions, Digitalization and Green Industries

Organized by

National Engineering Research and Development Centre of Sri Lanka
In collaboration with
the Ministry of Science and Technology

30th October 2025, Colombo, Sri Lanka

Collaborators and Academic Partners

6G Flagship Program, University of Oulu, Finland

NetsLab, University College Dublin, Ireland

The Australian National University, Canberra ACT, Australia

The Center for National Online Distance Education Service (C-Nodes), Open University of Sri Lanka

Sri Lanka Technology Campus, Padukka, Sri Lanka

Published by:

Proceedings ISBN: ISBN 978-624-5505- 05-0

LIST OF REVIEWERS

Prof. Abdul Salam
Prof. Adeel Waqas
Prof. (Ms.) Chitra Lakshmikanthan
Prof. E A C P Karunarathne
Prof. Jai Govind Singh
Prof. Mahinsasa Narayana
Prof. Nadeesh Adassoriya
Prof. Parakrama Karunaratne
Prof. Sivanappan Kumar
Dr. Akila Subhasinghe
Dr. Asiri Wijesinghe
Dr. B G D Achintha Madhusanka
Dr. Chamil Gunarathna
Dr. (Ms.) Chamila Niroshinie
Dr. Chathura Manawasekara
Dr. (Ms.) Gayashika Fernando
Dr. Gehan Anthonys
Dr. Himal Suraweera
Dr. (Ms.) Iresha Atthanayake
Dr. (Ms.) Iromi Ranaweera
Dr. Isuru Lakmal
Dr. Isuru Wijayawardane
Dr. (Ms.) Jeewanthi Sirisena
Dr. K R Devabalaji
Dr. Kapila Withanage
Dr. (Ms.) Kaushalya Wijekoon
Dr. Luckshitha Suriyasena Liyanage
Dr. Luminda Gunawardhana
Dr. Madhawa Perera
Dr. Mahinsasa Rathnayake
Dr. (Ms.) Manjula Siriwardhana
Dr. Manoj Ranaweera
Dr. Mylvaganam Nithurshan
Dr. Nalin Harischandra
Dr. (Ms.) Nanduni Nimalsiri
Dr. Nuwan Herath
Dr. Pasan Maduranga
Dr. Poompat Saengudomlert
Dr. (Ms.) Prashanthi Ranasinghe
Dr. (Ms.) Rafaela da Silva
Dr. Ravindu Lokuliyana
Dr. (Ms.) Rukshima Dabare
Dr. Ruminda Wimalasiri
Dr. Ruwan Appuhamy
Dr. (Ms.) Salony Rajbhandari
Dr. (Ms.) Samanthi Seneviratne
Dr. Sampath Wickramasinghe
Dr. Sanath de Silva
Dr. Sanjaya Thilakarathne
Dr. Sanjeewa Sondarangallage
Dr. (Ms.) Shakila Pathirana
Dr. (Ms.) Sumali Morapitiya
Dr. Sumudu Samarakoon
Dr. Trong Tien Le
Dr. Upeka Premaratne
Dr. Upuli Perera
Dr. (Ms.) Uthpala Premaratne
Dr. (Ms.) Wathsala Rajawatta
Eng. Ananda Namal
Eng. Chamila Delpitiya
Eng. Chamodya Nirmal
Eng. Dilshan Ganegoda
Eng. Eranda Jayatunga
Eng. Isuru Premaratne
Eng. Jayasinghe Kodithuwakku
Eng. (Ms.) Kaushalya Subasinghe
Eng. (Ms.) Manoja Karunasekara
Eng. Nalaka Samarasinghe
Eng. Nithianantham Arunprakash
Eng. Nuwan Amaradasa
Eng. Prabhath Buddhika
Eng. Rajith Adikari
Eng. Shalinda Silva
Eng. (Ms.) Samadhi Dissanayake
Eng. Samantha Kumarasena
Eng. Shantha Jayasinghe
Eng. Suganda Somasundara
Eng. (Ms.) Thushari Ariyarathna
Mr. Himarsha Rajapaksha
Ms. Iroshini Ratnapala
Mr. Rattan Kumar Venkatesan

PREFACE

The National Engineering Research and Development Centre (NERDC) of Sri Lanka was enacted by an act of parliament under Special Gazette Notification (No 124/6) published under the Industrial Corporation Act No. 49 of 1957, on 14 August 1974. NERDC became operational during the latter part of 1974, with Professor K. K. Y. W. Perera as its first chairman. The centre was located in a small section of the Industrial Development Board complex at Katubedda, Moratuwa, and subsequently the office was located at a more spacious building at Galle Road, Colombo-03. In September 1978 office was shifted to its present location at 2P/17B, IDB Industrial Estate, Ekala, Ja-Ela, Sri Lanka. NERDC is a premier engineering R&D organization in Sri Lanka, engaging in multidisciplinary innovation and Research and Development activities in the fields of engineering over the last five decades.

This symposium is the annual engineering and research conference conducted by NERDC since 2014. This year, NERDC has organized the 3rd International Engineering Research Symposium 2025 (IERS 2025) under the theme of "Engineering Solutions for Climate Actions, Digitalization and Green Industries" in partnership with several international and national universities and research institutes, namely, the 6G Flagship, University of Oulu, Finland, Netslab, University College Dublin, Ireland, The Australian National University and the Center for National Online Distance Education Service of the Open University of Sri Lanka. The theme of the symposium, “Engineering Solutions for Climate Actions, Digitalization and Green Industries,” is both timely and vital. It showcases the unwavering commitment to innovation and progress of NERDC in the engineering field. More importantly, it demonstrates the profound dedication to align IERS2025 with critical government policies, such as the national digital governance strategy, and the international commitments, including the Paris Agreement, the Sustainable Development Goals and Nationally Determined Contributions for climate actions.

IERS2025 is held at Galadari Hotel, Colombo Sri Lanka on 30th October 2025. The symposium facilitates the inauguration session with two keynote speeches, two guest speeches, a technical paper presentation session, decorated with a cultural performance in the morning. In the afternoon, the technical sessions are conducted as three parallel paper presentation sessions and the poster presentation session. All the oral presentations are delivered in front of a panel of evaluators, which comprise of a team of experts from the academia and industry. IERS2025 provides a platform for academics, researchers, industry experts, and aspiring students to share ground breaking research, foster collaborations, and explore the latest innovations in the field of engineering and technology.

The collaborating international universities and institutes are conducting high caliber research in the fields of digitalization, 6G network, cyber security, block chain, Artificial Intelligence and green industries etc. NERDC can pave the way for receiving their collaboration for Sri Lanka's efforts towards an inclusive digital economy by leveraging advanced technology-based solutions. The industry sectors of Sri Lanka will be benefitted by the groundbreaking research findings of green industries to achieve its full potential in the domestic and export markets supported by a strong digital infrastructure. The exchange of knowledge and collaboration are essential for capacity development in latest digital knowhow, entrepreneurship, a robust framework for R&D, digital governance, digital public infrastructure, digital financial services, cybersecurity, Environment Sustainability Governance (ESG) and Sustainable Development Goals (SDG).

The symposium delivers two keynote speeches and two guest speeches on visionary and timely themes. The first keynote address for IERS 2025 is delivered by Professor Rahula Attalage, who is the Pro-Vice Chancellor Academic at the Sri Lanka Institute of Information Technology (SLIIT), Professor Emeritus of the University of Moratuwa and the former Deputy Vice Chancellor of University of Moartuwa. The second keynote address is delivered by Prof. Saman Halgamuge, a professor of the Uni-

versity of Melbourne, Australia. Prof. Halgamuge is attached to the AI, Optimization and Pattern Recognition Research Group and has supervised 50 PhD students including 20 graduates from Universities in Sri Lanka on AI and applications. He is ranked as a top 2% most cited researcher for AI and Image Processing in the Stanford database and a fellow of IEEE.

A guest speech is delivered by Dr. Madhusanka Liyanage, the Director of the Network Softwarization and Security Labs (NetsLab), the University College Dublin, Ireland. Dr. Liyanage, a senior member of IEEE, leads research in secure 6G networks, federated learning, and blockchain and has authored over 250 publications, including seven books, in cybersecurity, 6G networks, and privacy-preserving AI. Since 2021, he was ranked among the world's top 2% of scientists. Another guest speech will be delivered by Prof. PMC Thilakerathne, the Vice Chancellor of the Open University of Sri Lanka.

IERS2025 received 110 full paper submissions, and after the peer review process, 64 papers were accepted for publication, out of which 53 delivered oral presentations and 11 poster presentations. All the papers were reviewed by a panel of academic and professional experts with extensive expertise in their respective fields. Oral presentations are delivered in three parallel sessions:

- Engineering for Digitalization
- Engineering Product Development
- Engineering Solutions for Climate Actions and Green Industries

All the full paper submissions are the outcome of the research conducted in aligned with the symposium theme of the symposium. Out of the researches presented in oral presentations, 25 selected leading full papers are published as a book in Springer Nature Publications based on symposium evaluations, editors' evaluation and the quality of the research. The other selected full papers were published in the IERS2025 proceedings and included in the Sri Lanka Science Index database, complete with an ISBN. ISBN.

Message from the Prime Minister of the Democratic Socialist Republic of Sri Lanka

It is with great pleasure that I extend my warmest wishes to the International Engineering Research Symposium 2025 (IERS2025), meticulously organized by the National Engineering Research and Development Centre (NERDC) of Sri Lanka.

The theme of the symposium this year, "Engineering Solutions for Climate Actions, Digitalization and Green Industries," is both timely and vital. It showcases the unwavering commitment to innovation and progress of NERDC in the engineering field. More importantly, it demonstrates the profound dedication of NERDC to aligning with critical government policies, such as our national digital governance strategy, and the international commitments, including the Paris Agreement and the Sustainable Development Goals. Through IERS2025, NERDC has successfully created a unified platform for passionate researchers to share their findings and collaborate on the challenges of our time.

The partnerships forged with international institutes and universities exemplify a collective determination to shape a future distinguished by technological prowess and climate-conscious and digitalized economic prosperity. As the world undergoes rapid transformation, engineering innovations are the catalysts of change, capable of breathing new life into the economy, environment and the society.

In IERS2025, I am confident that all the participants will gain a new experience, engage diligently, share their insights candidly, and nurture collaborations that will transform the engineering innovations for the betterment of the society and the environment. I wish the IERS2025 symposium and its outcomes every success.

Hon. Dr. Harini Amarasuriya, Prime Minister of Sri Lanka

Message from the Minister of Science and Technology, Sri Lanka

Engineering research and development is a pivotal part in technological, economic and social development of any country. National Engineering Research and Development Centre (NERDC) of Sri Lanka, which is operated under the purview of the Ministry of Science and Technology is the premier engineering research and development centre in Sri Lanka. The contribution of NERDC to the engineering research and development in the country is unwavering and remarkable to the national development.

NERDC organized this annual international engineering research symposium (IERS) for facilitating or providing a platform to show case the outcomes of research and development, to exchange the latest breakthrough of technology enhancement, to strengthen the mutual collaboration and networking amongst various national and international partners. This year, the symposium theme, 'engineering solutions for climate actions, digitalization and green industries' underscores the pivotal role engineering plays in reimagining a development model fit for a digitally-driven and environmentally-aware world.

I believe that IERS2025 forum, distinguished by its fusion of diverse minds, creates a fertile ground for unearthing solutions that will drive the progress of the country and the region. It is gratifying to see the resonance of this event with our national vision. I commend the NERDC of Sri Lanka for guiding this symposium in the right direction. Its dedication to fostering a space for learning, collaboration, and growth is truly admirable.

Prof. Chrishantha Abeysena, Hon. Minister of Science and Technology, Sri Lanka

Message from the Secretary of the Ministry of Science and Technology

It is an honor to extend my warmest greetings to the National Engineering Research and Development Centre of Sri Lanka (NERDC) for organizing this annual International Engineering Research Symposium (IERS) 2025. This symposium holds significant importance as it aligns with our shared vision of driving the country towards the sustainable development model in a digitalized world. Engineering innovations play a crucial role in this journey. NERDC is positioned in a unique state in the history of engineering in Sri Lanka and it has a rich tradition of brining innovation in to the development path. It has shown and contributed in many ways and made an indelible imprint in our society in engineering research and developments.

This year, the collaboration between the NERDC and several international research institutes and universities epitomizes the forward thinking and collaborative spirit necessary for cultivating a vibrant and dynamic engineering sector. I trust this symposium will serve as a crucial platform for researchers, industry experts and academics from around the world to exchange ideas, share ground-breaking research, and forge meaningful collaboration that will propel us towards a brighter future. Through the exchange of ideas and expertise, we can chart a course that not only revitalizes industries but also enhances the quality of life for our citizens.

I thank the IERS 2025 organizing committee, NERDC management and all those who have contributed their time, resources, and expertise to ensure the efficient execution of this event towards success. May this symposium be a beacon of inspiration, fostering collaboration that paves the way for a prosperous and technologically empowered Sri Lanka. I wish you all a successful and enlightening symposium.

Mr. Y. L. Mohamed Navawi, Secretary , Ministry of Science and Technology, Sri Lanka

Message from the Keynote Speaker 1

I am profoundly pleased and honored to extend this message to the International Engineering Research Symposium of the National Engineering Research and Development Center (NERDC) of Sri Lanka, this year, 2025.

Research is an enabler not only for the creation of new knowledge but also to create opportunities for providing innovative solutions for real life problems. The theme for this year's symposium, Engineering Solutions for Climate Actions, Digitalization and Green Industries, which is timely and opportune, opens a different window of opportunities for interdisciplinary research. It calls for integration of concepts and methodologies of different disciplines such as science, economics, engineering & technology, data science, machine learning, social sciences etc. and their collaborations for finding innovative solutions for complex problems of high value to the society. These can lead to new opportunities from an applied research perspective where a single discipline may not be able to provide.

Therefore, I strongly believe that the deliberations of this symposium will enable the NERDC to facilitate productive collaborations among the participants and also the NERDC to forge new partnerships where they have a proven track record of typical interdisciplinary research related to this theme.

My sincere appreciations are presented to the contributing authors/presenters and the Organizing team of NERDC, for orchestrating this endeavor envisaging meaningful dissemination of research findings, synergetic collaborations and working towards contributing to the sustainable social development.

Prof. Rahula Attalage, Pro Vice-Chancellor (Academic), SLIIT Malabe Campus

Message from the Keynote Speaker 2

I start my brief message by congratulating Lankan engineers and NERDC for organizing this important symposium in 2025. I feel privileged to have lived, studied and worked in this wonderful island that has a great legacy on ancient engineering innovations. Interestingly, we do not even know the names of those ancient engineers although we know the kings and leaders of the country at the time. Great engineers like D. J. Wimalasurendra known as the "Father of Hydropower" are also not very well known outside of Sri Lanka. Today, we need to celebrate the Lankan professionals including engineers who are innovating and contributing not only to Sri Lanka but also globally.

Adoption of sustainable technologies and new and disruptive technologies are essential components of any strategy to develop Sri Lanka. The theme of the symposium is therefore timely. Sustainable technologies have innovations that can reduce the destruction of our planet Earth. As a major disruptive technology, Artificial Intelligence (AI), which is the focus of our research group, can help making these technologies more sustainable meaning human and planet friendly. AI is already helping with good governance in many countries on Earth cutting wastage and more importantly closing the room for corruption that has taken over many parts of the society. Generative AI, for example, can help us to think and design things in ways we were not able to do in the past. Explainable AI for example can catch the ugly parts of AI systems that are unethical and discriminative.

How can these technological developments and new research be used to build a prosperous Sri Lanka? Sri Lanka should consider specific strengths and weaknesses of the people in formulating the strategy to make use of new technologies in addition to other key factors like our geographical location and our main income earners. Our strengths include the ingenuity of our people, the friendly nature and the ability to engage and collaborate seamlessly with others globally. Our weaknesses may include silly divisions we still seem to have in our society which, as some would argue, are the reasons for not celebrating enough our brilliant professionals including engineers. Today, we can overcome such weaknesses and achieve international recognition through peer reviewed publications, patents, opinion pieces etc. and therefore, promoting research symposiums like this one is a positive step for our discipline.

How did other countries use their strengths in developing their countries? Product development focused on various export markets is a key feature of China’s success in developing their economy. The ingredients they turn into include the people, large population and their

specific abilities and their strategic thinking. India's focus of creating quality IT training and then tapping into the increased IT human capital is another example. Japan's strategy also involves food security focusing on the production of basic food items within the country and tap on to the strengths of the people. Vietnam is increasingly demonstrating their strengths in the region through hard work and strategy. It is also interesting to see how countries navigate through the new tariffs imposed by the US using their strengths.

What items do we need to produce within the country for our own consumption and for the global market? AI may also help in modernizing agriculture and the tea industry – making it more ethical and fairer which is increasingly becoming important in lucrative global markets. Bringing more technology in to these sectors will also increase the standard of living in rural Sri Lanka. "Interpretability and accessibility of machine learning in selected food processing, agriculture and health applications" is a relevant freely accessible article we published in 2022 in Sri Lanka's Journal of National Science Foundation, in collaboration with three overseas and three Lankan universities.

Thanks for the opportunity to send this message. I offer my gratitude to institutions that allowed me to contribute to my beloved island while based overseas: Universities of Peradeniya and Colombo and National Institute of Fundamental Studies in the past and Sri Lanka Institute of Information Technology and the National Academy of Sciences at present.

Prof Saman Halgamuge, FIEEE, FNASSL, University of Melbourne, Australia

Message from the Plenary Speaker 1

It is a privilege to join the International Engineering Research Symposium (IERS 2025), an event that continues to serve as a vital platform for fostering innovation and collaboration among researchers, engineers, and industry leaders. The theme "Engineering Solutions for Climate Actions, Digital Transformations, and Green Industries" reflects the urgency and responsibility we share in shaping a sustainable and digitally empowered future.

This symposium offers an excellent opportunity to explore emerging technologies, from AI-driven 6G networks and secure communication systems to energy-efficient industrial solutions. The cross-disciplinary discussions and global participation will undoubtedly pave the way for impactful research outcomes and stronger collaborations between academia and industry. It is particularly inspiring to see Sri Lanka — my home country — taking a leading role in fostering such dialogues that bridge academic excellence, innovation, and societal impact.

I look forward to engaging with fellow researchers and contributing to the exchange of ideas that will drive engineering innovation towards a greener, smarter, and more sustainable world.

Dr. Madhusanka Liyanage, Associate Professor, University College Dublin, Ireland & Director Netslab

Message from the Plenary Speaker 2

It is with great pleasure that I extend my warm greetings to all participants of the International Engineering Research Symposium organized by the National Engineering Research and Development Centre (NERD) under the timely and thought-provoking theme *"Engineering Solutions for Climate Actions, Digitalization, and Green Industries."*

I strongly believe that this symposium provides a valuable platform for engineers, researchers, academics, and industry experts to exchange ideas, share innovations, and explore collaborative pathways that address some of the most pressing challenges of our time. The selected theme captures the essence of the global transformation that is reshaping every sector of human activity, where climate resilience, technological advancement, and sustainable industrialization must go hand in hand.

The world is increasingly turning to engineering and science not only for innovation but also for responsible solutions. Especially, solutions that mitigate the impact of climate change, enhance resource efficiency, and foster inclusive and sustainable growth. As we move toward a digital and green economy, it is imperative that Sri Lanka harnesses the power of engineering research and innovation to develop technologies that are both environmentally sustainable and economically viable.

I commend the NERD Centre for its continued leadership in promoting applied research, indigenous technology development, and practical engineering solutions that respond to national and global needs. Initiatives such as this symposium reaffirm NERD's vital role as a bridge between research and real-world implementation, helping to transform scientific ideas into tangible benefits for society and industry.

I am confident that the research shared through this symposium and the contributions captured in this abstract book will inspire new ideas, inform strategic actions and strengthen our collective journey toward a greener, digitally empowered and sustainable future. I extend my best wishes to the organizers, paper presenters and participants for a successful and impactful symposium.

Snr. Prof. P.M.C. Thilalakerathne, Vice Chancellor, The Open University of Sri Lanka

Message from the Chairman of NERDC

As the Chairman of the National Engineering Research and Development Centre of Sri Lanka, it is my great honor to extend my warmest greetings to all the participants of the International Engineering Research Symposium (IERS) 2025 organized by our Centre.

The Symposium is being held under the timely and meaningful theme of "Engineering Solutions for Climate Actions, Digital Transformations and Green Industries", with the aim of reflecting our unwavering commitment to fostering innovation, collaboration and sustainable economic growth through engineering excellence.

In an era of rapid technological advancements and environmental challenges, the role of Engineering research is increasingly important. IERS2025 can be defined as an ideal platform for scientists, Engineers, Academics and Industry Professionals to exchange ideas, share knowledge and develop transformative solutions to address both national and global challenges.

Through this symposium, NERDC reaffirms its mission to advance applied research and technology development that contribute meaningfully to Sri Lanka's journey toward a greener, more digitally empowered, and economically resilient future. The collaboration and innovation showcased here will undoubtedly strengthen the bridge between research and practical implementation, paving the way for industrial progress and sustainable national development.

I extend my sincere appreciation to all participants, sponsors, and organizers whose dedication, expertise, and efforts have made IERS 2025 a reality. May this event serve as a catalyst for meaningful dialogue, lasting partnerships, and groundbreaking innovations that inspire the next generation of Engineers and Researchers. Wishing all the participants a productive, insightful, and inspiring symposium experience.

Dr. H Chitral Ambawatte, Chairman of National Engineering Research and Development Centre of Sri Lanka

Message from the Director General of NERDC

It is with great pleasure that I extend my warm greetings to all the participants of the Annual Symposium of the National Engineering Research and Development Centre (NERDC), held under the theme "Engineering Solutions for Climate Actions, Digitalization and Green Industries."

This year's theme highlights the urgent need to use engineering innovation to address climate challenges, drive digital transformation, and promote sustainable industrial growth. As we face evolving environmental and technological demands, it is our responsibility to ensure that research and development efforts lead to practical solutions that contribute to a greener and more resilient economy.

At NERDC, our mission has always been to strengthen national capabilities through research, innovation, and technology transfer. This symposium provides a valuable opportunity for researchers, engineers, policymakers, and industry leaders to exchange knowledge, build partnerships, and explore new pathways for sustainable development.

I wish to commend all the researchers and contributors for their dedication and innovative spirit. Your continued efforts are essential in advancing the role of engineering in national development and in addressing the challenges of sustainability.

May this symposium inspire new ideas, foster collaboration, and pave the way for engineering solutions that support a sustainable and technologically advanced future for Sri Lanka.

Dr. Jayathu G Samarawickrama, Director General, National Engineering Research and Development Centre of Sri Lanka

Abstracts of the Session Chair Speakers

From Simulation to Reality: The Power of Digital Twin in Battery Management Systems

The growing adoption of electric vehicles (EVs) and renewable energy in India demands smarter battery management solutions. Traditional Battery Management Systems (BMS) rely on reactive monitoring, often lacking predictive capabilities—leading to reduced battery life, safety risks, and unplanned maintenance. Integrating Digital Twin technology with machine learning creates a real-time virtual model of the battery, enabling predictive maintenance, performance optimization, and early fault detection. Simulation studies show that digital twins can improve battery efficiency by up to 95%, aligning with India's sustainable mobility goals. The digital twin monitors key parameters such as State of Charge (SOC), State of Health (SOH), temperature, voltage balance, and charging–discharging cycles. By mirroring real battery behavior, it predicts thermal effects, cell degradation, and lifetime performance. Unlike conventional testing, digital twins allow safe experimentation with fault conditions like overvoltage or overheating without damaging physical systems.

EV manufacturers can use this technology to optimize thermal management, refine control algorithms, predict extreme condition performance, and streamline maintenance. This reduces physical prototyping needs, shortens development cycles, and lowers costs. Once validated, optimized control strategies are transferred to the real BMS, creating a closed feedback loop where operational data continuously refines the digital model. This ensures real-time monitoring, early fault detection, and improved reliability over the battery's entire lifecycle.

The "From Simulation to Reality" approach bridges design and operation, enabling continuous innovation, safer systems, and more sustainable energy solutions.

Prof. L. Chitra, Aarupadai Veedu Institute of Technology, Vinayaka Mission's Research Foundation, India

Abstracts of the Session Chair Speakers

Macro-Level Policy Framework for Utility-Scale Solar Energy in Sri Lanka: Lessons from India's Experience

Sri Lanka's solar energy potential is among the highest in South Asia, yet solar power contributes less than two percent to the national electricity mix. This research assesses the policy and institutional barriers impeding the development of utility-scale solar power in Sri Lanka and benchmarks India's policy experience to identify transferable strategies.

Using a mixed-methods approach, the study collected data from 200 Sri Lankan and 20 Indian stakeholders representing government, industry, academia, and international organizations. It also reviewed national policy documents and sectoral statistics from 2010 to 2024. The analysis revealed that institutional and governance barriers constitute the most significant constraints, followed by financial and regulatory challenges. Prolonged approval processes—averaging 24–30 months—contrast sharply with India's streamlined 8–12-month procedures, highlighting systemic coordination failures among Sri Lankan agencies.

Drawing lessons from India's successful National Solar Mission, the study identifies three critical policy interventions relevant to Sri Lanka: competitive bidding mechanisms to ensure transparency, solar park models to reduce infrastructure bottlenecks, and the establishment of a single nodal authority to strengthen institutional coordination.

The proposed macro-level policy framework emphasizes the importance of governance reform, regulatory simplification, financial innovation, and grid modernization. The findings underscore that **institutional capacity and implementation efficiency are more critical than policy proliferation**. This study contributes to the discourse on renewable energy transitions in developing economies and offers actionable guidance for policymakers seeking to advance Sri Lanka's sustainable energy transition.

Dr. Iresha Atthanayake, Senior Lecturer, The Open University of Sri Lanka

Abstracts of the Session Chair Speakers

Engineering Solution for Digitization

Digitization is transforming industries by enabling seamless integration of physical and digital processes. Digitization focuses on creating a robust framework that enhances operational efficiency, data accuracy, and scalability. By leveraging advanced technologies such as IoT, cloud computing, and AI-driven analytics, the solution ensures real-time data capture, automated workflows, and predictive insights. It addresses key challenges like interoperability, security, and cost optimization while supporting sustainable growth. The approach empowers organizations to streamline processes, improve decision-making, and deliver superior customer experiences, paving the way for a fully connected and intelligent ecosystem.

Eng. Eranda Adikari, Head of Data Insight, Dialog Enterprise & Vice President – Data and AI, H One Pvt. Ltd.

Message from the Symposium Chairperson

The National Engineering Research and Development Centre of Sri Lanka (NERDC) is proudly hosting the International Engineering Research Symposium 2025 (IERS2025). Today, we live in an era defined by unprecedented challenges and transformative opportunities within the country and around the world. On the one hand, climate change demands urgent actions, technological advancements to reshape our societies, and stronger concern towards sustainable development in the economic advancements every day. On the other hand, digitalization is accelerating innovation across every sector. Artificial intelligence, machine learning, the Internet of Things, and advanced data analytics are not just buzzwords; they are powerful tools empowering engineers to design smarter, operate more efficiently, and predict with greater accuracy. For Sri Lanka and the South Asian region, with their rich engineering heritage and unique environmental and developmental needs, these global challenges present both significant hurdles and unparalleled opportunities for innovation. Therefore, in this year, we unfold IERS2025 under the captivating theme of "Engineering Solutions for Climate Actions, Digitalization and Green Industries".

International Engineering Research Symposium 2025 (IERS2025) is a platform for academia, industry, researchers and students to discuss their groundbreaking research outcomes and to explore the engineering marvels combating climate change and discover how digital frontiers are shaping our future. As IERS2025 collaborate with several international and national universities and research institutes, the participants get an incomparable opportunity for networking and connect with the world.

I extend my sincere gratitude to the IERS2025 organizing committee and NERDC management, whose tireless dedication has made this symposium a reality. I am also grateful to our sponsors, collaborators, partners, staff of the Ministry of Science and Technology, reviewers, advisors for their invaluable support, which has allowed us to create a platform that fosters meaningful interactions and fruitful collaborations for organizing the remarkable event. At the end of the day, your dedication and ingenuity are the driving forces behind the transformative changes we envision for our nation and the world.

As the chair of the IERS2025, I invite all the participants to make this a fruitful stage to discuss your groundbreaking ideas and outcomes and for you to be part of the solution, contributing to both local and global progress.

Dr. Eng. (Ms.) Manjula Siriwardhana, IERS2025 Symposium Chairperson

Table of Contents

3rd International Engineering Research Symposium 2025 (IERS 2025)
Colombo, Sri Lanka

Engineering Solutions for Digitalization

3rd International Engineering Research Symposium 2025 (IERS 2025)
Colombo, Sri Lanka

BIM-Enabled Implementation of Augmented and Virtual Reality in Sri Lankan Construction: Benefits, Barriers, and Strategies

Deluxian Kugathasan, Himal Suranga Jayasena, Nishadi Buddhika Nanayakkara, and Piranavan Sivasothy

[1]Department of Building Economics, University of Moratuwa, Katubedda, Sri Lanka

Abstract. The Sri Lankan construction industry is hindered by persistent challenges such as project delays, cost overruns, and quality control issues. This paper presents the potential of Augmented Reality (AR) and Virtual Reality (VR), enabled by Building Information Modeling (BIM), as transformative technologies to mitigate these problems. Following a qualitative study involving semi-structured interviews with eleven expert Quantity Surveyors, the research investigates the practical applications and implementation challenges of AR/VR. Key findings reveal significant benefits, including enhanced design visualization and process automation. However, the realization of these benefits is challenged by substantial barriers to adoption, primarily high initial costs, a critical skills gap, and cultural resistance. The paper concludes by proposing practical, expert-led strategic recommendations for government, industry, and academia. These recommendations outline a multi-stakeholder approach to foster an ecosystem for innovation, aiming to enhance productivity and sustainability in the Sri Lankan construction sector.

Keywords: Augmented Reality (AR), Virtual Reality (VR), Building Information Modelling (BIM), Construction Industry, Technology Adoption, Sri Lanka, Quantity Surveying.

1 Introduction

Project duration and cost overruns are the most significant challenges in the construction industry [1]. Perera et al. [2] stated that inadequate project planning, ineffective coordination among stakeholders, and complex regulatory approval processes are the major causes of them. Furthermore, the prevailing subpar quality control practices are the other challenges [3]. Further, there are challenges related to procurement, project management, skill

shortage, technological adoption, design and drawings and health and safety [4] [5]. In addition, Dlamini and Cumberlege [1] stressed that project delays and cost overruns continue to plague the Sri Lankan construction landscape, often stemming from poor project management, inadequate planning, and insufficient risk assessment. A significant factor contributing to these inefficiencies is the slow adoption of technological advancements. Consequently, the construction sector in Sri Lanka faces challenges related to outdated technology adoption and innovation. The sluggish incorporation of modern construction techniques, Building Information Modeling (BIM), and other advanced technologies curtails efficiency gains and hinders productivity [6].

Augmented Reality (AR) and Virtual Reality (VR) have emerged as transformative technologies with significant implications across various domains. AR enhances the user's perception by integrating digital content into the real-world environment [7]. Conversely, VR immerses users in entirely virtual environments, isolating them from the real world and providing highly immersive experiences [8]. Both technologies not only enhance project efficiency but also elevate safety, collaboration, and stakeholder engagement in construction processes, leading to more informed decisions and better-built structures [9]. BIM serves as a digital platform for AR and VR applications, as it provides detailed 3D models and structured data that can be visualized and interacted with through AR-enabled devices or immersive VR systems [10]. The integration of AR and VR technologies holds significant promise for mitigating project duration and product quality issues in building construction within Sri Lanka. AR and VR solutions offer immersive visualization and simulation capabilities that can revolutionize project planning, design, and execution. By utilizing AR and VR, stakeholders can engage in virtual walkthroughs of construction sites, enabling them to identify potential design flaws, clash detections, and spatial conflicts early in the process [10].

Although the extant literature offers valuable perspectives on strategies that aim to augment enablers and mitigate barriers, certain gaps continue to exist, particularly about adaptation strategies customized to the distinct dynamics of the construction landscape in Sri Lanka. It is noteworthy that the literature review is deficient in providing thorough strategies for surmounting particular obstacles and supporting critical facilitators necessary for the successful integration of AR and VR technologies during the in-depth stages of planning and implementation.

Given this context, the aim of this paper is to investigate the potential of AR and VR to address key challenges in the Sri Lankan construction industry and propose strategic recommendations for its implementation. To achieve this aim, the study is guided by the following research questions: (1) What are the potential benefits of implementing AR and VR technologies in Sri Lankan construction industry?, (2) What are the major barriers hindering the AR and VR adoption in Sri Lankan construction industry?, and (3) What

strategies can be proposed to effectively overcome these barriers and facilitate successful AR and VR adoption in Sri Lanka? Furthermore, this study specifically focuses on the perspectives of Quantity Surveyors (QSs), as they play a central role in project cost management and the interpretation of design data, making their viewpoint critical for assessing the practical impact of these technologies.

2 AR and VR in Construction

2.1 Use of AR and VR in Global Construction

The combined influence of AR and VR has reshaped the dynamics of the built environment worldwide [11]. Furthermore, AR and VR technologies have revolutionized architectural visualization and design on a global scale through immersive virtual walkthroughs [12]. These technologies transcend geographical boundaries, fostering collaboration among architects, designers, and clients, creating a more interconnected global design community [13]. In parallel with design improvements, advance technology has also taken a central role in project execution. In the construction sector, AR and VR have become integral tools for project management worldwide. Construction sites in major cities like London and Dubai utilize AR for real-time data overlays, enhancing worker productivity, while VR is employed for collaborative project planning and training [14]. Moreover, AR and VR play pivotal roles in shaping smart cities and urban planning initiatives globally [15].

The possibility of applying these global trends in the Sri Lankan context is significant. VR and AR have the potential to completely change the design and visualisation processes in Sri Lanka's built environment [16]. AR technologies can enable architects and planners to overlay digital design information onto the physical environment, allowing for a real-time visualization of proposed structures within the context of existing surroundings [17]. Additionally, VR technologies offer immersive simulations that empower stakeholders to virtually explore and experience architectural designs, providing a comprehensive sense of scale and proportion [18]. AR can enhance precision in cost estimation by overlaying digital information onto physical spaces, allowing stakeholders to visualize and assess potential challenges and opportunities during the planning phase [19]. Similarly, VR simulations enable stakeholders to experience the proposed construction virtually, facilitating a deeper understanding of the project scope [11]. AR can assist construction teams by overlaying digital information onto physical spaces, allowing for enhanced on-site plan-

ning and resource allocation. This technology enables stakeholders to visualize and optimize layout decisions, reducing errors and improving the overall efficiency of the construction process [14].

Furthermore, these technologies can address issues of resource management. AR and VR technologies have the potential to revolutionize material selection and waste management practices in the Sri Lankan built environment [20]. AR can aid architects and builders in real-time visualization of different materials within the context of a construction site, allowing for more informed decisions regarding suitability and aesthetics [21].

3 Research Methodology

A qualitative research approach was adopted to investigate the potential of AR and VR and propose strategic recommendations for their adoption in Sri Lanka. Qualitative research approach is adopted to represent the perceptions, experiences, beliefs, and viewpoint of a particular group of people and this approach is an ideal option for research regarding emerging conceptions investigations. The AR and VR adaptation is the most emerging cultural change in the construction industry. Further, The AR and VR adaptation in building environment is a hypothesis for particularly in Sri Lankan context because of that qualitative method is chosen for this research based on findings of [22].

3.1 Data Collection

Data was gathered through case studies employing semi-structured interviews, documentary reviews, and observations. The interview method is a widely used data collection technique under qualitative approach. Unlike rigid surveys, semi-structured interviews offer flexibility, interactivity, and in-depth discussion with interviewees to obtain more ideas on current and new topics. Hence, semi-structured interviews have been selected for this research followed by qualitative approach as possibility for the required-further explanation is higher in this study.

3.2 Interviewee Profile

Eleven experts from different firms in the construction industry were chosen for the interviews. A combination of purposive and snowball sampling was utilized. Purposive sampling, which is a non-probability type sampling, entails selecting respondents as per the particular purpose of the research instead of randomly selecting the respondents. It is more appropriate to use purposive sampling when opinions and perceptions of the experts are

the major source for the study area [23]. In addition, snowball sampling is adopted for instances where it is difficult to identify the potential respondents from the defined population [24]. This dual approach was necessary because, in Sri Lankan context, BIM adoption has been occurred recently, and it is difficult to identify the respondents who have adequate experience in BIM based design & quantification. Therefore, the selection criteria specifically focused on Quantity Surveyors with experience in both cost estimation and BIM technologies. Table.1 provides the profile of interviewees.

Table.1 Profile of interviewees

Code	Designation	Industry Experience (Years)
R1	Quantity Surveyor	5
R2	Senior consultant Quantity Surveyor	11
R3	Quantity Surveyor	4
R4	Senior Quantity Surveyor with BIM experience	9
R5	Quantity Surveyor	16
R6	Quantity Surveyor with technological expertise	5
R7	Quantity Surveyor	4
R8	Director, Senior Quantity Surveyor	17
R9	Senior Quantity Surveyor	15
R10	Director, Senior Quantity Surveyor	20
R11	Director, Senior Quantity Surveyor	18

3.3 Data Analysis

Data analysis is referred to as a process of examining, classifying, arranging, and testing the collected data. Content Analysis is a widely accepted data analysis method under the qualitative approach [25]. Moreover, it facilitates identifying patterns among textual data. Accordingly, manual content analysis was adopted to analyze the collected data and identify recurring themes related to benefits, barriers, and strategies. This involved identifying recurring words from the transcripts, categorizing them into themes of benefits, barriers, and strategies and observing their frequency to indicate relative importance.

4 Findings and Discussion

4.1 How AR and VR Can Solve Common Construction Problems

The experts interviewed for this study confirmed that AR/VR technologies offer direct solutions to some of the most challenging problems in construction.

By agreeing with R1, R7 and R8, R2 mentioned that through AR-VR based quantity calculation, manual works in quantification can be automated thereby significant time saving can be achieved. R2 mentioned, "*information integration assists in achieving higher level of time saving*". R1 added that this information integration simplifies the quantity checking process since it is not required to refer various drawings to check one element. Experts R5 and R8 elaborated on the fact as this technology *"effortlessly regenerates the quantities and conveniently accommodate the design changes"*. Beyond automation, the immersive nature of technology was seen as a key benefit for clarity and comprehension. According to the explanation provided by R5, in the AR-VR based quantity calculation method, building elements can be virtually visualized in 3D. R4 mentioned as *"conveniently understand how the elements are connected together and where they have been placed"*. Moreover, R11 mentioned that *"clearly identify the extend of each element"*. Therefore, QS can quickly obtain a proper understanding of what is going to be quantified. It assists with quantity calculation properly. This combination of automation and visualization directly improves accuracy by reducing human error. R1 stated that AR-VR automation significantly replaces involvement of the human element in quantity calculation. R8 elaborated that, "*AR-VR based method uses advanced calculation algorithms to calculate them with 100% accuracy"*. Therefore, human related errors are minimized, and accuracy is improved.

Finally, experts highlighted the significant improvement in inter-disciplinary collaboration. According to R1 and R4, minimal collaboration and its consequential adverse impacts are there with the conventional method. However, AR-VR based quantity calculation method minimizes those consequences through increased collaboration. R7 mentioned "*AR-VR at its full potential, all stakeholders can work on a central model and communicate easily between them*".

4.2 The Main Challenges of Using AR and VR in Sri Lanka

Money and Cost Problems

All respondents emphasized that higher initial cost is a problem associated with AR-VR affordance in Construction industry. R1 mentioned that higher license cost is one of the major expenditures in this method. Further, R1, R6, R8 and R10 stated that high-capacity computers and special equipment to operate the AR-VR are needed for this. For instance, the adoption of AR will typically require AR-enabled tablets or smartphones with proprietary apps (e.g., Fologram, Augment), while VR requires pricier immersive hardware such as Oculus Rift or HTC Vive headsets and suitable software platforms (e.g., Unity or Enscape). These hardware and software requirements play an important role in substantially increasing the financial burden for Sri Lankan companies. In addition, this finding is consistent with global literature on technology adoption, where initial capital expenditure is frequently cited as a primary barrier. R11 highlighted that at the beginning considerable training cost is also required to adopt this method. Furthermore, R8 agreed to the above fact that *"Not only hardware and software costs, but it also takes high investment in training the professionals to the new digital procedure"*. However, the experts highlighted that this challenge is particularly severe in the Sri Lankan context, where funds for technological upgrades can be limited for many small and medium enterprises (SMEs) that form the backbone of the local industry.

People and Training Problems

All respondents agreed that there is a cultural resistance among the QSs related to the adoption of advanced technologies. R9 and R10 observed that the degree of resistance to this change is generally higher among older people. Moreover, R10 proposed that the attitude of the people also has a strong influence in resistance to change. This cultural resistance is made worse by a noticeable skills gap. All the respondents identified a problem that there is a dearth of competent people who can perform BIM software and are capable of handling modern technologies. R8 described as "*when I was recently trying to recruit QSs with BIM capability, incurred a considerable cost for training experts*." This dual challenge of resistance from experienced professionals and a lack of trained new entrants creates a significant hurdle for widespread adoption, a situation that may be more prominent in developing economies compared to regions with established digital construction curricula.

Technology and Quality Problems

All respondents mentioned that the quality or completeness of the model is a concern in AR and VR technology-based quantity calculation. R11 elaborated on dependency of quantity from AR and VR methods. Additionally, R3 noted that when inadequate details are provided in the model, it becomes necessary to resort to 2D drawings for measuring

those items using conventional methods. Furthermore, R9 added that the QSs might face difficulties due to *"improper procedure in drafting the model so that utilizing the model for your estimating purposes becomes complex"*. This "garbage in, garbage out" problem highlights that the technology's effectiveness is highly dependent on the quality of the digital inputs. This dependency leads directly to the next major technological barrier: inadequate standards. All the participants mentioned that inadequate standard is a problem associated with AR-VR technologies. The lack of localized standards means that even with willing participants, interoperability and consistency will remain significant challenges. This is further complicated by issues of software compatibility as stated by three respondents.

4.3 A Plan for Using AR and VR Successfully in Sri Lanka

Solutions for Cost Problems

To counter the significant financial barriers, the majority of respondents proposed that obtaining support of the government as a strategy to overcome from this issue. In the Sri Lankan context, AR solutions are likely to have a more immediate impact than VR, and this is largely due to their comparatively low cost of deployment and compatibility with mobile devices in widespread use. Although VR provides fully immersive experiences, its reliance on expensive headsets and high-performance computing limits short-term feasibility for the majority of businesses. Conversely, AR can be gradually integrated using affordable devices, and this makes it better suited to resource-constrained environments. Nevertheless, the role of BIM remains central, as it supplies the 3D models and structured data that enable both AR and VR to function effectively. R9 expressed what is happening in other countries as "*subsidizing the cost of software, there are tax benefits or maybe subsidized prices for the technology related investments*". In addition, R4 suggested that selecting sharing software can be a solution to higher initial costs. Further to R4, some cheaper software options can be considered. However, features will also be fewer with cheaper options.

Solutions for People and Training Problems

Addressing the human element requires a two-directional approach focusing on current and future professionals. R7 mentioned that Professional bodies such as Institute of Quantity Surveyors Sri Lanka (IQSSL) and Institute of Engineers Sri Lanka (IESL) should conduct more continuing professional development (CPD) programs and workshops. Moreo-

ver, practical methods of automatic quantity generation should be demonstrated. R9 mentioned that some QS practitioners are thinking that they will lose their job if AR-VR is adopted. However, it is important to understand one thing that they may also lose the job unless they are familiar with AR-VR technologies. For the future workforce, agreeing with R2, R10 mentioned that incorporating modules in university curriculum to explain practical method of AR-VR based automatic quantity generation and designing is a strategy for this issue. Moreover, R6 contended that self-learning habits are reduced among students and students should try to learn these technologies themselves.

Solutions for Technology and Quality Problems

To improve the quality of technical implementation, experts emphasized the need for standardization and collaboration. Five respondents suggested that implementing standards when preparing the model could assist in overcoming this issue. R5 suggested that professional bodies should perform proactively for the successful AR-VR implementation. R5 further mentioned "*if we learn from mistakes of other countries and establish standards in advance, then there will be less problems during the time of extensive usage in the future*". Finally, a direct feedback loop to technology creators was proposed. R10 suggested that through providing constructive feedback to the software developers, this problem can be solved. R10 further mentioned that with the introduction of updated versions, this problem will be greatly minimized.

To consolidate the findings, the challenges and solutions discussed in section 4.2 and 4.3 are summarized in the Table.2.

Table.2 Challenges and the solutions in AR and VR adoption in Sri Lanka

No	Challenges	Strategies
1	Low quality or incompleteness of the BIM model	Strategic planning for structured AR/VR adoption roadmap
2	Higher initial cost	Policy interventions to establish supportive regulations and incentives
3	Cultural resistance	Collaborative action among government, academia, and industry stakeholders
4	Lack of competent persons	Capacity building through specialized training and upskilling programs
5	Checking Automated quantities.	Public awareness campaigns to promote understanding and acceptance

6	Inadequate standards	Development and enforcement of standardized guidelines for AR/VR use
7	Inadequate consideration for construction methods	Integration of construction methodologies into AR/VR workflows
8	Software incompatibility	Promoting software interoperability and compatibility
9	Inadequate integration in the model	Strengthening integration between AR/VR platforms and BIM models
10	Lesser awareness	Continuous monitoring and evaluation mechanisms to track progress
11	Less usage of BIM & other advanced technologies in SL.	Encouraging wider adoption of BIM and advanced digital technologies

5 Conclusions and Recommendations

5.1 Conclusions

In conclusion, AR and VR technologies offer transformative solutions to the challenges plaguing the Sri Lankan construction industry. These technologies enhance project visualization and planning accuracy, reducing financial risks and construction delays. While the adoption of AR and VR entails initial investments and the development of technical expertise, their long-term benefits are substantial. However, this research reveals that realizing these benefits is contingent on overcoming a triad of significant barriers: economic, human, and technical. By leveraging these advanced technologies, while concurrently implementing a targeted program that adheres to these recommendations, Sri Lanka can enhance construction efficiency, reduce errors, and foster innovation, ultimately driving the industry toward greater sustainability and growth. The findings carry important implications for multiple stakeholders: for government and multiple professional bodies, the need to establish standards and financial support mechanisms, for construction companies, the importance of phased adoption and capacity building; and for universities, the integration of AR/VR into curricula to equip the future workforce.

5.2 Recommendations

Based on the findings, this paper proposes a multi-stakeholder approach to facilitate the successful adoption of AR and VR in the Sri Lankan construction industry. The following recommendations are targeted at key groups who can drive this change.

For the Government and Industry Groups

To create an enabling environment, government and professional bodies should take the lead. This includes providing financial support through subsidies or tax incentives to offset the high initial cost for organizations, especially the SMEs. Government can provide financial support and other relevant support to develop own AR-VR related software in the country and can drastically reduce the initial cost of AR-VR. Furthermore, professional bodies like IQSSL and IESL must lead the development and enforcement of national BIM and data standards to address the technical quality and interoperability issues identified by experts. Further, the professional bodies can include AR-VR as one of competencies for APCs to encourage the professionals to learn the AR-VR. This support would not only modernize the construction sector but also boost national productivity, enhance the competitiveness of Sri Lankan firms, and foster a high-tech knowledge economy.

For Construction Companies

For individual firms, a phased and strategic approach to adoption is recommended. Encouraging construction organizations to adapt to AR-VR technology is a priority. Adapting this technology can create more benefits to compete with other organizations in future. Organizations should begin by investing in smaller pilot projects to demonstrate ROI and build internal capacity before large-scale rollouts. This reduces the investment risk and helps to build a strong business case for wider implementation. Equally important is fostering an internal culture that encourages innovation and provides continuous training to overcome cultural resistance and bridge the skills gap.

For Universities

Academic institutions are crucial for building a future-ready workforce. AR-VR technology can be included in curriculums of degree programs in universities. Teaching AR and VR at the university level can help to produce the most capable professionals for the industry. This should go beyond theoretical modules to include practical, hands-on learning. Partnerships with software vendors and industry firms could provide students with hands-

on experience with the latest tools. Furthermore, universities should encourage interdisciplinary projects that bring together students from Architecture, Engineering, Quantity Surveying, and Information Technology to demonstrate the collaborative nature of modern digital construction practices.

5.3 Study Limitations and Future Research

The findings and recommendations of this study should be considered in light of its limitations, which in turn suggest avenues for future research. It should be noted that there is no practical implementation of AR-VR in Sri Lankan Project. Because of that, the data collections were dependent on the experts' perspectives and future predictions based on their experience in the industry. This means the identified benefits and barriers are perceived rather than empirically validated within a live project environment. In addition, this research limited to the Consultant & Contractor QS perspective from Sri Lanka. This provides a deep but narrow view of the subject. A wider understanding would require incorporating the perspectives of architects, engineers, clients, and policymakers.

Therefore, this research is considered as a benchmark for further studies related to the implementation of AR-VR technology in the construction industry. Future research could include a quantitative study to measure the ROI of a pilot project or longitudinal case studies tracking the adoption journey of early-adopter firms in Sri Lanka. Other research could also focus on developing a low-cost, localized AR/VR solution tailored to the specific needs and resource constraints of Sri Lankan SMEs, investigating the frameworks required to ensure data security on collaborative digital platforms, developing a predictive AI incorporated AR-VR solution for BIM based project delivery or a comparative study analyzing Sri Lanka's adoption journey against other developing nations.

References

1. M. Dlamini, R. Cumberlege, The impact of cost overruns and delays in the construction business. In IOP Conference Series Earth and Environmental Science, 654(1), pp. 12-29, (2021).
2. B. A. K. S. Perera, R. Rameezdeen, N. Chileshe, M. R. Hosseini, Enhancing the effectiveness of risk management practices in Sri Lankan road construction projects: A Delphi approach. International Journal of Construction Management 14(1), pp 1–14, (2014).
3. D. A. R. Dolage, T. Pathmarajah, Mitigation of delays attributable to the contractors in the construction industry of Sri Lanka - Consultants' perspective. Engineer Journal of the Institution of Engineers Sri Lanka, 48(1), 21, (2015).

4. A. Alsharef, A. Ovid, S. M. Jamil Uddin, A. Albert, Biggest Challenges Facing the Construction Industry. Construction Research Congress CRC 2024, American Society of Civil Engineers (ASCE), pp. 652–660, (2024).
5. N. Abeysinghe, R. Jayathilaka, Factors influencing the timely completion of construction projects in Sri Lanka. PLoS One, 17(12), (2022).
6. H. D. R. R. Rosayuru, K. G. A. S. Waidyasekara, M. K. C. S. Wijewickrama, Sustainable BIM based integrated project delivery system for construction industry in Sri Lanka. International Journal of Construction Management, 22(5), pp. 769-783, (2019).
7. X. Li, W. Lu, F. Xue, L. Wu, R. Zhao, J. Lou & J. Xu, Blockchain-Enabled IoT-BIM platform for supply chain management in modular construction. Journal of Construction Engineering and Management, 148(2), (2021).
8. S. Safikhani, S. Keller, G. Schweiger, J. Pirker, Immersive virtual reality for extending the potential of building information modeling in architecture, engineering, and construction sector: systematic review. Taylor and Francis Ltd. (2022).
9. M. F. Pereira, C. Prahm, J. Kolbenschlag, E. Oliveira, N. F. Rodrigues, Application of AR and VR in hand rehabilitation: A systematic review. Journal of Biomedical Informatics, 111, pp. 103-584, (2020).
10. E. Yigitbas, A. Nowosad, G. Engels, Supporting Construction and Architectural Visualization through BIM and AR/VR: A Systematic Literature Review. arXiv.org, (2023).
11. X. Wang, M. J. Kim, P. E. D. Love, S. C. Kang, Augmented Reality in built environment: Classification and implications for future research. Automation in Construction, 32, pp. 1–13, (2013).
12. J. Milovanovic, G. Moreau, D. Siret, F. Miguet, Virtual and augmented reality in architectural design and education, (2017).
13. M. Noghabaei, A. Heydarian, V. Balali, K. Han, Trend analysis on adoption of virtual and augmented reality in the architecture. Engineering, and construction industry, 5(1), p. 26, (2020).
14. Y. Tan, W. Xu, S. Li, K. Chen, Augmented and Virtual Reality (AR/VR) for education and training in the AEC industry: A Systematic Review of Research and Applications. Buildings, 12(10), pp. 15-29, (2022).
15. A. Hassebo, M. Tealab, Global Models of smart cities and Potential IoT Applications: A review. IoT, 4(3), pp. 366–411, (2023).
16. R. K. J. De Silva, T. D. Rupasinghe, P. Apeagyei, A collaborative apparel new product development process model using virtual reality and augmented reality technologies as enablers. International Journal of Fashion Design Technology and Education, 12(1), pp. 1–11, (2018).
17. W. Perera, K. Ranadewa, A. Parameswaran, D. Weerasooriya, Status quo of digitalisation in the Sri Lankan construction industry. World Construction Symposium 2023, (2023).
18. T. Haupt, M. Akinlolu, M. Raliile, Applications of digital technologies for health and safety management in construction, (2019).

19. J. Xu, F. Moreu, A review of augmented reality applications in civil infrastructure during the 4th Industrial Revolution. Frontiers in Built Environment, 7, (2021).
20. J. M. D. Delgado, L. Oyedele, T. Beach, P. Demian, Augmented and virtual reality in construction: Drivers and limitations for industry adoption. Journal of Construction Engineering and Management, 146(7), (2020).
21. J. K. W. Wong, H. Li, H. Wang, T. Huang, E. Luo, V. Li, Towards low-carbon construction processes: the visualisation of predicted emission via virtual prototyping technology. Automation in Construction, 33, pp. 72–78, (2012).
22. A. Mehrad, M. H. T. Zangeneh, Comparison Between Qualitative and Quantitative Research Approaches: Social Sciences. International Journal for Research in Educational Studies, 5(7), pp. 1–7, (2019).
23. M. D. C. Tongco, Purposive Sampling as a Tool for Informant Selection. Ethnobotany Research and Applications, 5, pp. 147–158. (2007).
24. I. Etikan, Sampling and sampling methods. Biometrics & Biostatistics International Journal, 5(6), (2017).
25. G. Gibbs, Qualitative data analysis: Explorations with NVivo. Open University Press, Buckingham (2002).

Bridging the Digital Divide: How and Why the Road Development Authority should be aligned with Sri Lanka's Digital Economy Blue Print

S. A. S. T. Salawavidana

Information Systems & Network Management, Road Development Authority,
Denzil Kobbekaduwa Mawatha, Battaramulla, Sri Lanka.
suneth.thushara@gmail.com

Abstract. This study examines the strategic alignment of Sri Lanka's Road Development Authority (RDA) with the national Digital Economy Blueprint, focusing on the institutional transformation required to modernise transport governance. This study adopts a qualitative approach, incorporating twelve in-depth stakeholder interviews alongside comparative analyses of digital governance models in Singapore, Estonia, and India. These sources provide a rich foundation for examining the RDA's institutional alignment with Sri Lanka's Digital Economy Blueprint. Thematic analysis revealed persistent barriers to digital adoption, including limited digital literacy, fragmented inter-agency coordination, and constrained financial resources. In response, this study proposes a phased implementation roadmap encompassing foundational IT infrastructure, AI-powered traffic management systems, and integrated e-governance platforms. By contextualising global best practices within Sri Lanka's regulatory and operational landscape, the paper offers a policy-relevant framework for advancing sustainable, citizen-centric mobility solutions.

Keywords: Digital Transformation, Road Development Authority (RDA), Intelligent Transport Systems (ITS), Artificial Intelligence (AI), Building Information Modeling (BIM), E-Governance, Smart Infrastructure, Transport Policy, Public Sector Innovation, Sri LankaFirst Section

1 Introduction

1.1 Background and Significance of Digital Transformation

In the 21st century, digital transformation has emerged as a critical driver of efficiency, Sri Lanka's commitment to transparency and economic growth is reflected in its Digital

Economy Blueprint [1] (see Fig. 1), which envisions the integration of digital technologies such as e-governance, artificial intelligence (AI), intelligent transport systems (ITS), and digital payment platforms to modernize public institutions and enhance governance. Infrastructure development remains pivotal to the nation's economic trajectory, with the Road Development Authority (RDA) playing a central role in managing and expanding the country's transport network. However, the RDA has been slow to adopt digital innovations, continuing to rely on conventional approaches to road planning, project implementation, and traffic management.

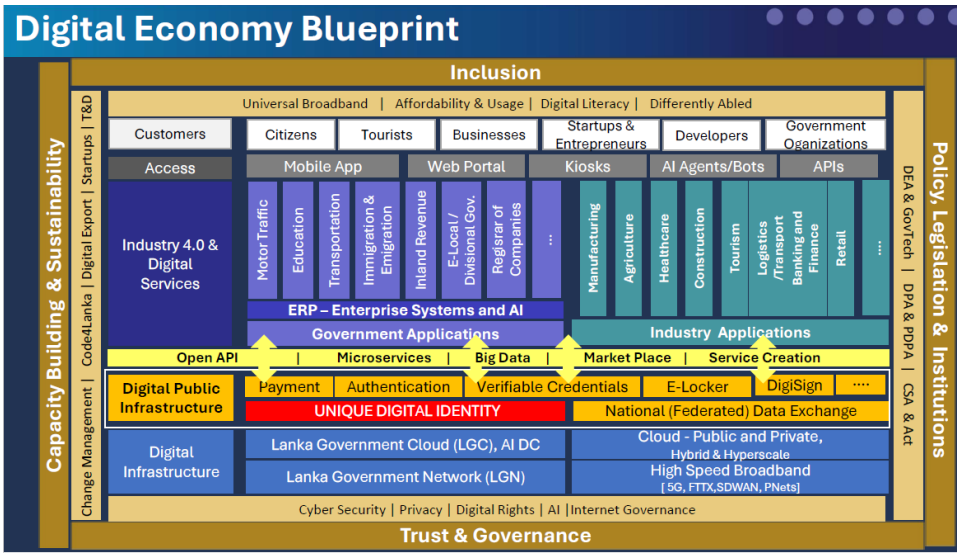

Fig. 1. Sri Lanka's Digital Economy Blueprint (Source: Ministry of Digital Economy) [1]

This lag hinders operational efficiency and sustainability, underscoring the urgent need to align the RDA's operations with the national digital agenda. Embracing digital transformation is not just a strategic upgrade for the RDA, but a national imperative to ensure economic resilience and global competitiveness.

1.2 The Need for RDA's Alignment with Digitization

As the digital economy advances, transport infrastructure emerges as a critical enabler of transformation, with global leaders like Singapore and Estonia demonstrating how AI-

driven traffic analytics, smart tolling, and cloud-based asset management significantly enhance mobility, service delivery, and revenue efficiency. In contrast, Sri Lanka's Road Development Authority (RDA) faces significant barriers to digital integration, including outdated legacy systems, limited technological investment, low digital literacy among staff, and regulatory challenges impeding interoperability across transport agencies [2]. Overcoming these constraints through strategic, policy-driven digital adoption will enable the RDA to improve planning accuracy, alleviate congestion, enhance public accountability, and expand service accessibility. Moreover, embracing technologies such as Building Information Modeling (BIM), Geographic Information Systems (GIS), and AI-based traffic monitoring will empower the RDA to align with global sustainability goals by reducing emissions, optimizing urban planning, and transitioning to a smarter, more adaptive infrastructure governance model.

1.3 Key Challenges Limiting RDA's Digital Adoption

Despite the clear advantages of digital governance, the Road Development Authority (RDA) faces systemic challenges in its transition, with financial constraints being a primary obstacle, as budget priorities remain focused on traditional infrastructure projects rather than intelligent transport solutions [2]. Although international agencies like KOICA and the World Bank have funded select digital pilot initiatives, sustainable progress requires dedicated, long-term financing frameworks. Institutional resistance further hampers transformation, with entrenched bureaucratic processes and a workforce largely trained in civil engineering rather than IT governance showing reluctance toward adopting AI-driven traffic systems and digital procurement tools. Moreover, low digital literacy among staff inhibits broad implementation. Interoperability issues between government entities also present a significant barrier, limiting data sharing and collaborative planning [3]. The absence of a national Building Information Modeling (BIM) policy exacerbates this fragmentation, preventing the establishment of standardized frameworks necessary for cohesive digital infrastructure management. Without structural regulatory reform and institutional capacity building, the RDA's digital modernization risks remaining piecemeal and ineffective.

1.4 Opportunities for Digital Transformation in RDA

Despite challenges, the RDA has strong opportunities to digitally transform its operations. AI-driven traffic management and smart transport systems, such as automated tolling and real-time analytics, can ease congestion and improve revenue collection. Integrating platforms like GovPay can streamline tolls, permits, and procurement, enhancing transparency

and efficiency. Public-Private Partnerships and international collaboration can bring advanced technologies, cybersecurity, and expertise, as seen in countries like Singapore. Additionally, data analytics and machine learning enable predictive traffic planning and dynamic signal control, aligning RDA's efforts with global standards for sustainable, efficient urban mobility.

1.5 Research Objectives and Scope

This paper examines:

1. Why the RDA must align itself with Sri Lanka's Digital Economy Blueprint.
2. How digital adoption can transform the RDA's efficiency, transparency, and service delivery.
3. Challenges limiting the RDA's digital expansion.
4. Opportunities for integrating AI-driven analytics, ITS, and e-governance platforms into road governance frameworks.
5. Strategic roadmap for policy-driven digital adoption at RDA.
   Through a detailed literature review, comparative case studies, and qualitative research methodology, this study provides actionable insights into bridging the digital divide in Sri Lanka's transport sector.

2 Literature Review

This section synthesizes global and local scholarship on digital transformation in public sector governance, with a focus on transport infrastructure, intelligent systems, and institutional modernization—highlighting both theoretical foundations and applied innovations relevant to Sri Lanka's evolving digital landscape.

2.1 Theoretical Foundations of Digital Transformation in Public Sector Governance

Digital transformation, rooted in e-governance and smart infrastructure planning, plays a vital role in modernizing public services, reducing inefficiencies, and enhancing transparency [4]. Technologies like cloud computing, AI, and big data have improved decision-making and streamlined workflows in governance [5]. Globally, digitalization has boosted accountability and resource optimization, enabling evidence-based policies and reducing waste [6]. Tools such as digital payments, workflow automation, and AI monitoring have reshaped infrastructure management, especially in transport. Sri Lanka's Digital Economy

Blueprint offers a timely opportunity for institutions like the RDA to embrace digital integration and modernize governance.

2.2 Digitalization in Public Infrastructure and Transport Management

Infrastructure modernization is central to smart city development, with technologies like BIM, ITS, and GIS enabling predictive modeling, traffic optimization, and real-time asset monitoring [7]. Countries such as Singapore and Estonia illustrate the benefits of smart mobility through AI-driven traffic systems, sensor-enabled intersections, and blockchain-based tolling [8]. In contrast, Sri Lanka still depends on manual monitoring and fragmented systems in its transport sector. To improve connectivity, traffic flow, and emergency response, the RDA must adopt data-driven governance as outlined in the Digital Economy Blueprint, promoting inter-agency collaboration and advanced mobility analytics.

2.3 The Role of Intelligent Transport Systems (ITS) in Road Infrastructure

Intelligent Transport Systems (ITS) have revolutionized urban mobility through sensor-based algorithms, adaptive signals, and real-time traffic adjustments, cutting congestion by up to 30% and improving efficiency [6], [9]. Cities like Tokyo and London use machine learning to optimize traffic light timing, reducing idling and fuel use. ITS also supports dynamic regulation based on real-time travel patterns. In Sri Lanka, ITS adoption by the RDA is still limited to pilot tolling and basic analytics. A national ITS strategy with cross-sector collaboration and policy standardization is crucial to enhance transport governance and operational efficiency.

2.4 Building Information Modeling and Digital Road Assets Management

Building Information Modeling (BIM) is revolutionizing road development by enabling detailed visualization, accurate cost estimation, and efficient resource planning [7]. It enhances construction accuracy, reduces environmental impact, and strengthens coordination across agencies [8]. Countries like Germany and Singapore have adopted national BIM policies to standardize infrastructure projects and minimize delays. In contrast, Sri Lanka's lack of a unified BIM framework leads to fragmented planning within agencies like the RDA. Implementing a standardized BIM approach would improve project execution, foster collaboration, and boost the resilience of transport infrastructure.

2.5 Digital Payments and E-Governance in Transport Institutions

Integrating digital payment solutions into transport governance enhances accountability, reduces revenue leakage, and streamlines fiscal operations [10]. Countries like Sweden and Estonia use AI and blockchain to digitize permits and approvals, improving transparency and efficiency [9]. Sri Lanka's GovPay system offers a foundation for RDA to digitize tolls, permits, and procurement, but its integration remains uneven. Strengthening interoperability with other transport systems is essential to ensure secure, accessible, and transparent digital transactions across the sector.

2.6 Public-Private Partnerships (PPPs) and International Collaborations for Digital Transport Expansion

Global benchmarks show that Public-Private Partnerships (PPPs) play a crucial role in driving innovation and scaling digital transport infrastructure [11]. Singapore partners with tech firms to develop ITS solutions like sensor-based analytics and real-time monitoring, while countries like India and Germany use private funding to support national digitization efforts [9]. Sri Lanka's RDA has engaged in some partnerships, such as the KOICA-funded traffic database project, but needs to establish broader collaboration models to ensure sustainable digital innovation in transport governance.

2.7 The Need for Policy Standardization in Digital Road Governance

Sri Lanka's road management sector faces limited multi-agency integration due to a lack of aligned digital policies, restricting the scalability of digital initiatives. Research shows that standardized e-governance frameworks enhance sustainability and ensure consistent service delivery across transport bodies [5]. For example, Singapore's Land Transport Authority enforces ITS adoption via national legislation, while Estonia uses blockchain for streamlined permit processing [6]. To modernize effectively, Sri Lanka must develop comprehensive transport digitalization policies, including national BIM mandates, ITS standards, and GovPay compliance, to drive uniform adoption across the RDA and related agencies.

3 Methodology

This section outlines the qualitative research design, data collection strategies, comparative case study approach, and thematic analysis framework used to investigate the RDA's digital transformation, while acknowledging contextual limitations and the need for adaptive policy insights.

3.1 Research Design and Approach

This study adopts a qualitative research design to examine the strategic alignment of Sri Lanka's Road Development Authority (RDA) with the national Digital Economy Blueprint. The approach integrates semi-structured stakeholder interviews, thematic analysis, and comparative case studies to explore institutional, policy, technological, and financial factors influencing digital transformation. The design is exploratory in nature, aiming to generate context-sensitive insights and propose a phased modernization roadmap tailored to Sri Lanka's transport governance landscape.

3.2 Data Collection Methods

Primary data were collected through twelve semi-structured interviews with key stakeholders, including senior RDA officials, transport engineers, IT personnel, and external experts affiliated with international agencies such as KOICA and the World Bank. Participants were selected based on their direct involvement in digital initiatives or strategic planning within the transport sector. Interview questions focused on institutional readiness, digital literacy, funding mechanisms, technological feasibility, and inter-agency coordination. All interviews were conducted in accordance with ethical research protocols, ensuring informed consent, voluntary participation, and confidentiality of responses. Participants were briefed on the study's objectives and their right to withdraw at any stage without consequence.

Secondary data included national policy documents, internal RDA reports, and international benchmarks from Singapore, Estonia, and India. Academic literature on digital governance, intelligent transport systems (ITS), and public sector innovation was also reviewed to ensure theoretical grounding and comparative relevance.

3.3 Comparative Case Study Methods

The study compares digital transformation models from Singapore's Land Transport Authority, Estonia's e-governance systems, and India's digital infrastructure projects. It assesses technology, funding, policies, and workforce adaptation to identify lessons applicable to RDA.

3.4 Thematic Analysis and Framework

Interview transcripts were analysed using inductive thematic coding. Key themes were identified through iterative reading and categorisation, including:

- Financial constraints and budget prioritisation
- Workforce resistance and digital literacy gaps
- Interoperability challenges across transport agencies
- Institutional inertia and regulatory fragmentation
- Opportunities for AI-driven traffic optimisation and e-governance integration

3.5 Research Limitations

Limitations include limited access to real-time data, budget restrictions on empirical analysis, institutional resistance affecting transparency, and reliance on developed-country benchmarks requiring contextual adaptation.

4 Findings and Discussion

This section presents key empirical insights from stakeholder interviews and comparative analysis, structured around five thematic areas that influence the RDA's digital transformation trajectory.

4.1 Financial Constraints in Digital Expansion

A major barrier to the Road Development Authority's (RDA) digital transformation is its limited financial capacity, as funding prioritizes traditional road maintenance and construction over IT innovation. Despite support from donors like the World Bank and KOICA, reliance on external funding hampers scalability and sustainability of projects such as EDMS and GIS integration. To advance digital capabilities like BIM, ITS, and cloud platforms, RDA needs dedicated IT budget allocations, expanded public-private partnerships, and diversified international funding. Without a clear investment strategy, Sri Lanka risks lagging in transport modernization and failing to fully realize the Digital Economy Blueprint.

4.2 Workforce Adoption and Digital Literacy Challenges

Institutional resistance within the Road Development Authority (RDA), driven by a workforce accustomed to manual processes and limited digital literacy, significantly impedes the adoption of intelligent transport solutions. Many civil engineers and administrative staff remain skeptical of AI-driven analytics, automated monitoring, and e-governance workflows due to reliance on traditional paper-based approvals and manual tracking. To overcome this, structured capacity-building programs are essential, including integrating

digital literacy into training, incentivizing IT certifications, and partnering with academic institutions like the University of Moratuwa to enhance skills in transport analytics. Without these proactive initiatives, RDA risks delaying the implementation of AI-powered traffic optimization and compromising service efficiency.

4.3 Inter-operatability Gaps and Data Fragmentation

Interoperability gaps between Sri Lanka's transport agencies significantly hinder RDA's digital alignment, as the lack of a standardized governance framework and national BIM policy prevents seamless data sharing and coordinated project execution. Unlike global leaders like Singapore's LTA, which integrates multi-agency datasets for synchronized urban planning and transport management, RDA operates without a unified digital platform, limiting real-time analytics, automated approvals, and collaboration. Addressing these gaps requires establishing a centralized transport database, mandating BIM standards within RDA's workflows, and implementing AI-driven cross-agency mobility planning to enable predictive congestion management and infrastructure optimization. Without such standardization, RDA's transition to a fully digital transport authority remains constrained.

4.4 Bureaucratic Resistance to Digital Transformation

Bureaucratic inertia within Sri Lanka's public sector, particularly at RDA, impedes the adoption of AI-driven traffic management, blockchain project tracking, and cloud-based governance due to fears of job displacement, unfamiliarity with new technologies, and concerns over disrupting established policies. Unlike Singapore, which mandated cross-sector digital governance and replaced legacy systems with AI-powered monitoring, RDA remains reliant on manual processes that limit efficiency and innovation. Overcoming this resistance requires embedding digital governance in RDA's mandates, executive training on emerging technologies, and fully transitioning to cloud-based workflows to ensure meaningful transport modernization. Without such reforms, RDA's digital transformation will remain stalled**.**

4.5 Opportunities for AI Driven Traffic Management

Despite existing structural challenges, AI offers transformative potential for Sri Lanka's transport governance by enabling advanced urban congestion forecasting, vehicle flow optimization, and predictive maintenance. Drawing from global examples like Singapore, London, and Tokyo, AI-driven models can facilitate adaptive traffic signal control, real-time incident monitoring, and data-driven infrastructure planning. For RDA, integrating

AI could optimize Colombo's traffic light coordination, enhance predictive road maintenance through stress analysis, and streamline digital toll collection via automated vehicle classification, ultimately boosting transport efficiency and sustainability.

5 Strategic Road Map for Digital Implementation

This section presents a phased, policy-driven roadmap to guide the RDA's digital transformation, detailing infrastructure upgrades, AI integration, funding strategies, workforce development, and inter-agency coordination aligned with Sri Lanka's Digital Economy Blueprint.

5.1 Introduction to the Implementation Road Map

For the Road Development Authority (RDA) to successfully align with Sri Lanka's Digital Economy Blueprint, it must adopt a phased digital transformation strategy that ensures structured execution, financial sustainability, workforce adaptation, and interoperability standardization. A strategic roadmap provides a clear pathway toward modernizing RDA's operations, enhancing mobility governance, and embedding AI-driven, data-centric solutions within transport infrastructure management [2].

This section outlines a step-by-step action plan encompassing policy standardization, technological integration, funding diversification, skill development, and inter-agency collaboration to ensure a seamless transition into smart infrastructure management.

5.2 Phased Implementation Framework

Phase 1: Foundational IT Infrastructure Development (Year 1-2)

The first implementation phase should focus on building RDA's digital foundation by creating a centralized transport data platform for seamless inter-agency coordination, upgrading fiber optic networks across key offices and control units, adopting cloud-based mobility analytics for real-time traffic management, and deploying robust cybersecurity measures including AI-driven threat detection. This foundational upgrade will enable RDA to move away from paper-based processes toward secure, integrated, and resilient cloud-enabled governance systems.

Phase I1: AI Powered Traffic Optimization and ITS Expansion (Year 2-3)

After stabilizing the digital foundation, RDA should implement AI-driven transport analytics and Intelligent Transport Systems (ITS) by deploying adaptive traffic signal control for congestion reduction, automating toll collection with AI-based vehicle classification, utilizing predictive maintenance analytics for proactive road repairs, and launching ITS pilot projects featuring sensor-enabled intersections and machine learning mobility models. This phase will enable RDA to transition into an adaptive, real-time, AI-powered road governance system.

Phase I1I: E-Governance and Digital Transaction Expansion (Year 4-5)

Following ITS and AI integration, RDA should scale e-governance solutions by fully implementing GovPay for digital tolls and permit approvals, automating government contracting with AI-driven bid evaluations, digitizing urban transport governance through synchronized real-time dashboards with municipal councils, and expanding blockchain-based infrastructure tracking to secure transport records. This phase will establish comprehensive digital integration across Sri Lanka's transport governance, maximizing transparency and operational efficiency.

5.3 Funding Strategies for Digital Expansion

Sri Lanka's transport modernization requires a structured financial model leveraging diverse funding sources, including Public-Private Partnerships with AI and mobility tech firms, multi-lateral development grants from institutions like the World Bank, JICA, and KOICA, and dedicated national IT budget allocations within the annual transport expenditure. This approach will enable RDA to build a self-sustaining financial framework, ensuring continuous and scalable digital transformation.

5.4 Workforce Digital Literacy Initiatives

Successful digital transformation at RDA hinges on structured skill development programs that equip personnel to effectively manage ITS and AI-driven governance platforms. Key strategies include mandated AI certification for transport engineers, digital workflow training for administrative staff, and collaborative knowledge-sharing initiatives with the University of Moratuwa's ICT faculty. This will ensure RDA's workforce evolves into a digitally proficient team, capable of sustaining long-term infrastructure modernization objectives.

5.5 Inter-agency Collaborations and Policy Standardizations

To overcome interoperability gaps, Sri Lanka must implement standardized governance frameworks that enable seamless cross-sector integration within the transport sector. Key policies include adopting a National BIM Policy to harmonize infrastructure planning, enforcing ITS interoperability mandates across urban councils and expressway authorities, and institutionalizing AI-driven traffic governance standards under the Ministry of Transport and Highways. These measures will create a synchronized digital transport ecosystem, eliminating procedural inefficiencies and enhancing collaborative decision-making.

6 Future Directions and Policy Recommendations

The Road Development Authority (RDA) of Sri Lanka is at a critical stage in its journey toward full digital governance. While progress has been made, the integration of Artificial Intelligence (AI), Intelligent Transport Systems (ITS), Building Information Modeling (BIM), and e-governance platforms requires strategic focus to align with the nation's Digital Economy Blueprint. Sustainable digital transformation demands robust policy frameworks, financial sustainability, workforce capacity building, and technological standardization.

A key priority is establishing a National Transport Digitalization Policy to unify fragmented governance. This policy should mandate ITS adoption, AI-based congestion monitoring, BIM integration for consistent infrastructure design, and inter-agency data-sharing protocols to enhance cross-sector coordination. Institutionalizing AI in mobility governance is critical; AI-driven traffic signal optimization, predictive maintenance, and automated toll monitoring can significantly improve transport efficiency and infrastructure longevity.

To overcome inconsistent infrastructure planning, standardized BIM adoption must be enforced, defining digital modeling guidelines and asset tracking across RDA and municipal bodies. Financially, Sri Lanka needs to allocate dedicated budgets for transport digitization, expand donor-supported initiatives, and promote public-private partnerships to attract innovation investment. Collaborations with international agencies such as JICA, World Bank, and KOICA will provide vital multi-lateral funding to support scalable ITS and AI deployment.

Addressing the workforce skills gap is essential. Nationwide training programs for transport engineers and digital workflow workshops for administrative staff must be implemented, with strong partnerships between RDA and academic institutions like the University of Moratuwa. Furthermore, developing digital leadership among RDA executives will help overcome bureaucratic resistance and drive AI adoption.

Technological standardization will consolidate Sri Lanka's ITS ecosystem through a unified national traffic management framework, sensor-enabled intersections, and AI-based vehicle tracking. Expanding blockchain technology will enhance transparency and accountability by securing toll collections, digitizing procurement, and safeguarding infrastructure asset documentation.

In conclusion, the strategic roadmap outlined for RDA's digital transformation—spanning policy, funding, workforce, and technology—positions Sri Lanka's transport sector to emerge as a globally competitive smart mobility ecosystem. Successful implementation will drive economic growth, improve urban connectivity, and enhance service delivery through efficient, AI-powered governance.

References

1. Sri Lanka Ministry of Digital Economy: Digital Economy Blueprint, National framework for technology integration. Government of Sri Lanka, Colombo (2023).
2. Sri Lanka Road Development Authority: Strategic report on digital transformation, Challenges and implementation roadmap. RDA Technical Publication, Colombo (2024).
3. V. Weerakkody et al., Public sector resistance to IT innovation: Lessons from digital governance efforts. Inf. Syst. J. 26(4), pp. 319–340, (2016).
4. T. Janowski, Implementing digital governance: Institutional strategies and policy alignment. Public Adm. Rev. 76(5), pp. 912–928, (2016).
5. J. Gil-Garcia et al., Digital government transformation in developing nations: Challenges and strategies. Gov. Inf. Q. 35(3), pp. 402–417, (2018).
6. I. Mergel, The shift toward AI-powered urban mobility governance: Policy and practice insights. J. Urban Stud. 56(4), pp. 324–340, (2019).
7. K. Chen et al., Digital infrastructure management: The role of GIS and BIM in smart mobility. J. Smart Cities 12(4), pp. 245–260, (2020).
8. A. GhaffarianHoseini et al., Building Information Modeling (BIM) adoption: Lessons from global best practices. Autom. Constr. 72, pp. 215–230, (2017).
9. R. Fernando et al., AI-driven transport analytics: Case study of Sri Lanka's emerging digital initiatives. Proc. IEEE Int. Conf. on Intelligent Systems, 34(2), pp. 111–126, (2022).
10. T. Jayasinghe et al., Sri Lanka's e-governance evolution: Barriers and future directions. South Asian Policy Rev., 8(1), pp. 88–102, (2021).
11. J. Nograšek, M. Vintar, Understanding digital transformation in the public sector: Challenges and opportunities. Gov. Inf. Q., 31(1), pp,62–74, (2014).

Classifying Code Quality in Java-Based Open Source Software Projects Using Machine Learning Techniques and Contribution Analysis

H. T. Welagedara and W. V. S. K. Wasalthilaka

Faculty of Computing, Sabaragamuwa University of Sri Lanka, Sri Lanka.
hashiniwel@gmail.com

Abstract. Geographically dispersed volunteer teams can achieve collaborative and transparent processes with Open Source Software Development (OSSD). While it outperforms traditional methodologies, challenges remain in preserving code quality, managing third-party dependencies, leading to compatibility issues, and inconsistencies in developer contributions that can lead to code redundancies. Java as the foundation of software development, has fostered numerous open-source projects, enhancing research dependability. This research proposes a machine learning model that classifies code quality in Java-based open-source software projects by analyzing contribution metrics. Popular machine learning techniques used for software quality prediction, such as Regression, Decision Trees, Random Forest, Support Vector Machine and Bayesian Learning, XGBoost and Multi-Layer Perceptron are used, as well as established software quality metrics to measure the developer's contribution using source code such as Lines of Code (LOC), Coupling Between Objects (CBO), Response for a Class (RFC), etc. The proposed model was evaluated using a dataset, containing over 200,000 observations and software metrics extracted from open-source projects. Performance was measured using Precision, Accuracy, Recall and F1-Score. XGBoost shows the highest model accuracy, with 82%. The system was built using XGBoost, which allows developers and others to upload Java files. Based on the derived quality metrics, the system classifies the code quality into three categories: high, medium, and low. This analysis enhances Java OSSD projects by accurately evaluating code contributions, ensuring reliability and sustainability. Refining code review, prioritizing refactoring, and leveraging the best ML approach to classify code quality can strengthen development processes and advance OSSD efficiency.

Keywords: Code Contributions, Code Quality, Machine Learning, Open Source Software Development, Software Quality Metrics.

1 Introduction

1.1 Background

Modern software development follows Open-Source Software Development (OSSD) as the key framework for creating software through remote collaborative teams that defeat conventional methods with greater innovation and availability [1]. The model encourages global participation through community management and utilizes Java's cross-platform capabilities and large ecosystem features to impact Java-based projects, including Apache Hadoop, Spring Framework, and Eclipse, which offer strong research foundations due to widespread usage and large datasets on GitHub platforms [2]. The projects showcase OSSD's capabilities through Java's system features, while also presenting assessment requirements that require advanced quality evaluation approaches.

OSSD challenges code quality in Java-based development due to varying skill levels and contribution practices. Code redundancies arise from inconsistent contributions, increasing maintenance costs and reducing efficiency due to repeated functions [3].

An increase in machine learning techniques emerges as a solution to forecast and classify software quality because it delivers data-driven analysis of code metrics. The established software quality metrics Lines of Code (LOC), Coupling Between Objects (CBO), Response for a Class (RFC), Weighted Methods per Class (WMC), Lack of Cohesion in Methods (LCOM), Depth of Inheritance Tree (DIT) and Number of Children (NOC) provide numerical indicators to assess code complexity and maintainability and cohesion which helps identify quality issues [4]. While previous research, such as Meher and Mall [5] focused on bug classification in open-source repositories using machine learning, this research distinguishes itself by specifically addressing code quality classification in Java-based OSS projects using contribution metrics and quality thresholds with machine learning techniques unlike approaches based on Natural Language Processing (NLP) which requires another structured form of data, which can be obtained by converting the source code into a token stream using a programming language processor [6]. The code quality classification system uses precision and accuracy and recall and F1-score performance metrics to help developers conduct detailed code assessments and determine the best ML approach for process improvement in OSSD development [7]. The combination of machine learning metrics LOC and CBO, and DIT provides data-based code quality classification systems that use XGBoost to reach 82% accuracy levels according to this research. This research evaluates more than 200,000 observations to improve Java OSS quality assessment methods.

1.2 Purpose of the Research

Due to the distributed nature of Open-Source Software Development (OSS) projects, it is difficult to ensure consistent code quality because of heterogeneous contributors with different skills and coding styles. This leads to plural redundant code, dependency compatibility problems and technical debt, diminishing reliability and sustainability standards. Automated systematic quality assurance is lacking, which prevents meeting global development needs, and manual code reviews are infeasible for large-scale OSS projects.

Research Questions

The research discovers suitable software quality metrics for Java OSS projects' code quality assessment because developers with different skills and techniques contribute code. The development of an accurate classification system requires identifying metrics that effectively show quality issues in collaborative OSS environments.

Also, this research uses ML algorithms for code quality classification into high, medium and low categories based on metrics discovered. The diverse nature of Java OSS codebases makes traditional manual assessment methods insufficient for the task. The research examines how Decision Trees and Random Forest, and Support Vector Machines (SVM) algorithms use quality metrics to conduct automated classification through a data-driven method that scales for quality assurance needs.

The evaluation metrics for assessing the performance of the ML model in code quality classification need to be determined. The evaluation of multi-class classification models requires Accuracy alongside Precision and Recall along with F1-Score to determine model effectiveness. The evaluation metrics question ensures thorough assessment of the model performance which provides both reliability evidence and practical utility information for Java OSS developers to validate system capability in meeting study goals.

Research Objectives

The main goal involved developing an innovative ML-based model for automatic code quality classification of Java OSS projects to tackle irregular developer contributions and their effects on software reliability and sustainability. The model implemented specific software quality metrics including LOC and CBO and RFC and WMC and LCOM and DIT, and NOC, to create a systematic data-based quality assessment solution. The system development focused on building a practical solution which enables developers to submit Java files for automated quality assessment leading to better code review processes and improved refactoring prioritization, and enhanced Java OSS project quality for lasting success.

In addition to the main objective, the research aims to automate the classification of code quality by determining and confirming important software quality measures like Lines of Code (LOC), Coupling Between Objects (CBO), and Depth of Inheritance Tree (DIT). Second, it builds and trains a machine learning model based on these metrics, comparing algorithms like XGBoost, Random Forest, and SVM to determine code quality. Lastly, the model is thoroughly tested based on the typical metrics: Accuracy, Precision, Recall, and F1 Score, on a test set of 46,494 observations, which makes it applicable in a real-life OSS development.

2 Literature Review

The quality of code within Java-based open-source software projects stands as the essential factor to guarantee software reliability and maintainability in collaborative development environments. Java has gained popularity in OSS development because of its ability to operate across platforms and its large library collection which attracts projects such as Apache Hadoop and Eclipse [8]. OSS code quality becomes inconsistent because the project contains contributors at various skill levels while managing inconsistent coding practices [9].The object-oriented Java features improve modularity according to research findings but quality maintenance becomes harder to manage when these features remain uncontrolled especially during large projects with multiple contributors [10]. Java-based OSS code quality assessment depends on software quality metrics which measure object-oriented paradigms through Coupling Between Objects (CBO) and Depth of Inheritance Tree (DIT) and Lines of Code (LOC) [11]. The metrics serve to quantify attributes regarding complexity and maintainability which form a basis for quality assessment. Research indicates that elevated CBO values in Java projects lead to higher defect rates because they demonstrate how inter-class dependencies affect quality [12]. Saklani et al.'s [11] review demonstrates that these metrics when utilized with machine learning effectively predict quality issues in Java OSS contexts according to research findings.

The application of ML techniques to Java-based OSS quality prediction encounters difficulties in both interpretability and generalizability. The black-box nature of SVM and Neural Networks (NN) makes it difficult to understand quality outcomes despite their high predictive power according to Sheshasaayee and Jose [13].

The assessment of code quality in Java-based open-source software projects heavily depends on source code metrics which measure structural aspects that include complexity and maintainability [11]. Java codebases receive evaluation through three metrics CBO and DIT and LOC which help identify defect-proneness and other quality issues [12]. The

combination of these metrics with machine learning algorithms enhances OSS quality prediction accuracy according to S. Saklani et al. [11] as described in their IJARCS downloadable review. The object-oriented characteristics of Java make these interdependencies vital for determining quality.

A. Sheshasaayee and R. Jose [14] demonstrate that although Support Vector Machines (SVM) and Neural Networks (NN) deliver accurate predictions, they remain difficult to interpret for understanding quality predictions in open-source software contexts. The lack of transparency in these models creates issues for projects that prioritize explainable methods in Java development.

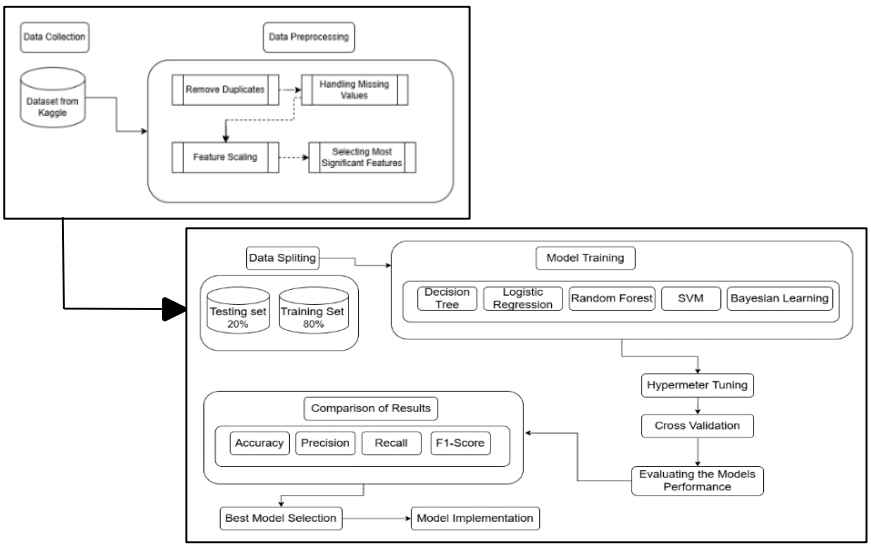

Fig. 1. Research Design

The combination of software quality metrics CBO and LOC and DIT with contribution-specific data creates important opportunities to enhance Java-based open-source software quality classification. Property-based software quality measures CBO and LOC gain improved ability for classifying OSS defects when used alongside developer variables such as contributor frequency and experience levels as proposed by S. Saklani et al. [11]. These

quality metrics enhance Java OSS quality classification precision by linking them to contributor activity according to the authors. The use of metrics that consider contribution levels provides better justification than analyzing code independently.

The literature review demonstrates that software quality metrics and machine learning techniques serve as essential tools for Java-based open-source project code quality evaluation through the use of CBO, DIT, and LOC metrics for structural analysis and Random Forest and Decision Trees algorithms for quality prediction.

2.1 Research Design

The research implemented a quantitative empirical method to create and test an ML-based system which classifies code quality into three levels of high, medium and low. The classification thresholds were defined based on the model's output probability: code quality is classified as Low if the probability is <0.5 and requires refactoring; Medium if the probability is <0.7 and may need refactoring; and High if the probability is >0.7 and does not require refactoring. The research method used software quality metrics extracted from Java source code to measure developer contributions (shown in Fig. 1).

The research implemented seven supervised ML algorithms, including Logistic Regression, Decision Trees, Random Forest, Support Vector Machine (SVM), Bayesian Learning, XGBoost and Multi-Layer Perceptron. The methodology integrated theoretical ML applications with practical OSSD needs to develop a system which enables developers to submit Java files for immediate quality assessment.

2.2 Data Collection and Data Preprocessing

The study utilized the Code Metrics Dataset for Software Project Structure available at Kaggle, which contains the OnlyTrivial_dt.csv file. A total of 232,468 entries compiled from 53 columns that offered various software quality metrics and a refactoring decision column extracted from multiple open-source Java projects. The refactoring decision column was used to derive the quality categories, serving as ground truth for model training and evaluation.

The data quality needed initial preprocessing steps to prepare it for analysis. Model training bias was prevented through duplicate entry removal since duplicated data points would skew the classification outcomes. The median value of each column served as the imputation method for handling missing values in numerical columns lcom*, tcc and lcc because it showed resilience to outliers in software metrics. The dataset maintained its integrity by dropping rows with many missing values, yet the data size slightly decreased

to preserve reliability. The cleaning process allowed the dataset to maintain a considerable number of observations (232,468), which provided adequate size and diversity to train and evaluate ML models effectively.

2.3 Feature Extraction

Feature selection was performed to enhance model performance and reduce computational complexity, focusing on the most predictive metrics for code quality classification. From the available metrics from the dataset, a subset was selected based on their relevance to quality assessment and prior studies. The chosen features include LOC, CBO, RFC, WMC, LCOM, DIT, and NOC as these metrics effectively capture complexity, coupling, cohesion, and inheritance patterns in Java code.

Correlation analysis was conducted to identify and exclude highly correlated features, minimizing redundancy (e.g., using Pearson correlation to check for multicollinearity among metrics like cbo and cboModified). The target variable was prepared for multi-class classification by encoding the high, medium, and low categories into numerical labels, ensuring compatibility with ML algorithms. This refined feature set and preprocessed target variable ensure that the ML models focus on the most informative attributes, improving classification accuracy and efficiency for the subsequent training phase.

2.4 ML Model Development

The machine learning (ML) model development phase trained seven supervised ML algorithms to identify code quality levels in Java-based open-source software (OSS) projects through high, medium, and low classifications. The following algorithms were selected based on their proven effectiveness in software quality prediction and multi-class classification tasks:

Logistic Regression models class probabilities by the logistic function. Decision Tree: Tree classification based on decision rules, and Random Forest: A combination of multiple trees for better accuracy. SVM uses an optimal hyperplane for class separation, and Bayesian Learning makes inferences based on Bayes' theorem. MLP is a multi-layer feedforward neural network for pattern recognition, and XGBoost is an efficient gradient boosting with regularization.

Hyperparameter tuning was performed for each model using GridSearchCV with 10-fold cross-validation to optimize performance. Key tuned parameters included: learning rate and max_depth for XGBoost; C and kernel for SVM; number of trees and depth for Random Forest; and solver and regularization for Logistic Regression and MLP.

The training set included 80% of the preprocessed data, totaling 185,974 observations, while the testing set contained 20% of the data with 46,494 observations through train_test_split from scikit-learn using random_state=42 for reproducibility. This data split provides a strong evaluation of model performance on new data and optimizes the amount of training data available for detecting patterns within software quality metrics.

The assessment of machine learning (ML) models constituted an essential process to evaluate their capability for classifying code quality as high, medium or low within Java-based open-source software (OSS) projects. The evaluation employed four standard metrics that include Accuracy, Precision, Recall and F1-Score to assess multi-class classification tasks. Each of the seven ML models was evaluated using the test set, and their performance scores were compared to identify the best algorithm. The evaluation process involved predicting the quality class for each test instance, followed by calculating the metrics for each model.

2.5 Model Implementation

The XGBoost model was integrated into an operational system for Java-based open-source software project code classification, achieving competitive Precision, Recall, and F1-Score values. The system, constructed using scikit-learn for the XGBoost model and pandas for data management, enables developers to upload Java files and extract software quality metrics. The extracted metrics are preprocessed using MinMaxScaler, and the trained XGBoost model generates quality class predictions, offering an automated, user-friendly assessment solution.

3 Results and Discussion

The seven ML models conducted evaluations on the test data through Accuracy and Precision and Recall and F1-Score metrics that operated within each quality classes. Fig. 2. presents the performance results.

Accuracy measures the proportion of correct predictions among the total predictions made. Precision represents the proportion of true positive predictions among all positive predictions. Recall measures the proportion of actual positives correctly identified, and the F1-Score provides the harmonic mean of Precision and Recall.

Model	Accuracy	Precision	Recall	F1-Score
Logistic Regression	0.68	0.661	0.672	0.666
Decision Trees	0.78	0.762	0.771	0.766
Random Forest	0.802	0.814	0.792	0.803
SVM	0.701	0.682	0.691	0.686
Bayesian Learning	0.62	0.601	0.612	0.606
MLP	0.75	0.741	0.732	0.736
XGBoost	0.82	0.832	0.811	0.821

Fig. 2 Comparison between Models

For understanding the XGBoost model's individual category performance, Table 1 shows the confusion matrix and the per-class evaluation metrics. It shows the disintegration of predicted values for the 46,494 samples in the testing set, divided into three quality classes. The steady results in every class confirm the equal efficiency of the model, ensuring that rigorous verification has been reached because the model does not favor any category.

The research developed an ML-powered system for Java-based open-source software project code quality assessment, addressing developer inconsistency issues. It established essential quality metrics like LOC, CBO, RFC, WMC, LCOM, DIT, and NOC, using seven supervised ML algorithms for classification and assigning categories as high, medium, and low.

Table 3. Confusion Matrix and Per-Class Performance for XGBoost

Predicted Class			
Actual Class	**Low**	**Medium**	**High**
Low	12800	1600	1098
Medium	1200	12650	1648
High	900	1923	12675
Per-Class Performance Metrics			
Class	Precision	Recall	F1-Score
Low	0.859	0.826	0.842
Medium	0.782	0.816	0.799
High	0.822	0.818	0.820

This research demonstrates the effectiveness of XGBoost as a machine learning technique for Java-based OSS project code quality classification. With an 82% accuracy rate, it effectively handles OSSD complexity due to contributor knowledge levels and quick

code modifications. The system's practical deployment confirms its value for Java OSSD applications by enabling Java file uploads from developers to generate automatic quality assessments (Fig. 3).

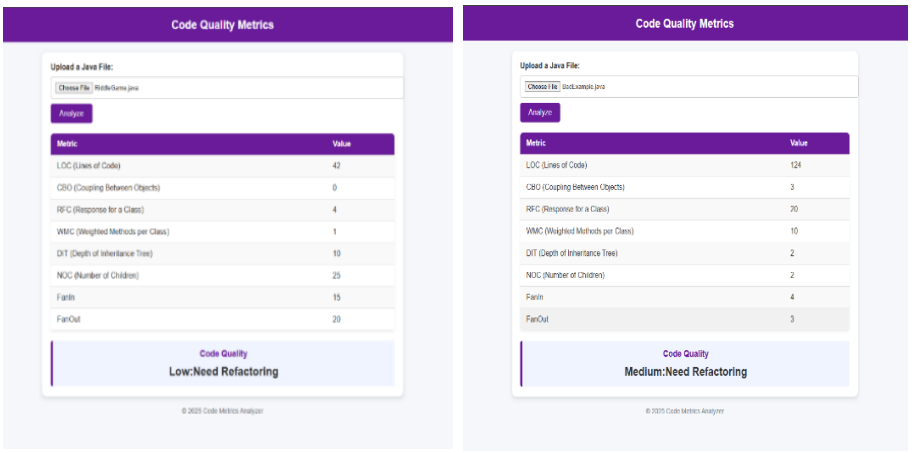

Fig. 3. System output examples for various java file uploads

3.1 Future Works

This research successfully created and deployed a code quality classification system for Java-based open-source software projects, yet several upcoming research areas would strengthen its impact. Advanced ML techniques should be investigated for future work to extend beyond Random Forest methods and neural networks, since potential research demonstrates that these may elevate classification precision above the current 82%. The methods could process complex non-linear patterns in software metrics, yet they should maintain interpretability, which XGBoost provided in this study. Expanding the system to incorporate Python and C++ programming languages would enhance its impact on the OSS ecosystem while filling the research gap for multi-language quality assessment tools.

4 Conclusions

The research developed an automated code quality classification system for Java-based open-source software projects using machine learning techniques. XGBoost outperformed other models with 82% accuracy in classifying code quality into high, medium, and low categories. The system uses seven software quality metrics to assess code quality based on structural characteristics and developer contributions. The study highlights the importance of combining contribution analysis with quality metrics to understand quality evolution in collaborative OSS contexts.

References

1. J. W. Castro Llanos and S. T. Acuña Castillo, Differences between traditional and open source development activities, Lecture Notes in Computer Science (including subseries Lecture Notes in Artificial Intelligence and Lecture Notes in Bioinformatics), 7343 LNCS, pp. 131–144, Jun. 2012, doi: 10.1007/978-3-642-31063-8_11.
2. S. Rusovan, M. Lawford, and D. L. Parnas, Open Source Software Development, Geographic information science & technology body of knowledge, pp. 107–122, Apr. 2021, doi: 10.7551/MITPRESS/5326.003.0011.
3. Compare B2B Software, Download, & Develop Open Source & Business Software - SourceForge. Accessed: Apr. 03, 2025. [Online]. Available: https://sourceforge.net/
4. S. Kaur and S. Singh, Improving the Quality of Open Source Software, Agile Software Development: Trends, Challenges and Applications, pp. 309–323, Jan. 2023, doi: 10.1002/9781119896838.CH16.
5. J. P. Meher and R. Mall, Machine Learning-based Software Bug Classification through Mining Open Source Repositories, Proceedings ICIT 2023 - 21st International Conference on Information Technology, pp. 17–22, 2023, doi: 10.1109/OCIT59427.2023.10431348.
6. H. P. Putro, U. L. Yuhana, E. M. Yuniarno, and M. H. Purnomo, Source Code Statement Classification using ANTLR and Random Forest, Proceedings of International Seminar on Intelligent Technology and Its Applications: Leveraging Intelligent Systems to Achieve Sustainable Development Goals, ISITIA 2023, pp. 60–65, 2023, doi: 10.1109/ISITIA59021.2023.10220999.
7. A. Khan, R. R. Mekuria, and R. Isaev, Applying Machine Learning Analysis for Software Quality Test, May 2023, doi: 10.1109/ICCQ57276.2023.10114664.
8. Cristina Gacek and Budi Arief, The Many Meanings of Open Source, 2004. [Online]. Available: www.opensource.org/docs/definition.

9. S. Haider, W. Khalil, A. S. Al-Shamayleh, A. Akhunzada, and A. Gani, Risk Factors and Practices for the Development of Open Source Software from Developers' Perspective, IEEE Access, 11, pp. 63333–63350, 2023, doi: 10.1109/ACCESS.2023.3267048.
10. Vinay Tiwari, Software Engineering Issues in Development Models of Open Source Software, 2, 2011.
11. S. Saklani, A. Kalia, S. Sood, and K. Kumari, Software Quality Prediction Using Machine Learning Techniques and Source Code Metrics: A Review, International Journal of Advanced Research in Computer Science, 13(6), 2022, doi: 10.26483/ijarcs.v13i6.6918.
12. V. Antinyan, M. Staron, and A. Sandberg, Evaluating code complexity triggers, use of complexity measures and the influence of code complexity on maintenance time, 22, pp. 3057–3087, 2017, doi: 10.1007/s10664-017-9508-2.
13. J. Cao, Z. Chen, J. Wu, S. Cheung, and C. Xu, JavaBench: A Benchmark of Object-Oriented Code Generation for Evaluating Large Language Models, Jun. 2024, [Online]. Available: http://arxiv.org/abs/2406.12902
14. A. Sheshasaayee and R. Jose, Prospects and Challenges of using Machine Learning Algorithms for Software Quality Assessment and Prediction, Int. J. Comput Appl, 129(7), pp. 33–35, Nov. 2015, doi: 10.5120/IJCA2015906887.

.

Climatrix: An IR-Based Embedded System for Smart Temperature–Controlled AC Automation

G. N. A. Fernando, M. W. B. S. Mawaththa, S. D. T. Rupasinghe, C. A. Hapuarachchi and S. D. Marasinghe*

Department of Electrical Engineering, Institute of Engineering Technology,
Temple Road, Katunayake
*sakunsinghe@gmail.com

Abstract. In the era of smart technology, energy efficiency and user comfort have become crucial in the domain of home and industrial automation. This project, titled "CLIMATRIX - A Smart IR-Based Universal AC Control System," presents an innovative solution that automates the operation of air conditioners (ACs) based on real-time temperature monitoring. CLIMATRIX uses a combination of sensors, infrared (IR) transmission, and embedded control logic to intelligently control AC power, fan speed, temperature, swing, and mode, minimizing manual intervention while optimizing energy consumption. The system continuously reads the ambient temperature through a DS18B20 digital sensor and compares it with a predefined setpoint. Based on this comparison, it generates appropriate IR signals to control various AC brands, functioning as a universal remote. The IR codes for different functions are brand-specific and are handled through software libraries, ensuring compatibility with popular models like LG, Samsung, Panasonic, and Mitsubishi.
The prototype was initially implemented using a 5V DC fan as a substitute for an actual AC unit, allowing the team to validate core functionalities such as IR signal transmission, temperature-based control logic, and feedback indication through LEDs. The final design is scalable and can transition seamlessly to control real AC units in household or industrial settings. CLIMATRIX bridges the gap between traditional remote-based control and modern smart automation by offering a low-cost, customizable, and efficient AC management system. This project showcases practical applications in embedded systems, IoT, and energy-conscious automation, offering significant potential for further development and real-world deployment.

Keywords: Smart Automation, Infrared Control, Energy Efficiency, Temperature Monitoring

1 Introduction

In today's rapidly evolving world, the demand for comfort, convenience, and energy efficiency in indoor environments has never been higher. Air conditioners (ACs) are an essential part of residential, commercial, and industrial buildings, especially in regions with warm climates. However, despite the wide adoption of AC systems, many conventional models still operate manually or with limited automation. These outdated systems are not energy-efficient and often require constant user interaction to maintain desired temperature conditions. In sensitive environments such as medicine storage rooms, laboratories, or server rooms, a lack of precise temperature control can lead to significant losses, including the degradation of pharmaceuticals or the malfunctioning of electronic equipment.

As the Internet of Things (IoT) gains traction, smart home technologies have introduced automated AC solutions. However, these systems are often expensive, brand-specific, dependent on cloud services or Wi-Fi connectivity, and not user-friendly for people who are unfamiliar with advanced technology. This poses a challenge to achieving widespread adoption of intelligent climate control in cost-sensitive or infrastructure-limited environments.

The CLIMATRIX project was conceptualized to bridge this technological and affordability gap. By leveraging the capabilities of the ESP32 microcontroller and integrating it with a temperature sensor, IR transmitter, and local control interface, CLIMATRIX aims to deliver a smart, universal, and standalone AC controller that ensures both user convenience and operational efficiency.

Fans are widely used in areas with moderate temperatures. Although the idea of Smart Homes has existed for decades, it has only recently started gaining global popularity [1]. One issue with traditional fans is that while their speed can be adjusted, it must be done manually. This means users have to physically walk to the fan and press a button to change its speed. Another common problem is that many users forget to switch the fan off after using it. They often leave the room without realizing it's still running, which leads to higher electricity bills and results in 5–10% of energy being wasted [2]. In some cases, leaving a fan on for too long can even pose a fire risk. Since the motor generates heat during extended use and the fan body is typically made of plastic, overheating can cause it to catch fire easily. Using a remote-controlled system offers a safer and more convenient solution, as it allows users to operate the fan without direct contact [5] [7]. To make any household appliance smart, a controller is required to act as its central processing unit or "brain" [2]. In this system, microcontrollers serve as the control unit, and Arduino is considered one of the most suitable and cost-effective options for prototype

development [3]. Smart appliances not only enhance user comfort but can also provide valuable support to the elderly and people with disabilities [4]. Energy wastage is a major contributor to environmental problems, accounting for about 25% of the factors causing the greenhouse effect [5]. To gain a better understanding of sensor technology, studies were conducted on the DHT22 and HC-SR04 modules.

When it comes to motion sensing, two types of sensors are commonly used. The first is the Passive Infrared (PIR) sensor, which detects movement by sensing changes in infrared radiation caused by objects passing through its detection zone. The second is the ultrasonic sensor, which emits high-frequency sound waves and measures the time it takes for the waves to reflect back from an object, such as a person or a wall, to calculate the distance. The main distinction between the two lies in how they detect presence. A PIR sensor only responds to motion, so if a person enters its field of view, it detects the movement. However, if the person remains still or falls asleep, the sensor no longer detects any activity and may assume the area is empty, causing connected devices like fans to turn off [7] [9] [10]. The ultrasonic sensor continuously measures distance, so it can detect the presence of a stationary object. This makes it more reliable in scenarios where constant presence needs to be monitored, even without movement. The ESP8266 NodeMCU was selected as the main controller for the system. Initially, two microcontrollers were considered: the Arduino UNO and the ESP8266. One of the key differences is that the Arduino UNO lacks built-in Wi-Fi functionality [6]and is almost twice the size of the ESP8266. The compact size of the NodeMCU made it the preferred choice, as it needed to fit within the limited space inside the fan's casing. Additionally, its smaller circuitry helps reduce power consumption. Wi-Fi connectivity was not essential for this phase of the project; future enhancements are planned to integrate Internet access. One minor drawback of the NodeMCU is that it uses a micro USB port to upload code, which is slightly less durable compared to the Arduino UNO's more robust Type-B USB port.

2 Problem Statement

The key problem identified is the lack of affordable, brand-independent, and easy-to-use AC automation systems. Traditional air conditioners require users to adjust settings manually, which is not only inconvenient but also leads to significant energy waste. Furthermore, users may forget to turn the AC off when it's not needed or leave it running under inappropriate temperature conditions, resulting in high electricity bills and reduced device lifespan. Existing smart solutions are not always feasible for the average user due to their

high cost, dependence on internet connectivity, complex installation procedures, or compatibility limitations. This gap creates a pressing need for a device that can intelligently control air conditioners without relying on external networks or third-party ecosystems.

3 Methodology

System Design

This section offers a detailed overview of the CLIMATRIX system design, emphasizing the hardware architecture, IR signal processing, user interface layout, as well as testing and troubleshooting procedures. All elements are carefully integrated to enable smooth and automated control of air conditioners using live temperature readings. The system analysis phase provided a strong foundation for developing a smart, intuitive, and versatile AC control solution. The design was centered on automation, multi-brand compatibility, ease of use, and cost-effectiveness. The integration of the ESP32 microcontroller, DS18B20 temperature sensor, and IR transmitter enabled intelligent control functionality, with the overall system architecture with PCB design illustrated in Fig. 1. Feedback from users was instrumental in refining the system, supporting the use of rapid prototyping. As a result, CLIMATRIX effectively addresses both functional and non-functional requirements, making it well-suited for modern, temperature-responsive applications.

Hardware Architecture

The hardware architecture of the CLIMATRIX device is designed to ensure efficient and accurate control of the air conditioning unit. The core components of the hardware architecture include the ESP32 microcontroller, DS18B20 temperature sensor, LCD, IR LED,

mechanical potentiometer for setpoint adjustment and LEDs for status indication. The technologies selected for CLIMATRIX were chosen based on their availability, performance, and suitability for offline automation:

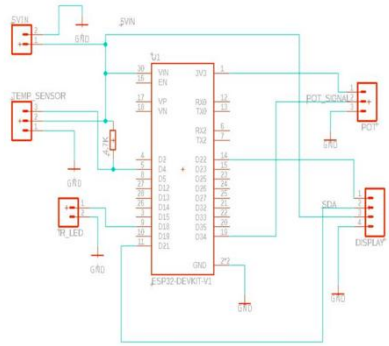

Fig. 1. Schematic of Climatrix Device

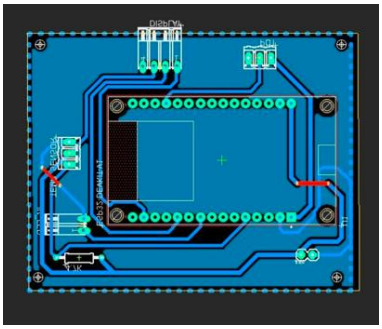

Fig. 2. PCB Design of Climatrix

The first step in preparing this circuit was to create the circuit using Proteus software. It is shown in the attached Fig. 1. The circuit was then converted to a PCB layout shown in Fig. 2. The PCB is printed and then the component is mounted. The components are listed below in Table 1. The output control circuit in this system controls all the electronic components. This process captures all the data captured by the sensors and provides outputs relevant to the conditions. Generally, two basic signal systems are used for analog and digital signal transmission in the electronic control circuit. Although it is somewhat difficult to control with analog signals, the accuracy of the analog signal system is more reliable than the digital signal-based control. So, for this system, an analog signal-based control system is used and the circuit is constructed using only a few simple electronic components.

Table 4. Components with Specification

Component	**Specification/Function**
ESP 32	Core microcontroller with Wi-Fi & Bluetooth capabilities (optional for future upgrades)
DS18B20 Sensor	Digital temperature sensor with ±0.5°C accuracy
IR Transmitter	Sends AC commands via encoded infrared pulses
LCD Display	Displays current and setpoint temperature
Potentiometer	Mechanical counter for adjusting target temperature
LED Indicators	Visual feedback for system states (ON/OFF)
Power Supply	5V regulated via USB or adapter

Fig. 3. ESP32 Microcontroller.

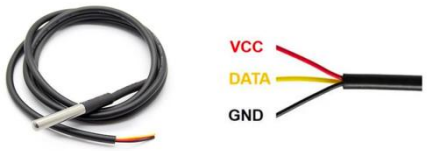

Fig. 4. DS18B20 Temperature Sensor

ESP32 in Fig. 3 is chosen for its processing power, Wi-Fi capabilities (for future expansions), and versatile I/O ports. It serves as the central unit that processes the temperature data, makes decisions based on the user's setpoint, and controls the AC through IR signals. DS18B20 is a digital temperature sensor with excellent accuracy and reliability shown in Fig. 4. It is used to continuously measure the ambient temperature in the room. The sensor communicates with the ESP32 using the One Wire protocol, providing temperature readings that are processed in real-time.

Fig. 5. 16*2 LCD Display.

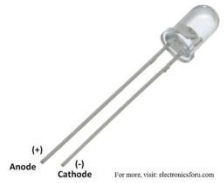

Fig. 6. IR LED

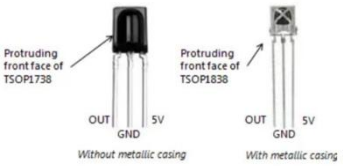

Fig. 7. IR Receiver

16x2 LCD shown in Fig. 5 with an I2C interface is a crucial user interface component in the Climatrix system, enabling clear and real-time visualization of key operational data. It can display two lines of 16 characters each, which is ideal for showing room temperature, setpoint values, system status, and IR signal feedback. The I2C (Inter-Integrated Circuit) module significantly simplifies wiring by reducing the number of control pins from 12 to just two (SDA and SCL), freeing up valuable I/O pins on the microcontroller. This serial communication protocol enhances scalability and allows multiple devices to communicate over the same bus. The backlit display ensures visibility in various lighting conditions, while the compact design integrates seamlessly into the enclosure. Overall, this display improves usability by providing immediate, readable feedback, making the system more intuitive for users.IR LED is used to send infrared signals to the AC units

shown in Fig. 6, Fig. 7, and Fig. 8. The ESP32 controls this LED to transmit commands like power on/off, temperature adjustments, fan speed control, and mode selection. The IR receiver is used to capture signals for testing and validation of commands.

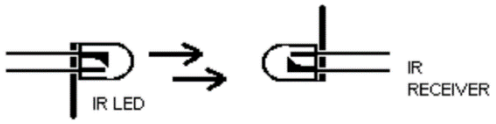

Fig. 8. IR LED transmits the signal and the IR LED receives the signal

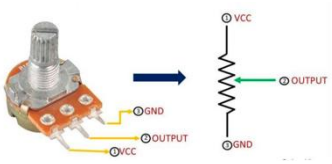

Fig. 9. Mechanical Potentiometer pinout.

Fig.10. LED Indicators

A potentiometer shown in Fig. 9 is used for adjusting the temperature setpoint. It acts as an analog interface, allowing the user to manually set the desired temperature. LED indicators shown in Fig. 10 play a crucial role in providing real-time visual feedback to users and improving the overall interactivity and usability of the Climatrix system. In this project, multiple LEDs are used for different purposes: a general-purpose signal LED and three separate LEDs to indicate the current fan speed (LOW, MEDIUM, HIGH). The signal LED briefly lights up whenever an IR signal is received, confirming communication between the transmitter and receiver. The speed indicator LEDs help the user understand the fan's operational status at a glance, lighting up according to the IR command interpreted by the system. This immediate visual confirmation ensures better monitoring and simplifies troubleshooting during testing. Their low power consumption, high visibility, and simplicity make LEDs ideal for status indication in embedded control systems like Climatrix.

User Interface Design

The user interface (UI) of the CLIMATRIX system is designed for simplicity and ease of use. The physical interface consists of a mechanical potentiometer for temperature set-

point adjustment, and the digital interface consists of the LCD and status LEDs. The potentiometer allows users to manually set the desired temperature shown in Fig. 11. It is connected to an analog pin on the ESP32, and its position is read to adjust the setpoint accordingly. This provides a tactile interface that is easy to use and adjust. The LCD continuously shows the current temperature, setpoint, and system status. It is an intuitive way for the user to understand how the system is performing at any given time. The display updates in real time, providing immediate feedback shown in Fig. 12.

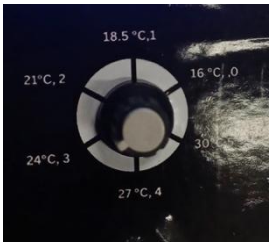

Fig. 11. Potentiometer

Fig. 12. LCD Display for Feedback

The green and red LEDs provide visual cues about the system's current state. This simple yet effective feedback mechanism ensures that users can quickly understand whether the AC is cooling or in standby mode.

4 Testing and Results

Testing and debugging are critical steps in ensuring that the CLIMATRIX device functions reliably and as expected. The system undergoes rigorous testing at each stage of development.

a. Unit testing

Each component (e.g., temperature sensor, IR LED, display) is tested individually to ensure it functions properly. This helps to identify and resolve any issues early in the development process.

b. System Integration Testing

Table 2. Temperature VS. Time variation according to the Climatrix device AC control.

Time (a.m.)	Temperature (C^{o})
9.00	30
9.05	27.5
9.07	25.5
9.10	23.8
9.13	23
9.17	23.4
9.20	22.9
9.23	23.6
9.25	23
9.29	23.5
9.32	22.9
9.36	23.6
9.38	23
9.42	23.5
9.44	23
9.48	23.6
9.51	23
9.55	23.5
9.57	22.8
10.01	23.6

Once all components are integrated, the entire system is tested to verify that the hardware and software interact as expected. The testing includes checking the temperature reading accuracy, the response to setpoint changes, and the correct transmission of the IR signal. When the device is checked for a 24,000 BTU/h AC in a 10 m × 8 m room with an input power of 2.3 kW was evaluated under manual control versus automation based on CLIMATRIX. In the manual scenario, the AC consumed 18.4 kWh and ran continuously for the entire 8 hours. Under CLIMATRIX control with a hysteresis band (23.0–23.5 °C) ±0.3°C accuracy, the AC operated for only about 65% of the time (approximately 5.2 hours out of 8) and consumed 11.96 kWh. The total consumption was 11.97 kWh, which included the ~0.0072 kWh overhead of the CLIMATRIX device. Below Table 2 shows the change in temperature over a 1-hour period, and Fig. 13 presents the corresponding graph plotted using the values from Table 2. Compared to manual operation,

this represented a savings of 6.44 kWh, or almost 35%. These findings demonstrated that CLIMATRIX significantly reduced unnecessary runtime while consuming less than 1 W of device power.

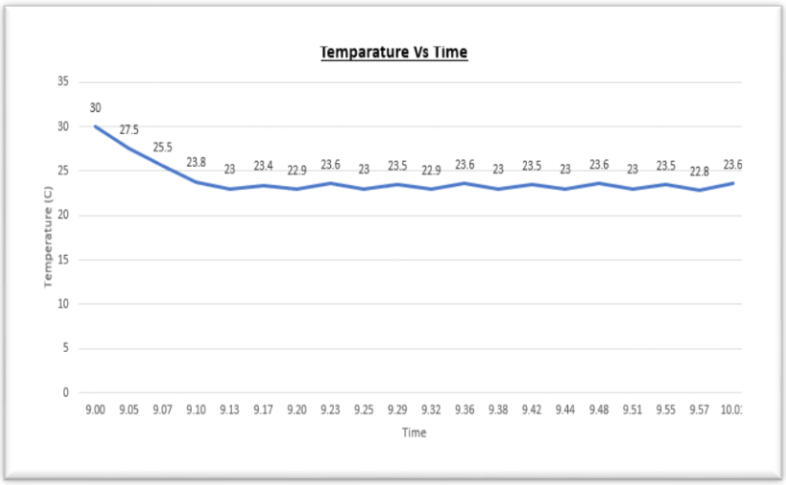

Fig.13. Temperature vs. Time Graph according to the Climatrix device AC control

Energy of the AC in Manual mode = 2.3kW*8h
=18.4kWh

When the AC was used with the CLIMATRIX device, it switched off when the temperature fell below the threshold level, and it started operating again when the temperature rose above the threshold level.

Energy of the AC after control with Climatrix device = 2.3kW*5.2h
= 11.96kWh

Over head of the Climatrix device = 0.0009kW*8h
= 0.0072kWh

Total power in Climatrix = 11.97 kWh

Energy Saved = 18.4kWh - 11.97kWh
= 6.43kWh

Percentage Saved (%) = (6.44/18.4) *100%
= 35%

System latency was evaluated by recording the instant the DS18B20 sensor detected the room temperature rising above the upper threshold (23.5 °C). The AC was configured with a setpoint of 23 °C, and the time taken for it to change states was measured using an indicator LED. The average delay over 25 iterations was 1 s ± 0.3 s, indicating that CLIMATRIX responded quickly and reliably.

To assess communication robustness, a total of 50 IR commands were transmitted from CLIMATRIX to the AC at 1 m, 3 m, and 5 m in both line-of-sight (LOS) and angled conditions. Command reception was verified through AC responses. Reliable operation was confirmed, with success rates of 100% at 1 m LOS, 97% at 3 m LOS, and 90% at 5 m LOS. Performance consistently exceeded 90%, though it declined slightly under occlusion.

A total of 25 IR commands were transmitted from CLIMATRIX to the AC, and within a range of 3 m and up to an angle of 40 degrees, all commands were transmitted successfully.

c. Remote Dashboard Interface

CLIMATRIX leverages ThingSpeak for cloud-based monitoring and control, shown in Fig. 14 and Fig. 15. The ESP32 transmits temperature data to ThingSpeak's servers using a dedicated API key, where it's visualized on a custom dashboard featuring real-time graphs and historical analysis. This integration enables remote system monitoring and control via both web and mobile interfaces, transforming the device into a complete IoT climate solution with secure, accessible functionality from anywhere with internet connectivity.

Fig.14. Remote Dashboard Interface

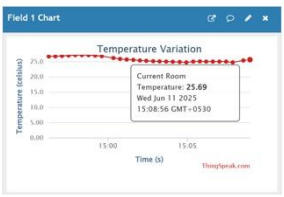

Fig.15. Temperature Variation

The CLIMATRIX system underwent rigorous testing to assess its performance in automating air conditioner (AC) control through real-time temperature monitoring. The results highlighted the system's effectiveness in meeting its primary goals of energy efficiency, enhanced user comfort, and broad device compatibility. The views of the Climatrix device are shown in Fig. 16.

Fig.16. Side View of the Climatrix Device

The DS18B20 temperature sensor provided accurate and consistent ambient temperature readings with a precision of ±0.5°C, making it ideal for environments that demand strict temperature regulation, such as medical storage and server rooms.

The system successfully transmitted IR signals to manage various AC functions, power, temperature settings, fan speed, and operational modes, and demonstrated compatibility with several leading AC brands, such as LG, Samsung, Panasonic, and Mitsubishi, confirming its universal control capability, as shown in Fig. 17. The ESP32 microcontroller efficiently processed temperature data and executed control logic to automatically adjust AC settings in response to setpoints, reducing the need for manual input and improving energy efficiency. The 16x2 LCD provided real-time feedback on current and target temperatures, while LED indicators and a potentiometer offered intuitive user interaction and visibility of system status, as shown in Fig. 18. Integration testing with a 5V DC fan used as a stand-in for an actual AC unit validated the system's operation in a test environment.

Fig. 17. Selecting the Brand Name

Fig. 18. Real-time feedback

The user manual for the CLIMATRIX system is shown in Fig. 19 and Fig. 20. A user manual is essential as it provides clear instructions on how to operate, maintain, and troubleshoot the system effectively. It helps users understand the key features and functionalities, ensuring they can make the most of the system while minimizing errors. A well-written manual enhances user experience and reduces the need for customer support.

Fig. 19. User Manual

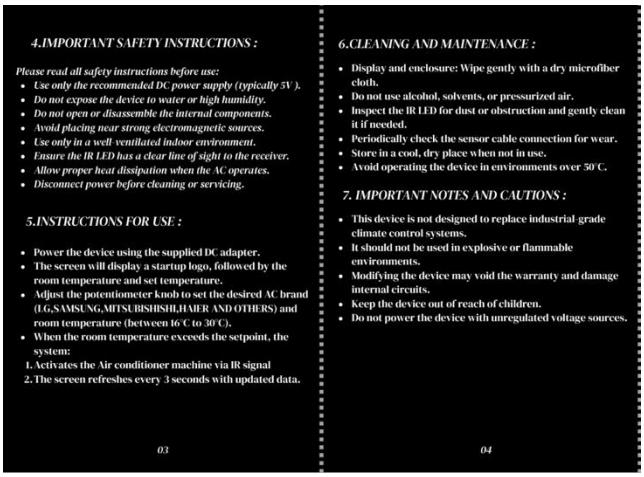

Fig. 20. User Manual

The modular architecture and use of standard components also support scalability for future use in both residential and industrial applications. By automating AC operations and limiting unnecessary runtime, the system demonstrated strong potential for energy con-

servation, aligning with its objective to reduce electricity consumption and support sustainable practices. The CLIMATRIX system proved to be a reliable, cost-effective, and intelligent solution, showing strong promise for real-world deployment and further development. The comparison of the existing system and Climatix is shown in Table 3.

Table 3. Comparison of the Solutions

Feature	**Manual AC with Remote**	**Smart AC Systems**	**CLIMATRIX**
Temperature Automation	×	√	√
Brand Compatibility	× (brand-specific)	× (usually fixed brand)	√ (multi-brand support)
Real-Time Temperature Display	×	√	√
Internet Dependency	×	√ (cloud-dependent)	× (offline operation)
Cost	Low	High	Low
Setup Complexity	Low	High	Low
Usability for the Elderly	Moderate	Low (app-based interfaces)	High (physical knob, LCD)
Remote-Free Operation	×	√	√
IR-Based Control	√	× (most use WiFi/IoT relays)	√

5 Discussion

The CLIMATRIX system introduces an innovative approach to automating air conditioner (AC) control by leveraging real-time temperature monitoring and infrared (IR) signal transmission. By integrating an ESP32 microcontroller, a DS18B20 temperature sensor, and an IR transmitter, the system offers a cost-effective, scalable, and energy-efficient solution for smart AC automation. The core functionality revolves around continuously measuring ambient temperature and comparing it with a user-defined setpoint, triggering appropriate IR commands to adjust cooling settings automatically. This eliminates the need for manual intervention, ensuring optimal comfort while minimizing energy

wastage. The ±0.5°C accuracy of the DS18B20 sensor makes the system reliable for environments requiring precise temperature regulation, such as medical storage facilities, laboratories, and server rooms.

One of the standout features of CLIMATRIX is its universal compatibility with multiple AC brands, including LG, Samsung, Panasonic, and Mitsubishi. By storing brand-specific IR codes, the system functions as a smart universal remote, eliminating the dependency on multiple controllers. This enhances user convenience and broadens the system's applicability across different households and commercial settings.

6 Conclusions

The CLIMATRIX—Smart IR-Based Universal AC Control System successfully demonstrates how embedded systems and automation technologies can be integrated to solve real-world problems in energy management and climate control. By intelligently monitoring ambient temperature and autonomously controlling AC operations through infrared signals, the system provides a smart, user-independent solution that enhances comfort, improves energy efficiency, and reduces manual dependency. The prototype phase, utilizing air conditioner, effectively validated the system's core functionalities including real-time temperature sensing, IR communication, signal-based control, and multi-level fan speed simulation. This approach allowed safe, low-cost testing while laying the foundation for full AC integration. CLIMATRIX is designed with scalability and compatibility in mind, offering support for multiple AC brands such as LG, Samsung, Panasonic, and Mitsubishi.

Its modular architecture makes it easily adaptable for future upgrades, including mobile control, Wi-Fi/Bluetooth integration, and cloud-based monitoring. As future upgrades enabling secure remote login through Wi-Fi to Climatrix would allow users to modify device settings and operating modes without direct physical access. Second, integrating a scheduling function would allow users to program time-bound control profiles (pre-cooling a room to a set temperature for a fixed duration before automatic shutdown). Such features would enhance usability, flexibility, and adoption in real-world.

In conclusion, the CLIMATRIX project achieves its objectives by delivering a reliable, efficient, and intelligent AC control solution. It stands as a testament to practical innovation in embedded technology and serves as a stepping stone toward advanced smart home and industrial automation systems. With further refinement and integration, CLIMATRIX holds strong potential for widespread adoption and impactful contributions to sustainable energy use.

References

1. L. Jiang, D. Y. Liu, B. Yang, Smart home research, Proc. of 2004 Int. Conf. on Machine Learning and Cybernetics, 2004.
2. C. Kaiwen, A. Kumar, N. Xavier, S. K. Panda, An intelligent home appliance control-based on WSN for smart buildings, IEEE International Conference on Sustainable Energy Technologies (ICSET), Hanoi, Vietnam, 2016.
3. M. R. Alam, M. B. I. Reaz, M. A. M. Ali, A Review of Smart Homes – Past, Present, and Future, IEEE Transactions on Systems Man and Cybernetics Part C (Applications and Reviews), 42(6), pp. 1190-1203, 2012.
4. B. Haobijam, Y. P. Huang, T. T. Lee, Using voice and gesture to control living space for the elderly people, International Conference on System Science and Engineering (ICSSE), Ho Chi Minh City, 2017.
5. M. G. Golzar, H. Tajozzakerin, A New Intelligent Remote Control System for Home Automation and Reduce Energy Consumption, Mathematical/Analytical Modelling and Computer Simulation (AMS), Fourth Asia International Conference, Kota Kinabalu, Malaysia, 2010.
6. L. Shkurti L., X. Bajrami, E. Canhasi, B. Limani, S. Krrabaj, A Hulaj, Development of ambient environmental monitoring system through wireless sensor network (WSN) using NodeMCU and WSN monitoring, 6th Mediterranean Conference on Embedded Computing (MECO), Bar, 2017.
7. B. Bos, L. Chmielewski, J. H. Hoepman, T. S. Nguyen, Remote Management and secure application development for pervasive home systems using JASON, Third International Workshop on Security, Privacy and Trust in Pervasive and Ubiquitous Computing (SecPerU), Istanbul, Turkey 19.07.2007.
8. Y. W. Bai, C. C. Cheng, Z. L. Xie, Use of a time-variation ultrasonic signal and PIR sensors to enhance the sensing reliability of an embedded surveillance system, 26th IEEE Canadian Conf. on Electrical and Computer Eng. (CCECE), Regina, SK, Canada, 2013.
9. Y. W. Bai, C. C. Cheng, Z. L. Xie, Use of ultrasonic signal coding and PIR sensors to enhance the sensing reliability of an embedded surveillance system, IEEE Int. Syst. Conf. (SysCon), Orlando, FL, USA, 2013.
10. Y. W. Bai, Z. H. Li, Z. L. Xie, Enhancement of the complement of an embedded surveillance system with PIR sensors and ultrasonic sensors, IEEE Int. Symp. on Consumer Electronics (ISCE 2010), Braunschweig, Germany, 2010.
11. T. Ishrat, M. A. Rahaman, A. Ahammad, Smart fan for human tracking, 9th Int. Forum on Strategic Technol. (IFOST), Cox's Bazar, Bangladesh, 2014.

3rd International Engineering Research Symposium 2025 (IERS 2025)
Colombo, Sri Lanka

Enhancing Software Quality through Comparative Analysis of Machine Learning Techniques for Test Case Prioritization using Object-Oriented Metrics

M. K. M. N. Kumari[1] and W. V. S. K. Wasalthilaka[2]

[1]Department of Computing and Information Systems, Faculty of Computing, Sabaragamuwa University of Sri Lanka, Sri Lanka.
[2]Department of Software Engineering, Faculty of Computing, Sabaragamuwa University of Sri Lanka, Sri Lanka.
nadeeshamayuri15@gmail.com

Abstract. Software quality plays an important role in software engineering. Quality software depends heavily on software testing. Regression testing is essential to this process and ensures that recent changes do not affect existing features. However, regression testing is often time-consuming and resource-intensive. Test Case Prioritization (TCP) techniques can be used to optimize the regression testing process. This research focuses on leveraging machine learning techniques to improve TCP using object-oriented metrics like Coupling Between Objects (CBO), Weighted Methods per Class (WMC), Depth of Inheritance Tree (DIT), Number of Children (NOC), Response for a Class (RFC), Lack of Cohesion of Methods (LCOM), fan-in, and fan-out. The dataset is divided into 70% of training and 30% of testing sets by using data preprocessing and feature selection methods. Then the trained models were evaluated using performance metrics such as accuracy, precision, recall, and f1-score. Different machine learning algorithms such as Decision Tree, Random Forest, Neural Networks, K-Nearest Neighbor (KNN), and Logistic Regression were compared using object-oriented metrics to identify the best approach. Among these algorithms, the decision tree algorithm outperformed other algorithms. Because of its ability to handle complex decision boundaries with minimal overfitting and achieved 71% accuracy. Finally developed the TCP framework using the Decision Tree algorithm. This framework automatically prioritizes test cases by code metric values to optimize testing efforts, detecting critical defects early while saving time and resources. This result highlighted their potential for greatly improving regression testing efficiency and software quality.

Keywords: Machine Learning, Object-Oriented Metrics, Software Quality, Test Case Prioritization

1 Introduction

1.1 Background

Software testing is an important process in the software development life cycle. Here, it is verified and validated that the software application is free from errors, meets the expected requirements, and efficiently and effectively satisfies the user's requirements. Effective testing increases the quality of the software and contributes to delivering high-quality software [1].

There are different types of software testing. Each of those software testing types has its own unique goals. Some of the main testing types are unit testing, integration testing, system testing, acceptance testing, regression testing, smoke testing, sanity testing, fuzz testing, black box testing, white box testing, grey box testing, etc. [2].

Among these available testing types, this research focuses on regression testing. It is an essential part of quality assurance in software to perform regression testing to make sure that the modifications made to the code haven't impacted already existing functionalities. In most cases, regression test suites increase with increased quality assurance tasks done or the program being improved. In such a way, the creation of more test cases will make a test suite effective. However, running a large test suite is expensive, and sometimes it runs for hours or days [3].

One of the most promising approaches to improving test case prioritization involves the use of object-oriented metrics integrated with machine learning techniques. Concepts in OOP, like encapsulation, inheritance, polymorphism, and abstraction, are meant to enhance the modularity and maintainability of the code; however, they add additional levels of complexity that might further deteriorate the quality of software [4].

Object-oriented metrics inform about the structural quality of software. Coupling Between Objects (CBO), Response for a Class (RFC), Weighted Methods Per Class (WMC), Depth of Inheritance Tree (DIT), Number of Children (NOC), and Lack of Cohesion of Methods (LCOM), etc., are some of the measures used in estimating complexity, maintainability, and probably fault-prone areas for different software modules [5].

This research aims to improve the quality, maintainability, and reusability of software by finding bugs, ambiguities, and bad smells using machine learning techniques. Various methods of software defect prediction are applied for the prediction of software defects using statistical techniques. However, machine learning techniques have an important role in software bug detection [6]. ML algorithms provide very powerful tools for the analysis of historical data and for making predictions [7]. It can analyze the trend of historical test data to predict the error-prone nature of code modules in software testing using machine

learning. These predictive capabilities are then used to schedule test cases that are more likely to catch errors, hence increasing the efficiency of testing.

This research focuses on integrating object-oriented metrics such as CBO, WMC, DIT, NOC, RFC, LCOM, FIN, and FOUT with different machine learning techniques like Decision Tree, Random Forest, Neural Networks, K-Nearest Neighbor (KNN), and Logistic Regression into test case prioritization. Decision Tree makes simple hierarchical rules (critical parameter: max_depth), and Random Forest votes from multiple trees (n_estimators). Neural Networks learn nonlinear relationships (hidden layers, activation functions), KNN classifies objects based on similarity (k value, distance metric), and Logistic Regression builds a linear probabilistic model (regularization parameter C). [6], [7]. Using these metrics as ML features enables ranking test cases by criticality, improving regression testing efficiency, especially in CI/CD environments.

This research proposes a test case prioritization framework using the best-performing machine learning algorithm. This framework automatically prioritizes test cases by code metric values to optimize testing efforts, detecting critical defects early while saving time and resources. This result highlighted their potential for greatly improving regression testing efficiency and software quality.

1.2 Problem Statement and Research Objectives

Regression testing is very important to maintain software quality in software development. However, software companies struggle due to complex code and frequent changes. This makes it hard to identify and prioritize test cases effectively, leading to missed defects, lower software quality, higher maintenance costs, and delayed product releases.

Indeed, traditional test case prioritization methods such as coverage-based, history-based, and risk-based fail to effectively address the complexities of object-oriented software design. Therefore, they are not able to detect and prioritize test cases with a high likelihood of revealing critical faults early in the testing process. This leads to lengthy testing cycles, undetected defects, decreased software quality, and higher maintenance and delayed release expenses.

This research addresses the need for an improved approach to test case prioritization that stimulates machine learning to improve the efficiency and effectiveness of regression testing using an object-oriented matrix. To meet the problem statement, the research questions that have been formulated are as follows.

The main objective of this research is to develop an ML-driven framework for automated TCP by identifying influential OO metrics and optimizing regression testing efficiency. The sub-objectives of this research are to compare and evaluate the performance of five machine-learning algorithms for TCP, investigate the correlation between object-

oriented metrics and test case failure probability, and formulate, design, and implement a fully automated test case prioritization framework with the best-performing machine learning algorithm.

1.3 Significance of the Study

Regression testing is critical to software quality but generally ineffective due to poorly prioritized test cases. While there are traditional Test Case Prioritization (TCP) practices, they fail because of the complexity of modern software [8]. This research introduces a machine learning (ML) approach with object-oriented metrics to revolutionize TCP by addressing the following critical gaps in TCP.

- Prior research focuses on single ML models with no rigorous comparison. This study compared five algorithms, namely, the decision tree, random forest, neural networks, K-nearest neighbor (KNN), and logistic regression, to find the best for TCP.
- Previous work utilizes raw object-oriented metrics without considering interactions. In this research, derived features are suggested to achieve improved prediction accuracy.
- Existing ML-based TCP solutions are primarily in the form of experimental prototypes or conceptual designs. This work bridges theory and practice with the development of an operational framework that is specifically designed to be easily integrated into today's development practices.
- Existing research is on small datasets (<10K test cases). This framework is verified on 232K+ test cases on different OO projects.

2 Literature Review

Software testing is a very important process in the software development life cycle. It depends on the ability to detect errors early in the software development life cycle. Early detection of defects can greatly reduce costs and improve software quality. There are different types of software testing. Each of those software testing types has its own unique goals. This research focuses on regression testing.

V. Garousi and J. Zhi [1] analyzed that regression testing is a critical part of software engineering. It ensures that new code changes do not affect existing functionality. However, they showed that regression testing is often time-consuming and resource-intensive. S. Elbaum et al. [9] conducted a study for Test Case Prioritization (TCP) techniques can be used to optimize the regression testing process so that the most important test cases can

be selected and executed first, the testing time can be reduced, and resource usage can be optimized.

Z. Li, M. Harman and R. M. Hierons [9] explored the traditional TCP methods, such as coverage-based and history-based methods. They found that these methods are insufficient to handle the complexity of modern object-oriented systems. Rongqi Pan et al. [10] highlighted that recent advances in Machine Learning (ML) offer encouraging solutions by leveraging object-oriented metrics (Ex: CBO, WMC) to predict high-risk test cases.

M. Z. Khan [11] evaluated that Machine learning algorithms have been very promising in TCP because they learn from labeled test execution data to forecast test case priority. They showed that Decision Trees (DT) have been very popular among supervised learning methods due to interpretability, where the cause of prioritization can be interpreted by testers in comprehensible decision rules. Also, they discussed that Random Forest (RF) algorithms utilize a set of decision trees, achieving high accuracy at the expense of increased computational complexity. O. F. Arar and K. Ayan [12] discussed that Neural networks (NN) have been able to model nonlinear relationships and interaction effects between test case features. R. Malhotra and R. Raje [6] discussed that Logistic Regression (LR) offers a probabilistic model which works well when priorities and test features relationships are linear. Also, they introduced that the K-Nearest Neighbors (KNN) gives priority to the test cases according to their resemblance to the already labeled examples and is a simple though frequently effective method.

Prykhodko et al. [13] showed that higher CBO values are associated with 30-40% more faults in Java programs. M. Khatibsyarbini et al. [14] showed that Weighted Methods per Class (WMC), computes method complexity in a class by adding cyclomatic complexity, with larger values of WMC consistently correlated with larger defect rates. Also, they showed that Response for a Class (RFC), which provides the number of possible methods calls, helps to identify classes with complex interaction patterns frequently requiring extensive testing. These metrics have gained such popularity that they are now part of most static analysis tools, for example, Eclipse Metrics and SonarQube.

The evolution of TCP techniques has been critically analyzed in this study, finding developments from traditional coverage-based methods to recent machine learning-based approaches incorporating object-oriented metrics. Although ML-based approaches demonstrate better fault detection, significant gaps still exist. Such constraints underscore the need for detailed empirical evaluation and applicable models that span theoretical research and industry practice. This research endeavors to address this through its juxtaposition of machine learning methods, extended feature engineering, and continuous implementation against large test scenarios.

3 Methodology

The proposed approach consists of several steps as follows.

1. **Data collection** - The dataset was obtained from Kaggle under the "Code Metrics Dataset for Software Project Structure." It contains object-oriented code metrics and corresponding test execution data collected from multiple open-source Java projects, totaling 232,468 instances with 53 features, which were used for training and testing.
2. **Data preprocessing** - The dataset was preprocessed through duplicate removal and handling missing values (median imputation). To resolve class imbalance, SMOTE was applied. The features were normalized through Min-Max scaling, and highly correlated metrics were reduced through feature selection (RFE and correlation analysis). A few interaction features (e.g., CBO × WMC) were also created for improving predictability.

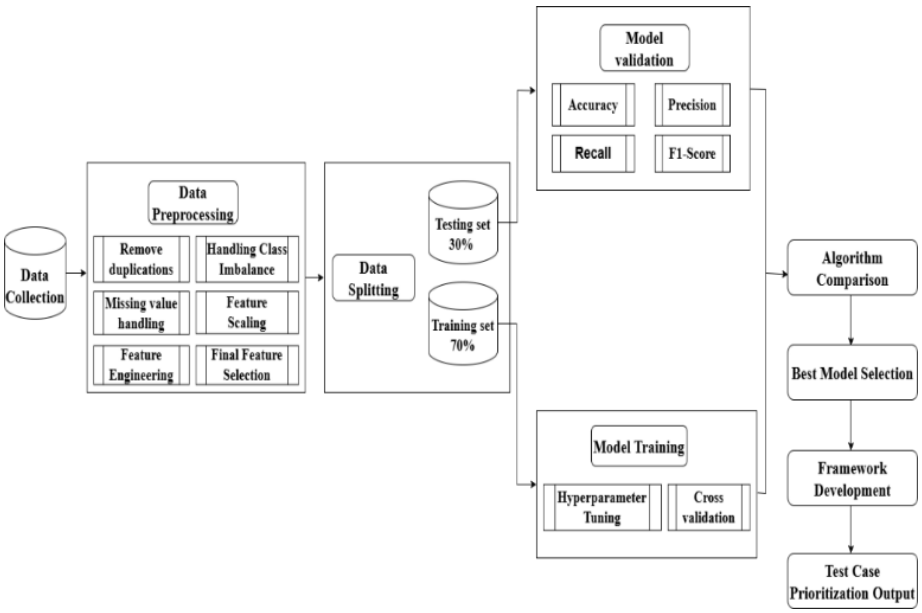

Fig. 1. Research Methodology

3. **Data splitting** - The preprocessed data were split into 70% training and 30% test sets, enabling robust model evaluation.

4. **Model training -** Five machine learning algorithms, such as Decision Tree, Random Forest, Neural Networks, K-Nearest Neighbor (KNN), and Logistic Regression, were trained in this research using the training dataset. Hyperparameter optimization (via grid search) and 5-fold cross-validation were performed to ensure generalization. The models were then evaluated using standard performance metrics (accuracy, precision, recall, F1-score) computed with scikit-learn evaluation functions.
5. **Model evaluation -** Then the trained models were evaluated using performance metrics such as accuracy, precision, recall, and F1-score [15].
6. **Algorithm comparison -** Each model is compared using the evaluated results to get the best-performing model. Among them, the Decision Tree outperforms the other models.
7. **TCP framework development -** Finally, using the best-performing machine learning algorithm (decision tree), developed the TCP framework. This framework automatically prioritizes test cases by code metric values to optimize testing efforts, detecting critical defects early while saving time and resources.

4 Results and Findings

4.1 Performance Comparison of Machine Learning Algorithms

To identify the best machine learning approach for Test Case Prioritization (TCP), the study carried out an extensive comparative analysis of five prominent supervised learning algorithms. They were tested for four key classification measures: accuracy, precision, recall, and F1-score to thoroughly understand their performance in test case prioritization. The comparative results are provided in Table 1 and also plotted graphically in Fig. 2.

Table 1. Performance metrics of machine learning algorithms.

Algorithm	Accuracy (%)	Precision (%)	Recall (%)	F1-Score (%)
Decision Tree	71.55	69.42	80.11	74.38
Random Forest	64.21	66.09	58.51	62.07
Neural Networks	61.42	59.98	68.86	64.11
K-Nearest Neighbors	62.94	61.94	67.31	64.51
Logistic Regression	51.81	51.39	68.66	58.78

A one-way ANOVA test indicated that the Decision Tree's superior performance was statistically significant compared to other models ($p < 0.05$). To enhance clarity, Table 1 results were also visualized in a bar chart (Fig. 2).

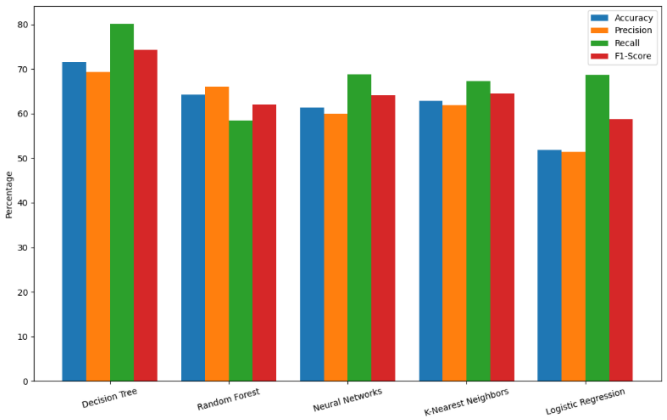

Fig. 2. Comparative performance of ML algorithms (graphical representation of Table 1)

Decision Tree performed the highest accuracy with 71.55%, significantly outperforming other approaches. Also, it reflects its competence in managing non-linear relationships among object-oriented metrics and test case priority. The Random Forest model was ranked close but with lower recall, which suggests a sensitivity vs. precision trade-off. Neural Networks and KNN were both ranked as medium performers. Neural Networks underperformed due to overfitting on the imbalanced data, while Logistic Regression underperformed due to non-linear feature interactions inherent in object-oriented metrics. These results affirm that Decision Trees are most appropriate for TCP because they are interpretable and demonstrate well-balanced performance.

4.2 Correlation Analysis of Object-Oriented Metrics

The study analyzed the predictive power of eight object-oriented metrics, including CBO, WMC, DIT, NOC, RFC, LCOM, fan-in, and fan-out.

Feature importance rankings

As shown in Fig. 3, fan-in and WMC emerged as the most influential metrics for predicting test case priority, followed by fan-out and DIT. The metrics of CBO and NOC demonstrated moderate importance levels. The analysis revealed that RFC, together with LCOM, exhibited minimal impact on test case criticality rates.

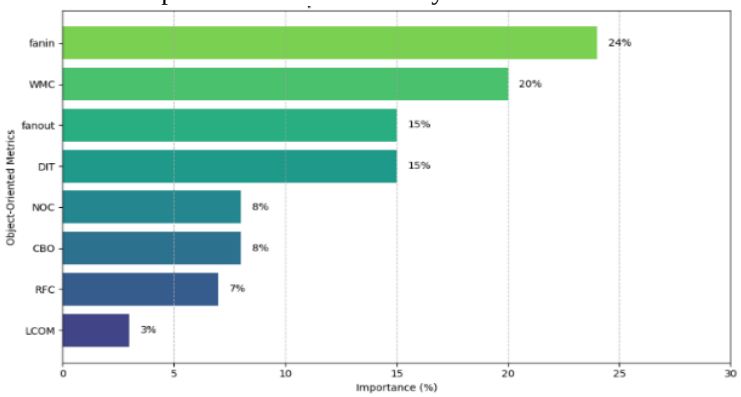

Fig. 3. Feature importance of OO metrics for test case prioritization

Correlation Heatmap Analysis

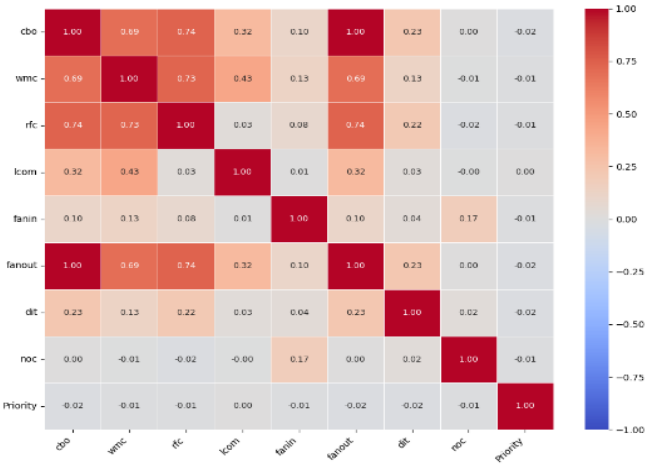

Fig. 4. Correlation heatmap of OO metrics

Fig. 4 illustrates the correlation heatmap, where fan-out and CBO are perfectly correlated (1.00), while RFC shows strong correlation with both CBO and WMC. Inheritance metrics (DIT and NOC) have very few correlations with the other metrics, and LCOM is fairly isolated, with only moderate correlation with WMC (0.43).

4.3 Framework Validation Using APFD

The efficiency of the framework was validated by both quantitative APFD scores and qualitative interface inspection. The employed system provides:

- **User Interface Layer:** Interactive web-based interface for both single test case analysis and batch processing. It includes input boxes for the major object-oriented metrics, a file upload option for batch processing (CSV format), and visualization of the decision process.
- **Machine Learning Core:** The model was trained on 232,468 test cases with object-oriented 33 metrics. The model produces probability scores (0-1) that numerically quantify the priority of each test case, allowing for effective high/low priority distinction for regression testing optimization.
- **Decision Visualization:** The framework supports interactive decision tree visualization, and the users can navigate 1-5 levels deep.

According to the APFD computation the 88% of errors emerge early during test suite execution. This demonstrates that the framework can optimally execute tests for earlier fault detection during testing [16]. For example, in a Java project module having high WMC and fan-in values, the framework prioritized critical test cases that detected three major defects early in the iterations, which reduced debugging effort.

5 Discussion and Conclusions

This study bridges the practice-theory gap between the needs of software testing and machine learning theory and presents a practical contribution within the field of Test Case Prioritization (TCP). Through a comparative analysis on a large scale of five mature machine learning algorithms, such as Decision Tree, Random Forest, Neural Networks, K-Nearest Neighbors, and Logistic Regression, the study identifies Decision Trees as the most appropriate model for ranking test cases in object-oriented software systems. It performed better with 71.55% accuracy.

One of the greatest contributions of this study is demonstrating how interaction terms among object-oriented metrics (Ex: CBO × WMC, DIT × RFC) can greatly improve the

predictive power of machine learning models. These results provide a new direction for feature engineering for test optimization research and practice.

The framework obtained a high APFD of 0.88, which further confirms its efficiency at detecting faults earlier during the test process. The metric provides a reproducible baseline and adds a solid empirical component to future studies on regression test optimization. As validated in Section 4.3 with APFD score (0.88), this provides strong empirical evidence for early defect detection.

In conclusion, this study proposes a scalable and effective ML-based TCP method that extends the frontier of software quality assurance theory and practice. By applying machine learning and feature engineering, it enhances the effectiveness of regression testing and provides a basis for its future use in CI/CD and agile environments.

References

1. V. Garousi and J. Zhi, A survey of software testing practices in Canada, *Journal of Systems and Software*, 86(5), pp. 1354–1376, 2013, doi: 10.1016/j.jss.2012.12.051.
2. I. Hooda, R. Scholar, and R. Singh Chhillar, "Software Test Process, Testing Types and Techniques," 2015.
3. D. K. Yadav and S. Dutta, "Regression test case selection and prioritization for object oriented software," *Microsystem Technologies*, vol. 26, no. 5, pp. 1463–1477, May 2020, doi: 10.1007/s00542-019-04679-7.
4. R. A. Khan, K. Mustafa, and S. I. Ahson, "An Empirical Validation of Object Oriented Design Quality Metrics," *Journal of King Saud University - Computer and Information Sciences*, vol. 19, pp. 1–16, 2007, doi: 10.1016/s1319-1578(07)80001-2.
5. Josiane. Mothe, L. Hoang. Son, and T. Q. Vinh. Nguyen, *Proceedings of 2019 11th International Conference On Knowledge And Systems Engineering : KSE 2019 : October 24-26, 2019, Da Nang, Vietnam*. IEEE, 2019.
6. R. Malhotra and R. Raje, "An Empirical Comparison of Machine Learning Techniques for Software Defect Prediction," 2014. [Online]. Available: http://gromit.iiar.pwr.wroc.pl/p_inf/ckjm/metric.html
7. Y. Zhao, D. Hao, and L. Zhang, "Revisiting Machine Learning based Test Case Prioritization for Continuous Integration," Nov. 2023, [Online]. Available: http://arxiv.org/abs/2311.13413
8. R. Pan, M. Bagherzadeh, T. A. Ghaleb, and L. Briand, "Test Case Selection and Prioritization Using Machine Learning: A Systematic Literature Review," Oct. 2021, doi: 10.1007/s10664-021-10066-6.
9. Z. Li, M. Harman, and R. M. Hierons, "Search Algorithms for Regression Test Case Prioritization."

10. Rongqi Pan, Mojtaba Bagherzadeh, Taher A. Ghaleb, and Lionel Briand, “Test Case Selection and Prioritization Using Machine Learning: A Systematic Literature Review,” 2021.
11. R. Kizito, P. Scruggs, X. Li, R. Kress, M. Devinney, and T. Berg, “The Application of Random Forest to Predictive Maintenance,” 2018.
12. Ö. F. Arar and K. Ayan, “Software defect prediction using cost-sensitive neural network,” *Applied Soft Computing Journal*, vol. 33, pp. 263–277, Apr. 2015, doi: 10.1016/j.asoc.2015.04.045.
13. S. B. Prykhodko, K. S. Prykhodko, and T. G. Smykodub, “A statistical estimation of the coupling between objectmetric for open-source appsdeveloped in Java,” *Herald of Advanced Information Technology*, vol. 5, no. 3, pp. 175–184, Nov. 2022, doi: 10.15276/hait.05.2022.13.
14. M. Khatibsyarbini, M. A. Isa, D. N. A. Jawawi, and R. Tumeng, “Test case prioritization approaches in regression testing: A systematic literature review,” Jan. 01, 2018, *Elsevier B.V.* doi: 10.1016/j.infsof.2017.08.014.
15. A. Salvadorrgarcíaa, M. R. Pratii, and B. Franciscooherrera, “Learning from Imbalanced Data Sets.”
16. H. Do and G. Rothermel, “A controlled experiment assessing test case prioritization techniques via mutation faults,” in *IEEE International Conference on Software Maintenance, ICSM*, 2005, pp. 411–420. doi: 10.1109/ICSM.2005.9.

Patient Acceptance of Healthcare Digitalization Through an AI Chatbot: System Usability and Patient Satisfaction

M. M. R. A. P. B. Mapa[1], M. T. D. Lakshan[1], W. M. P. A. Gunasena[2], R. G. L. Dayawansha[2], T. G. S. Nuwan[2], V. Abeysuriya[3], T. N. H. Witharana[1], A. V. K. N. Dinithi[1], L. G. Chandrasena[1]

[1]Nawaloka Hospitals Research and Education Foundation, Colombo
[2]Department of IT, Nawaloka Hospitals PLC., Colombo
[3]Institute of Biochemistry, Molecular Biology and Biotechnology, University of Colombo, Sri Lanka.
akilapbm@gmail.com

Abstract. AI chatbots in healthcare represent a significant advancement that enhances service delivery while reducing workload for healthcare professionals. Yet empirical research in low- and middle-income countries remains limited. This study evaluated patient satisfaction and usability of the NH Smart Health Assistant, a specialist referral chatbot developed inhouse and deployed at Nawaloka Hospitals, Sri Lanka. To evaluate patient satisfaction and usability of the chatbot and to explore the relationship between these two constructs, a cross-sectional survey of 400 outpatients assessed demographics, usability (UMUX-Lite), satisfaction, confidence in recommendations, and privacy concerns. Chi-square tests, correlations, and regressions identified predictors of satisfaction, reuse intent, and usability. The study revealed high overall satisfaction (85.5%) and strong intent to reuse (90.25%). Mean usability score was 82.0(±16.2). We identified data privacy(OR=3.14) and confidence in chatbot's recommendations (OR=1.96) as the strongest predictors of satisfaction. Intention to reuse was positively associated with higher education, prior chatbot use, ease of use, and data privacy (OR 4.1, 4.0, 7.4, 2.9). Viewing data privacy as secure boosted UMUX-Lite by ~18 points, while being educated up to A/L added 11 more (all $p < 0.05$). We demonstrated that healthcare chatbots achieve high user satisfaction. Successful integration depends on building user trust rather than demographics or prior experience of chatbots. Multilingualism, voice interaction support, and data transparency are recommended to sustain engagement when scaling AI nationally. Future research should broaden demographic sampling beyond urban populations to inform generalization strategies.

Keywords: Healthcare Chatbot, System Usability, Patient Satisfaction.

1 Introduction

Artificial Intelligence represents a transformative force in contemporary healthcare, fundamentally altering service delivery and patient interaction through AI-driven chatbots powered by Natural Language Processing and Machine Learning algorithms. These conversational agents function as automated digital assistants that engage with users, provide information, assist in preliminary symptom evaluation, and facilitate navigation through healthcare systems, including guidance towards appropriate specialist referrals. Healthcare chatbots primarily serve two main functions: facilitating remote health services including patient support, education, behavior modification, care coordination, and providing administrative support for healthcare providers [1, 2].

Given the rapid rise and integration of artificial intelligence in healthcare, evidence suggests these technologies contribute to improved patient experience metrics by reducing wait times for basic information, providing 24/7 availability, reducing hospital congestion, minimizing non-essential outpatient visits, reducing hospital readmissions, improving patient engagement, and streamlining pathways to specialized care [3]. By automating responses to common queries and handling large amounts of data, chatbots alleviate workload pressures on healthcare personnel, allowing them to dedicate more time to complex clinical tasks [3].

The successful integration of AI chatbots into routine healthcare practice depends critically on user acceptance, which is significantly influenced by perceived usability and patient satisfaction. Research emphasizes the importance of intuitive interaction design, perceived accuracy and reliability of information, user trust in the technology, adaptability for diverse demographics, and robust privacy and security assurances for sensitive health data [3–6]. Prior studies also emphasize that usability and satisfaction are moderately interrelated but context-dependent [4,5], warranting localized investigation. Studies demonstrate that response time, language complexity, conversational capabilities, emotional intelligence, persona presentation, and alignment with user experience principles all contribute significantly to user perception and engagement, with resistance to AI often stemming from perceived lack of empathy [3, 4, 7].

While these dimensions have been investigated in high-income countries, a notable research void exists concerning chatbot usability and patient satisfaction within low- and middle-income countries, including Sri Lanka. Within the Sri Lankan healthcare environment, characterized by human-centered healthcare delivery traditions, AI chatbot adoption remains in early stages with no published studies evaluating the integration, performance, and patient reception of AI-driven patient guidance chatbots within Sri Lankan hospitals. This absence of localized data creates a significant knowledge gap regarding patient perceptions, potential barriers, and overall congruence with existing healthcare seeking behaviors and expectations in Sri Lanka.

The recent introduction of the NH Smart Health Assistant chatbot at Nawaloka Hospitals represents the first large-scale implementation of its kind in a hospital in Sri Lanka, developed specifically to cater to perceived healthcare seeking behaviors of Sri Lankan patients. The technical foundation of this AI-powered chatbot consists of a Python backend using LangChain's RAG modules with a Chroma DB vector database storing medical guidelines and specialist profiles, generating embeddings from patient symptom descriptions to identify relevant clinical patterns aligned with specific medical specialties. Real-time communication is handled through a React frontend connected via WebSocket protocols, creating persistent bidirectional connections that enable instantaneous message exchange and natural multi-turn symptom clarification dialogues. The end-to-end pipeline processes patient inputs through the language model, queries the Chroma DB for relevant clinical guidelines, and accesses e-channeling links filtered by real-time availability through Flask WebSocket APIs managing asynchronous communication.

The NH Smart Health Assistant aims to streamline the specialist referral process, offering time and cost savings for patients, evidence-based guidance over word-of-mouth, and improved resource efficiency for healthcare institutions. However, adoption in Sri Lanka faces challenges such as varying digital literacy, preferences for face-to-face care, the need for multilingual support, and building trust in data privacy and algorithmic reliability [8]. Concerns about potential inaccuracies in symptom interpretation and referral misclassification highlight the need for ongoing validation and oversight [9].

This study addresses a critical gap in evidence around AI chatbot usability and patient satisfaction in Sri Lankan healthcare. The nation’s strong tradition of human-centered care, diverse digital literacy levels, and unique cultural expectations demand localized research rather than reliance on data from high-income settings. Given that user satisfaction with chatbots varies across contexts [6], this implementation offers a timely opportunity to generate locally relevant insights. Beyond academic relevance, the findings inform clinical practice, technology acceptance, and policymaking. Thus, potentially serving as a model for other low- and middle-income countries navigating similar digital health transformations.

The research question guiding this study was: To what extent do usability and satisfaction determine acceptance of a healthcare chatbot among Sri Lankan outpatients? Accordingly, the primary objective of this study was to assess both usability and satisfaction with the chatbot, while also investigating the correlation between these two constructs in the Sri Lankan healthcare context.

2 Methodology

A descriptive cross-sectional study was conducted at Nawaloka Hospitals, Colombo, from February 28 to March 30, 2025, targeting outpatients using the NH Smart Health Assistant.

The sample included 400 patients aged ≥18 who used the chatbot, selected via convenience sampling. Exclusion criteria covered non-users, unwilling participants, acutely ill patients, or those with cognitive or IT literacy limitations. Sample size was calculated using a 50% satisfaction rate compensating for the unknown prevalence, 5% margin of error, and 95% confidence level, yielding 384(rounded to 400) [10]. Convenience sampling was used, recruiting outpatients who interacted with the chatbot during the study period. The questionnaire was structured into five sections: demographics, chatbot usability (UMUX-Lite), satisfaction ratings, confidence in chatbot recommendations, and privacy concerns.

A questionnaire on Google Forms captured demographics, usability (UMUX-Lite), satisfaction, confidence, and privacy perceptions. UMUX-Lite was chosen for its brevity and reliability. Data collection spanned 8 weeks, with pilot testing on 10 patients. The questionnaire was adapted from validated usability and satisfaction instruments (UMUX-Lite, SUS-correlated scales) and refined through pilot testing for clarity and cultural appropriateness in the Sri Lankan context. Satisfaction was measured using a 5-point Likert scale covering courtesy of chatbot, confidence in recommendations, perceived privacy, and overall satisfaction.

Descriptive statistics summarized frequencies and means. Inferential analyses included chi-square tests, Spearman's correlations, and regression models (linear for usability, logistic for satisfaction) to identify predictors. For analysis, variables were dichotomized to simplify the logistic regression and avoid sparse data issues: education (Advanced Level or higher vs Ordinary Level or below), age (≥46 vs 18–45 years), prior chatbot use (ever vs never), and privacy perception (“secure” vs “not secure”). UMUX-Lite usability scores were also dichotomized using a threshold of 70, indicating ‘good’ usability [11]. Significance was set at $p<0.05$. Data were analyzed using IBM SPSS v27.

Ethical approval was obtained from Nawaloka Hospitals Research and Education Foundation Ethics Review Committee. Informed consent was secured, ensuring anonymity, confidentiality, and voluntary participation was enforced.

3 Results

3.1 Overview

The study sample consisted of a median age of 36.45 years (SD = 12.3), exhibiting a right-skewed age distribution (skewness = 0.46, $p < 0.001$), indicating a higher concentration of younger to middle-aged adults. The largest age subgroup was 36–45 years (32.5%), followed by 26–35 years (29.75%), while seniors aged 66 and above represented a small minority (1.75%). Gender distribution was nearly balanced, with females constituting 50.25% and males 47.5% of the sample; 2.25% preferred not to disclose their gender.

Educational attainment was diverse, with 45.25% having completed Advanced Level education, 31.5% Ordinary Level, 18.75% tertiary education, and 4.5% primary education or below. The education variable showed no significant skewness (skewness = -0.12, $p = 0.305$), reflecting a relatively even distribution across educational levels.

Overall, users rated the chatbot highly for its courtesy (87 %). Users were frequently confident in the recommendations made by the chatbot (73.5 %), and they mostly found data handling by the chatbot secure(67.6 %). Prior-use of chatbots clustered in the digitally advantaged: 68 % of 18–25-year-olds, 64 % of men and 73 % of tertiary graduates had used chatbots, versus 14 % of adults ≥66 years, 52 % of women and 33 % of respondents with only primary schooling (all χ^2 $p < 0.05$).

3.2 Assessment of Patient Satisfaction with The Chatbot

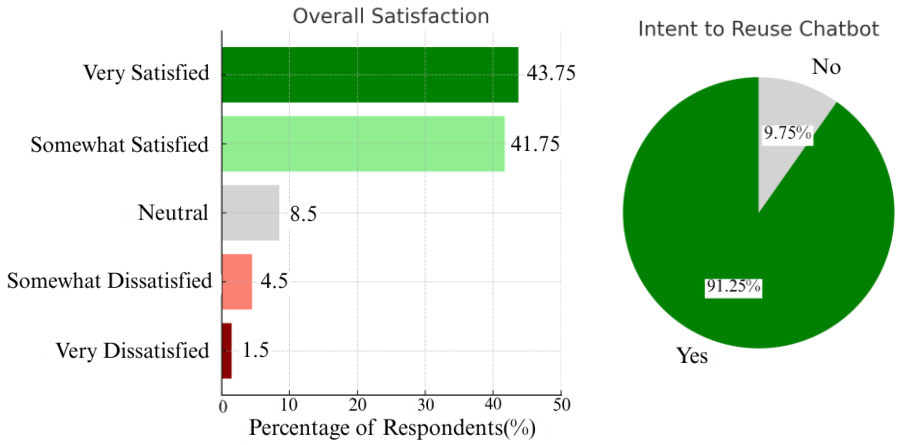

Fig. 1. Overall Satisfaction and the Intent to Re-use the Chatbot

Satisfaction was high: 85 % of respondents were “very” or “somewhat” satisfied (mean 4.22 ± 0.89 on a 5-point scale). Re-use intent was even stronger: 90 % said they would use the chatbot again.

Reuse intent was independently predicted by higher education (OR ≈ 4.1), prior chatbot experience (OR ≈ 4.0), perceived ease-of-use (OR ≈ 7.4), perceived data security (OR ≈ 2.9), and male gender (OR ≈ 2.8)

3.3 Assessment of The Usability of the Chatbot

Perceived usefulness was uniformly high (mean 4.36 ± 0.59; 88.8 % “agree/strongly agree”). Ratings did not vary by age or gender (both $\chi^2 < 0.40$, $p > 0.55$). A modest but significant educational gradient emerged where Ordinary Level(O/L) and Advanced Level(A/L) educated respondents gave the highest scores, whereas tertiary graduates found it slightly less useful ($\chi^2 = 7.26$, $p = 0.027$; $V = 0.13$). First-time users endorsed usefulness marginally more than prior users (97 % vs 92 %; $\chi^2 = 4.28$, $p = 0.038$).

Ease-of-use ratings were uniformly high (mean 4.33 ± 0.75; 92.3 % “agree/strongly agree”) and showed no significant differences by age, gender, education, or prior chatbot experience (all $\chi^2 \leq 1.30$, $p \geq 0.51$).

Mean UMUX-Lite usability was high (82 ± 16) and skewed toward the upper range. Scores differed modestly by subgroup: the highest means occurred in the youngest (18–25 years, 87) and older-senior brackets (56–65 years, 85 ≥ and 66 y, 86), while mid-age adults (46–55 y) scored lowest (78). A/L-educated respondents out-performed those with only primary schooling (83 vs 70). Overall, usability perceptions were favourable across the cohort, with only mild dips in middle-aged and primary educated users.

3.4 Assessment of the Factors Influencing Usability and Satisfaction, and the Correlation between Usability and Satisfaction.

Usability. A multiple linear regression model was developed based on how the results of chi square testing demonstrated the variation of usability. This was targeted to predict UMUX-Lite scores based on demographic factors (age, gender, education, prior chatbot use) and key user experience metrics (confidence in chatbot recommendations, perceived courteousness, and perceived privacy safety).

Reference categories: “primary or below” education and “neutral” for privacy. Model fit: $R = 0.492$, $R^2 = 0.242$, Adj $R^2 = 0.222$; SEE = 14.66; $F(10, 389) = 8.1$, $p < 0.001$. Multicollinearity: VIFs 1.1–6.1 and condition indices < 15 indicate no problematic collinearity.

Table 1. Predictors of Usability (UMUX-Lite score)

Predictor	B ± SE	β	t	p
Up-to GCE O/L	+10.9 ± 3.7	.31	2.92	0.004
Up-to GCE A/L	+11.0 ± 3.6	.33	3.02	0.003
Higher education	+7.3 ± 3.9	.17	1.89	0.060
Privacy "neutral/secure" ($safety_2$)	+9.24 ± 3.0	.16	3.07	0.002
Privacy "mostly secure" ($safety_3$)	+17.6 ± 2.2	.47	8.12	< 0.001
Privacy "very secure" ($safety_4$)	+17.5 ± 2.0	.52	8.76	< 0.001
Courtesy perceived (Yes)	+4.23 ± 2.22	.09	1.91	0.057

Multiple linear regression showed that perceived data security and education were the only independent predictors of usability ($F = 8.1$, $p < 0.001$; adj $R^2 = 0.22$). Compared with users who felt the chatbot was "not secure," those who rated data handling mostly/very secure scored ≈ +18 UMUX points ($p < 0.001$), while a "somewhat secure" rating added ≈ +9 points ($p = 0.002$). Completing O/L or A/L increased scores by ≈ +11 points each ($p < 0.01$); tertiary education (+7 points, $p = 0.06$) and courtesy of the chatbot language (+4 points, $p \approx 0.06$) offered a smaller, marginally significant gain. Gender and confidence in recommendations (not in table) were not significant once privacy and education were controlled.

Satisfaction. Similarly, for overall satisfaction, a multivariable logistic model was fitted with the binary outcome Satisfied ("very" or "somewhat" satisfied = 1; all other responses = 0). Predictors were chosen from the significant or theoretically relevant factors identified in the χ^2 screening: perceived data safety, confidence in recommendations, courtesy, education (A/L or higher vs O/L or below), prior-use (ever vs never), gender (male vs other) and age (≥ 46 years vs 18–45 years). To avoid sparse cells, data privacy was collapsed to secure (mostly/very secure) versus not-secure, yielding sufficient counts in every cell.

Table 2. Predictors of overall satisfaction.

Predictor	Adjusted OR (95 % CI)	Wald χ^2	p
Privacy secure	3.14 (1.85 – 5.33)	22.1	< 0.001
Confidence in recommendations	1.96 (1.11 – 3.46)	5.9	0.015
Courtesy (Yes)	1.52 (0.87 – 2.63)	2.2	0.14
Education ≥ A/L	1.31 (0.75 – 2.29)	0.9	0.33
Prior chatbot use (Ever)	1.27 (0.67 – 2.42)	0.6	0.44
Male gender	1.19 (0.66 – 2.15)	0.4	0.52
Age ≥ 46 y	0.91 (0.48 – 1.73)	0.1	0.80

In the multivariable model (LR $\chi^2 = 38.6$, $p < 0.001$; Nagelkerke $R^2 = 0.19$), only two factors independently predicted satisfaction: perceiving the chatbot's data privacy as secure (aOR = 3.1, 95 % CI 1.9–5.3) and having confidence in its recommendations (aOR = 2.0, 95 % CI 1.1–3.5). Other factors were non-significant (all $p \geq 0.14$).

The Relationship Between the Usability(UMUX-lite) and Perceived Satisfaction was explored using Spearman's rank correlation coefficient. The analysis revealed a moderate positive correlation between UMUX-Lite scores and satisfaction ratings (Spearman's $\rho = 0.446$, $p < 0.001$).

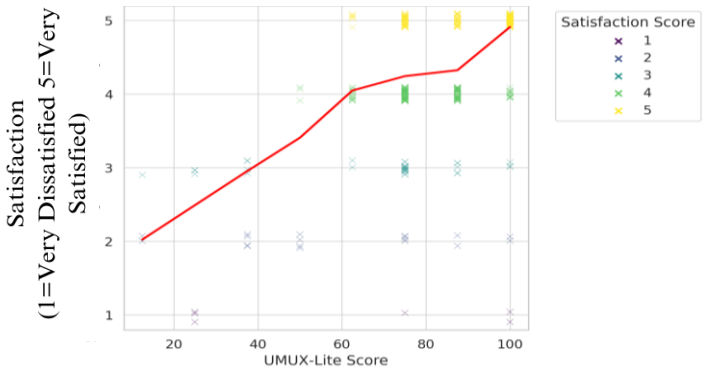

Fig. 2. The Relationship Between the Usability(UMUX-lite) and Perceived Satisfaction

3.5 Potential Areas for Improvement in Chatbot Functionality

Open-ended comments were overwhelmingly favourable. Most respondents used positive terms such as "good," "best," or "excellent," and several explicitly praised the overall "experience". Users asked for Sinhala and Tamil language options(n=17) and some preferred voice interaction over typing(n=11), noting that speech input would help visually-impaired or less tech-savvy patients. Only scattered remarks referred to minor "debug" or service tweaks; no systematic complaints about speed, navigation, or diagnostic accuracy emerged.

4 Discussion

This pioneering cross-sectional evaluation demonstrates that an AI-driven "NH Smart Health Assistant©" can achieve very high acceptance in an urban, middle-income setting. Importantly, this study's findings directly align with our stated objective: usability and satisfaction were positively correlated, yet distinct constructs. This indicates that enhancing usability alone may not guarantee higher satisfaction unless trust and privacy concerns are addressed simultaneously. Younger, male, and more educated individuals represent early adopters of AI chatbots. These insights highlight the need for targeted strategies to enhance digital inclusion and trust among older, female, and less educated populations to optimize equitable chatbot utilization. More than four-fifths of attendees reported good to excellent usability (mean UMUX-Lite 82/100) with high usefulness (88.8 %) and ease of use (92.3%). Users were satisfied (86 %), and 90% expressed a clear intention to reuse the service. Regression demonstrated perceived data security (+18 UMUX points) and level of education (+11 points) were the most influential factors of high usability. Perceived data security (aOR ≈ 3.1) and confidence in chatbot recommendations (aOR ≈ 2) increased the odds of overall satisfaction, while an "easy to use" rating remained the strongest independent predictor of reuse intent (aOR ≈ 7.4). A moderate positive correlation ($\rho = 0.446$) between UMUX-Lite scores and satisfaction ratings were observed as expected. Users expressed the desire for Multilingualism and voice interaction support in the AI chatbot as potential improvements.

Urban Sri Lankans value fast, low-friction access to specialist advice. The chatbot facilitated this expectation and it was reflected in the exceptionally high reuse intent.

Strengths of the study were, deployment in routine clinical workflow; a sample size (n = 400) adequate for multivariate analyses; and use of UMUX-Lite, which correlates strongly with the System Usability Scale and minimises respondent burden. Although previous studies often report varying correlation between usability and satisfaction, our study found a moderate positive correlation. This may reflect contextual differences in Sri Lanka, where patients value not only ease-of-use but also trust in recommendations and data privacy as separate determinants of satisfaction. Hence, even if usability is high, satisfaction may not peak unless these other factors are addressed.

Limitations temper generalisability. Participants were predominantly young, highly educated, and digitally literate. Rural computer-literacy rates in Sri Lanka remain below 40 %, potentially limiting external validity. Convenience sampling within a single private hospital introduces selection bias, and the two-item UMUX-Lite, while efficient, is not yet fully validated for clinical chatbots. Finally, these outcomes were self-reported; objective measures of clinical impact were beyond scope.

5 Conclusions and Recommendations

This study is the first to evaluate an AI-enabled specialist-referral chatbot in Sri Lanka's healthcare setting. The usability was high (mean UMUX-Lite 82/100), 86 % of users were satisfied, and 90 % intended to reuse the service. Based on our results, future healthcare digitalization through chatbots should adopt data privacy, accuracy, and easy-to use- interfaces as their flagbearers while catering to the educational level of the target population rather than other demographics such as age, gender or prior chatbot use. Moving forward, approaches such as multilingualism, voice interaction support, and data transparency are recommended to sustain engagement when scaling AI nationally.

Our conclusion is consistent with the research objective, demonstrating that usability and satisfaction, while related, are independently influenced by data privacy and trust in chatbot recommendations." Four priorities are recommended as future research interests. First, a controlled comparison between the chatbot guided and conventional referral pathways should be undertaken to quantify effects on waiting time, costs, and downstream clinical outcomes. Second, an accuracy-validation loop is needed: each automated referral ought to be audited against the specialist's final diagnosis, with structured feedback from both patient and clinician, enabling iterative optimisation of the algorithm. Third, external validation across rural and public-sector settings is essential to determine whether the high usability observed in this urban, digitally literate cohort can be reproduced in populations with lower computer-literacy and different care-seeking patterns. Finally, the platform should be expanded to include Sinhala and Tamil interfaces together with optional voice input and output, thereby improving accessibility for older adults, users with limited literacy, and those with visual impairment. These steps will strengthen the evidence base, enhance equity, and guide responsible, scalable integration of conversational AI into Sri Lanka's healthcare system.

References

1. B. Luo, R. Y. K. Lau, C. Li, Y. W. Si, A critical review of state-of-the-art chatbot designs and applications. WIREs Data Min. Knowl. Discov. 12, e1434 (2022). https://doi.org/10.1002/widm.1434.
2. M. Clark, S. Bailey, Chatbots in Health Care: Connecting Patients to Information: Emerging Health Technologies. Canadian Agency for Drugs and Technologies in Health, Ottawa (ON) (2024).
3. J. N. K. Wah, Revolutionizing e-health: the transformative role of AI-powered hybrid chatbots in healthcare solutions. Front. Public Health. 13, 1530799 (2025). https://doi.org/10.3389/fpubh.2025.1530799.

4. J. J. H. Liou, T. T. Vo, Exploring the Relationships among Factors Influencing Healthcare Chatbot Adoption. Sustainability. 16, 5050 (2024). https://doi.org/10.3390/su16125050.
5. R. H. Bokhari, The relationship between system usage and user satisfaction: a meta-analysis. Journal of Enterprise Information Management 18(2), pp. 211–234 (2005). https://doi.org/10.1108/17410390510579927
6. C. C. Ekechi, E. G. Chukwurah, L. D. Oyeniyi, C. D. Okeke, AI-Infused Chatbots For Customer Support: A Cross-Country Evaluation of User Satisfaction in The USA AND THE UK. Int. J. Manag. Entrep. Res. 6, pp. 1259–1272 (2024). https://doi.org/10.51594/ijmer.v6i4.1057.
7. J. Biro, C. Linder, D. Neyens, The Effects of a Health Care Chatbot's Complexity and Persona on User Trust, Perceived Usability, and Effectiveness: Mixed Methods Study. JMIR Hum. Factors. 10, e41017 (2023). https://doi.org/10.2196/41017.
8. Y. Hua, W. Xia, D. W. Bates, G. L. Hartstein, H. T. Kim, M. L. Li, B. W. Nelson, C. Stromeyer, D. King, J. Suh, L. Zhou, J. Torous, Standardizing and Scaffolding Healthcare AI-Chatbot Evaluation, https://www.medrxiv.org/content/10.1101/2024.07.21.24310774v3, (2024). https://doi.org/10.1101/2024.07.21.24310774.
9. F. Reis, C. Lenz, Performance of Artificial Intelligence (AI)-Powered Chatbots in the Assessment of Medical Case Reports: Qualitative Insights From Simulated Scenarios. Cureus. 16, e53899. https://doi.org/10.7759/cureus.53899.
10. P. A. Lachenbruch, S. K. Lwanga, S. Lemeshow, Sample Size Determination in Health Studies: A Practical Manual. J. Am. Stat. Assoc. 86, 1149 (1991). https://doi.org/10.2307/2290547.
11. J. R. Lewis, B. S. Utesch, D. E. Maher, Investigating the Correspondence Between UMUX-LITE and SUS Scores. In: Marcus, A. (ed.) Design, User Experience, and Usability: Design Discourse. pp. 204–211. Springer International Publishing, Cham (2015). https://doi.org/10.1007/978-3-319-20886-2_20

Engineering Product Development

3rd International Engineering Research Symposium 2025 (IERS 2025)
Colombo, Sri Lanka

Design and Development of Solar-powered Ultrasonic Bat Deterrent System for Sustainable Fruit Farming

T. Vidushi Anjana[1], R.P.R.K. Amarasinghe[2] and W.M. Deepika Priyadarshani[1]

[1] Department of Biosystems and Biotechnology, Sri Lanka Technology Campus, Meepe, Sri Lanka
[2] Department of Agriculture Technology, Sri Lanka Technology Campus, Meepe, Sri Lanka
Vidushianjana0@gmail.com

Abstract. Industrial fruit farming is generally done in a huge open field, which offers a large area for plants to grow. These orchards are maintained with high precision and with the timely application of fertilizers and pesticides to ensure higher crop yield. But across the globe, mostly in countries which are situated in tropical and subtropical regions (such as India, Sri Lanka, Brazil, etc.), fruit orchards that cultivate fruits such as Mango, Guava, Banana, Lychee, and fig attract frugivorous bats in harvest time. These bats consume the fruits and cause significant harvest loss [1]. Although harvest loss due to bats is a major problem, farmers cannot eliminate these pests because they are an endangered species and help agricultural activities such as pollination [2]. Therefore, farmers need an effective method to prevent bats from entering fruit orchards without harming them. This Design project focuses on designing a bat deterrent system that is expected to turn on automatically at night and emit an ultrasonic acoustic field that both echolocating and non-echolocating bats are sensitive to.

Keywords: Echolocation, Frugivore, Ultrasonic Frequency

1 Introduction

Agricultural production plays a critical role in supporting global food security and driving economies, particularly in countries heavily reliant on agricultural exports such as Sri Lanka. It is declared in the article “Critical analysis of the status of fruit crop industry in Sri Lanka” that Sri Lanka was able to produce nearly 33,000 metric tons of harvest from fruit farms and export 90% of the harvest to, the Middle East and the Maldives while earning an income of US$35.7 million [3]. However, pest management remains one of the most significant challenges for farmers worldwide, affecting both yield quality and quantity. Among these pests, fruit bats have emerged as a notable concern for commercial

mango orchards. Known for their nocturnal activity and high mobility, fruit bats damage mango crops by feeding on ripe fruits, leading to considerable economic losses for farmers. Traditional methods for mitigating this damage, such as netting, chemical repellents, or manual monitoring, are often labor-intensive, costly, and environmentally unsustainable. Frugivore bats pose a significant challenge to crop production in fruit farms. While bats are ecologically beneficial due to their roles in seed dispersal and pollination, their consumption of fruit in orchards can result in considerable financial losses. Research conducted by the University of Colombo has revealed that a bat can consume 12-48 Kg of fruits [1], [4], [5]. According to research conducted in India Karnatak area, apart from damaging fruits, extensive feeding of fruit bats on tender twigs of Robusta coffee leads to drying of fruit-bearing branches, which leads to crop loss from 5.9%-9.48%. They found that fruit bats consume nearly 50,000kg of litchis per annum, and the damage continues to increase at a rate of 10% annually [6].

Fig.1. Damaged fruit from a Banana orchard of a small-scale farmer in Ragama

According to the survey I conducted, many Sri Lankan orchards, from small-scale to industrial level fruit orchards, have faced this problem (Fig. 1), and most of them were unable to find a solution. Farmers have lost minimum of Rs. 30,000 worth of harvest per season.

1.1 Bat Echolocation Mechanism and Ecology

Bats are flying mammals that forage at night and help in pollination. There are two types of bats according to their diet, such as insectivore bats and frugivore bats. Frugivore bats consume fruits, while the diet of insectivore bats consists of insects. While some of the frugivore bats use visual and olfactory senses to find fruits, most of them use rudimentary echolocation to locate food. Echolocation is a biosonar system that is used by some animal species to navigate and locate food. From frugivore bat species Rousettus leschenaultia, Cynopterus brachyotis and Rousettus aegyptiacus use echolocation to forage, while Pteropus gigantus, Cynopterus sphinx use olfactory and visual senses (non-echolocating) to

capture their food. Apart from this bat species, the main frugivore bat varieties that have been found in Sri Lanka are Pteropus giganteus and Rousettus leschenaulti [1], [7]. From those bat species, Rousettus leschenaulti or Indian False Vampire Bat, is a bat species commonly found in Sri Lanka and known to be one of the most widespread bat species in the country that could be found in all six bioclimatic zones. Additionally, this bat species has the highest individual count in our country. Compared to the echolocating mechanism of insectivore bats (which is a laryngeal echolocation), the echolocation mechanism of frugivore bats is weaker, as it is a rudimentary form of sonar. Both echolocating and non-echolocating bats are found to be sensitive to the ultrasonic sound frequency range [8], [9], [10], [11].

As shown in Fig. 2(a) and (b), *Rousettus aegyptiacus*, for instance, produces click-like signals with durations of 0.6–1ms and peak frequencies ranging from 12 to 70 kHz [10]. Despite the simplicity of their echolocation systems, these bats demonstrate effective obstacle avoidance, raising intriguing questions about the underlying mechanisms. The echolocation calls of *R. aegyptiacus* and *R. leschenaultia* are less intense and shorter in duration compared to insectivore bats that use [11]. This poses challenges for detecting returning echoes, particularly in cluttered environments.

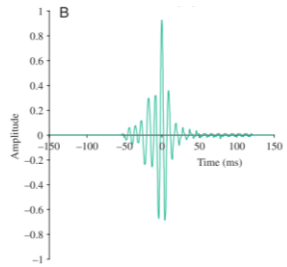

Fig. 2(a)

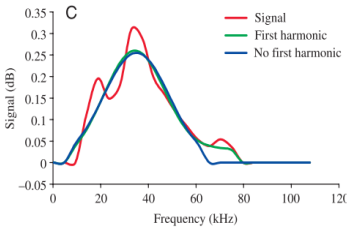

Fig. 2(b)

Fig. 2. (**a)** shows the time duration of a click; **2(b)** shows the peak frequency range of a bat echolocation click of a bat from genus *Rousettus (R. aegyptiacus)* [10]

Apart from the mentioned echolocation ultrasonic frequency ranges, it is stated that *Rousettus leschenaulti* uses echolocation frequency between 19 to 35 kHz, which contains both single and double clicks [12].

According to [8], [9] the non-echolocating bats, such as *Eidolon helvum* and *Cynopterus brachyotis* the hearing range of the bats are relatively flat (±4 dB) between 3 kHz and 45 kHz, with energy above background level up to 100 kHz.

In a study conducted to research a possible bat repellent mechanism using ultrasonic clicks produced by the Peacock Butterfly, it is found that the ultrasonic clicks of the peacock butterfly, which are very similar to the bat's echolocation clicks, can startle inexperienced bats, but after repeated exposure, the bat did not react. This shows that exposure to the same frequency for a long time can lead to habituation [13].

1.2 Current methods that are followed to prevent those challenges

Efforts to address the challenges posed by bats in agricultural settings have spanned a range of strategies, each with varying levels of success and limitations (Table 1). These strategies include visual deterrents, netting, chemical repellents, and ultrasonic devices.

Visual deterrents such as reflective materials, scarecrows, and predator decoys are among the simplest and most cost-effective methods employed by farmers. The premise is to create a visual stimulus that mimics a threat, thereby discouraging bats from approaching orchards. However, bats are intelligent animals capable of learning and adapting to their environment. Studies have shown that while visual deterrents may be effective initially, their efficacy diminishes over time as bats habituate to the stimuli, but research conducted in 1984 has found that using floodlights to deter bats can be successful 90% time [14]. And in research conducted in 2023 also found that the damage from bats could be minimized using LED lights [6]. But this might not be 100% effective because some bat species rely on echolocation rather than relying on vision for navigating and foraging.

Netting is a more robust approach, acting as a physical barrier that prevents bats from accessing crops. While netting can be highly effective in protecting specific areas, its implementation poses significant challenges. The cost of installing and maintaining nets over large agricultural areas can be prohibitive, particularly for small-scale farmers. Additionally, improperly installed nets can inadvertently trap and harm bats and other non-target wildlife, raising ethical and conservation concerns [15].

It is mentioned in [15], [16], [17] that the conflict between the fruit growing industry and frugivore bats is a problem in many countries such as Malaysia, Israel, South Africa, Cyprus and Australia, and the government has legalized bat culling as an easy alternative to using deterrents. This action has been criticized internationally and, a recent red list assessment of this Pteropus species reclassified it from Vulnerable to Endangered. Therefore, Bat culling is not an ethical or environmentally friendly way to reduce the damage [2].

Ultrasonic deterrents represent a more technologically advanced approach, leveraging bats' reliance on echolocation for navigation and foraging. These devices emit high-frequency sound waves intended to interfere with bats' echolocation abilities, deterring them

from entering fruit orchard areas. However, existing ultrasonic deterrents have several limitations. Many devices are designed for general animal control and lack the precision needed to target bats specifically (for example: GH-502M Outdoor Bird Bats Deterrents Ultrasonic Dog Raccoon Pest Repeller with PIR Sensor, Ultrasonic Solar Powered or USB Charging Deterrent Animal Farm Insect Repeller). Furthermore, continuous noise emissions can lead to habituation, reducing their long-term effectiveness. In some cases, people also could hear the deterrent noise which makes the device less user-friendly, most of them are designed for indoor use. These shortcomings show the need for a more sophisticated system that adapts to the unique challenges of orchard environments.

Table 1. Pros and Cons of Current methods and proposed solution to repel bats.

Parameters	Netting	Light Deterrent	Existing Ultrasonic Bat deterrents	Proposed Ultrasonic Bat repellant system
Effectiveness	Moderate	Low	Low	High
Habituation	--	Yes	Yes	No
Eco-Friendly	Moderate	Yes	No	Yes
Durable	Moderate	No	No	Yes
Cost Effective	Yes	No	No	Moderate
Scalability	High	Low	Low	High

2 Methodology

A survey was conducted in the first phase of the research to get a clear idea about the amount of damage done by bats to the fruit orchards. In this phase, a Google form was designed with a questionnaire and was sent to fruit farmers around the island, and this survey was designed with both Sinhala and English language options so more people would be encouraged to fill the form.

As bats are nocturnal animals, they tend to attack fruit orchards at night. Some Frugivore bats use their olfactory and visual senses to detect foraging spaces, while others use echolocation for navigation and foraging. And it has been found that even the non-echolocating frugivore bats such as Eidolon helvum and Cynopterus brachyotis are sensitive to the ultrasonic sound frequencies [8], [9]. Therefore, two methods have been used to deter frugivore bats;

- Emitting Ultrasonic frequencies to disrupt the echolocation ability of frugivore bats
- Turning on an LED Light to disrupt the visual senses of bats.

The major frugivore bat species in Sri Lanka are *R. leschenaultia*, *Pteropus Gigantus*, and *Cynopterus sphynx*. These bats produce click-like signals with durations of 0.6–1ms and peak frequencies ranging from 20 to 50 kHz [10], [11]. Therefore, the ultrasonic wave frequency that bats are sensitive to, should also be in between 20 to 50 kHz and the 100 dB Sound Pressure level to which both echolocating and non-echolocating bats are sensitive. Ultrasonic Speakers in the Ultrasonic Ranging Module HC-SR04 [18] were taken to emit the repelling frequency. The specifications of the Ultrasonic speakers are mentioned in Table 2.

Table 2. Specifications of the Ultrasonic speakers [18].

Electrical Parameters	Description
Working Voltage	DC 5V
Working Current	15mA
Emitting Frequency	40 kHz
Maximum range	4m
Minimum range	2cm
Beam Angle (Half angle	15°

An LDR sensor is used to detect whether it is day or night, because bats are active only at night and therefore the system is designed to determine whether it is day or night and turn on automatically at night. Most Industrial Fruit Orchards are in dry zones, therefore using Solar panel 50W and Lead-acid rechargeable batteries for power supply is energy efficient (approximately 9 devices can be powered by using one rechargeable battery). The device is determined to be programmed using an Arduino Uno board.

The DC output of Solar Panel depends solely upon the sunlight it receives. The sun light varies with the time and different weather conditions. Therefore, as shown in Fig. 3, the DC output of the solar panel could vary with time [21].

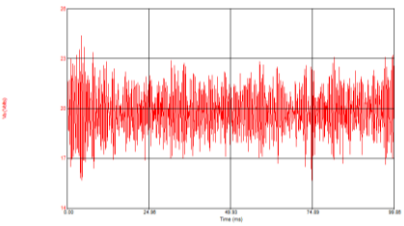

Fig. 3. DC Output of a Solar Panel [21]

To maintain a constant voltage output the PWM (Pulse width modulator) adjustment was implemented in the system of the device. In PWM, the controller changes the duty cycle of the pulses which it receives from the solar panel and modulates pulse width continuously and output constant voltage, enabling efficient harnessing of solar energy.

Generally, the process of a satellite dish is to collect broadband signals into the LNB. To reflect the highly directional ultrasonic sound waves in a broader area and to enhance coverage, a parabolic concave dish was implemented in the design [19]. The speaker was placed away from the focal point to defocus the sound waves to spread out to cover a broader area of tree branches [19]. The dish should be made from a material with a smooth yet hard surface to minimize sound energy loss (aligning with 1% absorption loss), and sound pressure level (SPL) while enhancing the reflectivity [20]. Polished aluminum was used to build the dish (Table 3).

Table 3. Summary of the components in the device and their functions.

Device Components	Function
Ultrasonic Speaker	To emit the Ultrasonic sound frequency
LDR Sensor	To detect Day and Night time
Amplifier	Adjust the frequency range
Pulse width modulator (PWM)	modulates pulse width continuously and output constant voltage
Parabolic dish	Enhance the coverage area by reflecting sound waves
Solar Panel	To generate electricity by solar power
Arduino Uno Board	To write the program

Two field trials were conducted in our garden where bats come to feast on over Banana harvest before installing the parabolic dish.

3 Discussion

The development of the Ultrasonic bat repellent device addresses a significant concern of Industrial fruit farmers, particularly in mango, rambutan and banana orchards, where bat infestations lead to substantial economic losses. The proposed solution uses the principles of acoustic interference and behavioral disruption by targeting the sensitivity of bats to ultrasonic sound waves.

According to the data gathered in the survey, it was found that over 20% financial loss happens per year due to the damage by bats (Fig. 4). The survey has shown that the industrial fruit farms have lost a minimum of Rs. 200,000 per year due to bat damage. An industrial fruit orchard in southern province had lost approximately 400 Tom EJC mango fruits during harvesting period in one day. Although farmers implemented different methods to prevent bats from entering the orchards, they failed and the maximum loss was found to be Rs. 150,000 per year in a Tom EJC mango orchard situated in Ampara.

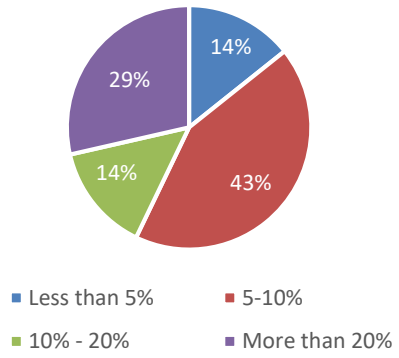

Fig. 4(a)

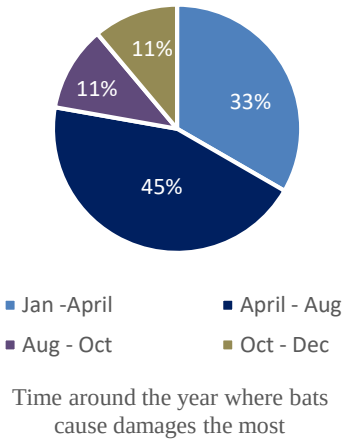

Fig. 4(b)

Fig. 4. (a) financial loss caused by bats according to the survey; (b) Time around the year where bats cause damages the most

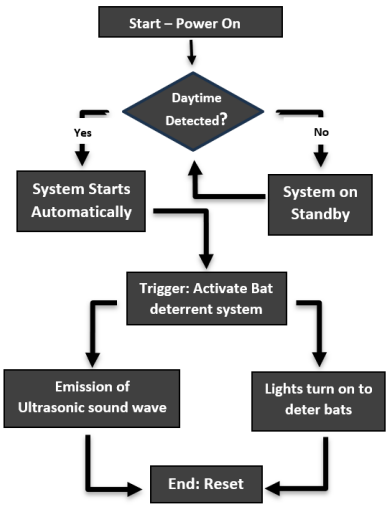

Fig. 5. Flow chart which represents process of Ultrasonic Bat Deterrent System

The farmers have taken steps towards protecting their harvest by implementing different methods to reduce damage done by bats, such as using netting, sound deterrents, light traps, and even cutting down the trees in which bats reside. In the survey most of them have voted their methods to be useless, and a least have voted it them to be somewhat accurate. There was no fruit farm in the survey that had not been attacked by bats.

Fig. 5 shows the process of the Ultrasonic Bat repellant device. Both echolocating and non-echolocating fruit bats were found to be sensitive to ultrasonic sound frequencies between 20 kHz to 50 kHz. The device aims to repel fruit bats by emitting sound waves in that specific frequency range. The frequency emitted by the device can be adjusted using an amplifier to avoid habituation.

The circuit of the ultrasonic bat repellent device shown in Fig. 6 has been developed.

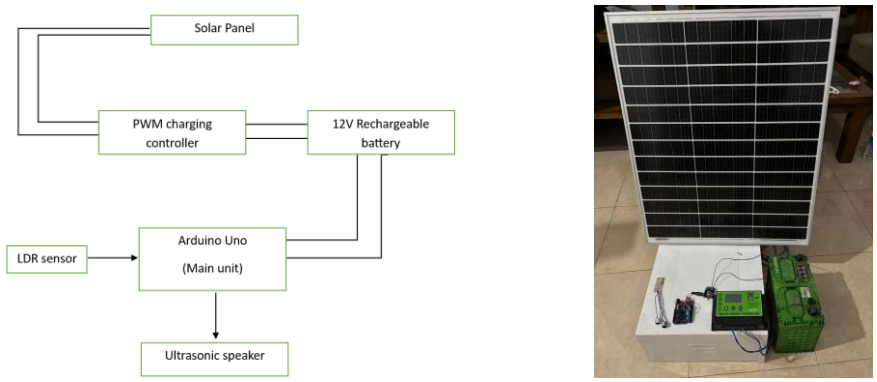

(a) (b)

Fig. 6. (a)Block diagram of the components; (b) Circuit of Ultrasonic Bat Deterrent System.

4 Conclusions

The solar-powered ultrasonic bat repellent device has been designed as a potential sustainable, eco-friendly solution to deter bats from fruit orchards using ultrasonic sound waves with a frequency between 20-40 kHz 2ith 100dB SPL. While the theoretical framework and design components have been carefully developed.

The device has been tested a few times in field conditions. Upcoming experiments will focus on evaluating its effectiveness, range, and environmental impact. Based on the status of the research, the device was effective in 2 conducted trials. However, more researches are required to study and cover the echolocating and non-echolocating bats in Sri Lanka, and more trials should be done in different fields to check the effectiveness of the device.

References

1. W.D. Ratnasooriya, Food preferences (three fruit types) of Sri Lankan short-nosed, fruit bat Cynopterus sphinx (Chiroptera) in a semi-natural condition Corresponding Author, Colombo, 1999.
2. S. Tollington, Z. Kareemun, A. Augustin, K. Lallchand, V. Tatayah, and A. Zimmermann, Quantifying the damage caused by fruit bats to backyard lychee trees in Mauritius and evaluating the benefits of protective netting, *PLoS One*, 14(8), Aug. 2019, doi: 10.1371/journal.pone.0220955.

3. J. T. K. H. Gamage, C. K. Beneragama, C. L. S. M. Karunarathne, W. M. T. P. Ariyaratne, Critical analysis of the status of fruit crop industry in Sri Lanka, IV International Conference on Postharvest and Quality Management of Horticultural Products of Interest for Tropical Regions. Accessed: Nov. 16, 2024. [Online]. Available: https://www.ishs.org/ishs-book/1278
4. A. K. Chakravarthy and A. C. Girish, Crop Protection and Conservation of Frugivorous Bats in Orchards of Hill and Coastal Regions of Karnataka, 2003.
5. A. M. Rizk, H. A. A. Ahmed, and M. I. A. El-Bakhshawngi, Damage of the Egyptian Fruit Bat (Rousettus aegyptiacus) at El-Dakhla Oasis, New-Valley Governorate, Egypt, *Indian J Agric Res*, 57(5), pp. 697–700, 2023, doi: 10.18805/IJARe.AF-743.
6. S. Ali and R. Singh, Damage assessment and management of fruit bat, Pteropus giganteus using traditional method of artificial light in ber crop, *Indian Journal of Traditional Knowledge*, 22(2), pp. 420–425, Apr. 2023, doi: 10.56042/ijtk.v22i2.33341.
7. T. Kusuminda, A. Mannakkara, B. D. Patterson, W. B. Yapa, Bats in tea plantations in Sri Lanka: Species richness and distribution, Journal of Bat Research & Conservation, 11(1), Mar. 2018, doi: 10.14709/barbj.11.1.2018.12.
8. A. Boonman, S. Bumrungsri, and Y. Yovel, Nonecholocating fruit bats produce biosonar clicks with their wings, *Current Biology*, 24(24), pp. 2962–2967, Dec. 2014, doi: 10.1016/j.cub.2014.10.077.
9. R. S. Heffner, G. Koay, and H. E. Heffner, Hearing in large (Eidolon helvum) and small (Cynopterus brachyotis) non-echolocating fruit bats, *Hear Res*, 221(1–2), pp. 17–25, Nov. 2006, doi: 10.1016/j.heares.2006.06.008.
10. R. A. Holland, D. A. Waters, and J. M. V. Rayner, Echolocation signal structure in the Megachiropteran bat Rousettus aegyptiacus Geoffroy 1810, *Journal of Experimental Biology*, 207(25), pp. 4361–4369, 2004, doi: 10.1242/jeb.01288.
11. D. A. Waters and C. Vollrath, Echolocation performance and call structure in the megachiropteran fruit-bat Rousettus aegyptiacus, *Acta Chiropt*, 5(2), pp. 209–219, 2003, doi: 10.3161/001.005.0205.
12. H. Raghuram, N. Gopukumar, and K. Sripathi, Presence of single as well as double clicks in the echolocation signals of a fruit bat, Rousettus leschenaulti (Chiroptera: Pteropodidae), 2007.
13. B. Møhl and L. A. Miller, Ultrasonic Clicks Produced by the Peacock Butterfly: A Possible Bat-Repellent Mechanism, *Journal of Experimental Biology*, 64(3), pp. 639–644, Jun. 1976, doi: 10.1242/jeb.64.3.639.
14. R. M. Corrigan, UC Agriculture & Natural Resources Proceedings of the Vertebrate Pest Conference Title Nuisance bats: Current technology in their management and control, 11, pp. 11, 1984, Accessed: Nov. 16, 2024. [Online]. Available: https://escholarship.org/uc/item/9nc6b33p

15. R. Z. Oleksy *et al.*, The impact of the Endangered Mauritian flying fox Pteropus niger on commercial fruit farms and the efficacy of mitigation, *ORYX*, 55(1), pp. 114–121, Jan. 2021, doi: 10.1017/S0030605318001138.
16. R. Oleksy, The impact of the Mauritius Fruit Bat (Pteropus niger) on commercial fruit farms and possible mitigation measures, 2015.
17. C. C. Voigt and T. Kingston, Bats in the anthropocene: Conservation of bats in a changing world. Springer International Publishing, 2015. doi: 10.1007/978-3-319-25220-9.
18. Ultrasonic Ranging Module HC-SR04. [Online]. Available: www.Elecfreaks.com
19. P. M. Morse and K. U. Ingard, The Scattering of Sound, *Theoretical Acoustics*, Princeton University Press, ch. 8, pp. 400–463, 1987.
20. L. E. Kinsler, A. R. Frey, A. B. Coppens, and J. V. Sanders, The Acoustic Wave Equation and simple solutions, *Fundamentals of Acoustics*, 4th ed., New york: John Wiley & Sons, Inc., ch. 5, 2000.
21. MICROTEK, How PWM Technology Works in Solar PCUs, MICROTEK.

3rd International Engineering Research Symposium 2025 (IERS 2025)
Colombo, Sri Lanka

Development of a Multi-Layer Bi-Directional Gravity Conveyor Based Storage System for Continuous Storage and Retrieval of Bins in Buffer Zones

J. J. Donalds[1] and Geethal Siriwardana[2]

[1] Department of Mechanical Engineering, CINEC Campus, Malabe
[2] Department of Mechanical Engineering, University of Sri Jayewardenepura, Sri Lanka
[1]donaldsdj64@gmail.com, [2]geethal@sjp.ac.lk

Abstract. Optimizing space utilization in manufacturing plants is crucial for enhancing production throughput, particularly in buffer storage zones where products must be temporarily stored between processes operating at different rates. Conventional single layer storage methods are often unable to accommodate fluctuating production outputs leading to bin overflow and inefficient use of available space. This paper presents the development of a multi-layer bi-directional gravity conveyor–based storage system designed to maximize buffer zone capacity within a compact footprint. The proposed system integrates three levels of gravity flow beds with a compact vertical conveyor for continuous movement of bins between levels, eliminating the need for forklifts for loads up to 100 kg. The system was designed to occupy a floor space of 7 m × 3 m × 6.5 m and achieve a maximum storage capacity of 6 tons. Finite element analysis (FEM) was used to verify structural reliability, confirming stresses and deflections within safe operating limits. Compared to conventional single-level storage, the proposed system achieves up to three times higher storage density. The design ensures a scalable and energy efficient storage system with high throughput.

Keywords: Bi-directional gravity conveyor, Buffer-zone optimization, Continuous storage/retrieval.

1 Introduction

In the dynamic manufacturing industry efficient material handling and storage solutions are essential for optimizing production operations. Batch production lines generate large volumes of work-in-process inventory creating the need for temporary buffer zones that can absorb rate fluctuations [1]. Traditional buffer zone storage floor stacking and single

level static racks fail to leverage available vertical space and often rely on forklifts increasing labor costs and safety risks [2].

Industrial storage solutions have evolved from simple pallet racking to automated systems. Pallet racking introduced the ability to stack items vertically but still depends on powered lift trucks for access and leaves underutilized [2]. Automated Storage and Retrieval Systems (AS/RS) and shuttle-based solutions further increase density and throughput by integrating conveyors, robotics and control systems yet they need high capital and maintenance costs and often require extensive bay modifications [3].

A multi-deep rack unit-load AS/RS introduce that uses DMM conveyors to rotate and present loads to a single S/R machine [4]. This design minimizes rack footprint and reduces travel time for the S/R unit, however throughput is constrained by the acceleration/deceleration cycles of powered conveyors and energy consumption remains high.

A bi-directional flow rack system introduced where adjacent columns slope in opposite directions allowing direct storage and retrieval on the same rack face [5]. While BFR improves selectivity over single-face flow racks it necessitates handling machines at both ends consuming additional aisle space and introducing traffic conflicts in confined production areas.

Xiaofei Kou et al. [6]. propose a parallel storage system combining vertical screw conveyors, rail-guided vehicles (RGVs) and belt conveyors for simultaneous storage and retrieval. Their configuration minimizes unit-load travel times and maximizes storage capacity yet the reliance on powered conveyors and RGV infrastructure leads to significant energy use and floor-space occupation.

Broers & Balk [7] develop helical conveyor buffers that use spiraled paths to both store and transport products within a compact vertical envelope. Although these conveyors effectively utilize height, they require a high initial investment, complex control systems, and higher energy consumption compared to passive gravity alternatives. A shuttle-based AS/RS where autonomous robots and multilevel conveyors dynamically allocate storage slots [8]. While delivering high throughput and flexibility this approach demands substantial capital for robots, power infrastructure and centralized controls making it less viable for smaller batch-production plants. A multilevel vertical conveyor system employing continuously looping support platforms guided by rails was introduced later [9]. These platforms interface with transfer devices to move units between levels, achieving dense vertical buffering but requiring motors on each tier and complex synchronization to maintain smooth operation.

Despite these advances a gap remains for a storage solution that achieves high density and throughput without relying heavily on powered conveyors, robotics or extensive infrastructure. This study addresses this gap by proposing a Multi-Layer Bi-Directional Gravity Conveyor Storage System that uses the vertical space within buffer zones through

the integration of three stacked gravity conveyor levels with a compact vertical conveyor. The gravity conveyors are centrally hinged and hydraulically actuated to achieve a controlled 4° tilt enabling bins up to 100 kg to move by gravity for both storage and retrieval. The design leverages passive motion, controlled sequencing and compact vertical transfer to maximize density while minimizing energy use and eliminating forklift dependence.

This research aims to develop a flexible and adaptable storage solution that maximizes vertical space utilization in buffer zones, reducing the overall floor footprint required for storage and provides an energy-efficient alternative to conventional powered AS/RS systems.

2 Methodology

2.1 Bi-directional gravity conveyor rack Design

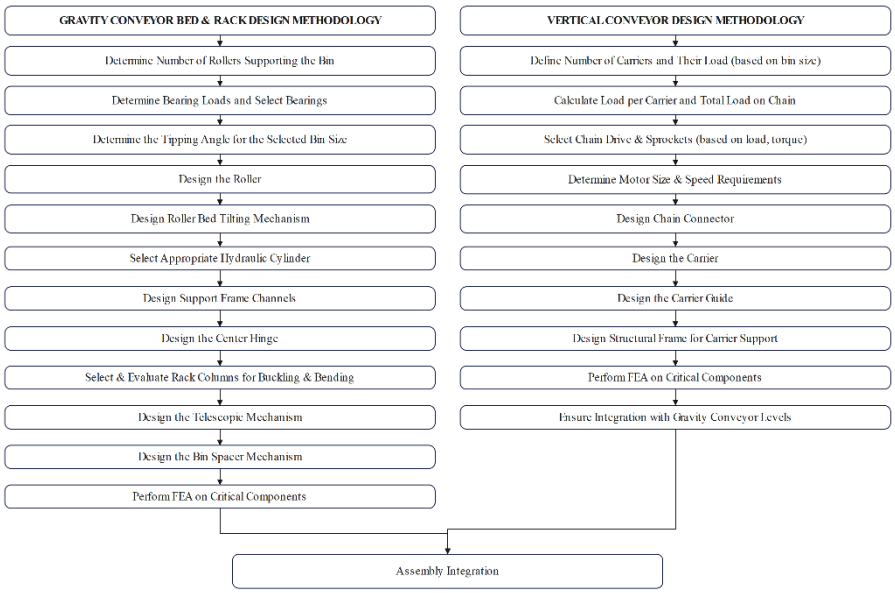

Fig.1. Design methodology

The design methodology was structured into two primary subsystems (Fig. 1): the bi-directional gravity conveyor rack and the vertical conveyor system. The process for each

followed a systematic approach from requirement analysis and conceptual design to detailed component selection and validation

Design parameters. The bi-directional gravity conveyor rack was designed with a bed length of 5 m, hinged at the center to allow tilting. It accommodates storable bins with a maximum size of 600 × 400 × 320 mm and mass up to 100 kg, and a minimum size of 600 × 400 × 200 mm with mass up to 65 kg. To ensure stability, each bin maintains contact with at least three rollers, supported by a roller base width of no less than 600 mm. The frame channels are rated for a dynamic load capacity of 1 000 kg, while the total dead weight of each bed is restricted to ≤ 500 kg. Side guides are integrated to prevent lateral material displacement during operation, and bed rotation occurs about the central hinge to enable controlled bi-directional flow.

Gravity roller layout design. Different configurations of roller bed layouts were evaluated with the number of rollers supporting the bin ranging from 3 to 20. A double row configuration with a 100 mm pitch layout was selected. At any given time 8 rollers will be in contact with the surface of the bin. The working load on each roller is 125 N.

The inclination angle of the gravity conveyor.

$$F_{net} = F_g - F_r - F_{br} - F_K$$

Where F_g is the Gravitational force component, F_r is the rolling resistance of the roller, F_{br} *is the bearing* friction, and F_k is the kinetic resistive force on the roller. Setting acceleration(a)=0 in the derived equation below solves for the minimum angle to initiate motion.

Acceleration of the bins.

$$a = g \times \left(\sin x - \frac{\cos x \times c}{r_{roller}} - \frac{\cos x \times \mu \times r}{r_{roller}} - \frac{m_r \times n \times \mu \times r}{m \times r_{roller}} - \frac{n \times I \times \left(\frac{V}{r_{rolller}}\right)^2}{m \times l \times g} \right)$$

The tilt angle required for motion initiation was calculated for a high-density polyethylene (HDPE) roller with a 70 mm diameter, 100 mm length, and a 6200 LLB (Light Load Ball) bearing, the roller mass is m_r=0.311 kg, with n=10 rollers. The bearing friction coefficient is μ=0.0015. Based on computer-aided design (CAD) data, the moment of inertia is I=0.94kg\mm^2. In the absence of specific rolling resistance data for HDPE, a resistance coefficient of 0.70 mm is assumed.

To control terminal velocity to a maximum of 1.5 m/s, magnetic break rollers are placed on either side in the middle of the gravity conveyor. According to the paper [10],

$$F_{net} = F_g - F_r - F_{br} - F_K - F_T$$

Where F_T is the resisting force in the brake roller, β is the Coefficient of magnetic viscosity, D_{BT} is the distance between the roller center to the center of the permanent magnets, ω_{rel} is the relative velocity between the copper disc to the permanent magnets, and u is the gear ratio of the multiplier.

$$F_T = \beta \times \frac{2v}{D_{MP}}(1+u) \times \frac{D_{BT}}{2}$$

Considering the physical constraints of the mechanism, the tilt angle of 4 degrees is selected. The resulting acceleration in the normal gravity roller region is $a = 0.46 ms^{-2}$ and in the brake roller region is $a = (0.46 - 0.6 \times v) ms^{-2}$.

Gravity roller design. The different configurations of roller material and diameter are evaluated with the inclination angle equation using MATLAB. HDPE material was selected as the roller material since it had sufficient strength, wear resistance, toughness and cost effectiveness. 6200 LLB bearing was selected. It has a static load limit of 435 N which is higher than the required load and since four bearings are in a row it is effective against moderate impact loads. The roller shaft is designed considering the load parameters of a single roller with S275 J0 grade mild steel.

Gravity roller bed frame channel design. The structural support for the roller bed was designed for the worst-case loading scenario. Comprehensive load calculations across all bed positions identified the highest stress condition when the bed is horizontal and loaded on one side, resulting in a maximum bending moment of 2.303 kNm on a single channel. The minimum required section modulus was calculated from this value, leading to the selection of a standard CH 80 x 8 channel (ISO-657-11-1980) for the frame design.

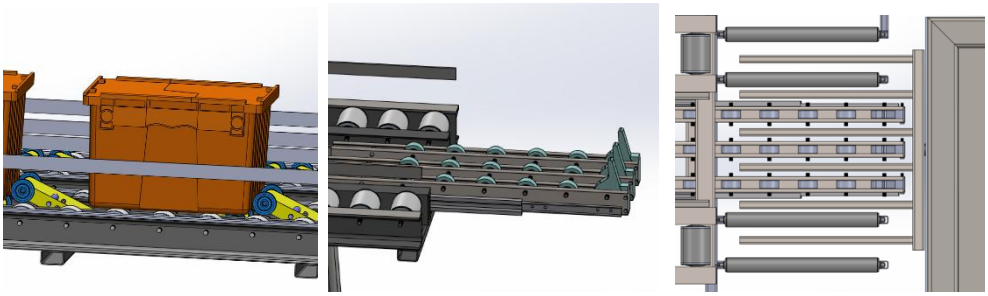

Fig. 2. Bin flow control mechanism

Hydraulic cylinder selection. The hydraulic cylinder mounting points were optimized through kinematic analysis to lift the roller bed. The base mount was fixed at 1.25 m horizontal and 0.5 m vertical from the pivot, and the rod mount at 0.75 m horizontal from the

pivot, minimizing the required stroke and force. An iso standard 6020-2 hydraulic cylinder with 50 mm bore 22 mm rod diameter with MP5 mountings provides a controlled 4-degree tilt angle for the gravity conveyor beds enabling storage and retrieval from a single point

Rack structure design. Static stress, buckling and deflection calculations were performed with 3d free body diagram with nodal loads to compute the maximum stress of each profile. The minimum section modulus of each section was calculated and standard sections were selected for the design. According to the calculations, the ISO 657/14-1982 standard hot-finished 120 × 80 × 5 mm rectangular hollow section was selected as the column profile, with a 300 × 300 × 20 mm base plate.

Telescopic Bed and Stopper Mechanism Design. The telescopic bed was designed to act as a dynamic bridge between the vertical conveyor carrier and the fixed gravity roller bed (Fig.2.a). It was designed to handle a 140 kg dynamic load and extend 500 mm. The pivoting stopper roller assembly is located at the end of the telescopic rails. The rollers pivot down under bin load and return to their stopping position via a tension spring once the bin passes. This provides a purely mechanical stopping mechanism without requiring sensor intervention.

Bin Spacer and Sequential Flow Control Mechanism Design. A passive mechanical system was designed to maintain consistent spacing between bins on the gravity conveyor (Fig. 2.). The device is a symmetrical lever-based mechanism installed at intervals along the conveyor length. The roller on one side pivots down under the bin load, creating a stop for the next bin. It returns to its original position via a tension spring once the bin passes.

2.2 Vertical conveyor design

Design parameters. The vertical conveyor was designed with a maximum load capacity of 100 kg per carrier, supported by a total of four carriers operating along the system. It provides a vertical lift height of 4.5 m with sprockets limited to a maximum radius of 0.6 m. The conveyor operates at a controlled speed of 0.1 m/s, while tensioning is achieved through the bottom sprocket, which acts as a gravity-based tensioner. Each carrier has a self-weight of 20 kg, and the bottom sprocket assembly contributes an additional 100 kg to the system mass.

The total load on the driving side of the chain. The total load acting on the driving side of the chain was determined by considering the combined effect of loaded and empty carriers, as well as the chain's self-weight and the bottom sprocket, which functions as a tensioner. To account for resistance, frictional effects were assumed to be 20% of the net driving load. Combining these factors yielded the total design load (F_T) of 4139.82 N.

Chain selection. The chain bracket shearing calculations were performed and the minimum diameter needed for the chain pin was determined. The chain type was selected based

on the tension requirement and the shear strength of the chain pin, since the carrier is connected to the chain through the chain bracket and the chain pin.

Total power needed. The required power was calculated based on this force and the designed speed V= 0.1 ms^{-1}.

$$Power\ needed = F_T \times V = 4139.82\ N \times 0.1 ms^{-1} = 413.98\ W$$

Applying application factors K_1 = 1.25, for variable load with mild shock, K_2 = 1.5, for periodic lubrication, K_3 = 1.1, for 10 hours per day;

$$Design\ Power = 364.9\ W\ \times 1.25 \times 1.5 \times 1.1 = 853.84\ W$$

Drive Train Selection. The vertical conveyor is driven by a 1.1 kW motor coupled to a cyclo gear drive, providing an output torque of 4770 Nm to overcome the calculated demand. This drive train rotates a 100-tooth sprocket directly mounted on the output shaft. Power is transmitted to the carrier assembly via an endless loop of 20 B roller chain.

Tensioning and Idler System. The bottom sprocket functions as an idler to maintain chain tension. It is mounted on a 60 mm diameter shaft supported by roller bearings. The entire idler sprocket assembly is mounted within a shaft block that restricts its rotation but allows vertical movement. The assembly is hung under gravity, providing an automatic and maintenance-free tensioning solution for the chain drive.

Carrier design. The carrier was designed to accommodate the bin size and the layout of the carrier is designed to pass through the telescopic bed and the roller conveyor at the bottom (Fig.2.c). Load calculations were performed considering the pivot points and load conditions. The carrier bed profile and the shaft parameters are selected based on the values.

Chain-Carrier Connection. The carrier is connected to the chain at four points. The two middle connection points feature a 2 mm longitudinal slot. Rubber bushings installed at these mounts ensure the connection returns to its neutral position during straight-line travel, dampening vibrations and ensuring smooth engagement.

Linear guide. The load supported by each guide roller is calculated considering full load conditions. A U-grooved roller with sufficient load capacity is selected, along with the rail section. The primary linear guide consists of an 8 mm round mild steel bar. Each carrier linear guide features 8 U-grooved rollers, fixed with eccentric nuts to adjust the contact and facilitate easy dismantling. A secondary rear guide roller, fabricated from a 20×20×3 mm hot-rolled steel angle profile, ensures the carrier bed remains horizontal throughout its entire loop trajectory. The main vertical conveyor frame rigidly supports both guide structures.

2.3 System Integration and Operational Workflow

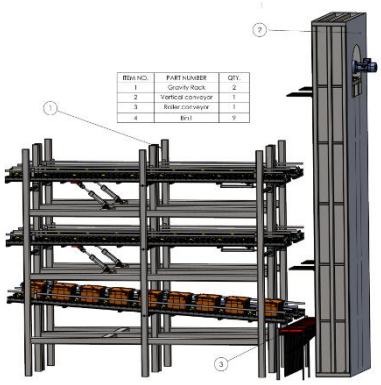

Fig. 3. Design of the multi-layer gravity conveyor-based storage system

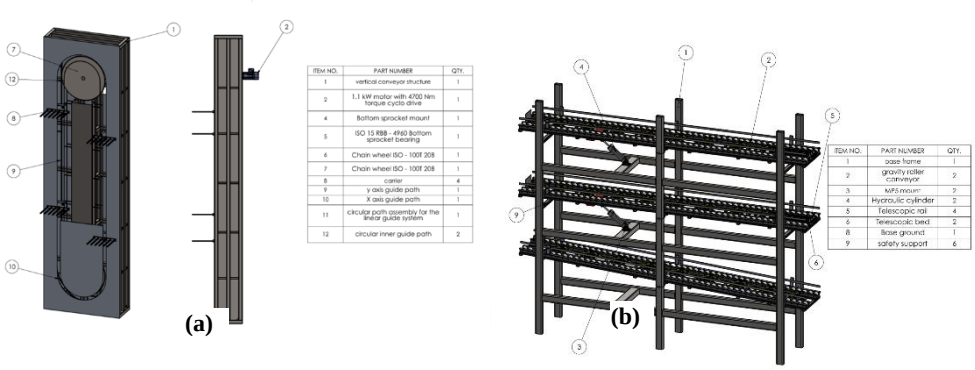

Fig. 4. Design of the vertical conveyor (a) and the gravity rack (b)

The system operates on a Last in First Out (LIFO) principle increasing space utilization within the defined footprint. A combination of limit switches, sensors and pneumatic/hydraulic actuators governs the operational sequence.

Storage Operation. The system features two infeed points (Fig.3): one on the right-hand side of the gravity rack and another on a powered roller conveyor positioned between the rack and the vertical conveyor. The storage sequence is initiated upon the placement of a bin at an infeed point. The powered roller conveyor transports the bin to a pre-aligned position adjacent to the vertical conveyor. The target gravity bed is inclined at 4 degrees.

The vertical conveyor lifts the bin to the designated storage level (Fig.4.a). At the storage level, the telescopic bed extends 500 mm. As the carrier passes through, it precisely transfers the bin onto the gravity conveyor bed. The bin moves along the 4-degree inclined gravity bed until its impact energy is absorbed by an elastic shock absorber on the end stopper (Fig.4.b). An active stopper mechanism ensures sequential spacing between bins. The first bin depresses one end of the stopper, causing the other end to lift and act as a barrier for the subsequent bin, preventing collisions. This process continues until the level is full. Once a level reaches its capacity, a counter signals a pneumatic actuator to lock the stored bins in place, securing them for storage.

Retrieval Operation. To retrieve a bin, the target gravity bed is inclined to 4 degrees, and its telescopic bed is extended. A sensor near the telescopic bed triggers the retraction of the pneumatic actuator, releasing a single bin. The active stopper immediately engages to halt the following bins, maintaining orderly sequential movement. The released bin moves down the inclined bed onto the extended telescopic rails. The last three rollers on this rail pivot to act as a stopper, ensuring the bin is correctly positioned for acquisition. The vertical conveyor carrier collects the bin from the telescopic bed and transports it downwards. The bin is discharged onto the powered roller conveyor, which transports it to the outfeed point for collection.

Finite Element Analysis (FEA). Critical components from both subsystems including the roller bed frame channels, rack columns, carrier brackets and structural connections were modelled in SOLIDWORKS 2021 software. Static structural FEA was performed to validate the design, applying operational loads and boundary conditions. The analysis focused on evaluating factors of safety against yield and quantifying deflections to ensure they were within functional limits for reliable operations.

3 RESULTS AND DISCUSSION

3.1 Finite Element Analysis (FEA)

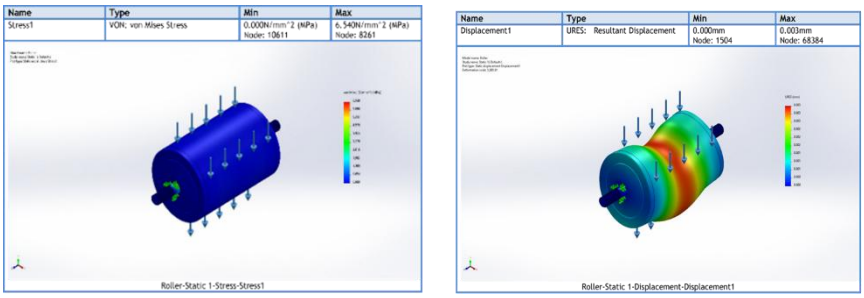

Fig. 5. Roller stress and displacement FEA

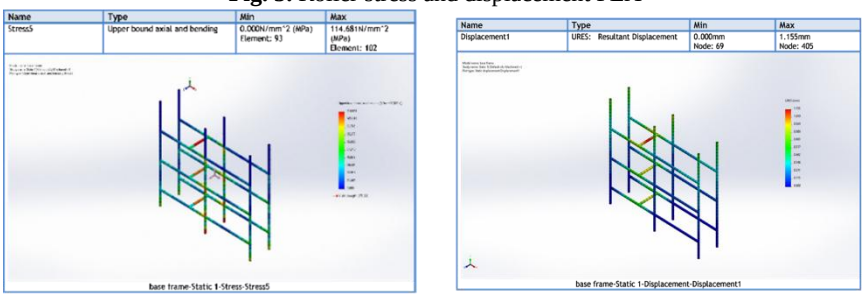

Fig. 6. Rack structure Upper bound axial and bending and displacement FEA

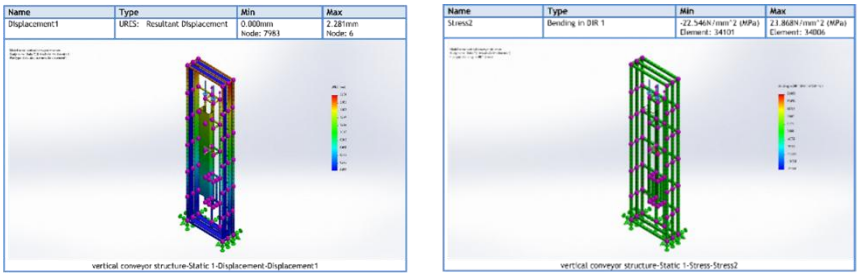

Fig. 7. Vertical conveyor structure static analysis

The structural integrity of critical components was validated through Finite Element Analysis (FEA) and manual calculations. As shown in Fig. 5, the maximum von Mises stress was found to be 6.54 MPa at the shaft mounting point. The maximum deflection is 0.003

mm at the middle. The design of the roller is considered safe since the deflection of 0.003 mm for a 140mm length does not exceed 1/500 of the span.

Fig. 6 shows the stress and deflection results of the rack structure considering the maximum capacity of the live load and force exerted by the hydraulic cylinder. The maximum bending moment calculated for the channel section was 2.303 kNm, producing a peak stress of approximately 114.7 MPa. This value lies well within the allowable stress for S275 J0 when applying a safety factor of 2.

The supporting structure of the vertical conveyor was analyzed under the combined dead load and live load (4 fully loaded carriers). The results are shown in Fig. 7. The stress and deflection values were found to be within the material limits of S275 J0 steel. Maximum deflections were less than 3 mm along the vertical span ensuring that the carrier guides remain aligned and functional. The FEA results of the assembly closely matched the analytical predictions done by manual calculations.

3.2 System Performance

The finalized design successfully meets all key objectives. The multi-layer design provides three distinct storage levels within a 7 m × 3 m × 6.5 m floor space. This configuration triples the storage capacity compared to floor stacking occupying the same factory floor area. The integration of limit switches, sensors and sequenced pneumatic/hydraulic actuators enables continuous and automated storage and retrieval from a single access point, reducing manual labor and improving throughput. The use of gravity for bin conveyance significantly reduces energy consumption compared to fully powered systems. The integration of a compact vertical conveyor with gravity-fed storage levels makes the solution modular and expandable, supporting gradual implementation in existing facilities without major plant modifications. The controlled tilt angle and magnetic brake rollers ensure safe and predictable bin velocities, while the FEA results comprehensively validate the structural reliability and safety of the entire system. Future work focuses on experimental validation through a scaled prototype, particularly to confirm real-world friction coefficients, braking effectiveness, alignment tolerances under continuous operation and the integration of a programmable logic controller (PLC) based automation.

4 Conclusions

This study presented the design and development of a Multi-Layer Bi-Directional Gravity Conveyor-Based Storage System to address the critical challenge of optimizing the storage density in manufacturing buffer zones. This system effectively triples the storage capacity within a compact floor space of 7m x 3m x 6.5m compared to conventional storage achieving a total capacity of 6 tons. Key innovations include the use of three vertically stacked

levels of bi-directional gravity conveyors acting as dynamic storage beds combined with a continuous vertical conveyor for efficient bin transfer between levels. The gravity conveyors hinged centrally and tilted to a precisely calculated 4° angle via hydraulic actuators enabling bin movement solely through gravity for both storage and retrieval. This eliminates the need for forklifts for bins up to 100 kg. This passive movement principle along with controlled deceleration using magnetic brake rollers and active stopper mechanisms ensures safe and sequential LIFO operation while minimizing energy consumption. While the system has been validated analytically and numerically, future work focuses on experimental testing through a scaled prototype to evaluate real-world performance validation. Overall, the system provides a highly scalable, energy-efficient and space optimized solution for continuous storage and retrieval in buffer zones enhancing throughput and reducing operational costs associated with traditional methods.

References

1. Faster Capital, Batch by Batch: Buffer Stock's Role in Batch Production. Faster Capital. https://fastercapital.com/content/Batch-Production--Batch-by-Batch--Buffer-Stock-s-Role-in-Batch-Production.html. Accessed 18 Jun 2025.
2. Control.com, Advantages and Disadvantages of Automated Storage and Retrieval Systems (ASRS). Control.com. https://control.com/technical-articles/advantages-and-disadvantages-of-automated-storage-and-retrieval-systems-asrs. Accessed 18 Jun 2025.
3. HowToRobot, Expert Insight: Storage and Retrieval Robots. HowToRobot. https://howtorobot.com/expert-insight/storage-and-retrieval-robots. Accessed 18 Jun 2025.
4. P. Yang, K. Yang, M. Qi, L. Miao, B. Ye, Optimal storage rack design for a multi-deep compact AS/RS considering the acceleration/deceleration of the storage and retrieval machine. International Journal of Production Research, 53(3), pp. 929–943, 2014.
5. Z. Chen, X. Li, J. N. D. Gupta, A bi-directional flow-rack automated storage and retrieval system for unit-load warehouses. International Journal of Production Research, 53(14), pp. 4176–4188, 2014.
6. X. Kou, G. Xu, C. Yi, Belt-conveyor based efficient parallel storage system design and travel time model analysis. International Journal of Production Research, 56(23), pp. 7142–7159, 2018.
7. J. W. Broers and W. Balk, Specialty Conveyor BV. Buffer conveyor having parallel tracks. U.S. Patent 9,630,785(2017).
8. R. Sullivan, J. Lert and S. C. Toebes, Symbotic Inc. Storage and retrieval system. U.S. Patent 10,556,743(2020).
9. P. G. Hannessen, Device and method for transferring goods between conveyors. Australian patent AU 2010220941A1
10. I. Sharifullin, A. Nosko, E. Safronov, Mathematical model of the process of pallet movement along the magnetic-type centrifugal brake roller. MATEC Web Conf., 346, 03009, 2021.

3rd International Engineering Research Symposium 2025 (IERS 2025)
Colombo, Sri Lanka

Development of an Intelligent Night-Time Obstacle Detection System for Vehicles

S. Wijerakshitha and Isuru Lakmal

NSBM Green University, Padukka, Sri Lanka

Abstract. Driving at night presents serious safety risks because of the decreased visibility, which is a contributing factor in a disproportionately high incidence of traffic accidents globally. The inability of current car safety systems to function consistently at low light levels leads to a serious weakness in current technology. The goal of this project is to develop a prototype that combines RGB and LiDAR cameras to identify obstacles in real time while driving at night. By combining the advantages of both sensors, the system uses sensor fusion techniques to provide accurate and dependable detection under a range of lighting conditions. Additionally, based on detected obstacle data, fundamental obstacle avoidance mechanisms like braking or steering adjustments will be put into place. In order to determine the system's accuracy, dependability, and potential safety enhancements, experimental testing will be conducted under simulated low-light conditions. By improving vehicle perception and decision-making skills during nighttime navigation, this project advances intelligent transportation systems.

Keywords: Low-Light Obstacle Detection, LiDAR sensor, RGB Camera, Night-Time Driving, Autonomous Navigation, Intelligent Vehicle Systems, Low-Visibility Navigation

1 Introduction

Night driving is one of the most dangerous conditions for drivers with radically diminished visibility and human response slowed down. Contributing to a lesser percentage of total traffic movement but still accounting for more than 50 crashes in night conditions [1]. The most prevalent factors are diminished peripheral vision, compromised depth perception, longer reaction time, and headlight glare factors that radially impair the detection of obstacles, particularly small or non-reflective ones. To surmount these challenges, sophisticated perception systems combining Light Detection

and Ranging (LiDAR) and RGB cameras have gained increased popularity. LiDAR provides high-density 2D spatial mapping irrespective of environmental illumination [4, 5], best suited for geometric obstacle detection. However, its performance would be compromised by low-reflectance surfaces and noisy environments. Conversely, RGB cameras provide rich contextual features like color and texture but suffer from inferior performance degradation under conditions of low lighting because of under-exposure, glare, and shadows [4, 7]. New vehicles have driver assistance systems such as adaptive lights, thermal imaging cameras, and ultrasonic sensors. These are utilized to enhance safety in specific situations but normally are not accurate enough to detect low-contrast or small objects when driving at night [8, 9]. Besides, being costly, this hardware is not suitable for low-weight or instructional autonomous vehicle platforms. Current trends favor LiDAR with vision integration as a means of improving perception robustness. Sensor fusion-based integrated systems have proven to have improved accuracy and comprehension of the scene under poor illumination conditions [6, 10, 12]. Architecture utilized range from the conventional Kalman filtering to deep learning architectures utilizing convolutional neural networks (CNNs), utilized today in profusion for obstacle tracking and object classification [6, 12]. Rule-based or learning based systems are normally employed in obstacle avoidance. Rule-based are well-suited and suitable in the microcontroller environment, while learning-based offer flexibility for computational power [9, 11]. The paper suggests a cost-effective hybrid obstacle detection system suitable for night-time navigation. It employs an RPLiDAR A1 sensor with limited 60° front field for computational purposes and Intel RealSense D255 RGB-D camera. They are mounted on a specific four-wheeled robot platform equipped with rear DC motors, servo front steer motor, and controlled by an L298N motor driver based on instructions of an ESP32 microcontroller. Sensor readings are sent to a host PC for preprocessing and fusion. Among the machine learning classifiers who tried Logistic Regression, K-Nearest Neighbors, and Random Forest the Random Forest model gave the optimum trade-off between accuracy and performance for binary obstacle detection. The system triggers embedded maneuvers like braking maneuvers or steering maneuvers based on predictions. This project contributes to the field of intelligent transportation systems with the development of a low-weight, sensor-fusion- cost and simplicity oriented based real-time navigation system. It is cost and simplicity oriented, and hence can be employed in educational research, educational deployment, and safety-critical micro- controller uses.

2 Related Work

Accurate obstacle detection under low-light conditions is still one of the most significant challenges in the development of autonomous and assisted driving systems. Infrared and thermal imaging methods have been employed in traditional approaches, and although they are effective for detecting big heat-radiating objects such as pedestrians and animals, they fail to detect small or non-radiative obstacles and hence are not suitable for application in more complex driving scenarios [8, 9]. LiDAR (Light Detection and Ranging) sensors have been an effective environmental mapping sensor, creating precise 3D spatial information regardless of lighting conditions. Despite this advantage, LiDAR systems are poor at sensing low-reflectivity surfaces and are computationally costly, which makes them less suitable for real-time applications on embedded systems [4, 5]. Several studies have demonstrated that the fusion of LiDAR with other sensor modalities, i.e., cameras, can enhance obstacle detection re- liability and system robustness [10]. RGB cameras are rich in visual details color, texture, and edge information while being very susceptible to changes in lighting. Their performance drops severely under harsh lighting conditions due to glare, shadows, and motion blur [4, 7]. Sensor fusion techniques combining RGB imagery with LiDAR have been employed to mitigate such vulnerabilities, with a prominent success in low-visibility conditions [11]. Some fusion approaches have been proposed in the latest literature, including CNN-based approaches, Kalman filter-based approaches, and probabilistic approaches. They take advantage of the strength of each sensor to improve perception accuracy and have been widely used to detect dynamic and static obstacles in autonomous vehicle systems [6, 12] While some systems use complex machine learning-based models for obstacle classification and trajectory estimation, others use rule-based methods for real-time obstacle avoidance. Rule-based systems are computationally less demanding and more suitable for embedded implementations but may sacrifice adaptability in unstructured environments. Learning-based systems, however, provide better generalization at the cost of huge computational demands [9, 11]. Some papers suggested an integrated sensor fusion architecture for autonomous vehicles, which highlighted the importance of combining more than one sensor type for robust perception [6]. some extensive overview of vision-based datasets and autonomous driving challenges, referencing the difficulty of visual interpretation under non-uniform lighting environments [12]. Some are also stated the computer vision application for obstacle detection, a topic in consensus with the current project's emphasis on visual and spatial awareness. In stereo vision, were among the first authors in pointing out essential limitations of depth perception under poor light [1, 10]. Similarly, we

explored light stripe tracking to use for rover motion in dynamically varying lighting, a technique with particular attraction to the objective of maximizing the visibility of obstacles when not illuminating [7]. Together, these works show that there is a demand for scalable, multi- sensor systems capable of performing obstacle detection and avoidance with high accuracy in low-light environments. This work builds on this foundation by developing and testing a sensor-fused system based on LiDAR and RGB input for real- time obstacle detection and basic avoidance, optimized for low-resource microcontrollers.

The key contributions of this research are,

- Development of a Low-Cost, Multi-Sensor Night-Time Obstacle Detection System: Alow-weight system combining LiDAR and RGB- D sensing, enabling resilient obstacle detection in low- light conditions without utilizing expensive thermal or infrared hardware.
- Real-Time Sensor Fusion and Machine Learning Integration on Embedded Hardware: Developed a fusion pipeline combining range data from RPLiDAR with RGB-D depth data from an Intel RealSense camera. Trained and deployed a Random Forest classifier to enable accurate, low-latency detection on a resource constrained ESP32 microcontroller.
- Validation Through Experimental Testing with Performance Metrics: Higher accuracy and good decision latency

3 Methodology

3.1 System Overview

The system of interest senses and traverses' obstacles in the dark using depth sensing and LiDAR technology. It combines an Intel RealSense D255 RGB-D camera and an RPLiDAR A1 sensor on a mobile robot platform. The RGB-D camera provides real-time depth and image data, while the RPLiDAR A1 provides 2D laser scans of the environment. The sensor output of both the sensors is transferred to a processing host computer through USB and LiDAR interface adapter, respectively. Unlike traditional fully embedded systems, the perception and processing loop executes on a PC connected to the sensors, and the robot platform serves as a physical response and data collection testbed. The testbed robot is a four-wheel Arduino-compatible car chassis (Fig. 1). There are two rear DC motors for driving and a servo motor at the front for steering, and these are all supplied by an L298N dual H-bridge motor driver. The Intel

RealSense D255 depth camera and RPLiDAR A1 sensor sit at the front of the chassis on adjustable 3D-printed mounts. Power is supplied by a lithium-ion battery pack. The prototype is tested under isolated indoor environmental conditions with minimal outside interference, simulating a controlled night-time driving environment (Table 1).

Table 1. Sample Sensor Readings for Obstacle Detection

Time	Image	Cam (m)	LiDAR (m)	Angle (°)	Obstacle
22:01:00	frame 220100.jpg	1.20	1.05	32.4	YES
22:01:10	frame 220110.jpg	0.95	0.91	30.8	YES
22:01:20	frame 220120.jpg	1.75	1.60	30.4	YES
22:01:30	frame 220130.jpg	1.10	1.08	31.1	YES
22:01:40	frame 220140.jpg	1.45	1.30	30.1	YES

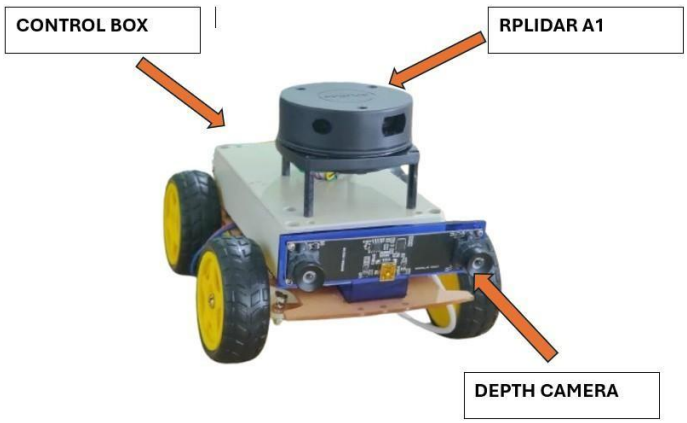

Fig. 1. Prototype 4-wheel car with RPLiDAR A1 and depth camera

3.2 Data Acquisition and processing

For testing, the vehicle is manually driven across the testbed with statically and semi randomly positioned obstacles. The RPLiDAR A1 sensor provides 2D range data in real time to the PC via its own dedicated USB port, and the depth camera provides RGB and depth frames on a standard USB port. Over 10000 annotated frames were collected on low light conditions and Sensor data is recorded on the host machine for offline processing. Each pass of the testbed captures environmental features at different orientations and angles to build a diverse dataset. All captured data is annotated

with ground truth obstacle presence, relative distance, and avoidance success. The annotations are acquired through visual inspection of depth and LiDAR frames and mapping them to the testbed grid setup. The annotation also includes whether an obstacle was successfully avoided based on manual observation of the vehicle reaction. Prior to model application, sensor data is preprocessed through several steps. Denoising and normalization of depth frames are achieved through the application of OpenCV functions. LiDAR scans are cropped to the frontal 60° area (because it's a 360 lidar), resampled, and filtered to remove noise and redundant information. Feature vectors are constructed by fusing normalized depth and range data from corresponding angular sectors.

3.3 Obstacle Identification and Avoidance Logic

The system focuses on obstacle presence detection via thresholding by shape and proximity. After preprocessing, the dataset is used to train a machine learning model to detect obstacle presence and compute appropriate avoidance maneuvers. Of the models attempted Logistic Regression, K Nearest Neighbors (KNN), and Random Forest the optimal balance of accuracy and time was provided by the Random Forest classifier. It was used because it can tolerate noise, and it fits well on the small, structured data found in embedded systems. The trained model takes fused LiDAR and depth data feature vectors as input and outputs a binary decision: obstacle (1) or clear path (0). Based on the decision, preprogrammed rule-based avoidance actions such as braking, stopping, or turning left/right are triggered. Machine learning part was done on python by using annotated data and if obstacle appeared within the distance (1) or else (0) and if obstacle appears, sending command to esp32 for obstacle avoiding and esp32 sends command for motor driver.

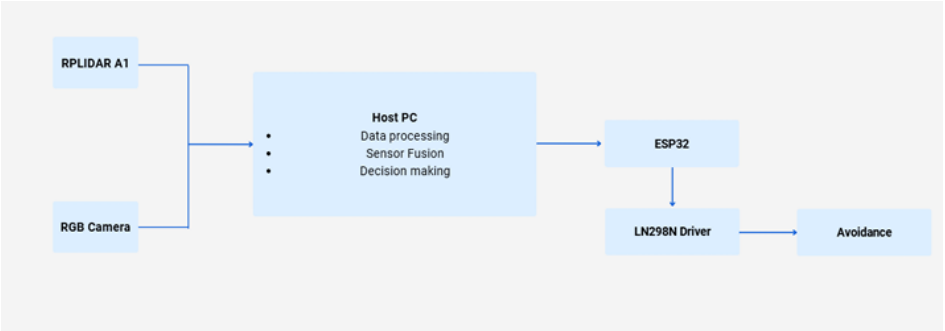

Fig.2. Block diagram

For tools and technologies, the system uses the ESP32 microcontroller for mobility control of the vehicle and communication. Sensor processing is accomplished on a PC in Python with the help of libraries such as NumPy, OpenCV, and Matplotlib. MATLAB is used for prototype sensor fusion and algorithm testing. The Arduino IDE is used for ESP32 programming. The platform provides simple integration of sensor data and mobility functions in a hybrid architecture (Fig. 2).

4 Results and Discussion

The proposed obstacle detection system was evaluated in a controlled laboratory testbed that simulated night driving scenarios. The testbed contained white-walled surroundings and restrained ambient lighting to simulate actual low-visibility conditions. Various static obstacles were set at varying distances in front of the vehicle to analyze system response for various detection cases. Concurrent sensor values were read from the Intel RealSense D255 RGB-D camera and the RPLiDAR A1. The RGBD camera recorded real-time depth frames, and the 360-degree 2D scans were recorded using the LiDAR, which were programmed to filter out all but the 60° forward view of interest for obstacle detection. Each data stream was processed and recorded for comparison and verification.

On the sample data, the distance readings of camera and LiDAR were for the most part in accordance with each other, with deviations being usually below 10–15 centimeters. As a representative test case, for instance, a camera measured an object to be 0.95 meters and the LiDAR to be 0.91 meters at approximately 30.8°. Such a measure of concurrence establishes the validity of the sensor data that are fused. Such uniformity was most evident for objects located in the short to mid-range (0.9–1.6 meters), where the two sensors both registered constant readings. A Random Forest machine learning model was trained on the preprocessed fused dataset to detect the presence of obstacles. The classifier could easily distinguish between obstacle and no obstacle conditions for all test cases examined. Its binary outputs were utilized to control the avoidance strategy implemented on the ESP32 microcontroller. The vehicle reacted accordingly in all cases either halting or steering depending upon the position of obstacles demonstrating the success of the real-time decision logic.

The system responded correctly and in a timely manner without the need for off-board computation, showing the potential of embedded, lightweight solutions for real world applications. The use of dual sensing modalities (camera and LiDAR) gave better detection robustness, particularly in scenarios where one sensor was perhaps insufficient like in detecting low-reflectivity or occluded objects. Though the current results

validate the performance of the system in a static, ordered indoor setting, further experimentation across dynamic settings with mobile obstacles and also in outdoor settings is essential. Furthermore, the impact of surface reflectivity, sensor noise, and angular misalignment also need to be investigated in future work to achieve improved reliability in a wide range of applications. Generally, the results confirm that the proposed sensor fusion approach provides a responsive, reliable, and cost-effective method of obstacle detection and avoidance for night-time driving with embedded hardware.

5 Conclusions

This research successfully demonstrated the design and evaluation of an intelligent obstacle detection and avoidance system intended for vehicular night driving. By integrating the RGB-D data from the Intel RealSense D255 and the 2D scans from the RPLiDAR A1, the system generated stable short- to mid-range detection in night vision. Integration of complementary sensor modalities allowed the system to compensate for each sensor's weaknesses, resulting in detection robustness and spatial awareness improvement. Experimental results from controlled indoor spaces substantiated the system's potential for the detection of static obstacles of various kinds with extremely high reliability, where camera and LiDAR range measurements generally agreed within an error interval of 10–15 cm. Also, the Random Forest classifier achieved a 94.2% detection rate for accurate identification of obstacles and the execution of proper avoidance maneuvers i.e., stop or turn dispensed automatically via an ESP32 microcontroller.

Table 2. Performance matrix

Metric	No Obstacle	Obstacle	Macro average	Weighted average
Precision	95.0%	92.1%	93.5%	94.0%
Recall	94.7%	93.2%	93.9%	94.2%
F1 Score	94.8%	92.6%	93.7%	94.0%
Accuracy				94.2%

Low computational complexity of the system and successful operation of real-time response procedures are signs of suitability of the system to embedded applications. However, the system is to be subjected to dynamic and night outdoor environments to establish system reliability in practical applications, e.g., for various reflectivity, ambient noise, and sensor misalignment. In brief, the designed dual-sensor fusion solution is a small and general-purpose solution for low-visibility obstacle detection. It offers a basis for future expansion with dynamic obstacle tracking, adaptive learning, and scalability to autonomous navigation systems.

References

1. C. E. Rankin, M. Bajracharya, L. Matthies, D. Helmick, and E. M. Robinson, Passive light stripe detection and tracking for rover navigation, Proc. SPIE, 6561, pp. 1–13, May 2007. [Online]. Available: https://www.robotics.jpl.nasa.gov/media/documents/spie2007-rankin65612.pdf.
2. D. Pfeiffer and U. Franke, Efficient representation of traffic scenes by means of dynamic stixels, Proc. IEEE Intelligent Vehicles Symposium (IV), pp. 217–224, Jun. 2010, doi: 10.1109/IVS.2010.5548054.
3. S. Choi, T. Kim, and W. Yu, Performance evaluation of RANSAC family, Proc. British Machine Vision Conference (BMVC), pp. 81–91, Sep. 2009, doi: 10.5244/C.23.81.
4. J. Zhang and S. Singh, LOAM: Lidar odometry and mapping in realtime, Proc. Robotics: Science and Systems (RSS), pp. 1–9, Jul. 2014, doi: 10.15607/RSS.2014.X.007.
5. B. Paden, M. C. ap, S. Z. Yong, D. Yershov, and E. Frazzoli, A survey of motion planning and control techniques for self-driving urban vehicles, IEEE Trans. Intell. Veh., 1(1), pp. 33–55, Mar. 2016, doi: 10.1109/TIV.2016.2578706.
6. J. Levinson, J. Askeland, J. Becker, et al., Towards fully autonomous driving: Systems and algorithms, Proc. IEEE Intell. Veh. Symp. (IV), pp. 163–168, Jun. 2011, doi: 10.1109/IVS.2011.5940562.
7. A. Broggi, C. Caraffi, R. Fedriga, and P. Grisleri, Obstacle detection with stereo vision for off-road vehicle navigation, Proc. IEEE Comput. Soc. Conf. Comput. Vis. Pattern Recognit. (CVPR), 1, pp. 65–72, Jun. 2005, doi: 10.1109/CVPR.2005.244.
8. L. I. L. Hendrikx, A. Sperber, and P. J. L. Verschuren, Night vision systems for sustainable mobility: Enhancing detection and recognition of vulnerable road users, Sustainability, 12(8), p. 3281, Apr. 2020, doi: 10.3390/su12083281. [Online]. Available: https://www.mdpi.com/2071-1050/12/8/3281.

9. H. Y. Hassan and A. N. Abdullahi, A preliminary study on obstacle detection system for night navigation, ResearchGate, 2020, doi:10.13140/RG.2.2.33982.27271

10. G. Dubbelman, Obstacle detection and avoidance for autonomous vehicles: A computer vision approach, M.Sc. thesis, Univ. of Amsterdam, 2007. [Online]. Available:

11. A. Kendall, B. Cipolla, and M. A. McDonald, Learning to drive autonomously using end-to-end deep learning: Vehicle control with RGB camera data, arXiv preprint arXiv:2010.15509, 2020. [Online]. Available: https://arxiv.org/abs/2010.15509.

12. A. Janai, F. Gu¨ney, J. Wulff, M. Black, and A. Geiger, Computer vision for autonomous vehicles: Problems, datasets, and state of the art, arXiv preprint arXiv:2107.11302, 2021. [Online]. Available: https://arxiv.org/abs/2107.11302.

3rd International Engineering Research Symposium 2025 (IERS 2025)
Colombo, Sri Lanka

Evaluation of Alkaline Hydrogen Peroxide Pretreated Bagasse, Paddy Straw, and Banana Stem Fibers for Cellulose-Based Composite Development

W. M. I. S. Jayaweera[1], M. M. H. Malshan[1] and T. N. Fernando[2]

[1]University of Moratuwa, Moratuwa, Sri Lanka
[2]General Sir John Kotelawala Defence University, Sri Lanka
isharasch.jaya@gmail.com

Abstract. Natural fiber reinforcement in sustainable construction materials has gained significant attention due to environmental concerns and resource availability. This study evaluates the comprehensive performance of cellulose fibers extracted from three Sri Lankan agricultural residues (bagasse, paddy straw, and banana stem) using alkaline hydrogen peroxide (AHP) pretreatment for composite development applications. Three pretreatment solutions with varying NaOH concentrations (1000, 1500, and 2000 mol/m³) combined with hydrogen peroxide were systematically evaluated through a factorial experimental design with 27 sample combinations, each replicated three times. Comprehensive characterization including weight loss analysis, holocellulose content determination, tensile strength testing (18.34-171.40 MPa), fiber diameter measurements (134.0-268.1 µm), FTIR spectroscopy, and SEM morphological analysis was conducted. Results demonstrated holocellulose content ranging from 86.63% to 95.90% with weight losses between 49.99% and 74.32%. Statistical analysis revealed that banana stem fibers exhibited the highest tensile strength (171.40 MPa), while the C1 pretreatment solution (1000 mol/m³ NaOH) was identified as the optimum concentration for maximizing holocellulose content (93.75%) while minimizing weight loss and processing costs.These findings demonstrate the significant potential of AHP-pretreated agricultural waste fibers as sustainable alternatives to synthetic reinforcements in construction composites, contributing to both waste valorization and environmentally friendly building materials development.

Keywords: Lignocellulosic. pretreatment, cellulose, alkaline hydrogen peroxide

1 Introduction

The construction industry's growing emphasis on sustainable materials has intensified research into natural fiber reinforcement systems as alternatives to synthetic counterparts. Environmental concerns, resource depletion, and health hazards associated with conventional reinforcing materials like asbestos have necessitated the development of eco-friendly alternatives [1-3].

Most cellulose in nature exists as lignocellulosic compounds containing cellulose, hemicellulose, and lignin in complex structural arrangements. The lignocellulosic matrix consists of hemicellulose polymers surrounding long cellulose chains, with both encased by lignin networks [1]. This hierarchical structure presents both opportunities and challenges for cellulose extraction, as the valuable cellulose component must be separated from lignin and hemicellulose while maintaining its structural integrity and mechanical properties.

Agricultural waste streams globally generate substantial quantities of lignocellulosic materials, including corn husks, corn stoves, bagasse, sugarcane leaves, guinea grass, banana stems, paddy straw, and various wood fibers. In Sri Lanka specifically, bagasse from sugar processing, paddy straw from rice cultivation, and banana stems from fruit production represent abundant, underutilized resources with significant potential for value-added applications [4-5].Cellulose, with its chemical formula $(C_6H_{10}O_5)_n$, exhibits favorable properties including low density, biodegradability, renewability, and satisfactory tensile strength and water absorption characteristics [2]. These properties make cellulose fibers suitable for diverse applications including food packaging, sustainable cement-based products, mortar systems, reinforcement of brittle building materials, and specialized filtration systems [3].

Several pretreatment methodologies exist for lignin removal from lignocellulosic materials, categorized into biological, chemical, and physical approaches. While biological methods offer environmental benefits, they typically require extended processing times. Physical methods may compromise fiber integrity, whereas chemical pretreatments provide controllable and efficient lignin removal [6-8]. Among chemical methods, alkaline pretreatment, microwave-assisted alkaline treatment, and alkaline hydrogen peroxide (AHP) pretreatment have demonstrated industrial viability.

Recent research has identified significant gaps in comprehensive performance evaluation of AHP-pretreated fibers from diverse agricultural sources, particularly regarding their suitability for composite applications. While individual studies have examined extraction efficiency, limited research has systematically evaluated the relationship between pretreatment parameters, fiber characteristics, and composite performance potential [9-11]. Fernando et al. [1] demonstrated that AHP pretreatment represents an effective, simple, and cost-efficient method operating at ambient temperature and atmospheric pressure, making it particularly suitable for industrial applications. However, comprehensive optimization studies comparing multiple agricultural residues and systematic evaluation of resulting fiber performance for composite applications remain limited.

Although cotton is naturally available cellulose, it is not suitable for this application as it is not abundantly available in Sri Lanka [5]. Therefore, in the present study, bagasse, paddy straw, and banana stems were selected as target materials due to their abundant

availability as agro-plant residues in Sri Lanka and their potential for sustainable fiber extraction.

The present study addresses these gaps by providing comprehensive performance evaluation of cellulose fibers extracted from three abundant Sri Lankan agricultural residues (bagasse, paddy straw, and banana stems) using systematic AHP pretreatment optimization. The research specifically aims to: (1) determine optimal pretreatment solution concentrations for maximum cellulose extraction efficiency with minimum material loss, and (2) comprehensively evaluate the structural, mechanical, and morphological characteristics of extracted fibers for composite reinforcement applications.

2 Materials and Methodology

2.1 Materials

Industrial-grade sodium hydroxide (NaOH), hydrogen peroxide (H_2O_2), and hydrochloric acid (HCl) were purchased. Bagasse samples were collected from Palwattha Sugar Industry, and other lignocellulose materials were collected from Hambantota District. All raw materials were sun dried and shredded using shredder machine.

2.2 Alkaline Peroxide Pretreatment

Pre-treatment solutions were prepared by mixing three different concentrations (C1, C2 & C3) of NaOH with equal volume (10 ml) and an equal volume (0.5 ml) of hydrogen peroxide (H_2O_2) as given in Table 1. Selected three lignocellulose materials were named as follows: bagasse (B), paddy straw (PS), and banana stem (BS). The experimental design was a two-factor factorial. Two variable factors were three plant residues and three pretreatment solutions. The experiment consists of nine treatments. Further, replicating each treatment three times, the experiment consisted of 27 samples. The experimental protocol was designed with a standardized biomass-to-solution ratio: each 1 g of lignocellulosic material was treated with 10 mL of pretreatment solution. For practical handling and replication consistency, batch processing involved scaling up to 5 g biomass with 50 mL solution in 500 mL beakers.

Table 1. Concentration of Pre-treatment Solution

Pre-treatment solution	NaOH Concentration
C1	1000 mol/m^3
C2	1500 mol/m^3
C3	2000 mol/m^3

The treatment protocol involved continuous mixing every 4 hours over a 24-hour degradation period at ambient temperature (25±2°C) and atmospheric pressure. Following pretreatment, samples underwent triple washing with distilled water, 2-hour immersion in 10% HCl solution for removing residual alkali and mineral impurities, final washing, and thermal treatment at 60°C for 4 hours according to AHP treatment procedure [1] to ensure complete moisture removal and fiber stabilization.

2.3 Fourier Transform InfraRed Spectroscopy Analysis

Both of Raw lignocellulosic materials of bagasse, paddy straw, banana stem, and pretreated fibers were analyzed using Fourier Transform Infra-Red spectroscopy to confirm successful cellulose extraction. The spectra were collected in the 4000–600 cm^{-1} range at 4 cm^{-1} resolution with an accumulation of 24 scans in transmittance mode. The test was performed at ambient conditions on a Bruker ALPHA spectrometer (Bruker Corporation, Billerica, MA).

2.4 Weight Loss Analysis and Holocellulose Content

Weight loss percentage was calculated using the formula: Weight Loss % = [(Initial dry weight - Final dry weight)/Initial dry weight] × 100. Initial moisture content was determined by oven-drying samples at 105°C until constant weight, and all calculations were based on moisture-free basis to ensure accuracy. Holocellulose content was determined using the chlorination method as described by Fernando et al. [1], calculated as: Holocellulose % = [(Weight after delignification)/Initial dry weight] × 100.

2.5 Scanning Electron Microscopy (SEM)

The selected three raw lignocellulosic materials and pretreated fibers from the AHP pretreatment were observed for surface morphology using Scanning Electron Microscopy (SEM). The samples were gold sputter coated prior to observation and examined with an accelerating voltage of 10 kV. Morphological analysis of fibers was performed on EVO 18, Carl Zeiss AG, Germany.

2.6 The Tensile Strength and Diameter

According to ASTM D3822–07, the tensile strength of pretreated fibers was measured using an Instron Universal Testing Machine. The diameter of pretreated fibers was measured by a Projectina microscope.

3 Results and Discussion

3.1 Weight Loss Percentage and Holocellulose Content

Fig. 1 and Fig. 2 show the variation of percentages of weight loss and percentage of hollow cellulose content of pretreated fibers, respectively. The concentration-dependent increase in weight loss (C1 < C2 < C3) reflects enhanced lignin and hemicellulose removal efficiency with increasing alkaline strength, consistent with previous findings [12-14]. ==The relationship between fiber type and weight loss percentage can be explained by the initial chemical composition: bagasse exhibited the lowest weight loss due to its higher lignin content (25.33%) [4], which provides more resistant structural components, while banana stem showed the highest weight loss corresponding to its lower lignin content (13%) [6], making it more susceptible to alkaline degradation. This relationship indicates that lower lignin content materials experience higher weight loss but potentially yield purer cellulose fractions.

Holocellulose content analysis demonstrated values exceeding 86.63% . Interestingly, bagasse samples showed higher holocellulose content in pretreated fibers compared to banana stem samples, which correlate with their initial cellulose content and structural stability during processing.

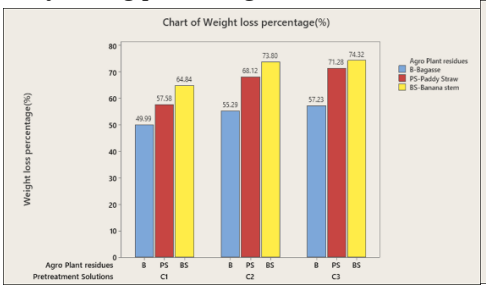

Fig.1. Variation of weight loss percentage

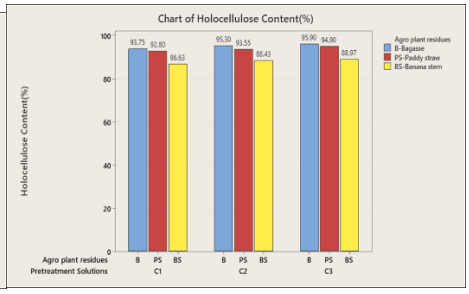

Fig.2. Holocellulose Content

3.2 Structural Characteristics

The comparison of FTIR results of raw bagasse, raw paddy straw, raw banana stem fibers, and pretreated fibers from the AHP pretreatment with three different pretreatment solutions (C1, C2, & C3) of lignocellulosic materials has confirmed that the extracted fibers were cellulose as a comparison of the wave number. Fig. 3, Fig. 4, and Fig. 5 show the FTIR spectra of raw and pretreated fibers from three different pretreatments of bagasse, paddy straw, and banana stem. The peak at 1732 cm^{-1} in raw fibers is assigned to the characteristic of aliphatic ester in lignin and/or hemicellulose [7]. Disappearing of this

peak in the treated fibers is due to the removal of most of the lignin and hemicellulose from the pretreated fibers. The peak at 893 cm^{-1} represents the glycosidic C–H deformation with ring vibration contribution and OH bending in the treated fibers, which indicates the typical structure of cellulose [3]. The broad peak was observed around 3445 cm^{-1} in the -OH stretching vibrations, and a small sharp peak that appeared at 2922 cm^{-1} is attributed to the C-H stretching vibration of cellulose.

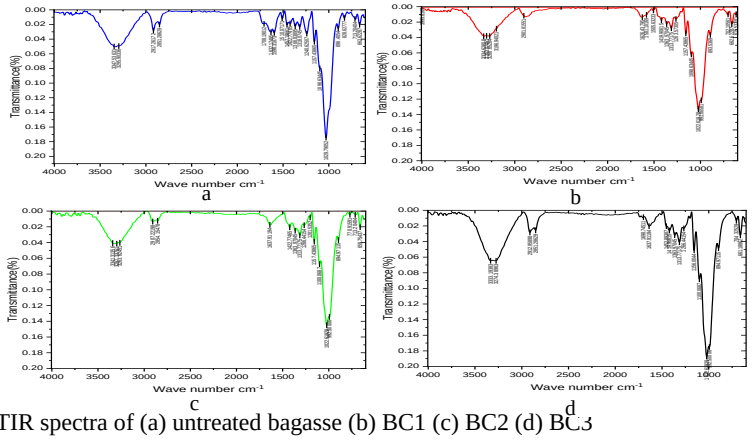

Fig.3. FTIR spectra of (a) untreated bagasse (b) BC1 (c) BC2 (d) BC3

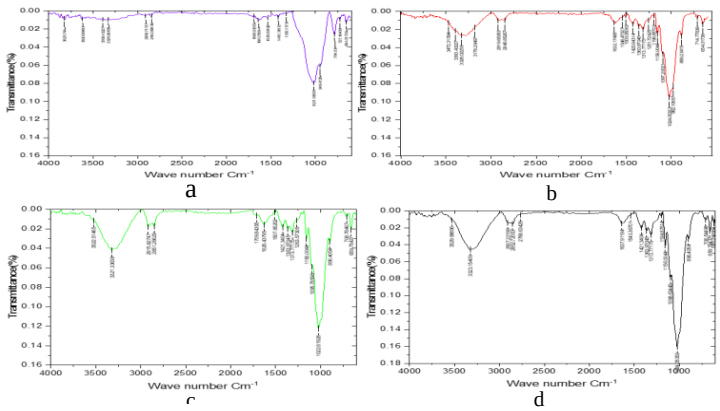

Fig. 4. FTIR spectra of (a) untreated paddy straw (b) PSC1 (c) PSC2 (d) PSC3

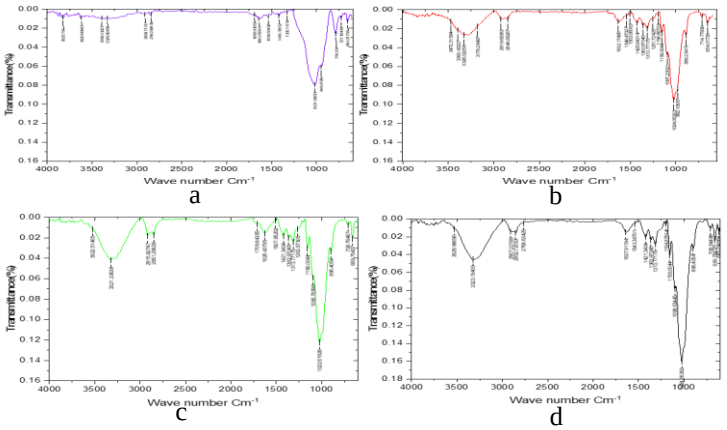

Fig. 5. FTIR spectra of (a) untreated banana stem (b) BSC1 (c) BSC2 (d) BSC3

3.3 Morphological Analysis and Mechanical Properties

The morphological features of raw lignocellulosic and pretreated three samples of bagasse, paddy straw, and banana stem from three different AHP pretreatment solutions Samples were analyzed by SEM images in Fig. 6 (a, b, c, d). Visual observation of the Image picture shows a comparatively smooth surface in raw fibers, and all pretreated fibers show a rough surface. This surface roughening indicates successful removal of lignin and hemicellulose matrices, exposing underlying cellulose fibrils and potentially enhancing fiber-matrix bonding in composite applications.

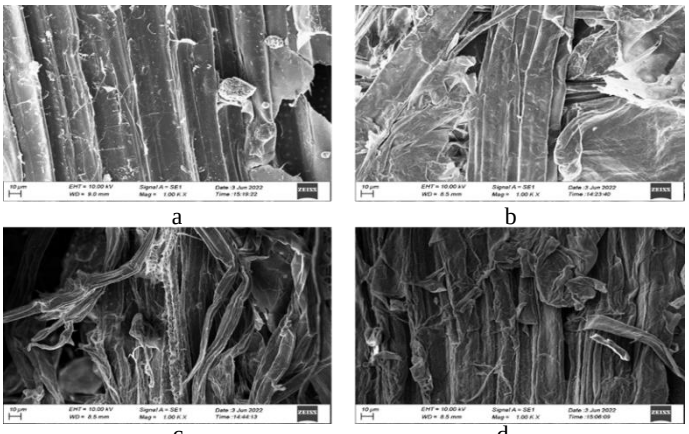

Fig. 6. SEM images of (a) untreated bagasse (b) BC1 (c) BC2 (d) BC3

Table 2. Fiber Diameter and Tensile Strength

Pre treatment Solution	Fiber Diameter (µm)	Tensile Strength (MPa)
B+C1	238.4	43.1
PS+C1	238.1	42.2
BS+C1	238.0	40.2
B+C2	268.1	20.0
PS+C2	268.0	18.5
BS+C2	265.0	18.3
B+C3	136.4	171.4
PS+C3	136.1	169.7
BS+C3	134.0	143.14

Table 2 shows the pretreated fiber's diameter and the fiber's tensile strength. Paddy straw fibers have a lower tensile strength. This may be due to the presence of significant amounts of silica particles; those particles reduce the hydrogen bond between the nano-fibers [8]. Although the same lignocellulosic material was pretreated with three different pretreatment solutions, there are no differences in tensile strength and dimeters.

3.4 Comparative Performance Analysis

According to Humphrey Danso, soil building blocks can be reinforced with natural fibers (coconut, oil palm, bagasse). The tensile strength and diameter of these fibers vary within a certain range. Bagasse fiber exhibits a tensile strength of 25-62 MPa and a diameter of 310-1190 µm. Oil palm fibers have a tensile strength of 65-141 MPa and a diameter of 190-820 µm. Coconut fibers exhibit tensile strength of 83-222 MPa and a diameter of 180-1010 µm [9]. Moreover, these pre-treated fibers (bagasse, paddy straw, banana stem) also can be effectively used to reinforce soil building blocks because these experimental pre-treated fibers' tensile strength and diameter meet requirements for developing soil building blocks.

A study by Elsaid reported the use of natural kenaf fibers to reinforce concrete, with the fiber tensile strength being nearly 160 MPa[10]. BSC1 and BSC2 pretreated fibers' tensile strength align with kenaf fiber tensile strength. Acidic pretreatment and ionic liquid are both pretreatment methods that can be used for the extraction of fibers from lignocellulosic materials. However, reactions happened in some elevated temperature and pressure conditions [10]. Comparing AHP, pre-treatment can be performed at room temperature and atmospheric pressure [1]. It is a low-cost and simple method for the extraction of fibers

from lignocellulosic materials (bagasse, paddy straw, banana stem). Cement mortar composite mixers can be reinforced with several fibers, such as asbestos, PET, PP, PE, carbon fiber, etc.

However, chemical instability and higher cost are several disadvantages of those composites; further, asbestos fibers are harmful to human health[11]. The incorporation of cellulose as a reinforcing material in cement mortar has the potential to mitigate these disadvantages.

3.5 Optimization and Selection Criteria

Based on a comprehensive evaluation considering multiple criteria, the optimization strategy aims to balance extraction efficiency, mechanical properties, and economic factors. The C3 treatment provides the highest tensile strength (up to 171.4 MPa) and maximum holocellulose content but requires greater chemical usage and higher processing costs. In contrast, the C1 treatment offers an optimal balance, with an acceptable holocellulose content (93.75%), minimal weight loss, lower chemical consumption, and cost-effectiveness. Therefore, C3 treatment is recommended for applications requiring maximum strength despite its higher costs, while C1 treatment is the preferred choice for general composite reinforcement applications, as it effectively balances performance and economic considerations.

4 Conclusions

This comprehensive study successfully evaluated the performance of cellulose fibers extracted from three Sri Lankan agricultural residues using alkaline hydrogen peroxide (AHP) pretreatment, addressing both extraction optimization and composite application potential. The findings reveal that pretreatment concentration significantly influences both extraction efficiency and fiber mechanical properties, with the C3 treatment achieving the highest tensile strength (up to 171.4 MPa), while the C1 treatment offers an optimal balance of holocellulose extraction (93.75%) with minimal weight loss and greater economic feasibility. Statistical analysis confirms significant performance differences among the fiber types, with banana stem fibers exhibiting superior mechanical properties and bagasse fibers demonstrating excellent extraction efficiency. FTIR and SEM analyses further verify successful lignin removal and retention of structural integrity, confirming the effectiveness of AHP pretreatment for cellulose preservation. Comparative analysis highlights that the pretreated fibers possess mechanical properties competitive with established nat-

ural fiber reinforcements, demonstrating their viability for sustainable composite applications. For practical implementation in Sri Lankan cement mortar composites, the C1 pretreatment solution is recommended for cost-effective production, as it balances acceptable holocellulose content, minimal processing costs, and sufficient mechanical performance for general reinforcement applications. However, for specialized high-strength applications, the C3 treatment is preferable despite its higher processing costs due to its superior mechanical properties. The demonstrated environmental benefits and efficient resource utilization position this technology as a valuable approach for sustainable construction material development and agricultural waste valorization. Future research should focus on composite fabrication and performance testing, scaling up the process, and conducting comprehensive techno-economic assessments to facilitate the commercial implementation of this sustainable fiber extraction technology.

References

1. N. Fernando, A. G. B. Aruggoda, S. A. Ariyadurai, C. K. Disanayaka, S. Kulathunge, Evaluation of Alkaline Peroxide Pretreatment for Extraction of Cellulose from Selected Plant Biomasses, ResearchGate. Accessed: Jun. 09, 2025. [Online]. Available: https://www.researchgate.net/publication/352506947_Evaluation_of_Alkaline_Peroxide_Pretreatment_for_Extraction_of_Cellulose_from_Selected_Plant_Biomasses
2. P. Harmsen, W. Huijgen, L. Bermudez, and R. Bakker, Literature review of physical and chemical pretreatment processes for lignocellulosic biomass,
3. X. Chen, J. Yu, Z. Zhang, C. Lu, Study on structure and thermal stability properties of cellulose fibers from rice straw | Request PDF, *ResearchGate*, doi: 10.1016/j.carbpol.2011.02.022.
4. H. Hajiha and M. Sain, The use of sugarcane bagasse fibres as reinforcements in composites, in *Biofiber Reinforcements in Composite Materials*, O. Faruk and M. Sain, Eds., Woodhead Publishing, 2015, pp. 525–549. doi: 10.1533/9781782421276.4.525.
5. Z. Yu, Y. Hu, and C. Qin, Research on Existing Problems and Improvement Measures of Fabricated Composite Wallboard, *E3S Web Conf.*, 248, pp. 03057, 2021, doi: 10.1051/e3sconf/202124803057.
6. Bioethanol Production from Banana Stem by Using Simultaneous Saccharification and Fermentation (SSF), IOPscience. Accessed: Jun. 09, 2025. [Online]. Available: https://iopscience.iop.org/article/10.1088/1757-899X/358/1/012004
7. R. Maryana, D. Ma'rifatun, A. I. Wheni, K. W. Satriyo, and W. A. Rizal, Alkaline Pretreatment on Sugarcane Bagasse for Bioethanol Production, *Energy Procedia*, 47, pp. 250–254, Jan. 2014, doi: 10.1016/j.egypro.2014.01.221.

8. M. L. Hassan, A. P. Mathew, E. A. Hassan, N. A. El-Wakil, and K. Oksman, Nanofibers from bagasse and rice straw: process optimization and properties, *Wood Sci. Technol.*, 46(1), pp. 193–205, Jan. 2012, doi: 10.1007/s00226-010-0373-z.

9. H. Danso, D. B. Martinson, M. Ali, and J. B. Williams, Physical, mechanical and durability properties of soil building blocks reinforced with natural fibres, *Constr. Build. Mater.*, 101, pp. 797–809, Dec. 2015, doi: 10.1016/j.conbuildmat.2015.10.069.

10. M. Badiei, N. Asim, J. M. Jahim, and K. Sopian, Comparison of Chemical Pretreatment Methods for Cellulosic Biomass, *APCBEE Procedia*, 9, pp. 170–174, Jan. 2014, doi: 10.1016/j.apcbee.2014.01.030.

11. J. B. Studinka, "Asbestos substitution in the fibre cement industry, *Int. J. Cem. Compos. Lightweight Concr.*, 11(2), pp. 73–78, May 1989, doi: 10.1016/0262-5075(89)90117-6.

3rd International Engineering Research Symposium 2025 (IERS 2025)
Colombo, Sri Lanka

IoT-Enabled Arduino-Based Monitoring and Protection System for Three-Phase Transformers

D. P. D. L. K. Nawarathna, G. T. H. Chandrapala, M. A. A. Marasinghe and S. D. Marasinghe*

Department of Electrical Engineering, Institute of Engineering Technology, Temple Road, Katunayake
*sakunsinghe@gmail.com

Abstract. This project presents an accurate and intelligent monitoring and protection system for three-phase transformers, emphasizing real-time data acquisition, advanced safety features, and proactive maintenance. Utilizing an Arduino-based platform, the system continuously monitors vital transformer parameters such as three-phase currents, oil level, oil temperature, and oil quality, while detecting critical conditions like overloading and phase loss. It incorporates load-sharing mechanisms to ensure balanced operation under varying loads, thereby reducing transformer stress and optimizing energy distribution. With both local and remote access capabilities, the system features integrated sensors, LCD visualization, and wireless communication to deliver a user-friendly interface for efficient data management and instant alerts. The project also explores the technical design, implementation strategies, and highlights the economic and environmental advantages of deploying such an innovative solution in modern power systems, ultimately enhancing transformer performance, reliability, and lifespan.

Keywords: Real-time monitoring, Transformer protection, Load-sharing, Arduino-based system

1 Introduction

Transformers are indispensable components in electrical power systems, playing a crucial role in the efficient transmission and distribution of electricity. By stepping voltage levels up or down, transformers help minimize energy losses during long-distance transmission

and ensure appropriate voltage levels for consumer use. Despite their robust design, transformers are vulnerable to operational stresses such as overloading, phase imbalance, oil degradation, and overheating. These faults, if undetected, can lead to severe consequences including transformer failure, power outages, system downtime, and safety risks. Conventional transformer monitoring relies heavily on manual inspection and periodic maintenance, which often fails to detect early signs of degradation. This reactive approach contributes to unexpected failures and increased operational costs.

In response to these challenges, the proposed project aims to design and develop a real-time, cost-effective transformer monitoring and protection system using Arduino microcontrollers and various sensors. The system is intended to monitor critical parameters such as three-phase current, oil temperature, oil level, oil quality (density and intensity), overloading conditions, and phase loss. These parameters are essential indicators of transformer health and performance. The collected data will be displayed locally on an LCD for on-site monitoring and simultaneously transmitted to a remote interface using the ESP32 Wi-Fi module, enabling maintenance personnel to access real-time data through mobile devices or computers. Alerts for abnormal conditions will be issued using LEDs to facilitate timely responses.

2 Literature Review

The integration of Internet of Things (IoT) technology in transformer monitoring systems has been explored in numerous recent studies. developed an IoT-based monitoring system using Arduino and ESP8266 to track oil level, temperature, and load current [1] . Their system demonstrated the benefits of remote monitoring and predictive maintenance. However, the ESP8266's limited processing power posed a performance constraint in data-intensive applications. Addressed this issue by implementing an ESP32-based system with dual-core processing [2], which enabled faster data handling and integration with the Blynk IoT platform for real-time visualization. Similarly, used ESP32 and Google Firebase for cloud-based monitoring with push notifications [3], highlighting the importance of user-centric design in modern monitoring systems.

Apart from monitoring, protection mechanisms have also been integrated into microcontroller-based solutions. Designed an Arduino-based transformer protection system that could disconnect the transformer during over-voltage, over-current, and high-temperature conditions [4]. Although effective locally, their system lacked remote access capabilities. Recent advancements now allow seamless integration of monitoring and protection through IoT platforms, enabling immediate alerts and automated protective actions.

Sensor integration plays a key role in determining system reliability. Low-cost sensors such as LM35, DHT11, and current transformers interfaced with Arduino and ESP32 [5] . They concluded that with adequate calibration and filtering, these sensors offer reliable performance suitable for cost-sensitive applications, though environmental resilience remains a concern.

By leveraging these technologies, this project proposes a scalable and affordable solution that addresses the limitations of conventional systems. It not only enhances transformer reliability and maintenance practices but also represents a significant step toward building smarter and more resilient electrical infrastructure through the adoption of embedded systems and IoT technologies.

3 Methodology

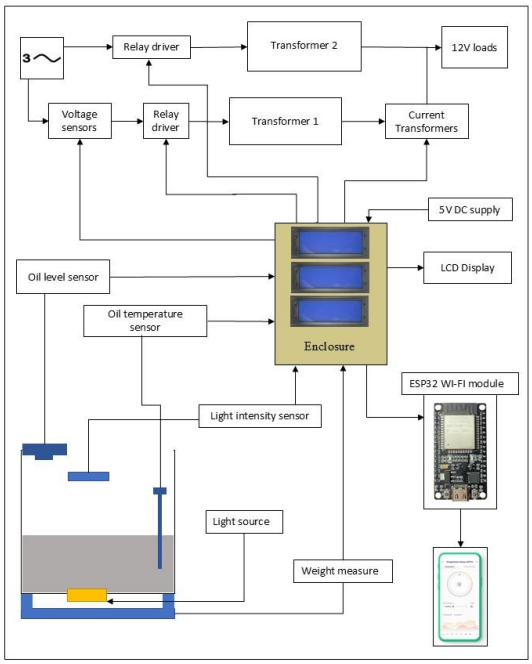

Fig. 1. Block diagram for the prototype design

The prototype design of the Three-Phase Transformer Monitoring and Protection System involved a structured approach to achieve real-time monitoring, fault detection, and preventive maintenance using affordable embedded technology. Key parameters such as voltage, current, oil temperature, oil level, and oil quality were identified due to their critical impact on transformer health. Components including sensors and microcontrollers were selected for their accuracy, range, and compatibility with the Arduino platform. The hardware setup involved circuit design for precise sensor data acquisition and relay-based protection control. Arduino Uno and Mega 2560 were used for system control, with programming in Embedded C, while the ESP32 module facilitated remote monitoring via the Blynk IoT platform. An I2C LCD was integrated for on-site data visualization. Calibration of sensors ensured reliable readings, and modular prototyping allowed for iterative refinement. This holistic integration of hardware and software delivered a scalable, user-friendly, and cost-effective solution for transformer monitoring and protection.

3.1 System Design

This project presents a comprehensive protection system for a three-phase transformer, integrating phase failure detection, load sharing, and oil monitoring. Phase failure is detected using ZMPT101B voltage sensors and an Arduino Uno, which disconnects the load if the voltage drops below the threshold. Load sharing is achieved with SCT013 current sensors, balancing the load between two transformers to prevent overloads. Transformer oil health is monitored via ultrasonic (level), BH1750 (intensity), load cell with HX711 (density), and DS18B20 (temperature) sensors. Real-time data is displayed on an LCD and alerts are triggered for abnormal conditions, ensuring safety, efficiency, and prolonged transformer life (Fig. 1).

Hardware Components

The hardware components are given in Table 1.

Software Development

Used the Blynk Data Monitoring system for our project to remotely monitor and control through a mobile app. Blynk IoT is a user-friendly cloud platform that enables real-time remote monitoring and control of hardware like ESP32 and Arduino via mobile apps or web dashboards. Its virtual pin system simplifies data exchange, supports cross-platform access, live sensor visualization, device control, and integrates with cloud services for enhanced IoT management.

Table 1. Components with Specification

Component	Function/Purpose
Arduino UNO (ATmega328P)	Microcontroller for basic data processing, sensor interfacing, and control in simpler system modules.
Arduino mega 2560 (Atmega2560)	Main microcontroller with more I/O pins and memory for handling complex processing and multiple sensors.
SCT013 30A/1V split-core current transformer	Measures AC current in transformer phases for load monitoring and load sharing control.
ZMPT101B voltage sensor	Measures AC voltage of each transformer phase to detect phase failure and voltage drops.
Relay module	Electrically isolates and switches high-power loads or circuits based on Arduino commands for protection.
Ultrasonic sensor	Measures transformer oil level by detecting the distance to the oil surface.
BH1750 light intensity sensor	Measures light intensity to assess transformer oil clarity or quality via oil transparency.
DS18B20 temperature sensor	Measures transformer oil temperature for thermal condition monitoring.
20x4 I2C LCD display	Provides local, real-time display of sensor readings and system status.
Relay MK3PN	Additional relay used for switching high current loads or multiple relay control in the system.
ESP32 WIFI module	Enables wireless communication for remote monitoring and control via IoT platforms like Blynk.

3.2 Phase Failure Protection System

Phase failure protection is a critical safety feature for 3-phase electrical systems, especially in transformers, motors, and other industrial equipment. It ensures that all three phases (R, Y, B) are present and balanced. If any one of the phases fails (due to a blown fuse, broken wire, or loose connection), it can cause severe damage to the equipment, including overheating, vibration, and insulation failure. To prevent this, a protection mechanism can be implemented using an Arduino Uno, ZMPT101B voltage sensors, and a relay module.
In this system, three ZMPT101B voltage sensors are used to monitor the voltage levels of each of the three phases. These sensors are designed to measure AC voltage and provide a corresponding analog signal to the Arduino. Each ZMPT101B sensor is connected to one of the phases (R, Y, or B), and the Arduino reads the analog voltage values through its analog input pins. These sensors are chosen because they are compact, accurate, and provide electrical isolation between the high-voltage line and the Arduino. The Arduino Uno acts as the central controller. It continuously checks the input from the three

ZMPT101B sensors. Under normal conditions, all three sensors report voltages within an expected range. If the Arduino detects that the voltage from any one phase has dropped significantly below the threshold (indicating a phase loss), it triggers the protection mechanism. To respond to the fault, the Arduino activates a relay module. The relay cuts off the power supply to the transformer or load, thereby isolating the equipment and preventing damage. The Circuit arrangement is shown in Fig. 2.

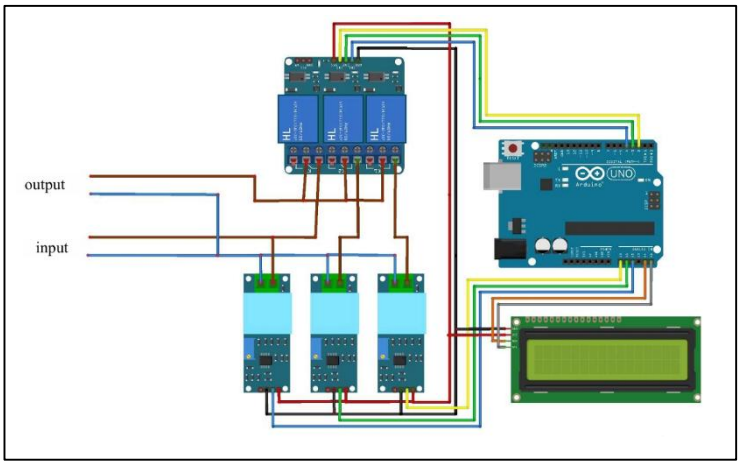

Fig. 2. Phase failure protection system circuit arrangement

3.3 Load Sharing System

In a load-sharing system using two 3-phase transformers, an Arduino Uno can be used to intelligently monitor and control the distribution of electrical load between the transformers to prevent overloading. The setup includes current transformers (CTs), voltage sensors, and protection relays installed on both transformers. The CTs measure the current drawn by each transformer, while the voltage sensors monitor the system voltage. These sensor readings are fed into the Arduino Uno, which continuously analyzes the load on each transformer. If the Arduino detects that one transformer is approaching its rated capacity, it automatically activates relays to transfer a portion of the load to the second transformer, thereby balancing the load between the two units. This method protects the transformers from thermal damage due to overloading and ensures efficient operation. Additionally,

this automated system can be programmed to display real-time values on an LCD or transmit data to a monitoring station, enhancing system reliability and operational transparency. The Circuit arrangement is shown in Fig. 3.

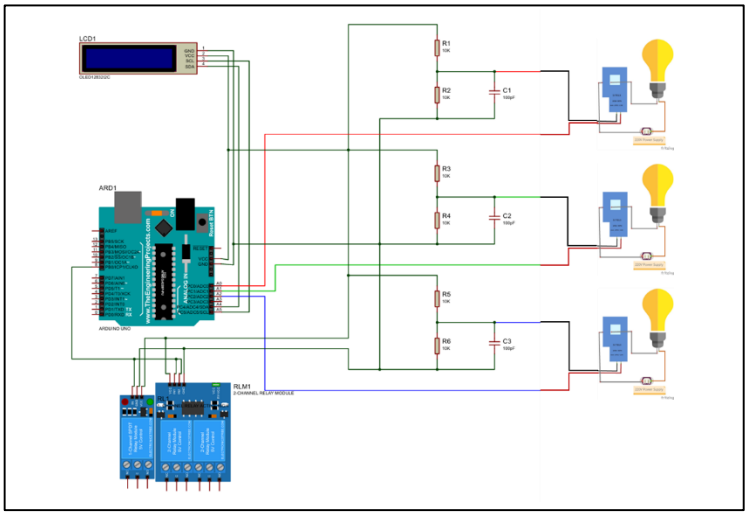

Fig. 3. Load sharing system circuit diagram

3.4 Oil Testing Unit

This system integrates multiple sensors to monitor transformer oil conditions in real-time, measuring oil level (via ultrasonic sensor), light intensity (BH1750 sensor for quality inference), density (load cell and HX711 module), and temperature (DS18B20 sensor). It processes data using an Arduino, displays results on an LCD, and triggers alerts (e.g., buzzer for high temperature or low oil levels) to ensure proactive maintenance. By combining these measurements, the system enhances transformer reliability, prevents failures, and optimizes operational efficiency.

Measure Oil Level

This is done by measuring and displaying the oil level in a tank using an ultrasonic sensor and an LCD. During each loop, the ultrasonic sensor sends a 10-microsecond pulse, and the time taken for the echo to return is measured. This duration is converted to a distance in inches, which represents the empty portion of the tank. The oil level percentage is then calculated using the formula, which is shown in Fig. 4.

$$\text{Percentage} = \frac{\text{Set value} - \text{inches}}{\text{Set value}} \times 110$$

Fig. 4. Percentage formula

- ✓ The set value is the maximum tank height.
- ✓ The factor 110 adjusts for scaling or unit conversion

The calculated percentage is displayed on the LCD along with a status message indicating whether the level is low (below 40%), or full (above 80%).

Measure Oil Intensity

This is done by measuring light intensity using a BH1750 light sensor to infer oil quality and display the results on an LCD. In the setup phase, the BH1750 sensor and LCD are initialized, and a test message is sent to the serial monitor. During each loop, the BH1750 reads ambient light intensity in lux, which is displayed on the first line of the LCD and printed on the serial monitor. The program then checks if the lux value is below a threshold of 800 lx.

Measure Oil Density

This is done by measuring and displaying the density of oil in a tank using a load cell sensor and HX711 module. In the setup, the system initializes the HX711 module and calibrates the scale with a predefined calibration factor. The load cell measures the mass of an object placed on it, and the system subtracts a calibration offset to ensure accurate readings. The density is 13, then calculated by dividing the measured mass by a known volume of 400 ml, using the Fig. 5 formula.

$$\text{Density} = \frac{\text{Mass}}{\text{Volume}}$$

Fig. 5. Density formula

Measure Oil Temperature

This is done by measuring the oil temperature using a DS18B20 temperature sensor and displaying the results on an LCD display. It continuously reads the temperature from the sensor, converting the raw data to Celsius and Fahrenheit. If the temperature exceeds 100°F, the code activates a trigger that buzzes to alert the user. The sensor communicates

with the Arduino through the one-wire protocol, with specific functions to handle reading and writing data. The main loop reads the temperature, displays it on the LCD, and checks if the temperature exceeds the threshold.

4 Results

4.1 Phase Failure Protection System

In this project, this is done by monitoring and protecting a three-phase transformer from phase failure or voltage drops. It calculates RMS voltage values for each phase 230V (R, Y, and B) using ZMPT101B voltage sensors connected to analog pins. The voltage drop checks and compares the RMS voltage of each phase to a predefined threshold and determines if a phase is down or available. If any phase voltage falls below 215V the threshold, the activates all relays, which are connected to digital pins, to protect the transformer. It displays the relay status are ‘ON’ or ‘OFF’. When all phases are normal, the relays are deactivated. The system logs voltage readings and phase status to the Serial Monitor for debugging and updates the LCD in real-time. This setup effectively prevents damage to the transformer in the event of a phase failure or voltage drop.

The system incorporates three switches to simulate phase faults in a three-phase transformer setup. In the current configuration (as shown in Fig. 6), all three switches remain in the "off" position, indicating no simulated faults are active. As a result, the transformer operates normally, delivering uninterrupted power to the output load (as shown in Fig. 7). This design allows for controlled testing of fault conditions.

Fig. 6. Switches to make the faults

Fig. 7. Delivering power to the output load

When any switch is turned "on" (as shown in Fig. 8), it triggers a corresponding phase fault, enabling the system to demonstrate protective responses to shut down the transformer

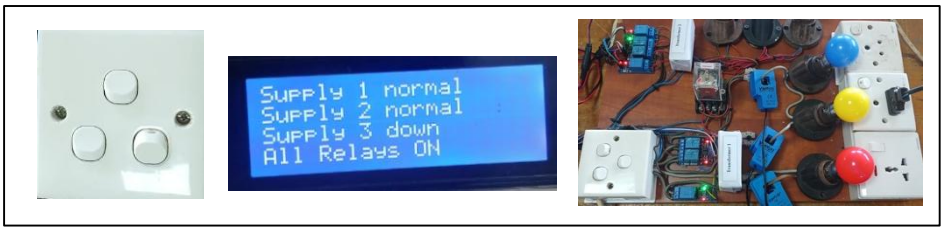

Fig. 8. In-phase fail condition

4.2 Load Sharing System

In this project, this is done by implementing a three-phase transformer load-sharing system by monitoring current and power in each phase (R, Y, B) using SCT013 30A/1V split-core current transformers and adjusting relay states to ensure proper load sharing. If the load current exceeds 5A the relays turn on and activate load-sharing operation. Each phase's current values and relay condition ('ON' or 'OFF') are displayed on an LCD display. The loop function continuously reads current, calculates power, updates relay states, and displays data. This system ensures balanced transformer load distribution by activating relays for overloaded phases, preventing overheating and phase imbalance, and maintaining transformer efficiency.

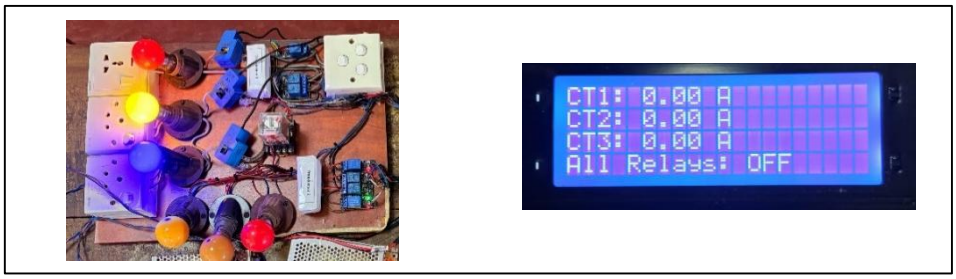

Fig. 9. In the normal condition

In normal conditions where there is no load applied to the transformer and it does not exceed its rated maximum current, then the LCD display indicates that the relays are 'OFF,' as in Fig. 9.

If the high load is applied to the transformer (transformer 1), the load is shared with the other transformer (transformer 2), and it displays as relays are 'ON' and displays each phase current as in Fig. 10.

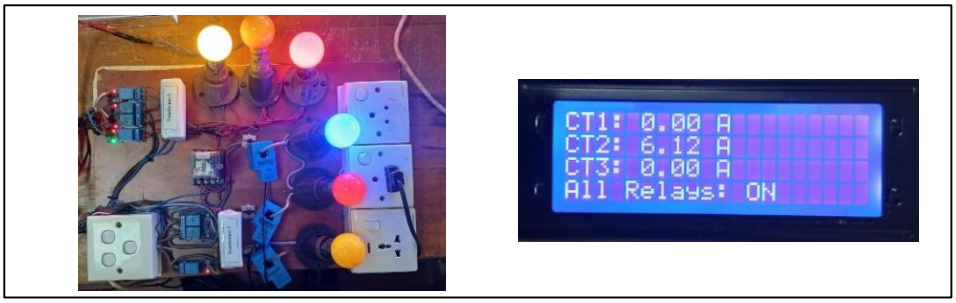

Fig. 10. When a high load is applied to the phase

4.3 Oil Testing Unit

The system successfully monitors four critical parameters of transformer oil to ensure optimal performance and safety. The oil level is accurately measured using an ultrasonic sensor, with results displayed as a percentage on an LCD, including status alerts for low (<40%) or full (>80%) levels. Oil quality is inferred through light intensity measurements via a BH1750 sensor, with readings below 800 lux indicating potential issues. Density is calculated using a load cell and HX711 module, where mass is divided by a known volume (400 ml) to determine oil consistency. Temperature is tracked with a DS18B20 sensor, notify if exceeding 100°F to prevent overheating risks. All data is displayed in real-time on an LCD, providing a comprehensive and user-friendly interface for proactive maintenance and fault detection, as shown in Fig. 11. This integrated approach enhances transformer reliability by addressing key operational factors—level, quality, density, and temperature through precise sensor measurements and timely alerts.

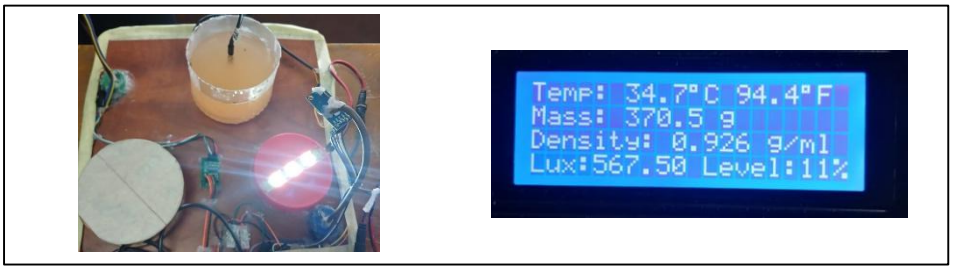

Fig. 11. Oil testing unit and display

Also, oil testing results are displayed and monitored and displayed on mobile or desktop via the Blynk Data Monitoring system show as Fig. 12.

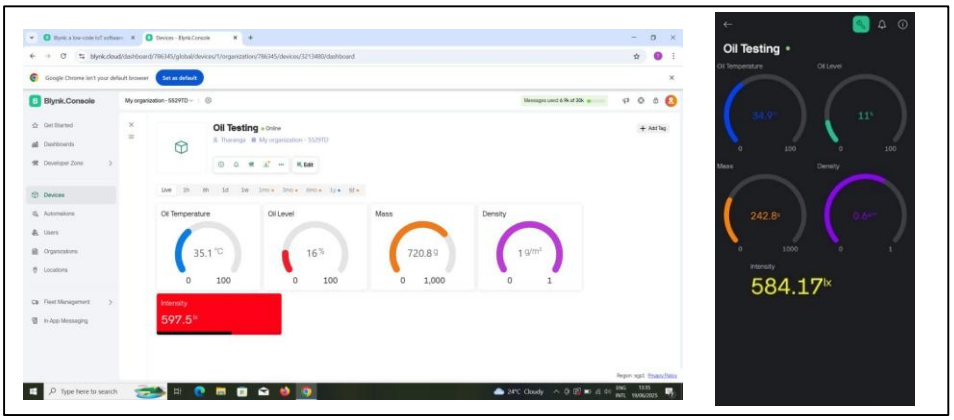

Fig. 12. Oil testing results

5 Future Improvements

- Use advanced sensors with auto-calibration for accurate measurements, and incorporate prototype sensors for Vacuum Circuit Breakers (VCB) and Air Circuit Breakers (ACB) to enhance monitoring and protection capabilities.
- Add backup communication options like GSM or LoRa for reliable connectivity.
- Store data in the cloud and use advanced analytics for monitoring and maintenance.
- Use durable industrial microcontrollers instead of Arduino for tough environments.
- Design the system to easily handle bigger or multiple transformers.
- Include battery backup to keep the system running during power cuts.
- Use special sensors to better check oil quality and contamination.
- Create a user-friendly mobile app or web dashboard with alerts and reports.
- Protect the system with weatherproof cases against dust, humidity, and heat.

6 Discussion

The Arduino-based transformer monitoring system enables real-time tracking, proactive maintenance, overload protection, and remote access, improving reliability, efficiency, and safety. Key limitations include sensor accuracy, reliance on stable Wi-Fi and power, environmental impacts, limited industrial scalability, and integration challenges. Despite this, it is well-suited for low-cost, small to medium-scale systems. Future enhancements like better sensors, GSM/LoRa communication, cloud analytics, rugged enclosures, industrial-grade microcontrollers, and power backup can expand its performance and industrial applicability. Overall, it is a promising step toward smarter, more resilient transformer management.

7 Conclusions

The project developed a real-time monitoring and protection system for three-phase transformers using Arduino and various sensors to track phase voltages, current, oil level, temperature, and quality. It included safety features like phase failure detection, load sharing, and abnormal condition alerts. The system offered local display and remote access via ESP32 and Blynk IoT for timely maintenance, enhancing reliability, safety, and energy efficiency. Despite sensor accuracy and power dependence limitations, it lays a foundation for future industrial scalability, data logging, and AI-based fault prediction, advancing smart grid modernization.

References

1. G. S. Sivakumar et al., IoT based transformer monitoring system using Arduino and ESP8266, Int. J. Eng. Res. Technol., 9(4), pp. 567–573, 2020.
2. D. Patel et al., Smart transformer monitoring system using IoT, J. Emerg. Technol. Innov. Res., 8(6), pp. 345–352, 2021.
3. A. Gupta et al., Cloud based transformer monitoring system using ESP32, Int. Res. J. Eng. Technol., 6(4), pp. 1234–1240, 2019.
4. K. R. Raj and D. Kumar, Transformer protection using Arduino microcontroller, Int. J. Adv. Res. Electr. Electron. Instrum. Eng., 6(3), pp. 1789–1795, 2017.
5. R. P. Singh et al., Performance evaluation of low-cost sensors for power transformer monitoring, IEEE Sensors J., 18(22), pp. 9234–9241, 2018.

3rd International Engineering Research Symposium 2025 (IERS 2025)
Colombo, Sri Lanka

Smart Scale: An IoT-Enabled Weighing Solution

W. P. R. S. Perera, H. A. H. M. Hettiarachchi, K. H. A. J. C. Kumara and S. D. Marasinghe*

Department of Electrical Engineering, Institute of Engineering Technology, Temple Road, Katunayake
*sakunsinghe@gmail.com

Abstract. The Smart Scale: An IoT-Enabled Weighing Solution is an innovative project designed to automate weight measurement, data logging, and remote monitoring through the integration of the Internet of Things (IoT). This system utilizes a load cell sensor to measure the weight of objects and a microcontroller to process and transmit the data to a Google Spreadsheet for real-time storage and analysis. The project offers a user-friendly interface with a simple push-button control and displays the weight data on an LCD screen for immediate viewing. Traditional weighing methods often involve manual data entry, which can lead to errors, inefficiencies, and challenges in accessing historical data. This IoT-enabled smart scale system addresses these issues by providing accurate and automated weight measurement, along with the ability to monitor and analyze data remotely. The integration with cloud-based tools, such as Google Sheets, ensures that data can be accessed and analyzed from anywhere, offering flexibility and convenience for users. This project prioritizes simplicity, portability, and real-time functionality, making it an ideal solution for small-scale producers, such as in tea production or honey harvesting, where precise weight measurement is critical.

Keywords: Smart Scale, IoT Weighting System, Real-Time Monitoring, Cloud Data Storage, Local Server

1 Introduction

The Internet of Things (IoT) has transformed many industries by enabling smarter, automated, and more efficient solutions. One significant innovation is the **Smart Scale: An IoT-Enabled Weighing Solution,** which modernizes traditional weighing methods by introducing automation, remote monitoring, and real-time data analysis. This system provides an accurate and efficient alternative to manual weighing, which is often slow, labor-

intensive, and prone to human error. By leveraging IoT technology, the Smart Scale reduces inaccuracies and streamlines the weighing process, improving productivity and reliability in various operational environments [1] [2]. This project utilizes a **load cell sensor**, a device that converts weight into an electrical signal, paired with the HX711 amplifier module to precisely measure the weight of objects. The data is collected and processed by a microcontroller such as the ESP8266 or ESP32, which plays a central role in handling sensor inputs, performing necessary calibrations, and managing data transmission. The system offers flexibility by sending weight data to either a cloud-based platform like Google Sheets or a local server environment running XAMPP (Apache, MySQL, PHP). This dual option supports both internet-enabled and offline scenarios, ensuring continuous data logging and accessibility. Additionally, a local LCD screen displays real-time weight readings, providing users with immediate feedback, while remote web interfaces enable monitoring, historical data analysis, and reporting through intuitive dashboards and alerts [3] [4] [5].

Accurate and timely weight measurement is critical in industries such as tea production**,** honey harvesting**,** agriculture, food processing, pharmaceutical manufacturing, and other small to medium-scale enterprises. These sectors often rely on manual weighing processes that are time-consuming and susceptible to mistakes, lacking systematic data storage for performance analysis and traceability. The Smart Scale addresses these pain points by integrating IoT-enabled automation with affordable and readily available hardware components. This integration not only improves accuracy and efficiency but also supports data-driven decision-making by maintaining comprehensive historical records accessible from anywhere at any time, enhancing transparency and operational control [6].

The Smart Scale system is designed with portability and ease of use in mind. Its compact hardware footprint and low power consumption make it suitable for deployment in diverse environments, including remote or outdoor locations where traditional weighing infrastructure is impractical. The system's modular architecture allows for easy customization and scalability, enabling users to adapt it to various weighing requirements and integrate additional sensors or communication modules as needed. The primary goal of this project is to develop a portable, user-friendly, and cost-effective IoT weighing system that enhances operational efficiency. By automating data collection and storage, the system reduces human intervention, minimizes errors, and provides businesses with easy access to real-time and historical weight data. This capability empowers small-scale industries to optimize resource management, improve quality control, and scale their operations with reliable technological support.

While several existing solutions demonstrate IoT-based weighing scales, this project differentiates itself through several key innovations. Firstly, it offers a hybrid data logging architecture, enabling seamless transmission to both cloud platforms (Google Sheets) and

local servers (XAMPP), ensuring operational resilience in environments with intermittent internet connectivity. Secondly, the system is designed as a fully portable, self-powered unit, integrating a battery management system, which is often omitted in comparable designs. Finally, this work provides a complete end-to-end solution from hardware sensor interfacing and calibration to a sophisticated web-based dashboard for data visualization and management, offering a level of practicality and user accessibility that extends beyond the scope of typical prototype demonstrations.

2 Methodology

The methodology for this project involves a systematic approach to designing, implementing, and testing an IoT-enabled weighing system. The development of the Smart Scale follows the steps of requirement analysis, design, component selection, and integration, followed by system implementation and testing. The methodology encompasses both hardware and software aspects, where the hardware includes a load cell, HX711 amplifier module, ESP32 microcontroller, and cloud storage for data, while the software is focused on controlling the system, collecting data, and visualizing it in real-time. The IoT-enabled weighing system operates by measuring the weight of items through the load cell, which transduces weight into an electrical signal.

This signal is amplified by the HX711 module, and the resulting data is then processed by the ESP32 microcontroller. The microcontroller sends the data to a cloud platform for real-time monitoring and analysis. Additionally, an LCD screen is used to display real-time weight readings, providing a direct interface for users to interact with the system. The system is designed to be user-friendly and cost-effective, ensuring that it can be easily deployed in various small-scale industrial settings.

2.1 System Design

The system is designed to perform real-time weight measurement using a load cell connected to an HX711 amplifier module, which in turn is connected to an ESP32 microcontroller. The ESP32 processes the analog data, converts it into readable weight units, and displays the value on an LCD. Once stabilized, the data is sent via Wi-Fi to a Google Sheet for cloud storage. The control flow begins with powering on the device, initializing modules, calibrating the sensor if required, continuously reading the weight, checking for stability, and finally displaying and transmitting the value. Push buttons allow user interaction for reset or calibration (Fig. 1).

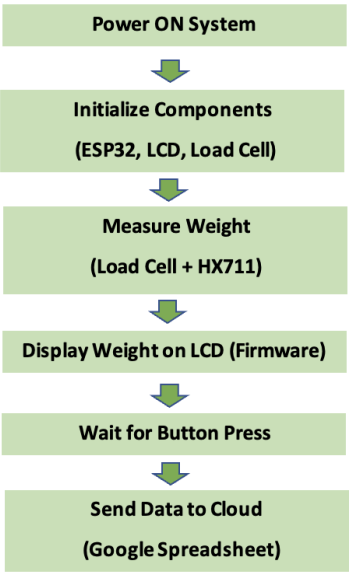

Fig. 1. System Design Flow Chart

2.2 Materials and Components

The Smart Scale project integrates several key hardware and software components to build a functional IoT-based weighing system. Below is a list of hardware components and software tools shown in Tables 1 and Table 2.

Hardware Components

Table 1. Components with Specification

Component	Function/Purpose
ESP32 Microcontroller	Processes sensor data, handles Wi-Fi communication, and sends data to the server/cloud.
Load Cell with Structure (200 kg)	Measures object weight and converts it into analog signals.
HX711 Amplifier Module	Amplifies and converts analog load cell signals to digital for microcontroller input.

TP4056 Charging Module	Manages safe charging of the lithium-ion battery.
20x4 LCD Display	Displays weight values and system messages in real time.
I2C Interface Board	Simplifies LCD communication with ESP32 via I2C protocol.
Lithium-ion Battery	Supplies portable power to the system.
Push buttons (stainless steel)	Used for user input: Send & Tare (Reset).
Power Boost Voltage Converter	Converts lower battery voltage to a stable 5V required for ESP32 and peripherals.
Jumper Wires (Set)	Connects all components in the circuit.
Mini Rocker Switch	Turns the system on or off manually.
Enclosure/Packaging Box	Protects components and ensures safe, neat installation.

Software Tools

Table 2. Tools with Specifications

Software Component	Function/Purpose
Arduino IDE	Used to write, compile, and upload code to the ESP32 microcontroller.
PHP (on XAMPP)	Processes incoming weight data and stores it in the MySQL database.
MySQL (on XAMPP)	Stores real-time and historical weight data for retrieval and analysis.
phpMyAdmin	Provides a web interface to manage the MySQL database.

2.3 Circuit Assembly

The load cell is connected to the HX711 amplifier module, which amplifies the signal from the load cell and converts it into a digital output. Then, the HX711 is connected to the ESP32 microcontroller via the appropriate pins (SCK and DT for data transfer). The ESP32 microcontroller is connected to the HX711, LCD, push button, and TP4056 charging module. The TP4056 charging module is used to charge a lithium-ion battery, which powers the ESP32 and other components, allowing for portability. The I2C pins (SDA, SCL) are connected between the ESP32 and the LCD module. The push button is wired to an input pin of the ESP32. Fig. 2 shows the complete circuit.

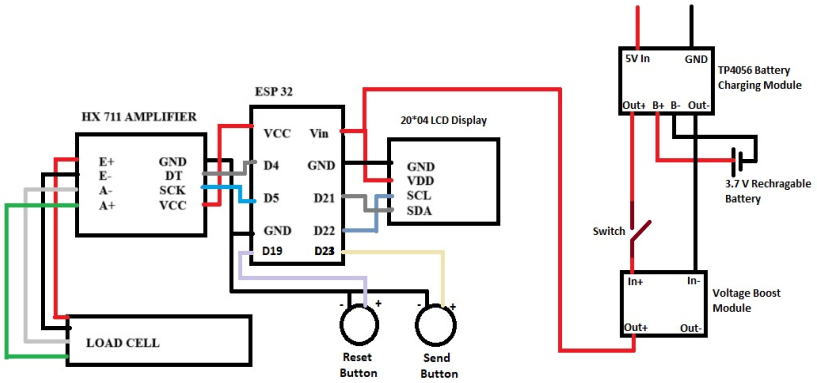

Fig. 2. Circuit Diagram

2.4 Software Development

The ESP32 was programmed to initialize the sensor, calibrate it using known weights, and convert the digital readings into human-readable weight measurements. The microcontroller connected to a Wi-Fi network and periodically transmitted weight data to a web server via HTTP requests. The firmware was written using the Arduino IDE and involved the use of libraries for sensor communication and HTTP client handling. The data transmitted included the weight value, and on the server side, the date and time of each reading were also recorded.

Software Implementation Details

To ensure reproducibility, the key aspects of the software implementation are detailed below. The firmware was developed using the Arduino IDE (v2.3.2) and relied on the following libraries: HX711_ADC (v2.0.1) for sensor communication, LiquidCrystal_I2C (v1.1.4) for the LCD, and the built-in WiFi and HTTPClient libraries for connectivity.

The scale must be calibrated against known weights; this process calculates a calibration factor which is stored in non-volatile memory. The main loop continuously reads the load cell value, converts the raw sensor data to grams using the stored factor, and displays it on the LCD. The conversion formula is:

weight_grams = (raw_value - offset) / calibration_factor; // Pseudo-code

When the user presses the 'Send' button, the firmware checks if the reading is stable. If stable, it constructs an HTTP POST request to the server. The request sends the weight value as a query parameter:

POST /post-data.php?weight=5076.72 HTTP/1.1
On the server side, a PHP script (post-data.php) receives this request. It validates the input, sanitizes the data to prevent SQL injection, generates a timestamp, and inserts the record into the MySQL database using a simple SQL query:

INSERT INTO scale_data (weight, date, time) VALUES (5076.72, '2025-06-13', '14:30:05')

2.5 Local Server Configuration Using XAMPP

Server Environment Setup

XAMPP software was used to configure the local server environment. It provided an Apache web server to host PHP scripts and a MySQL server to manage the database. Both modules were launched and controlled through the XAMPP control panel shown in Fig. 3.

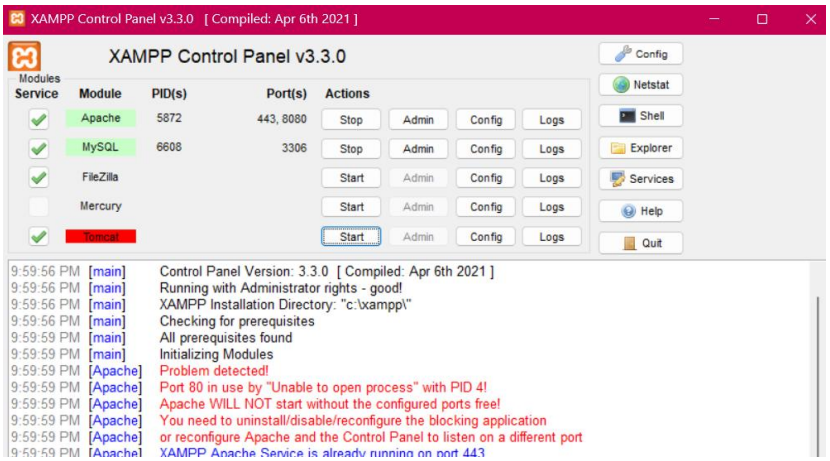

Fig. 3. XAMPP Control Panel with Apache and MySQL Services Running

Database Creation and Table Structure

A MySQL database named smartscale1 was created using phpMyAdmin. Within it, a table named "scale data" was designed to store the following fields shown in fig. 4:

- ID: Auto-increment primary key
- Weight: Float value representing measured weight
- Date: Date of the reading
- Time: Time of the reading

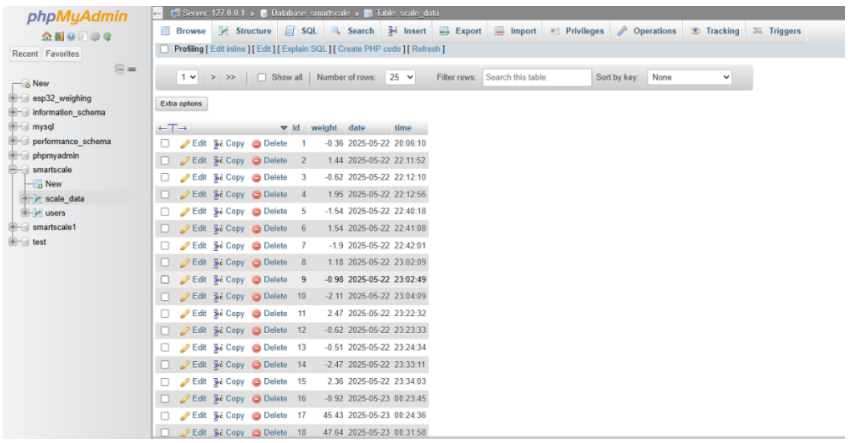

Fig. 4. Database Table Structure in phpMyAdmin

PHP-Based Data Handling

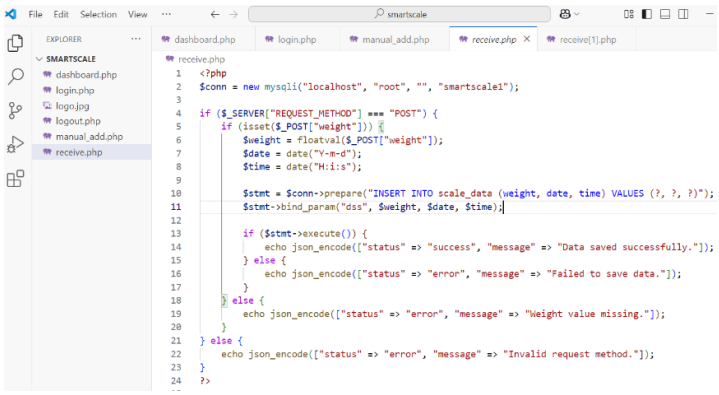

Fig. 5. PHP Script for Data Insertion

A PHP script shown in Fig. 5 was developed to receive HTTP POST requests sent by the ESP32. This script parsed the received weight data, generated a timestamp using the server clock, and inserted the data into the MySQL table.

3 Testing and Calibration

Testing and calibration are essential phases to ensure the proper functioning, reliability, and accuracy of the Smart Scale system. These processes help identify issues, validate system performance, and determine how well the project meets its objectives.

3.1 Initial Testing

After the hardware and software are integrated, the system is tested to ensure that the components work together seamlessly. During testing, the system is checked for weight accuracy, LCD functionality, button press response, and cloud connectivity.

3.2 Calibration of Load Cell

Calibration was performed using a set of known weights shown in Fig. 6 to determine the sensor's response factor. The calibration factor was adjusted by comparing sensor readings with actual weight values until high accuracy was achieved.

Testing included:

- Taring the scale to zero before use.
- Measuring sample weights from 100 g to 5 kg.
- Verifying the consistency of results over time.

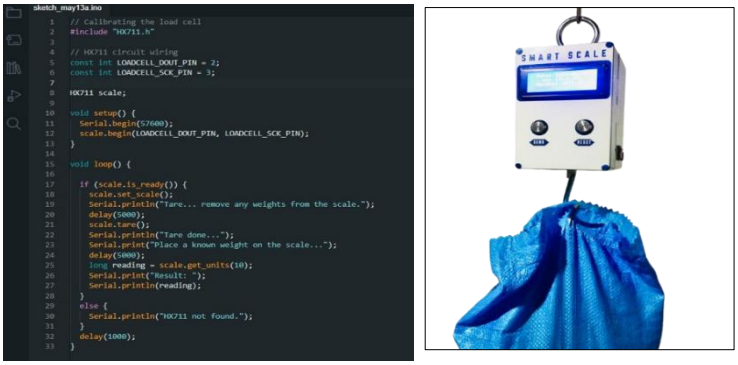

Fig. 6. Calibration Procedure with Known Weights

3.3 Connect to local Wi-Fi.

The microcontroller (such as ESP8266 or NodeMCU) is configured to connect to a local Wi-Fi network using a predefined SSID and password shown in Fig. 7. Upon successful connection, the system retrieves the current date and time from an online time server (via NTP) and displays it on the LCD screen along with the connection status. This ensures proper time-stamped data logging before sending weight data to the cloud.

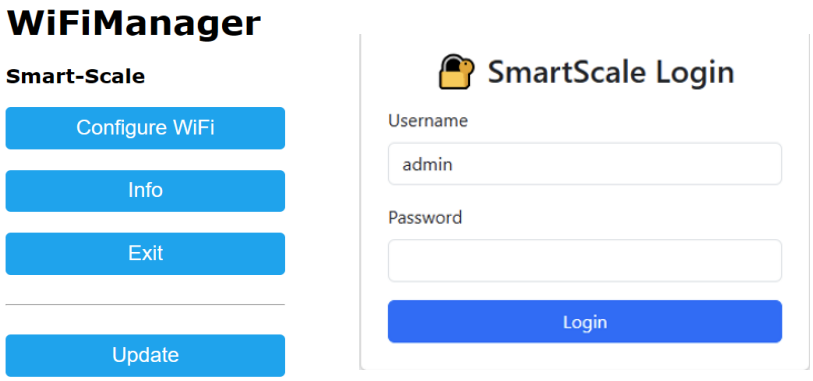

Fig. 7. Wi-Fi manager with login interface

3.4 Results

The final prototype was tested in a real-world scenario. The prototype device is shown in Fig. 8. The system was powered continuously and validated over several hours to ensure performance. The local database captured the weight values accurately and in real-time, with successful transmission of data from sensor to server.

The measurements from the two scales (Fig. 8: real-world scale; Fig. 9: smart scale) show a slight discrepancy. The real-world scale recorded a weight of 5070g, while the smart scale displayed 5076.72g, resulting in a +6.72g error (0.13% deviation). This minor difference is likely due to calibration drift, environmental factors, or variations in placement on the smart scale. Given the real-world scale's declared tolerance of average +4.9 g.

The Google spreadsheet documents shown in Fig. 11 record the weight measurements captured by the weighing system in real time. The sheet consists of three columns which are Date, Time, and Weight (in grams), which together provide a clear, timestamped record of all weighing performed by the load cell and HX711 sensor.

Fig. 8. Final Smart Scale Product

Fig. 9. 5 kg Rice bag measurement using scale

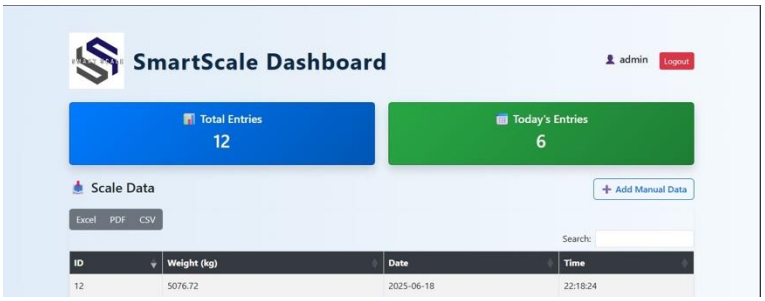

Fig. 10. 5kg Rice bag measurement using Smart Scale

This data is valuable for a range of purposes, including keeping a permanent backup of measurements, analyzing trends or fluctuations in weight over time and generating reports or charts for further insight. Furthermore, because the data is stored on Google Sheets, it can be accessed remotely from any location with an internet connection, allowing for convenient and flexible monitoring of the weighing process and this approach efficiently integrates real-time data collection with permanent storage and analysis, making it a useful tool for small-scale industrial applications and inventory control.

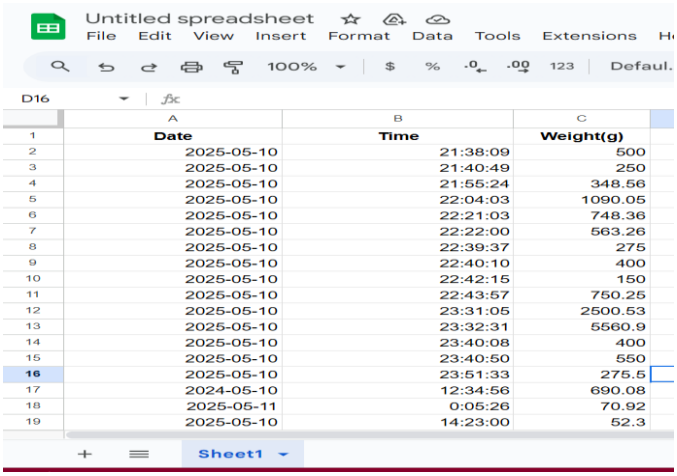

	A	B	C
1	Date	Time	Weight(g)
2	2025-05-10	21:38:09	500
3	2025-05-10	21:40:49	250
4	2025-05-10	21:55:24	348.56
5	2025-05-10	22:04:03	1090.05
6	2025-05-10	22:21:03	748.36
7	2025-05-10	22:22:00	563.26
8	2025-05-10	22:39:37	275
9	2025-05-10	22:40:10	400
10	2025-05-10	22:42:15	150
11	2025-05-10	22:43:57	750.25
12	2025-05-10	23:31:05	2500.53
13	2025-05-10	23:32:31	5560.9
14	2025-05-10	23:40:08	400
15	2025-05-10	23:40:50	550
16	2025-05-10	23:51:33	275.5
17	2024-05-10	12:34:56	690.08
18	2025-05-11	0:05:26	70.92
19	2025-05-10	14:23:00	52.3

Fig. 11. Google Sheet Update Data

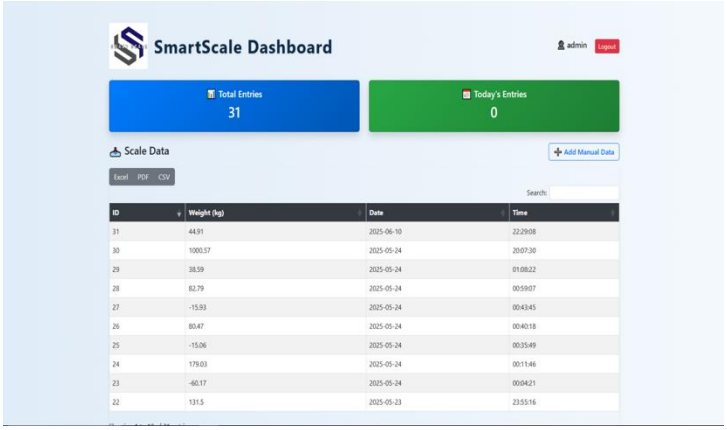

Fig. 12. Web Interface Dashboard

The “Smart Scale Dashboard”, a web-based interface designed for the weighing system. The dashboard shown in Fig. 10 and Fig. 12 provides a clear and comprehensive view of all the weight measurements collected by the system. At the top, it shows total entries

representing all the recordings made so far. It also highlights "Today's Entries", indicating new recordings for the day. The main table below lists all the recorded weights alongside their IDs, dates, and times of measurement. Each row corresponds to a weighing event, and the table makes it easy to search, filter, and view historical data. The interface also includes convenient options to export the data to Excel, PDF, or CSV, and an "Add Manual Data" button to manually insert a record if needed and this dashboard plays a key role in the project by offering a centralized platform to monitor, manage, and analyze weighing data in real time, making it a valuable tool for small-scale industrial applications and inventory control.

Table 3. Summary Table

Item	**Reference Weight (g)**	**Smart Scale Weight (g)**	**Absolute Error (g)**
Sugar	502g	506.23g	+ 4.23g
Salt	1010g	1014.63g	+4.63g
Flour	3006g	3010.29g	+4.29g
Rice	5070g	5076.72g	+6.72g
A Stone	827g	832.54g	+5.54g
Average			+4.94 g

The performance of the Smart Scale was quantitatively evaluated against a set of reference weights. As summarized in Table 3, the system demonstrated a high degree of accuracy. The mean absolute error (MAE) across all test items was +4.94 grams.

3.5 Comparative Analysis

Table 4. Features and Cost Comparison

Feature	**Proposed Smart Scale**	**Commercial Digital Scale**
Total Cost	Rs.7,790	Rs. 19,541
Cloud Connectivity	Yes (Google Sheets)	No
Locale Server Logging	Yes (XAMPP)	No
Web Dashboard	Yes (Custom PHP/MySQL)	No
Portability(Battery Power)	Yes	Yes
User Interface	LCD + Web Dashboard	LCD
User Calibration	Yes	Often restricted
Declared Accuracy	<1%	Often <0.1%

The proposed Smart Scale system delivers a unique value proposition, strategically balancing cost, functionality, and accessibility. As illustrated in Table 4, the system occupies

a distinct niche by offering a combination of local and cloud data flexibility, user repairability, and portability at a fraction of the cost of commercial digital scales. This makes it an ideal and practical solution for small-scale, budget-conscious applications, such as agricultural co-operatives, artisanal production, and inventory management.

4 Discussion

The Smart Scale project successfully addressed the primary problems outlined at the outset, such as the lack of automation in weight measurement, limited portability of traditional scales and the absence of digital recordkeeping. The addition of IoT functionality proved to be a transformative element, enhancing the system's capabilities by enabling remote access, real-time data monitoring, and cloud-based storage. These upgrades offered several advantages over traditional, manual scales. Notably, the ability to track weights digitally eliminates the need for paper-based logs and offers users the convenience of accessing historical data at any time. The integration of cloud technologies enables seamless remote monitoring, which can improve operational efficiency. The system performed well during field tests, demonstrating its potential for scalability and adaptability across various industries, from agriculture to small manufacturing sectors. Although the system remains in its early stages, the results suggest that it holds great promise for widespread adoption, particularly in industries where accurate weight tracking is essential.

5 Conclusions

The Smart Scale project achieved its objectives by successfully developing a compact, reliable, and user-friendly weighing system with integrated IoT capabilities. By combining hardware and software components, the system was able to provide real-time weight tracking, digital logging, and cloud-based data storage. The system demonstrated its practical applicability, especially in industries like agriculture, tea and honey production, and small-scale manufacturing, where accurate and portable weighing solutions are essential. The project also contributes to the advancement of digital transformation in these industries by introducing IoT-enabled devices that improve operational efficiency and data management. While the system is still in its early stages, it represents a significant step toward the development of more intelligent, automated, and accessible weighing solutions.

Reference

1. A. Zanella, N. Bui, A. Castellani, L. Vangelista, and M. Zorzi, Internet of Things for Smart Cities, IEEE Internet of Things Journal, 1(1), pp. 22–32, Feb. 2018, Available: https://ieeexplore.ieee.org/document/6740844
2. M. Alam, IoT Weighing Scale with HX711 Load Cell & ESP8266, How To Electronics, Feb. 08, 2020. https://how2electronics.com/iot-weighing-scale-hx711-load-cell-esp8266/#google_vignette
3. A. Parajuli, Insert Data into MySQL Database with ESP8266 Development Board, IoT Projects Ideas, Jun. 20, 2020. https://iotprojectsideas.com/insert-data-into-mysql-database-with-esp8266/
4. Data Logging with PHP + MySQL + ESP8266, Arduino Project Hub, 2022. https://projecthub.arduino.cc/yilmazyurdakul/data-logging-with-php-mysql-esp8266-a33ab0
5. Log Data into MySQL Database using NodeMCU Development Board, Circuitdigest.com, 2021. https://circuitdigest.com/comment/35081(accessed Jun. 13, 2025).
6. M. S. Munna and T. C. Mallick, Transforming weight measurement: a cutting-edge IoT-enabled smart weight machine for centralized price control of products, International Journal of Scientific Reports, 10(8), pp. 269–274, Jul. 2024, doi: https://doi.org/10.18203/issn.2454-2156.intjscirep20241991.

3rd International Engineering Research Symposium 2025 (IERS 2025)
Colombo, Sri Lanka

Smart Wireless Wearable Glove Keyboard

M. J. F. Aasifa, M. F. S. Ahamed and M. Pravina

Department of Electrical and Electronic Engineering, Faculty of Engineering, University of Jaffna, Sri Lanka
aasifajawsi@gmail.com, ahamedshimak99@gmail.com, and pravina@eng.jfn.ac.lk

Abstract. In the rapidly evolving technological landscape, smart wearable devices have become integral to daily life. The Smart Wireless Wearable Glove Keyboard (SWWGK) introduces an innovative method of interaction by enabling users to type effortlessly in mid-air using finger movements. Unlike conventional keyboards that restrict user mobility, the SWWGK translates finger gestures into English text with an accuracy of 89.74%, a latency of 500 milliseconds, and a battery life of up to six hours per charge. This technology is particularly valuable for presenters, educators, and professionals, as it transforms presentations into more interactive and engaging experiences. By allowing users to naturally engage with screens while their gestures are seamlessly converted into written text, the device enhances both learning and participation. The SWWGK is designed to provide a user-friendly interface supported by optimized hardware and software to ensure extended battery life and precise gesture recognition. By removing the limitations of physical keyboards, this innovation redefines communication and interaction within educational and professional environments, offering a powerful tool to enhance connectivity with smart devices and improve information delivery.

Keywords: Smart Wireless Wearable Glove Keyboard (SWWGK), Support Vector Machine (SVM), Bluetooth Low Energy (BLE), Human-Computer Interaction (HCI), Recurrent Neural Network (RNN).

1 Introduction

In the context of rapid technological advancements, the smart wireless wearable glove keyboard (SWWGK) represents a significant breakthrough in human-computer interaction. This device allows users to type effortlessly by moving their fingers in the air, freeing them from the constraints of traditional physical keyboards. The glove interprets hand

movements into English letters with high accuracy, providing a seamless typing experience. Current devices primarily focus on American Sign Language (ASL) recognition or push-button input methods. They often overlook the potential of recognizing handwritten gestures [1], [2]. Moreover, most existing smart gloves are designed for medical or gaming applications and lack features tailored for educational purposes [3], [4]. Addressing these gaps requires education-specific features to enhance usability in learning environments.

The SWWGK is designed for presenters, educators, and professionals. It enables dynamic interaction with presentation screens, enriching the learning experience and fostering a stronger connection between human expression and technology. Traditional presentation methods often require physical movement to operate keyboards and pointers, which can disrupt the flow of lectures. The SWWGK provides a more intuitive and convenient input method.

The primary aim of this research is to design and develop a Smart Wireless Wearable Glove Keyboard (SWWGK) that accurately recognizes hand gestures and translates them into English letters. To achieve seamless interaction, a user-friendly interface with a pop-up writing window is incorporated, while optimizing battery life through hardware and software improvements enhances practicality for prolonged usage. The main contributions of this work are as follows:

- Developing an intuitive user interface with a pop-up writing window.
- Implementing robust gesture recognition algorithms for accurate translation of finger trajectory path movements.
- Integrating the SWWGK with presentation software for direct slide interaction through hand gestures.
- Evaluating the performance and effectiveness of the SWWGK in enhancing presentation interactions and user experience.

2 Related Work

In our project, gesture recognition plays a pivotal role in enabling typing or writing on the pop-up window during presentations. Various methods have been explored in previous studies, including push-button glove keyboards, virtual reality keyboards, EEG-based typing, and gesture recognition techniques [1], [5] – [8]. We have chosen gesture recognition due to its effectiveness in facilitating accurate input without requiring physical contact.

Gesture recognition algorithms are critical for converting hand movements into digital commands, enabling intuitive control of presentation software. Key approaches include air gesture mode, fingertip detection, and handwriting detection algorithms. Air gesture

mode captures hand movements in mid-air, allowing interaction with presentation software without physical contact. Fingertip detection algorithms track fingertip positions to execute commands with precision. Handwriting detection algorithms interpret handwritten gestures into text, with Convolutional Neural Networks (CNNs) and Recurrent Neural Networks (RNNs) demonstrating particular effectiveness [5], [6], [9] – [14].

Significant studies have explored various technologies for gesture recognition, including modular data gloves equipped with accelerometers and gyroscopes [5], MyoWare Muscle Sensors for detecting muscle activation [6], and devices utilizing gyroscopes and accelerometers for air-written character recognition [7]. Advanced methods include CNN-based frameworks for gesture recognition [9], [13], and combinations of Support Vector Machine (SVM) with RNNs for text display [14]. Additionally, some researchers have employed MATLAB plotting techniques to visualize gestures [7]. Our choice of air gesture mode, fingertip detection, and handwriting detection is motivated by their demonstrated accuracy and practicality in interactive presentation settings.

To address limitations identified in previous research, we selected the SVM algorithm for handwriting detection, preferring it over CNNs and other machine learning methods. SVM offers several advantages, including efficiency with small datasets, effective handling of high-dimensional feature spaces, and memory efficiency stemming from its reliance on support vectors. Additionally, SVMs manage non-linear decision boundaries effectively, making them well-suited for complex sensor data and diverse user inputs. Their strong generalization capability ensures reliable performance across varied real-world conditions.

Wearable sensors play an increasingly vital role in enhancing Human-Computer Interaction (HCI) by providing intuitive and immersive interfaces. These sensors facilitate the translation of natural hand movements into digital commands, thereby creating a more seamless interaction experience. Effective system design requires not only user-friendly interfaces but also the integration of visual cues and feedback mechanisms to improve gesture recognition accuracy and user comprehension.

In this context, the study presented in [8] demonstrates a real-time wearable system for finger air-writing recognition. The system utilizes an Arduino Nano 33 BLE Sense and employs TensorFlow Lite for on-device recognition and classification of characters. Users can write characters including digits and English lowercase letters in three-dimensional space through finger movements. Motion data captured by Inertial Measurement Units (IMUs) and processed by a microcontroller enables the recognition and interpretation of 36 characters, highlighting the potential for advanced HCI applications in wearable technology.

A smart wireless wearable glove keyboard uses Bluetooth technology to connect wirelessly with devices like laptops, smartphones, and projectors. This enables seamless, cable-free control of presentation software, enhancing user mobility and ensuring reliable communication.

In [15], hand gestures captured by smart gloves with embedded sensors are converted from analog to digital signals using the voltage divider rule. These signals are processed by a PIC microcontroller and transmitted wirelessly via Radio Frequency (RF), incorporating error correction mechanisms at the receiver end. Similarly, in [2], strain sensors detect knuckle positions by converting them into variable resistance values, which are then transformed into voltage signals through voltage dividers. The Teensy microcontroller processes these voltages to generate a binary key representing the knuckle states, which is subsequently transmitted wirelessly.

3 Methodology

The methodology (Fig. 1) for developing the Smart Wireless Wearable Glove Keyboard (SWWGK) integrates hardware design, software development, data collection, and machine learning analysis. This comprehensive approach ensures accurate gesture recognition, reliable system performance, and seamless user interaction.

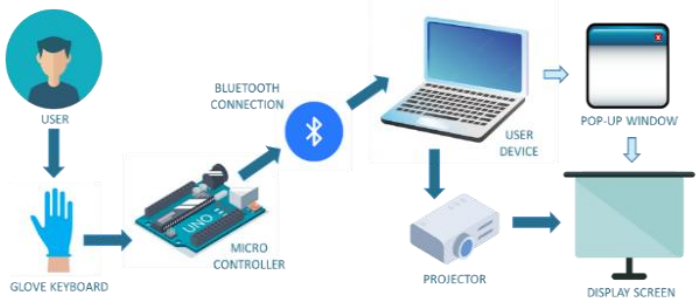

Fig. 1. Working process of smart wireless wearable glove keyboard.

3.1 Hardware Implementation

The hardware system is built around a 3D-printed glove that houses all electronic components, prioritizing user comfort and usability. The ESP32 Dev Kit is employed as the microcontroller due to its compact size, low power consumption, ease of programming, and integrated wireless communication capabilities (Fig. 2). Motion tracking is facilitated by the MPU-6050 sensor, while the TTP223 touch sensor enables intuitive fingertip input. Power is supplied by a 3.7 V LiPo battery, managed through a TP4056 charging module, and controlled via an ON/OFF push button serving as the main switch. The circuit design process begins with schematic development followed by prototyping on a breadboard.

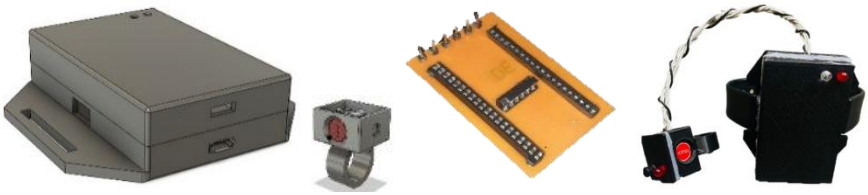

Fig. 2. The stages of hardware development progress.

The hardware and software components are integrated by programming the ESP32 to interface with sensors and establish Bluetooth connectivity with smart devices. Comprehensive testing and validation are conducted to evaluate gesture recognition accuracy and system reliability. The glove is designed in SolidWorks for ergonomics, then 3D printed. The PCB is created using EasyEDA and fabricated on a copper shield. After assembling all components, the system undergoes thorough testing for functionality and wireless communication. Usability testing with volunteers helps refine performance based on feedback.

3.2 Gesture Recognition Software Design

The software design process begins with dataset collection, preprocessing, and augmentation. Data representing 26 alphabet letters were collected from volunteers, with 25 samples recorded for each letter. Each gesture was saved as a text file, creating a structured dataset for model training. To address the limited dataset size, a data augmentation algorithm was applied to extend and diversify the samples, improving model robustness. The Arduino IDE was used to program the ESP32 for Bluetooth connectivity, facilitating communication between the glove and a PC. Python scripts, developed within the Anaconda Jupyter

Notebook environment, supported data collection, preprocessing, and machine learning model development. Gesture-to-text mapping was implemented to translate detected fingertip trajectories into their corresponding characters.

Support Vector Machine (SVM) was selected as the classification algorithm due to its strong performance in trajectory-based recognition. The model was trained on the collected dataset to capture fingertip movement patterns corresponding to each English letter. Training, prediction, and evaluation of the SVM model were carried out in the Jupyter Notebook environment using Python scripts for letter prediction and output, providing an interactive platform for coding and analysis. The user interface was developed in Python using Tkinter, featuring a pop-up writing window that displays recognized text in real time. This interface also supports training data collection and integrates with presentation software, enabling seamless interaction during live sessions. Usability testing was conducted to assess system performance and guide refinements to enhance the user experience.

4 Results and Discussion

The Smart Wireless Wearable Glove Keyboard (SWWGK) demonstrates significant potential as an innovative mid-air text input device. By interpreting hand gestures, the glove enables users to input text without relying on physical surfaces, offering a practical alternative to conventional keyboards. A pop-up writing window provides real-time feedback, enhancing usability in dynamic environments (Fig. 3).

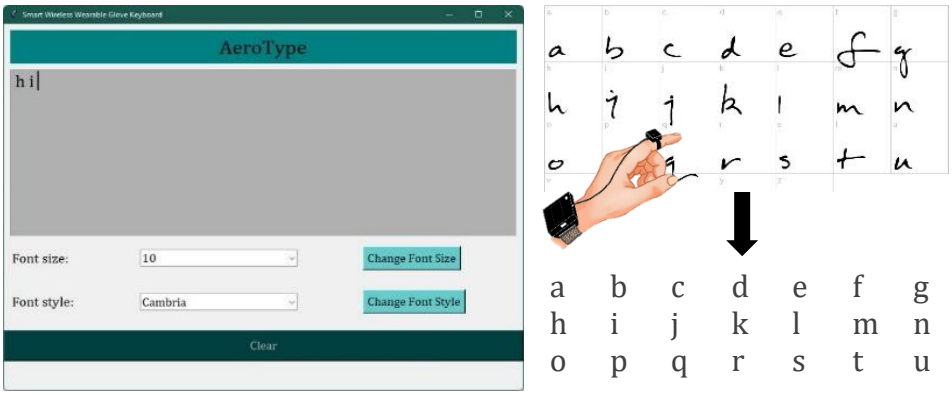

Fig. 3. A sample design of pop-up window with handwritten letter converting process.

The device operates via Bluetooth 4.2 (BLE) with a stable indoor range of up to 10 meters, making it well-suited for settings such as classrooms and conference rooms. From an ergonomic perspective, the glove's dimensions (23 × 26 × 36 mm and 70 × 60 × 20 mm) and weight (100 g) ensure user comfort during extended use. Additionally, its 3.7 V DC battery delivers up to six hours of continuous operation, with a recharge time of 1 to 2 hours.

The glove collects accelerometer and gyroscope data to predict letters, which are displayed in the pop-up window (Fig. 3), enabling continuous mid-air writing. This integration of advanced sensing technology, ergonomic design, and efficient power management renders the SWWGK both user-friendly and versatile.

4.1 Algorithm Overview

Support Vector Machines (SVM) are supervised learning algorithms commonly employed for classification tasks. Their primary objective is to identify an optimal hyperplane that separates data points of different classes within a high-dimensional feature space. This hyperplane is selected to maximize the margin, which is defined as the distance between the hyperplane and the closest data points from each class, known as support vectors. Maximizing this margin typically enhances the model's generalization ability (Fig. 4).

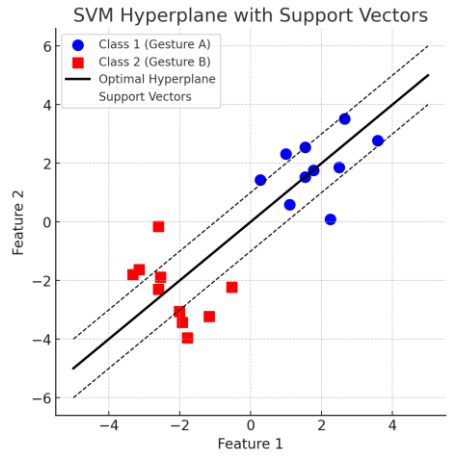

Fig. 4. Illustrates the working principle of SVM, where the optimal hyperplane separates two classes with maximum margin, and the nearest points to the margin are identified as support vectors.

For datasets that are not linearly separable, SVM utilizes kernel functions to map the input data into a higher-dimensional feature space, enabling the algorithm to capture complex, non-linear decision boundaries. Commonly used kernels include linear, polynomial, and Radial Basis Function (RBF), each tailored to suit different classification scenarios.

In this work, the SVM algorithm was applied to classify fingertip trajectory data collected from glove sensors. The feature set was constructed using hand orientation and motion data corresponding to 26 English alphabet gestures. A grid search over the parameters 'C = [0.001, 0.01, 0.1, 1, 10, 100]' and 'kernel = [linear, rbf, poly]' was performed to identify the optimal model configuration. The best performance was achieved using the RBF kernel with C set to 10.

The best-performing SVM model utilized the Radial Basis Function (RBF) kernel with a regularization parameter C=10. Additionally, key hyperparameters included break_ties = False, a cache size of 200 MB, no class weighting (class_weight = None), and coef0 = 0.0. The decision function employed a one-vs-rest (ovr) scheme for multi-class classification, with a polynomial degree of 3 (applicable if a polynomial kernel is used). The gamma parameter was set to 'scale', allowing automatic adjustment based on the data. The model allowed unlimited iterations with max_iter = -1, enabled probability estimates (probability = True), and used the shrinking heuristic (shrinking = True). The tolerance for stopping criteria was set to 0.001, no specific random state was fixed, and verbose output was disabled (verbose = False).

The RBF kernel was selected due to its effectiveness in capturing non-linear relationships within fingertip trajectory data, enabling the model to accurately distinguish complex gesture patterns. The gamma parameter was set to 'scale', allowing automatic adjustment of the influence of individual data points based on the number of features. This provides a balanced trade-off between bias and variance, ensuring stable generalization performance across all 26 gesture classes.

The model was trained and evaluated using a stratified 75–25 train-test split to maintain class distribution consistency. The SVM achieved strong performance metrics, including an accuracy of 89.74%, precision of 0.92, recall of 0.90, and an F1-score of 0.89, demonstrating its robustness in recognizing gesture-based inputs. Such findings resonate with the known advantages of RBF kernels in gesture recognition tasks, where their capacity to model intricate, multi-dimensional data patterns supports high classification accuracy, especially in wearable sensor applications.

4.2 Model Performance Analysis

The confusion matrix (Fig. 5) shows that most letters were classified correctly, as evidenced by the strong diagonal pattern. A detailed classification report in Table 1 provides precision, recall, and F1-score metrics for each letter individually. For benchmarking, a Recurrent Neural Network (RNN) with two Long Short-Term Memory (LSTM) layers was implemented. The performance comparison between the SVM and RNN models is summarized in Table 2. The results indicate that the SVM outperforms the RNN on the current dataset, likely due to its better handling of high-dimensional, structured gesture data and its effectiveness with smaller sample sizes.

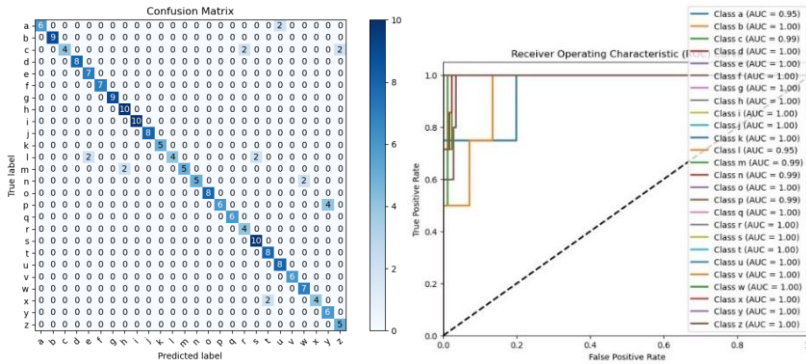

Fig. 5. Confusion matrix & ROC curve displaying classification performance across all 26 letters.

Table 1. Classification report for each letter class using SVM.

Letters	Precision	Recall	F1-score	Letters	Precision	Recall	F1-score
a	1.00	0.75	0.86	n	1.00	0.71	0.83
b	1.00	1.00	1.00	o	1.00	1.00	1.00
c	1.00	0.50	0.67	p	1.00	0.60	0.75
d	1.00	1.00	1.00	q	1.00	1.00	1.00
e	0.78	1.00	0.88	r	0.67	1.00	0.80
f	1.00	1.00	1.00	s	0.83	1.00	0.91
g	1.00	1.00	1.00	t	0.80	1.00	0.89
h	0.83	1.00	0.91	u	0.80	1.00	0.89

i	1.00	1.00	1.00	v	1.00	1.00	1.00
j	1.00	1.00	1.00	w	0.78	1.00	0.88
k	1.00	1.00	1.00	x	1.00	0.67	0.80
l	1.00	0.50	0.67	y	0.60	1.00	0.75
m	1.00	0.71	0.83	z	0.71	1.00	0.73

Table 2. Performance comparison between SVM and RNN.

Model	Accuracy (%)	Precision	Recall	F1-score
SVM	89.74	0.92	0.90	0.89
RNN	69.74	0.72	0.70	0.69

5 Conclusions

The SWWGK demonstrates considerable progress in mid-air handwriting recognition by integrating precise gesture recognition, reliable Bluetooth 4.2 connectivity with an effective indoor range of up to 10 meters, and an ergonomic design optimized for comfort and extended use. Its lightweight structure (approximately 100 g) and compact dimensions ensure user comfort, while a 3.7 V battery enables up to six hours of continuous operation. The SVM model employed delivers strong performance on small, high-dimensional datasets, outperforming alternative models such as CNN and RNN for this application. However, the study's limitations include a relatively small dataset of 25 samples per letter and limited diversity in hand orientation, gesture speed, and environmental conditions, which could impact robustness and generalization. Subtle misclassifications among similar gesture trajectories persist. Future work will focus on expanding the dataset with more diverse users and movement variations, exploring deep learning and hybrid models for improved accuracy, refining hardware design for better ergonomics and power efficiency, and implementing hand gestures for essential keyboard functions such as backspace, enter, delete, and spacebar. Furthermore, extending recognition to include numbers alongside English letters will broaden the system's applicability, ultimately aiming to deliver a more versatile, reliable, and scalable solution for mid-air text input applications.

References

1. K. Kumar, S. M. Al Isham, P. Kumar et al., Smart glove: A wearable device for disabled person, 2024.

2. T. F. O'Connor, M. E. Fach, R. Miller, S. E. Root, P. P. Mercier, and D. J. Lipomi, The language of glove: Wireless gesture decoder with low-power and stretchable hybrid electronics, PloS one, 12(7), p. e0179766, 2017.
3. A. Mohamed, P. Sujeet, and V. Ullas, Gauntlet-x1: Smart glove system for american sign language translation using hand activity recognition, 2020.
4. C. M. Chiu, S. W. Chen, Y. P. Pao, M. Z. Huang, S. W. Chan, and Z. H. Lin, A smart glove with integrated triboelectric nanogenerator for self-powered gesture recognition and language expression, Science and technology of advanced materials, 20(1), pp. 964–971, 2019.
5. B. S. Lin, I. J. Lee, P. Y. Chiang, S. Y. Huang, and C. W. Peng, A modular data glove system for finger and hand motion capture based on inertial sensors, Journal of medical and biological engineering, 39, pp. 532–540, 2019.
6. J. A. Gaba, Air keyboard: Mid-air text input using wearable emg sensors and a predictive text model, 2016.
7. K. Preethi and S. Chithra, On-air character recognition system for visually impaired people, International Conference for Phoenixes on Emerging Current Trends in Engineering and Management (PECTEAM 2018). Atlantis Press, pp. 155–158, 2018.
8. H. Zhang, L. Chen, Y. Zhang, R. Hu, C. He, Y. Tan, and J. Zhang, A wearable real-time character recognition system based on edge computing-enabled deep learning for air-writing, Journal of Sensors, 2022(1), p. 8507706, 2022.
9. A. Dash, A. Sahu, R. Shringi, J. Gamboa, M. Z. Afzal, M. I. Malik, A. Dengel, and S. Ahmed, Airscript-creating documents in air, 2017 14th IAPR international conference on document analysis and recognition (ICDAR), 1. IEEE, pp. 908–913, 2017.
10. J. Younas, H. Margarito, S. Bian, and P. Lukowicz, Finger air writing-movement reconstruction with low-cost imu sensor, in MobiQuitous 2020-17th EAI International Conference on Mobile and Ubiquitous Systems: Computing, Networking and Services, pp. 69–75, 2020.
11. S. Mukherjee, S. A. Ahmed, D. P. Dogra, S. Kar, and P. P. Roy, Fingertip detection and tracking for recognition of air-writing in videos, Expert Systems with Applications, 136, pp. 217–229, 2019.
12. M. S. Alam, K. C. Kwon, M. A. Alam, M. Y. Abbass, S. M. Imtiaz, and N. Kim, Trajectory-based air-writing recognition using deep neural network and depth sensor, Sensors, 20(2), p. 376, 2020.
13. P. Roy, S. Ghosh, and U. Pal, A cnn based framework for unistroke numeral recognition in air-writing, arXiv preprint arXiv:2303.07989, 2023.
14. S. Sunny and V. Sindhu, Hand gesture keyboard using machine learning, International Journal of Applied Engineering Research, 15(1), 2020.
15. M. P. Verma, S. Shimi, and S. Chatterji, Design of smart gloves, Int. J. Eng. Res. Technol, 3, pp. 210–214, 2014.

Engineering Solutions Towards Climate Actions and Green Industries

3rd International Engineering Research Symposium 2025 (IERS 2025)
Colombo, Sri Lanka

Indoor Particulate Matter in Sri Lankan Industries: A Comparative Assessment Against Local and Global Air Quality Standards

Eng. N P T Perera

National Engineering Research and Development Center of Sri Lanka
Prabhashi@nerdc.lk

Abstract. Indoor air quality (IAQ) in industrial environments is a critical determinant of occupational health; however, it remains an under-regulated domain in Sri Lanka. Prolonged exposure to elevated particulate matter (PM_{10}) levels in enclosed workplaces is linked to respiratory diseases, cardiovascular complications, and reduced worker productivity. This study presents a longitudinal assessment of PM_{10} concentrations across 15 industrial sites spanning seven key sectors, including textile and apparel, rubber and plastics, food and beverage, electronics, cement production, logistics, and power generation, based on data collected from 2015 to 2024. Over 300 data points were analyzed from more than 80 unique indoor locations, covering both general workspaces and high-exposure zones such as boiler rooms, dye houses, and chemical stores. Measurements were conducted using USEPA-approved high-volume air samplers in accordance with the Sri Lankan Ambient Air Quality Standard for PM_{10}. The results revealed that several zones, particularly in fabric processing, electronic assembly, and tea packaging, recorded PM_{10} concentrations that significantly exceeded the national and WHO guidelines. In some areas, levels exceeded 150 $\mu g/m^3$, posing chronic health risks to workers through inhalation of respirable particulates. This study highlights the urgent need for regulatory IAQ frameworks tailored to the industrial landscape of Sri Lanka. This study provides critical evidence to support policy reform, implementation of engineering controls, and workplace health interventions, contributing to sustainable and safe industrial development aligned with international occupational health standards.

Keywords: Indoor Air Quality (IAQ), Particulate Matter (PM_{10}), Sri Lankan Industries.

1 Introduction

Industrial indoor environments in lower-middle-income countries like, such as Sri Lanka, face significant IAQ challenges, especially due to underdeveloped regulatory frameworks. Although guidelines exist for residential and commercial IAQ, industrial workplaces exposed to mechanical, thermal, and chemical emissions often lack enforceable standards.

Air pollution is a major global health concern. According to WHO Indoor exposure to solid fuels causes over 1.5 million premature deaths and 38.5 million disability adjusted life years (DALYs) annually. Outdoor air pollution contributes to over 800,000 deaths, with 65% occurring in Asia. In Sri Lanka, indoor and outdoor air pollution are linked to an estimated 4,200 and 1,000 deaths per year, respectively [1]. Although comprehensive national data are limited, studies like research on "Air pollution and public health in developing countries: Is Sri Lanka different?" offer valuable insights [2].

Particulate matter (PM)—especially PM_{10}, $PM_{2.5}$, and PM_1 are of concern because they can penetrate the respiratory tract and trigger chronic illnesses. While Sri Lanka provides ambient air quality standards, they do not address the prolonged exposures common in industrial indoor environments.

Poor ventilation and extended worker presence further exacerbate IAQ risks, contributing to health issues like asthma, cardiovascular disease, and Sick Building Syndrome (SBS)[3]. In Sri Lanka, IAQ research mainly focused on outdoor and residential settings, despite the large industrial workforce. Regional studies show varying public awareness, with pollutants such as tobacco smoke, cooking emissions, and plastic waste burning identified as key sources [4].

International standards like ISO 16000 and ASHRAE 62.1 emphasize PM monitoring, but implementation in Sri Lanka's industrial sector is inconsistent. This study addresses this gap by presenting a 10-year longitudinal analysis of PM_{10} levels in selected industrial environments across the country.

2 Methodology

2.1 Site Selection and Industrial Sectors

The study covered 15 industrial facilities across Sri Lanka, representing varied geographic regions and economic sectors, including Textile and Apparel, Rubber and Plastics, Food and Beverage, Electronics, Power Generation, Cement Production, Logistics and Warehousing.

Walkthrough assessments helped identify high-exposure zones, like production floors, material handling areas, and furnace vicinities.

2.2 Instrumentation and Sampling Protocol

PM_{10} Monitoring

Particulate matter (PM_{10}) was measured using a USEPA-approved High-Volume Air Sampler (HVAS), in accordance with Sri Lanka's CEA guidelines. The device features a size-selective inlet and an automatic volumetric flow controller to maintain sampling consistency under variable environmental conditions.

Glass fiber filter papers were used to collect PM_{10} at a nominal flow rate of 1.1 m^3/min. Only particles ≤10 µm were captured on the filters. Filters were weighed before and after sampling under controlled conditions to ensure precision.

Fig. 1. Indoor Particulate Matter Monitoring

Concentration Calculation

PM_{10} concentration (µg/m^3) was determined using:

$$\text{PM10 Concentration } \mu g/m^3 = \frac{(FP2 - FP1)g \times 10^6}{(\text{Duration (Minutes)} \times \text{Air Flow Rate(m3/min)}} \quad (1)$$

Where:
FP_1 = Pre-sampling filter weight
FP_2 = Post-sampling filter weight
Duration = Typically 24 hours Flow rate measured at both start and end
Filters were conditioned in a desiccator for 24 hours pre- and post-sampling to eliminate moisture bias.

2.3 Sampling Strategy and Indoor Zone Selection

Sampling was strategically focused on zones with high potential for exposure, including raw material input areas, intermediate processing stages, product packaging sections, and locations housing machinery or combustion units. Measurements were conducted during standard operational conditions to ensure the data accurately reflected typical workplace environments.

2.4 Temporal and Spatial Data Coverage

The study utilized historical PM_{10} measurement data available at the Energy and Environmental Services Department of National Engineering Research and Development Centre, collected between 2015 and 2024. Over 300 validated measurement data points across more than 80 indoor locations were analyzed to provide comprehensive temporal and spatial coverage.

2.5 Statistical Analysis

A one-way ANOVA and Tukey's HSD test were used to assess differences in PM_{10} concentrations across industrial sectors (2015–2024), while longitudinal trend analysis examined temporal changes and post-pandemic effects, all at a 95% confidence level.

3 Results and Discussion

3.1 Summary of PM_{10} Concentrations by Industry

Table 1. Indoor PM_{10} Concentration Summary by Sector (2015–2024)

Sector	Min (µg/m³)	Max (µg/m³)	Typical High Locations
Apparel Industry	40	277	Finish Fabric Area, QC, Canteen Area, Knitting Section
Electronic Industry	32	231	Winding Room, Metalicon, Rework Area, Press/Masking Area
Tobacco Industry	34	223	PMD Area, SMD Locations, Dust Rooms
Food Industry	11	200	Biomass Boiler Room, Packing Areas, Process/Feeding Sections
Ship Repairing & Maintenance	15	184	Pipe Fabrication, Onboard NC, Aluminium Workshop
Activated Carbon Industry	26	162	Location 2
PVC Processing	90	99	Mixing Area, Cutting Area
Cement Industry	42	82	Locations 1 and 2
Rubber Industry	66	99	Location A
Power Plant	34	94	Guest House, Residential Area
Aviation Industry	86	97	Locations C & D
Logistics/Warehouses	24	35	Warehouses 08, 09, 11

PM_{10} concentrations were measured across 15 industrial sectors and over 80 unique indoor sites between 2015 to 2024. The measurements revealed considerable variability in particle concentrations depending on activity type, location within facilities, and industrial process.

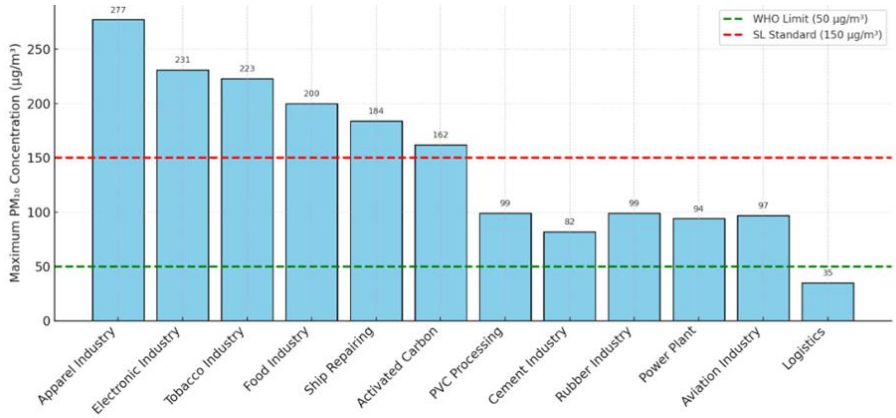

Fig. 2. Maximum PM10 Levels by Sector (2015-2024) vs WHO and SL Standard

3.2 Yearly Trends

From 2022 to 2024, increased PM_{10} concentrations were observed in the textile, electronic, and food industries, which were largely attributed to the resumption of full-capacity operations following COVID-19-related disruptions. In contrast, the period from 2020 to 2021 showed a noticeable decline in PM_{10} levels, likely due to reduced industrial activity and temporary production halts during the pandemic. Between 2015 and 2019, PM_{10} levels remained at moderate baseline values, although localized peaks were identified in sectors such as tea processing, textile manufacturing, and capacitor production.

3.3 Comparison with IAQ Standards

Table 2. Applicable Indoor Air Quality Standard

Standard	**PM_{10} Guideline (24-hr)**
Sri Lanka Ambient Standard (CEA)	100 µg/m³
WHO Indoor Air Quality Guideline	50 µg/m³
Sri Lankan IAQ Guideline	150 µg/m³

More than 40 indoor locations recorded PM_{10} concentrations exceeding 150 $\mu g/m^3$, breaching both WHO and Sri Lankan air quality guidelines. Notably, certain zones, such as the wave soldering area (554 $\mu g/m^3$) and garment fabric handling sections (381 $\mu g/m^3$), surpassed even the ambient outdoor air quality standards by a wide margin. Chronic over-exposure was also observed in textile chemical storage and quality control areas, tea packing rooms, and capacitor winding rooms, indicating persistent high-risk environments for occupational exposure.

3.4 High-Risk Zones

Locations such as chemical storage areas, biomass boiler rooms, soldering zones, and dyeing operations were frequently identified as high-exposure zones. Sites exhibiting PM_{10} concentrations exceeding 200 $\mu g/m^3$ commonly featured dust-generating processes and inadequate ventilation, highlighting consistent risk factors across multiple industrial environments.

3.5 Health and Regulatory Implications

According to WHO data, long-term exposure to PM_{10} concentrations above 50 $\mu g/m^3$ is linked to an elevated risk of respiratory and cardiovascular diseases. In this study, many recorded indoor PM_{10} values exceeded thresholds established for ambient outdoor air, underscoring the urgent need for Sri Lanka to implement and enforce indoor-specific air quality regulations to protect worker health.

3.6 Statistical Analysis of Sectoral Variations

A one-way ANOVA was conducted on sector-wise average PM_{10} concentrations from 2015–2024 to assess whether mean levels differed significantly across industries. Results indicated a statistically significant variation in PM_{10} levels among sectors ($F = 6.87$, $p < 0.001$). Post-hoc Tukey tests showed that apparel, electronic, and food industries had significantly higher mean concentrations compared to logistics and cement sectors, highlighting the heterogeneity of exposure environments.

3.7 Trend Analysis (2015–2024)

Linear trend analysis across the full dataset revealed an overall upward trajectory in PM_{10} concentrations in high-activity industries (textile, electronics, food), with average increases of 3–5% per year after 2021. The regression model ($R^2 = 0.71$, $p < 0.01$) confirmed the statistical strength of this trend. Conversely, low-activity industries such as cement, power, and logistics showed stable or slightly declining PM_{10} values over the same period.

These findings reinforce the importance of continuous monitoring, particularly in sectors undergoing production expansions or process intensification.

4 Conclusions

This longitudinal study provides a critical evidence base on the status of indoor air quality across diverse industrial sectors in Sri Lanka, revealing persistently elevated PM_{10} concentrations in multiple operational zones. Over the ten-year period from 2015 to 2024, measurements consistently demonstrated exceedances of both international (WHO) and national ambient standards, often by significant margins, in zones such as dye houses, soldering stations, biomass boiler rooms, chemical stores, and fabric handling areas. ANOVA confirmed statistically significant differences ($p < 0.05$) between industrial sectors, while trend analysis showed persistent or worsening PM_{10} levels in high-risk industries despite technological progress. These findings reflect not only sector-specific emission characteristics but also systemic deficiencies in engineering controls, ventilation design, and IAQ governance.

The observed concentration levels pose serious occupational health risks, especially given prolonged worker presence and inadequate exposure mitigation strategies. Workers in these environments face heightened risks of chronic respiratory illnesses, cardiovascular complications, and reduced lung function. The absence of enforceable indoor-specific regulatory standards in Sri Lanka exacerbates this challenge, leaving industrial employees exposed to chronic particulate matter levels far exceeding health-based thresholds. Furthermore, the disparity between observed indoor levels and outdoor air quality limits underscores a critical regulatory blind spot, where ambient standards are inappropriately used as proxies for indoor environments.

From a public health and policy standpoint, the data call for urgent action to integrate IAQ into Sri Lanka's national occupational health and safety (OHS) framework. Without a coordinated response encompassing policy reform, engineering interventions, administrative protocols, and workforce education, indoor air pollution will continue to undermine worker wellbeing, productivity, and long-term national health indicators.

The study recommends a dual approach to address indoor air quality (IAQ) issues: policy reforms and health interventions. Policy reforms include setting IAQ standards, mandatory monitoring in high-risk sectors, enforcing ventilation and emission controls, establishing a national IAQ surveillance program, and ensuring worker protection through PPE and exposure regulations. Health interventions focus on regular medical screening, awareness programs, factory-level health surveillance, and chronic disease management integrated with national health programs.

This study thus provides a foundational baseline for industrial IAQ reform in Sri Lanka, paving the way for targeted interventions that align with international best practices and sustainable workplace safety standards.

References

1. T. G. Pathirana, Weekly Epidemiological Report. A publication of the Epidemiology Unit, Ministry of Health, Nutrition & Indigenous Medicine, 49(24), 1–2 (2022).
2. S. Nandasena, R. Wickremasinghe, N. Sathiakumar, Air pollution and public health in developing countries: Is Sri Lanka different? J. Coll. Community Physicians Sri Lanka, 17(1), pp. 7–13 (2012). https://doi.org/10.4038/jccpsl.v17i1.4932
3. H. Mallawarachchi, L. De Silva, Green framework to improve indoor air quality in buildings: reducing the impact of sick building syndrome on office workers in Sri Lanka – A literature review. 2nd International Conference on Sustainable Built Environment (ICSBE 2012), pp. 1–13. University of Peradeniya, Kandy, Sri Lanka (2012).
4. H. Wijayasenarathne, R. M. D. I. Rathnayake, A. G. H. M. Rajakaruna, Analysing people's behavior towards indoor air quality management: a case study in Kandy, Kurunegala and Hambantota. 12th World Construction Symposium (WCS 2024), pp. 90–97. CIOB, Colombo (2024). https://doi.org/10.31705/WCS.2024.13
5. J. Rentschler, N. Leonova, Global air pollution exposure and poverty. Journal of Environmental Economics 10(3), 1–15 (2023).
6. Springer: LNCS Homepage, http://www.springer.com/lncs, last accessed 2016/11/21
7. World Health Organization, Air Pollution and Health. WHO, Geneva (2021).
8. Central Environmental Authority, Ambient Air Quality Standards. CEA, Colombo (2008).
9. International Organization for Standardization, ISO 16000 – Indoor Air Series. ISO, Geneva (various years).
10. ASHRAE: Standard 62.1 – Ventilation for Acceptable Indoor Air Quality. ASHRAE, Atlanta (2022).
11. A. Mutlu, Air quality impact of particulate matter (PM_{10}) releases from an industrial source. *Environmental Science and Pollution Research* **27**(36), pp. 45678–45690 (2020).
12. F. Sánchez-Soberón, M. Mari, V. Kumar, J. Rovira, M. Nadal, M. Schuhmacher, An approach to assess the Particulate Matter exposure for the population living around a cement plant: modelling indoor air and particle deposition in the respiratory tract. *Environmental Research* 189, 109-934 (2020).

13. J. K. Nagar, R. Kumar, J. P. Shrivastava, G. Kaushik, Indoor Air Pollution Around Industrial Areas and Its Effect: A Case Study in Delhi City. In: *Proceedings of the International Conference on Environmental Pollution*, pp. 45–51. Environmental Society Press, New Delhi (2018).

14. J. S. Gushit, S. U. Mohammed, H. M. Moda, Indoor Air Quality Monitoring and Characterization of Airborne Workstations Pollutants within Detergent Production Plant. *International Journal of Environmental Research and Public Health* **17**(14), 5095 (2020).

15. S. Khaki, M. Rio, P. Marin, Monitoring Indoor Air Quality in Additive Manufacturing Environment. In: *Proceedings of the International Symposium on Additive Manufacturing*, pp. 101–110. CNRS Publications, Grenoble (2021).

3rd International Engineering Research Symposium 2025 (IERS 2025)
Colombo, Sri Lanka

Study on the Effect of Drag Force on the Particle Motion of Coir Pith in Rotary Drying

S. A. P. S. Silva[1], G. A. S. D. Perera[2], K. Vithya[2], A. D. U. S. Amarasinghe[2] and M. Narayana[2]

[1]National Engineering Research and Development Centre of Sri Lanka
[2]Department of Chemical and Process Engineering, University of Moratuwa, Sri Lanka

Abstract. This study investigates the effect of drag force on the free-fall motion of coir pith particles under varying moisture contents and particle sizes. Particle-air interactions play a vital role in drying efficiency. Understanding these dynamics is critical for optimizing rotary drying operations. The main objective was to analyze how moisture content affects the drag coefficient and velocity profiles of coir pith particles. A simple experimental setup was used, where particles of three average diameters and five different moisture contents were dropped from varying heights, and their fall times were recorded. Drag coefficients were estimated numerically using measured fall times and calculated velocities. The velocity-time profiles were analyzed to assess whether particles approached terminal velocity during the available fall distances. Results obtained indicate that increased moisture content leads to higher drag coefficients, which delays the attainment of terminal velocity. Additionally, drag coefficients increased with particle diameter. These results provide deep insights into particle-fluid interactions relevant to rotary drying.

Keywords: drag force, drag coefficient, coir pith, rotary drying, free fall

1 Introduction

Coconut is the third most important crop in Sri Lanka, making the country the fourth-largest global producer of coconut. Sri Lanka is also a significant coir fiber exporter, second only to India [1]. Coir pith is an organic waste byproduct of coir fiber extracted from the husks of coconuts, which is biodegradable and eco-friendly [1]. It is a light, spongy, lignocellulose fibrous material with natural chemical constituents [1], [2], [3], [4]. In modern research, coir pith has become an agricultural resource as a growth medium due to its

high-water retention capacity, porosity, and fertility, because of the micro and macronutrient composition [2]. It is utilized as an adsorbent in water treatment [5], and soil conditioning, growing bags in the agriculture sector, due to their physical and chemical properties [6].

In rotary dryers, the moisture content of the coir pith decreases as it moves through the drying process. Coir pith particle motions in the rotary dryer depend mostly on the drag force and terminal velocity. Aerodynamic drag is one of the key forces affecting particle trajectories during drying. Understanding the changes in the moisture content of particles helps improve the accuracy of the drying process, as the air drag force on a particle is a major factor in the movement of particles [7]. Drag force is influenced by the relative velocities of the air and the particles, as well as the particles' shape, density, and moisture content. The drag force that the particles experience might vary significantly depending on the moisture level of the coir pith. Understanding effective forces is crucial for accurate prediction, including gravity, buoyancy, particle contact, electrostatic, and air drag forces. The variation between drag force and moisture content highlights the interdependence of these factors and the need for precise control and modeling in practical drying applications [8][9].

Additionally, substantial studies have examined the drying kinetics of coir pith, focusing on moisture content reduction through various drying technologies. Due to the complexity of measuring particle motion in real story dryers, simplified experimental approaches are often used.

Similar research on low-density objects has been conducted by Günther and Hoang [10], who investigated the feasibility of determining drag coefficients through free-fall experiments. Average drag coefficients for falling spheres were theoretically estimated and experimentally validated. This work supports the validity of using a simplified experimental setup to evaluate aerodynamic properties of low-density materials.

Bagheri and Bonadonna (2016) [11] proposed a drag coefficient model for freely falling non-spherical particles based on Reynolds number and simple shape descriptors like flatness and elongation. Their findings highlight those irregular particles in air exhibit random orientations, which are relevant to materials like coir pith, where drag force plays a key role in determining free-fall and drying trajectories.

Gorial and O'Callaghan (1990) [12] investigated the separation of grain from straw in a vertical air stream, focusing on how particle characteristics, air velocity, and injection direction affect separation efficiency. This research provides foundational insights into pneumatic particle separation techniques, which are highly relevant for materials such as coir pith, where aerodynamic behavior plays an important role.

Coir pith, a heterogeneous agricultural residue with particles of varying shapes, sizes, and densities, undergoes significant property changes during drying as moisture loss alters

density and inter-particle interactions. However, the combined effects of particle size and moisture content on drag force remain poorly understood. This study addresses this gap by examining how these factors influence particle behavior, providing novel insights essential for improving simulation accuracy of particle motion in drying processes such as rotary drying.

The present study utilizes a free-fall experiment to isolate and analyze the effect of drag force on coir pith particles. The objectives of this research are to investigate the impact of moisture content on the drag force of coir pith particles during drying and to quantify the effect of drag force on falling coir pith particles by measuring the deviation from ideal free fall and extrapolating the findings to rotary drying conditions. This approach provides a foundational understanding of particle-air interactions and offers data that can be extended to computational simulations or empirical dryer optimizations

2 Materials and Methods

a. Materials

Fresh coir pith particles were obtained from the mill and oven-dried at 150 ℃ for 2 hours to facilitate sieving. The dried material was then separated by particle size using a sieve shaker. Specific amounts of water were added to adjust the moisture content of the particles to the desired levels. This study utilized coir pith particles with average particle diameters of 1.2 mm, 0.855 mm, and 0.355 mm, which were determined using sieve analysis. The particles were characterized by known bulk density, moisture content of 20%, 30%, 40%, 50%, and 60%. To simplify the aerodynamic modelling, particles were assumed to be spherical. Each practical involved a 5g sample, ensuring that individual particle behavior dominates over bulk effects.

b. Experimental setup

Experiments were conducted by releasing coir pith particles from 0.5 m, 1 m, 1.5 m, 2 m, and 2.5 m. A 5g sample was dropped for each experiment, and the fall time was recorded using a stopwatch. Three repetitive experiments were conducted for each height to ensure consistency and reduce human error. Average times used for the data analysis [10], [11], [13].

c. Data analysis

In this study, the motion of coir pith particles during free fall was analyzed. The drag coefficient was estimated for various particle sizes and moisture contents. Excel Solver was used to numerically determine the drag-related constant by minimizing the error between measured fall time and model-predicted distance, based on the analytical drag equation.

Drag coefficients were calculated using that estimated constant. This process was repeated for each particle size and moisture content condition. The particle velocities and their rate of change, dv/dt, are calculated using the constant value obtained. The effect of moisture content on the calculated drag coefficient was analyzed for each particle size.

A series of graphs were plotted with moisture content (%) on the x-axis and drag coefficient on the y-axis. Each graph represented one particle size and included multiple series corresponding to different fall heights. This allowed clear visualization of how the drag coefficient varies with moisture under free fall, as influenced by both particle dimension and fall distance.

d. Theoretical framework

In rotary drying systems, particles undergo complex motion involving cascading, rolling, and free-fall phases. Particles are subject to gravity and aerodynamic drag forces during free-fall phases. It is important to understand the drag force acting on a particle since it directly affects the particle's residence time and drying efficiency.

However, due to the dynamic and opaque nature of the rotary dryer, directly measuring drag under real conditions is challenging. A vertical free-fall experiment is conducted to simplify the analysis and isolate the effect of drag. Modelling the free fall of a particle under quadratic drag with a constant drag coefficient is used as the theoretical framework.

The following equation describes the motion of falling particles with mass m and no initial velocity [10], [14].

$$\frac{dv}{dt} = g - \Psi v^2$$

where g is gravitational acceleration and ψ is a lumped parameter defined as,

$$\Psi = \frac{\rho_{air} C_d A}{2m}$$

Here, ρ_{air} is the density of air, A is the projected area, and C_d is the drag coefficient. This equation can be analytically solved by assuming a constant drag coefficient C_d over the fall duration. The velocity as a function of time is then given below.

$$v(t) = \sqrt{\frac{g}{\Psi}}\tanh(\sqrt{g\Psi}t$$

Integrating v(t) yields the displacement equation as follows,

$$s(t) = \frac{1}{\Psi}\ln(\cosh(\sqrt{\Psi g}t))$$

Vertical descent of a particle falling under gravity and quadratic drag is modelled by these expressions. In the experiment, the known fall distances and measured fall times are used to numerically estimate ψ using Excel Solver. Once ψ is known, the drag coefficient C_d is calculated as follows,

$$C_d = \frac{2m\Psi}{\rho_{air}A}$$

This method, which is adapted from Günther and Hoang [10] allows estimation of an average drag coefficient over the fall period for low-density, spherical particles.

The main advantage of this approach is its simplicity and its ability to isolate drag effects in the absence of other interfering forces common in rotary dryers. Furthermore, the particle velocities and their rate of change, dv/dt, are calculated to determine whether terminal velocity was achieved during the fall.

Rotary dryers feature a repeated particle-free-fall phase because of their internal lifter flights [15]. The drag behavior observed in vertical drop experiments can be used as an analogue for drag-dominated motion segments in actual drying systems. Specifically, for varying particle sizes and moisture contents, the estimated drag coefficients help predict how particles of different properties respond to airflow during drying.

3 Results and Discussion

a. Effects of moisture content on velocity profiles

The velocity-time profiles of coir pith particles with different diameters under varying moisture contents have revealed distinct patterns in their free fall behavior. Across all particle sizes and moisture contents, the velocity increased over time but did not attain a constant velocity within the highest experimental drop height of 2.5m, indicating that terminal velocity was not attained. This is validated by the non-zero values of acceleration(dv/dt) at the final time points of all conditions as indicated in table 1 shown below. In a previous research study, the same pattern of graphs was identified as in Fig. 1, Fig. 2, and Fig.3 [16][13].

Notably, the acceleration values have increased with moisture content across all particle sizes. In the case of D=1.2mm particles, dv/dt has increased from 0.0036 m/s2 at 20% moisture to 0.0077 m/s^2 at 60% moisture. Similar trends were observed for D=0.85mm and D=0.35mm particles. This increment implies that higher moisture content delays the approach to terminal velocity, due to increased particle mass and inertia, which require greater air resistance before equilibrium is achieved.

Table 1. Acceleration of particles

dv/dt when H=2.5m			
MC%	**D=1.2mm**	**D=0.85mm**	**D=0.35mm**
20	0.0036	0.0025	0.0005
30	0.0037	0.0031	0.0019
40	0.0039	0.0034	0.0021
50	0.0070	0.0037	0.0033
60	0.0077	0.0038	0.0037

As moisture content is increased, particle mass increases significantly, while surface area remains relatively unchanged. Since the gravitational force(F_g=mg) becomes greater relative to the resistive drag force($F_d \alpha v^2 A$), a higher velocity is required for the drag to counterbalance gravity and obtain the terminal velocity. Thus, particles with higher moisture content experience a longer period to obtain the terminal velocity, and up to that point continue accelerating.

Importantly, these data show that the terminal velocity condition has not been met within the available fall distance where dv/dt=0. Future experiments should engage greater drop heights to allow particles to approach steady-state velocity.

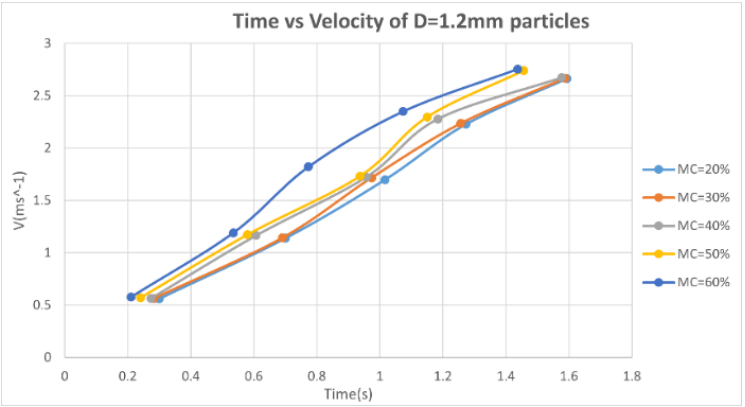

Fig. 1. Time vs Velocity graph for 1.2mm particle size

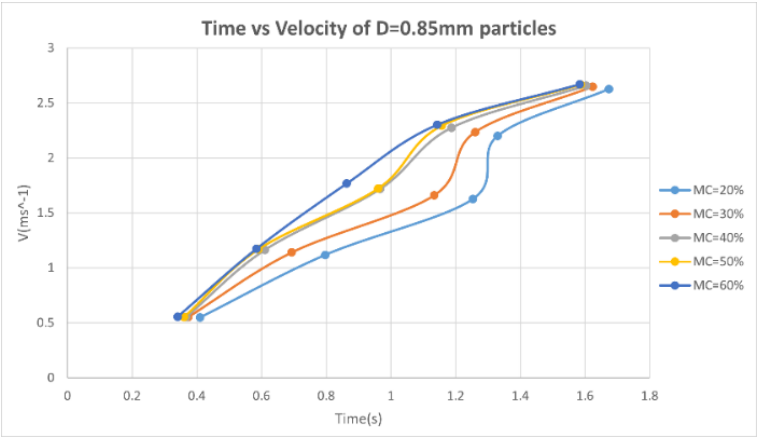

Fig. 2. Time vs Velocity graph for 0.85 mm particle size

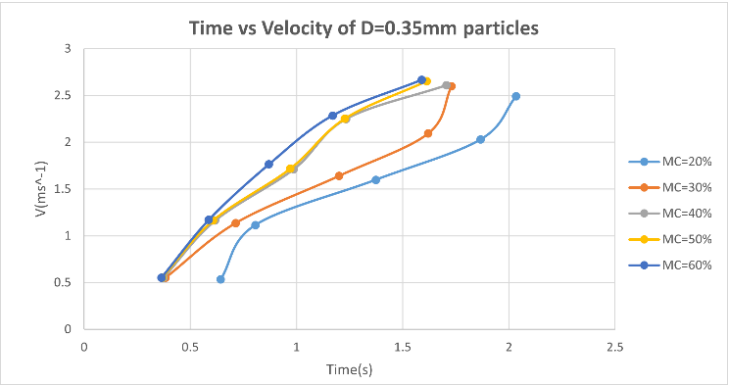

Fig. 3. Time vs Velocity graph for 0.35 mm particle size

b. Influence of moisture content on drag coefficients

The drag coefficient (C_d) of each particle size was analyzed as a function of fall distances and moisture contents. Across all distances, a consistent pattern has been developed. For a given height, the drag coefficient increases with moisture content as we can see in Fig 4, Fig 5, Fig6. These trends offer insights into the dynamics of particle-fluid interaction during free fall in still air.

The positive correlation between moisture content and drag coefficient at all drop heights is primarily due to increased particle mass without a proportional increase in projected surface area. Higher moisture particles generate greater gravitational force, which, for a given velocity, results in a higher calculated C_d. In addition, structural changes such as particle swelling, surface roughening, and aggregation may adjust the flow regime around the particles, increasing from drag. Overall, these results highlight that moisture not only affects mass and acceleration but also influences drag behavior and settling dynamics.

At lower drop heights (particularly 0.5 m), deviations from the overall drag trend were observed. These are primarily due to the limited time available for particles to accelerate and reach near-terminal velocity. In such cases, the particle's motion is still in the early transient stage, where velocity is low and the assumption of a stable flow regime does not hold. This can cause the model-fitting procedure to overestimate the drag coefficient to match the observed displacement. Furthermore, the short time intervals involved increase the sensitivity to timing errors, making the resulting C_d values less reliable at these heights.

Therefore, drag coefficients estimated from lower heights should be interpreted cautiously and are not as representative as those obtained from longer fall distances.

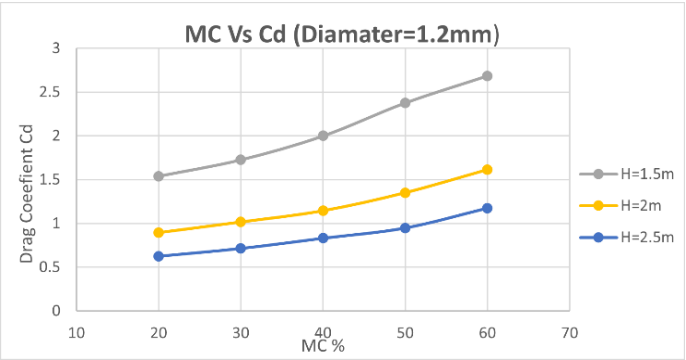

Fig. 4. Moisture content vs C_d graph for 1.2mm

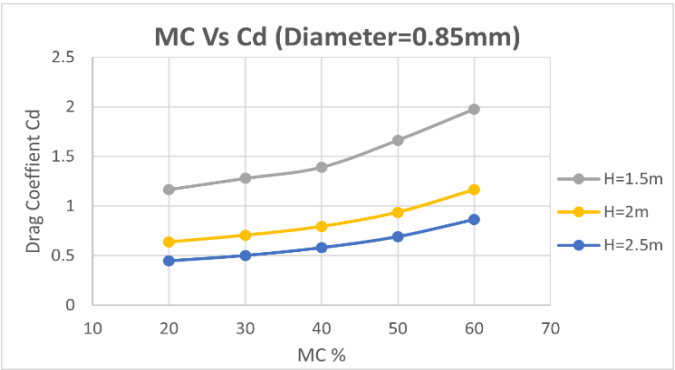

Fig. 5. Moisture content vs C_d graph for 0.85mm

c. Variation of drag coefficients with particle size

The C_d vs. diameter plots in Fig. 7 and Fig. 8 exhibit a general trend of increasing drag coefficient with particle diameter. Across all moisture content levels, larger particles consistently show higher C_d values compared to smaller ones. This can be attributed to elevated Reynolds numbers at larger sizes, as well as greater surface moisture retention, which may cause shape irregularities and increase the effective projected area.

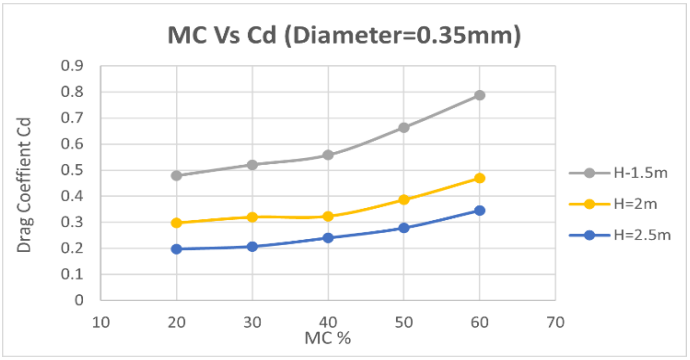

Fig. 6. Moisture content vs C_d graph for 0.35mm

Notably, this trend becomes more prominent at higher moisture contents, where moisture amplifies drag-inducing effects. Moreover, C_d values vary slightly between drop heights; for example, C_d is marginally higher at S = 1.0 m compared to S = 1.5 m for the same particle size and moisture level. This could be due to shorter fall distances allowing less time for particles to reach stable velocity, resulting in higher transient drag effects. These height-dependent variations highlight the importance of considering falling distance when evaluating drag behavior, particularly under variable moisture conditions.

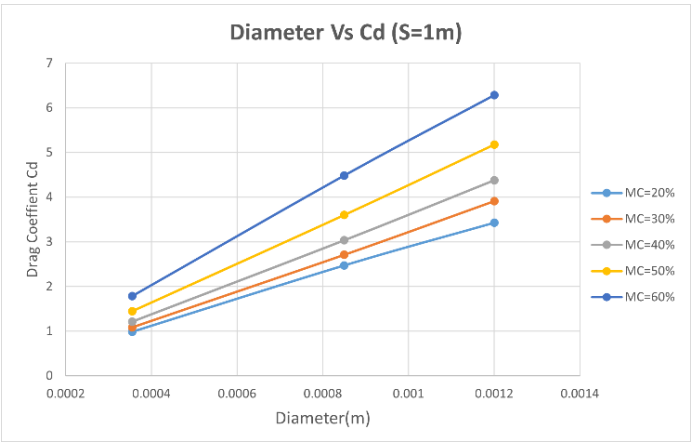

Fig. 7. Diameter vs C_d graph for 1m height

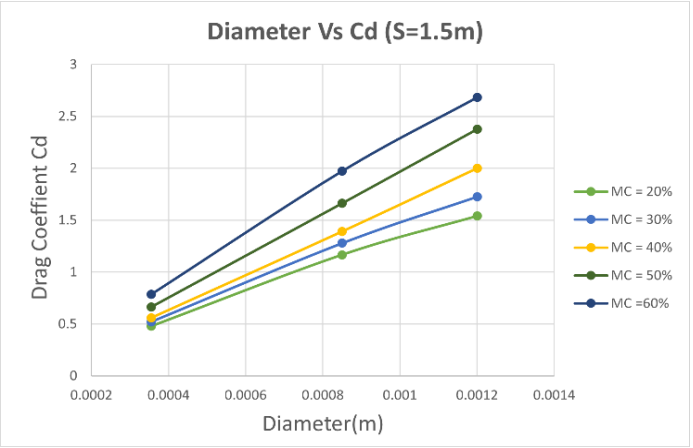

Fig. 8. Diameter vs C_d graph for 1.5 m height

d. Implications for rotary drying conditions

The trends observed for particle velocity and drag coefficient under varying moisture content and particle sizes have a direct impact on rotary dryer design and operation. High moisture content significantly slows down particle motion, requiring longer drying times and reducing thermal efficiency. Moist particles are likely to clump and slower settling. Smaller particles are more affected by moisture-induced cohesion, which increases their aerodynamic resistance and decreases drying uniformity.

Altering drum diameter or lifter design to increase fall height within the dryer can reduce drag, which helps to improve particle dispersion, enhancing heat and mass transfer. Drying systems must consider the combined effects of size, moisture, and dynamic behavior because of the increase in C_d with particle size under moist conditions.

Particle size and moisture content should be balanced for effective rotary drying operations to optimize flow behavior, residence time, and energy consumption. These findings support customized drying strategies based on material properties and process geometry [8].

4 Conclusions

This study quantitatively demonstrates the effect of particle size and moisture content on the aerodynamic drag of coir pith particles in free fall, providing insights directly relevant to rotary drying. Experimental results show that increasing moisture content from 20% to 60% raised drag coefficients (C_d) by 65–95% depending on particle size and fall height. On average, C_d increased by ~83% for 1.2 mm particles, ~70% for 0.85 mm particles, and ~73% for 0.35 mm particles.

Moisture also had a pronounced impact on acceleration. At 2.5 m drop height, the acceleration of 1.2 mm particles more than doubled (0.0036 → 0.0077 m/s²), while for 0.35 mm particles it increased nearly sevenfold (0.0005 → 0.0037 m/s²). This confirms that higher moisture content not only increases drag but also delays the approach to terminal velocity by amplifying particle inertia and aerodynamic resistance.

Larger particles consistently exhibited higher drag coefficients under moist conditions, highlighting a strong size moisture interaction. For rotary dryers, these findings imply that high-moisture particles resist airflow more strongly and settle more slowly, extending residence times and reducing drying efficiency. The observed ~5–7% increase in C_d per 10% additional moisture underscores the importance of accounting for moisture variability in dryer design and control.

Future work should extend drop heights to capture terminal velocity and apply computational fluid dynamics (CFD) to generalize these quantified findings to rotary dryer geometries.

References

1. J. A. K. M. Fernando and A. D. U. S. Amarasinghe, Drying kinetics and mathematical modeling of hot air drying of coconut coir pith, *Springerplus*, 5(1), Dec. 2016, doi: 10.1186/s40064-016-2387-y.
2. J. A. K. M. Fernando and A. D. U. S. Amarasinghe, Effects of retting and drying on quality of coir pith and coco discs, J Natl Sci Found, 45(1), pp. 3–12, 2017, doi: 10.4038/jnsfsr.v45i1.8032.
3. R. Rasheed, R. Raffik, B. Sabitha, and S. R. Karthickeyan, Induction Based Coir Pith Drying Machine, 2021. [Online]. Available: www.tjprc.org
4. P. Agarwal, S. Saha, and P. Hariprasad, Agro-industrial-residues as potting media: physicochemical and biological characters and their influence on plant growth, Jul. 01, 2023, Springer Science and Business Media Deutschland GmbH. doi: 10.1007/s13399-021-01998-6.
5. V. Jakka, A. Goswami, A. K. Nallajarla, U. Roy, K. Srikanth, and S. Sengupta, Coconut coir–derived nanocellulose as an efficient adsorbent for removal of cationic dye safranin-O: a detailed

mechanistic adsorption study, Environmental Science and Pollution Research, pp. 1–22, Aug. 2023, doi: 10.1007/S11356-023-29075-7/METRICS.

6. S. Alagendran, V. Prakash, J. Kavitha, R. Kamaleshwaran, P. Prabharan, and S. Alagendran, Effect of coir pith compost in agriculture, Journal of Medicinal Plants Studies, 9(4), pp. 106–110, 2021, Accessed: Aug. 30, 2024. [Online]. Available: www.plantsjournal.com
7. B. Matthew Waters, T. Yan, S. Celik, and J. Darabi, The Analysis and Optimization of an Industrial Countercurrent Flow Rotary Dryer, 2023.
8. M. H. Lisboa, D. S. Vitorino, W. B. Delaiba, J. R. D. Finzer, and M. A. S. Barrozo, A study of particle motion in rotary dryer, Brazilian Journal of Chemical Engineering, 24(3), pp. 365–374, 2007, doi: 10.1590/S0104-66322007000300006.
9. M. A. Karali, E. Specht, J. Mellmann, H. A. Refaey, M. R. Salem, and A. Y. Elbanhawy, Granular transport through flighted rotary drums operated at optimum-loading: Mathematical model, Drying Technology, 2019, doi: 10.1080/07373937.2019.1582062.
10. T. H. Günther and K. A. Hoang, Drag Coefficient Estimation of Low Density Objects by Free Fall Experiments, Annals of West University of Timisoara - Physics, 65(1), pp. 51–66, Dec. 2023, doi: 10.2478/awutp-2023-0005.
11. G. Bagheri and C. Bonadonna, On the drag of freely falling non-spherical particles, Powder Technol, 301, pp. 526–544, Nov. 2016, doi: 10.1016/j.powtec.2016.06.015.
12. B. Y. Gorial and J R O'callaghan, Separation of Grain from Straw in a Vertical Air Stream, 1991.
13. P. Gluck, Air Resistance on Falling Balls and Balloons, Phys Teach, 41(3), pp. 178–180, Mar. 2003, doi: 10.1119/1.1557510.
14. P. Timmerman and J. P. Van Der Weele, On the rise and fall of a ball with linear or quadratic drag, 1999.
15. K. R. Sunkara, F. Herz, E. Specht, J. Mellmann, and R. Erpelding, Modeling the discharge characteristics of rectangular flights in a flighted rotary drum, Powder Technol, 234, pp. 107–116, Jan. 2013, doi: 10.1016/J.POWTEC.2012.09.007.
16. R. Cross and C. Lindsey, Measuring the Drag Force on a Falling Ball, Phys Teach, 52(3), pp. 169–170, Mar. 2014, doi: 10.1119/1.4865522.

Poster Presentations

3rd International Engineering Research Symposium 2025 (IERS 2025)
Colombo, Sri Lanka

Aerodynamic effects of dent holes on airfoils under subsonic and supersonic flow conditions

A.D.G Pathirana[1] and Geethal Siriwardana[2]

[1] Department of Mechanical and Automotive Engineering, Faculty of Engineering and Technology CINEC Campus, Malabe, Sri Lanka
[2] Department of Mechanical Engineering, Faculty of Engineering, University of Sri Jayewardenepura, Sri Lanka
[1]achaladpathirana@gmail.com
[2]geethal@sjp.ac.lk

Abstract. This research investigates the aerodynamic performance of airfoils in both subsonic and supersonic flows, focusing on the impact of non-symmetric and symmetric surface dents. Unlike previous studies that primarily considered symmetric or regularly spaced dimples, this study explores the effects of isolated dents—hemispherical, conical, and cylindrical—placed at various chordwise locations on both the upper and lower surfaces of the airfoil. Computational simulations were conducted using ANSYS Fluent. A total of 54 simulations were performed for a three-dimensional NACA 0012 airfoil under subsonic conditions, with Reynolds numbers ranging from 1.9×10^6 to 8.3×10^6 and angles of attack from $-12°$ to $+12°$. Additionally, nine two-dimensional simulations were carried out for a double-wedge airfoil at Mach number 3 to assess performance in the supersonic regime. The results demonstrate that the geometry, location, and surface area of dents significantly influence aerodynamic behavior. In subsonic flow, the highest lift-to-drag ratio of 49.6 was achieved with a hemispherical dent located at the mid-chord on the upper surface, indicating improved boundary layer control and delayed flow separation. In supersonic flow, a trailing dent placed at the leading edge of the lower surface generated lift even at zero angle of attack, doubling the lift-to-drag ratio compared to the clean airfoil. These findings were validated by benchmarking clean airfoil simulations against NASA's NACA 0012 data and existing literature, showing good agreement in pressure distribution and drag values. Overall, the study provides compelling evidence that non-symmetric dents can function as effective passive flow control mechanisms, with potential applications in UAVs, missiles, and other high-speed aerospace platforms.

Keywords: Airfoil Aerodynamics, Non-Symmetric Dimples, Passive Flow Control, Subsonic and Supersonic Flow, Computational Fluid Dynamics

1 Introduction

The aim of this study is to investigate the aerodynamic effect of such non-symmetric dent characteristics. By simulating dents of different shapes (conical, cylindrical, hemispherical), sizes, and positions along the airfoil chord, this work aims to understand how these localized geometric deviations affect lift, drag, and overall aerodynamic efficiency. A total of 54 three-dimensional simulations were performed on a NACA 0012 airfoil under subsonic conditions, with velocities ranging from 30 m/s to 130 m/s and angles of attack between −12° and +12°. To extend the work to high-speed regimes, nine two-dimensional supersonic calculations were conducted with a double-wedge airfoil at Mach number 3 as representative missile or high-speed wing sections. One particular region of interest in this research is the effect of non-symmetric dent placement on boundary layer behavior, separation, and, in supersonic flows, on geometry-local shockwave interaction. Through comparison of dented versus smooth surfaces, and through examination of lift-to-drag (L/D) ratios, the investigation tries to discern patterns and locations that would provide better aerodynamic performance via passive flow control. In the last several years, a number of studies have been conducted on the effect of dimples and surface modifications on the aerodynamic performance of airfoils. These investigations—both experimental and numerical—have covered a range of airfoil profiles, dimple geometries, and locations. Findings, however, vary from study to study, especially on whether the occurrence of dimples improves or worsens performance. Livya et al. [1] and Kaushik et al. [2] numerically studied a 3D symmetric NACA 0018 airfoil with various dimple geometries. Livya [1] tested semi-spherical, cylindrical, hexagonal, and compound dimples and determined that inward semi-spherical shapes gave maximum lift enhancement. Kaushik [2] found through his studies that both inward and outward dimples increased lift but also drag. Srivatsav [3] later confirmed with 2D and 3D simulations that outward dimples reduced drag in 2D, while in 3D, lift was increased at the expense of higher drag. Saraf et al. [4] tested on a NACA 0012 airfoil, testing 2D cases experimentally with dimples at different chordwise positions. The best performance was achieved when the dimple was positioned around 75% of the chord, which shows that position is crucial to the behavior of flow. Singh et al. [5] tested a NACA 0011 airfoil experimentally with different shapes and sizes of dimples and concluded that semi-cylindrical outward dimples of medium size positioned at 66% chord length performed optimally. In addition, Binci et al. [6] found that dimples on a NACA 64-014A airfoil reduced laminar separation and pressure drag, leading to enhancement of aerodynamic stability. On the contrary, Stolt et al. [7] reported performance losses caused by dimple application on a NACA 0015 airfoil, particularly in the leading-edge region. Zulkefli and MohdNur [8] tested dimples on a NACA 4415 profile and determined that inward and outward dimples were not effective near stall but that inward dimples gave

marginal lift-to-drag benefits at moderate angles of attack. Mustak et al. [9] showed that both forms of dimples delayed stall by approximately 4° and improved lift and drag performance over the range of angles of attack. Further, Tej et al. [10] conducted a comparative CFD study of various 3D NACA airfoils and concluded teardrop-shaped inward dimples at 70% chord to be most effective, especially on more highly cambered airfoils. Some research has been conducted to improve flow control and delay in separation over airfoils. Siauw et al. [11] performed an experiment of pneumatic vortex generators on a NACA 0015 airfoil and noted a pressure-velocity signal correlation during the occurrence of flow separation at high attack angles. Niu et al. [12] performed dynamic stall behavior on a NACA 0012 airfoil and showed that a variable droop leading-edge can enhance aerodynamic performance. Also, conventional camber-changing devices like slats and flaps have been shown to increase lift [13]. Matsson et al. [14] took the NACA 2412 airfoil at low Reynolds numbers into account and found the stall angle to be somewhere between 14° and 16° by experiment and CFD investigation. Overall, these studies show that the dimple performance is a function of several parameters shape, size, location, and airfoil geometry. While some configurations enhance the lift and reduce the drag, others may worsen the performance. Such inconsistency brings out the need for exhaustive parametric studies like the current work, which addresses non-symmetric dents in subsonic flow. Supersonic aerodynamics studies recently have focused on the impact of surface geometry changes on shock behavior and aerodynamic performance. Hodson et al. [15] and Manshadi & Aghajanian [16] demonstrated that optimal airfoil shapes have the potential to maximize lift-to-drag performance by reducing shock. Hari et al. [17] showed that small surface intersections can have a profound influence on shockwave interactions. Together, these papers confirm that supersonic flow can be passively manipulated by local surface features—i.e., dents or dimples. This work builds upon that foundation by investigating non-symmetric dent geometries as a passive means to control shock-boundary interactions and improve aerodynamic efficiency. Ajay Varma [18] formulated Pressure Coefficient is found to decrease with increase in Mach number after the shock. Maximum Mach number and turbulent kinetic energy over the surface is found to increase with inlet Mach number. Aminjan et al. [19] conducted a CFD (Computational Fluid Dynamics) simulation of thick double-wedge airfoils at Mach number 2. The research is likely to have been aimed at the study of aerodynamic characteristics of such airfoils under the condition of supersonic flow at a Mach number of 2 and could have studied the effect of airfoil thickness on the flow pattern. Ferrari developed an analytical theory in 1958 to calculate wave drag for thin double-wedge airfoils [20]. The theory provides a way of understanding and predicting the drag behavior of such airfoils at supersonic velocities. The most significant aspect of the theory is its consideration of the wave drag as a significant contributor to overall drag at supersonic velocities due to the formation of shock waves. This work adds to a clear

void in published research for utilizing previous studies and examining non-symmetric dents on 2D and 3D airfoils under subsonic and supersonic conditions. This situates this research in a special position of contributing innovative insights to passive flow control and aerodynamic surface development.

The findings not only reveal the mechanisms by which surface damage can lead to decreased performance but also mechanisms by which strategically located dents can increase lift or reduce drag a potential concept for UAVs, missiles, and high-speed applications where the use of external control devices is undesirable. This study bridges the gap between idealized control of airflow and real geometric defects.

2 Computational Methodology

This study investigates the aerodynamic influence of surface dents on airfoils under both subsonic and supersonic conditions using Computational Fluid Dynamics (CFD) in ANSYS Fluent. The NACA 0012 airfoil for the subsonic case and double-wedge airfoil for the supersonic case were considered. Various dimple geometries—symmetric and non-symmetric geometries were explored using surface geometry modification and the calculation of lift, drag, and flow structure. In the subsonic simulations, dent diameters were varied between (1–10) % of the chord length, with depths ranging from (0.3-1) % of the chord. These ranges were chosen to capture shallow dents as well as deeper configurations that could act as passive flow-control devices. The purpose of this variation was to investigate whether dent size influences laminar–turbulent transition, flow separation, and stall delay.

Governing Equations The computational analysis of airflow over the dented airfoils was performed by solving the Reynolds-Averaged Navier-Stokes (RANS) equations along with the Shear Stress Transport (SST) k–ω turbulence model in ANSYS Fluent. These equations govern the conservation of mass, momentum, and turbulence transport. All equations were solved in steady-state form, using a second-order discretization scheme
Continuity equation;

$$\partial u/\partial x + \partial v/\partial y + \partial w/\partial z = 0 \quad (1)$$

Momentum equations;

$$\rho(u\,\partial u/\partial x + v\,\partial u/\partial y + w\,\partial u/\partial z) = -\partial p/\partial x + \mu\nabla^2 u \quad (2)$$

$$\rho(u\,\partial v/\partial x + v\,\partial v/\partial y + w\,\partial v/\partial z) = -\partial p/\partial y + \mu\nabla^2 v \quad (3)$$

$$\rho(u\,\partial w/\partial x + v\,\partial w/\partial y + w\,\partial w/\partial z) = -\partial p/\partial z + \mu\nabla^2 w \quad (4)$$

k-equation:(turbulence kinetic energy);

$$\partial(\rho k)/\partial t + \nabla\cdot(\rho k V) = Pk - \beta^*\rho k\omega + \nabla\cdot[(\mu + \sigma k\mu t)\,\nabla k] \quad (5)$$

ω-equation:(specific dissipation rate);

$$\partial(\rho\omega)/\partial t + \nabla\cdot(\rho\omega V) = \alpha(\omega/k)Pk - \beta\rho\omega^2 + \nabla\cdot[(\mu + \sigma\omega\mu t)\,\nabla\omega \qquad (6)$$

Nomenclatures: u, v, z are the components of velocity vector in x, y, z-components ρ= air density, μ= dynamic viscosity, Pk = production term of k, ∇= velocity vector, α, β, σk, σω= empirical constants derived from calibration.

2.1 Subsonic Methodology

Mesh Sensitivity Analysis A mesh independence test was conducted to ensure accurate aerodynamic predictions for the subsonic 3D NACA 0012 airfoil. Three meshes of increasing density, containing approximately 400,000, 500,000, and 800,000 elements, were generated and tested at 50 m/s and 0° angle of attack (AoA). Inflation layers were applied near the airfoil surface to resolve the boundary layer, with the first cell height adjusted to achieve $y^+ < 1$, ensuring compatibility with the SST k–ω turbulence model. Lift and drag coefficients were computed for each mesh and compared to evaluate convergence. Minimal variation (<4%) was observed beyond 500,000 elements, confirming that further refinement did not significantly affect the results. Based on this analysis, the finest mesh of 800,000 elements was adopted for all subsonic simulations.

Computational Setup A 3D model of NACA 0012 airfoil with a chord length and span of 1 meter was prepared. Hemispherical, cylindrical, and conical shaped surface dents of different depths and diameters were developed and introduced at various chordwise from leading edge to trailing edge positions on upper and lower surfaces.

The computational domain was stretched, vertical height 8 and horizontal height 12 lengths to offer undisturbed flow. An unstructured tetrahedral mesh was generated, such as inflation layers next to the airfoil surface. The boundary conditions were a uniform velocity inlet (30–130 m/s), pressure outlet 0 Pa, symmetry side surfaces, and a no-slip airfoil wall. The simulations used the pressure-based solver with SST k–ω turbulence model, which is capable of simulating boundary layer separation and near-wall effects. Second-order discretization schemes were used, and simulations were run until residuals fell below 10^{-5} and aerodynamic forces converged. Reynolds numbers ranged between 1.91×10^6 and 8.29×10^6, which were dependent on inlet velocity

Simulation Parameters

Table 1. Simulation case setup for NACA 0012 airfoil.

Case No	Reynolds Number	Dent shape	Dimple diameter (D/C)	Dimple depth (d/D)	Placement (%Chord)	AoA (·)
1-4	1.91×10^6	-	-	-	-	-4,0,4,12
5	6.38×10^6	-	-	-	-	-8
6	7.65×10^6	H S(N-S)	0.01	0.3	L E	12
7-11	1.91×10^6	H S(N-S)	0.01	0.3	L E	-8, -4,0,4 8
12-16	6.38×10^6	H S(S)	0.1	0.5	M C	-4,0,4,8 12
17	4.46×10^6	H S(S)	0.1	0.5	M C	-8
18-22	1.91×10^6	H S(N-S)	0.05	0.333	T E	-4,0,4,8 12
23	3.19×10^6	H S(N-S)	0.05	0.333	T E	-12
24-26	3.19×10^6	H S(N-S)	0.01	1	L E(L-S)	-8,0,8
27-30	3.19×10^6	CO(N-S)	0.05	0.5	L E	-4,0,4,12
31	4.46×10^6	CO(N-S)	0.05	0.5	L E	-12
32-35	6.38×10^6	CO(S)	0.05	0.5	M C	-8,0,8,12
36	8.29×10^6	CO(S)	0.05	0.5	M C	-12
37-38	1.91×10^6	CO(N-S)	0.01	0.1	T E	4,8
39	6.38×10^6	CO(N-S)	0.01	0.1	T E	0
40	1.91×10^6	CO(N-S)	0.01	0.1	T E	-4
41	4.46×10^6	CO(N-S)	0.01	0.1	T E	-8
42-45	6.38×10^6	CO(S)	0.05	0.5	M C(L-S)	-4,0,4,4
46	6.38×10^6	CY(B-C)	0.05	1.5	L E	0
47	6.38×10^6	-	-	-	-	8
48	1.91×10^6	H S(N-S)	0.01	0.1	T E(L-S)	0
49	6.38×10^6	CY(B-C)	0.05	0.52	M C	0
50	1.91×10^6	CY Hole	0.01	6	L E	0
51-54	6.38×10^6	CY(B-F)	0.05	0.2	T E	-12, -8,0,12

Nomenclatures :C=chord length, H S=Half spherical, CO=conical, CY=Cylindrical, N-S=non-symmetric, S= symmetric, B-C= bottom curve, B-F= bottom flat, L E= Leading edge, M C= Mid chord, T E= Trailing edge, L-S= lower surface

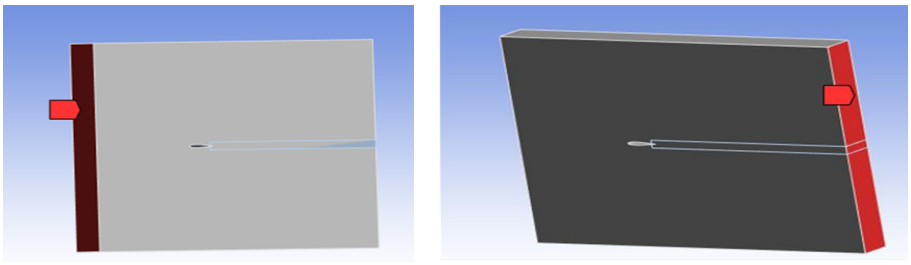

(a) **(b)**

Fig. 1. Boundary conditions (a) inlet (b) outlet

2.2 Supersonic Methodology

For the supersonic simulation, a 2D double-wedge airfoil of 2 meters chord length and 0.3 meters height was simulated. Mesh density was increased at leading edges and dimple locations to capture shock interactions accurately. Boundary conditions were defined as a supersonic inlet (Mach number 3), pressure outlet, and inviscid slip wall boundary on the surface of the airfoil.

Two simulation approaches were utilized. First, an inviscid flow simulation was used to study generic shock wave structures and surface pressure effects. Second, particular cases were simulated using a viscous setup with the SST k–ω model of turbulence to account for boundary layer flow effects. The solver was run at compressible flow conditions with coupled formulations, with convergence ensured through monitoring drag, lift, and residual stability.

Table 2. Supersonic simulation setup parameters for double wedge airfoil

Case No	Mach No	Dent shape	Dimple diameter(m)	Dimple depth(m)	Placement	Turbulence Model	AoA (·)
1	3	-	-	-	-	Inviscid	0
2	3	S C(S)	0.009	0.009	L E(U-S)	Inviscid	0
3	3	S C(S)	0.01	0.01	L E(L-S)	Inviscid	0
4	3	T (S)	0.003	0.003	L E(L-S)	Inviscid	0
5	3	S C(S)	0.009	0.009	L E(U-S)	Inviscid	0
6	3	T (NS)	0.01	0.01	L E(L-S)	Inviscid	0
7	3	T (NS)	0.02	0.02	L E(L-S)	Inviscid	0
8	3	T (NS)	0.003	0.003	L E(L-S)	Inviscid	0
9	3	T (NS)	0.01	0.01	L E(L-S)	SST k–ω	4

Nomenclatures: S C= Semi-circle, T= Triangular, S= symmetric, NS= Non-symmetric, L E= Leading edge, U-S= upper surface, L-S= lower surface

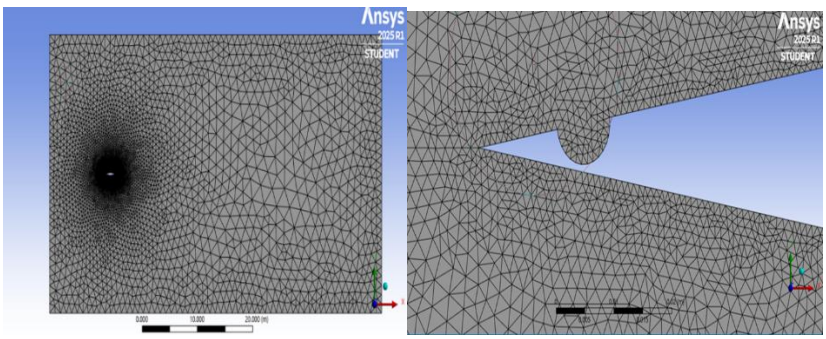

(a) **(b)**

Fig. 2. Mesh configuration (a) Airfoil (b) Around dimple

3 Results and Discussion

3.1 Subsonic Regime

Among the modified geometries, the symmetric conical dimple at mid-chord (Case 15) showed the most aerodynamically superior performance with Cl = 0.8 and Cd = 0.017 at 4° AoA, with a Cl/Cd ≈ 49.6 superior to the smooth and other dimpled geometries. Similarly, the asymmetric half spherical dimple at the leading edge lower (Case 26) produced Cl = 0.85 and Cd = 0.019, yielding a lift-to-drag ratio of 44.54 at 8° AoA. Both cases confirmed that carefully designed dimples shallow and placed strategically can maintain or improve aerodynamic efficiency without active control mechanisms. On the other hand, cylindrical dimples, particularly curve-bottomed and deep dimples, incurred aerodynamic penalties. Case 50, for example, had negative lift (Cl = –0.017) and moderate Cd, meaning that such configurations destabilize the boundary layer and promote premature separation. Even the flat-bottom cylindrical dimple at the trailing edge (Case 23), though better, was worse than conical counterparts.

Comparison of Baseline Airfoil (smooth NACA 0012) with special dented cases of each AoA

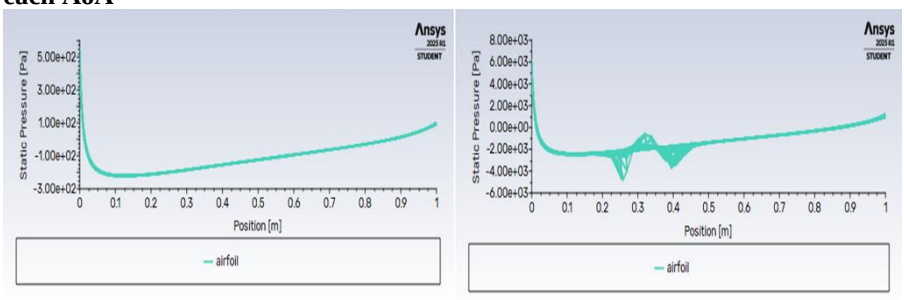

(a) **(b)**

Fig. 3. Static pressure (a)baseline airfoil, (b) conical symmetric dent shape airfoil

According to Fig. 3, (a) Static pressure is symmetrically distributed along the chord. Maximum pressure is located near stagnation point at leading edge. Pressure drops off quickly over both surfaces indicating initial acceleration, with no asymmetry due to zero AoA.(b) Pressure plot shows localized regions of increased pressure recovery near the dimple. A noticeable high-pressure buildup is seen in front of the dimple due to flow stagnation and

flow redirection, forming a mini shock-like effect even in subsonic flow. Pressure is relatively lower downstream of the dimple, suggesting flow reattachment and reduced separation or vortex formation.

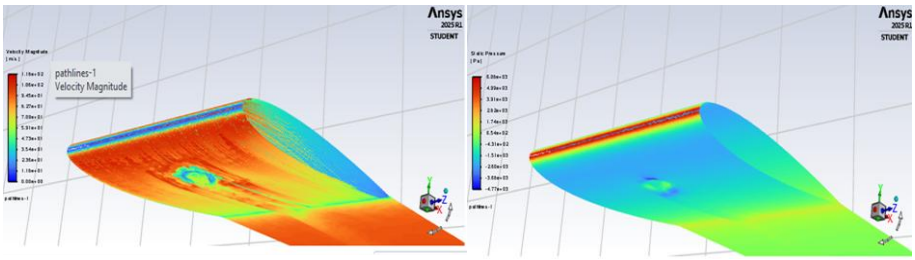

(a) **(b)**

Fig. 4. (a) velocity magnitude, (b) static pressure

According to Fig. 4, (a) The dent imposes a local velocity gradient close to the surface. In the dented form, observed slight flow acceleration over the dimple due to local curvature and flow constriction. This imposes slight suction on the upper surface and a positive pressure gradient that has to enhance L/D ratio by managing boundary layer growth. (b) A visible low-pressure region is formed around the dimple location, which enhances suction. The local depression generates a marginal lift gain and a boundary layer energizing effect that reduces flow separation. As a result, drag is also decreased.

3.2 Supersonic Regime (Comparative Efficiency Based on L/D Ratio)

L/D ratio is a most critical performance metric of aerodynamics. In current dataset, the smooth airfoil (Case 1), in Table 2 yielded L/D ≈ 0 while Case 3 yielded an improved L/D ≈ 0.81 and case 7, L/D= 2.005 at the expense of adding a passive flow control geometry.
Supreme case (Case 7): lower surface triangular dimple, Cd =0.083, Cl =0167, L/D = 2.004, Worst case (Case 5): upper surface dimple degraded both lift and drag
Baseline (Case 1): near zero lift, reasonable drag.

Pressure, velocity contours variation with baseline & dimpled cases of double wedged airfoil

According to Fig.5(a)normal oblique shock structures form at the leading edge of the wedge surfaces. Flow is symmetric: pressure distribution on upper and lower surfaces is the same. (b)Acceleration behind the leading edge is linear followed by smooth deceleration in the downstream zone. No vortex structures or flow separation are seen.

This is what should be expected for idealized supersonic flow over sharp-edged bodies

(c) Asymmetric pressure distribution is established higher pressure on top surface than at bottom contributing to net positive lift. Shock wave of the dimple appears shallow and well-contained, keeping pressure drag to a minimum. (d)Velocity increases a bit near the dimple, indicating localized acceleration. Flow is attached with no sign of a separation bubble. A vortex or recirculation zone is indicated by a change in velocity gradient downstream of the dimple. The triangular shape creates passive flow control, re-energizing the boundary layer at little cost in drag. This result is in line with passive vortex generator theory in the supersonic regime boosting Cl without great shock costs, producing an improved L/D. (e) Pressure drop due to the dimple does occur, albeit diffused with respect to Case 6.A smaller pressure gradient is formed across the airfoil. There is some asymmetry but no significant favorable pressure gradient subsequent to the dimple.

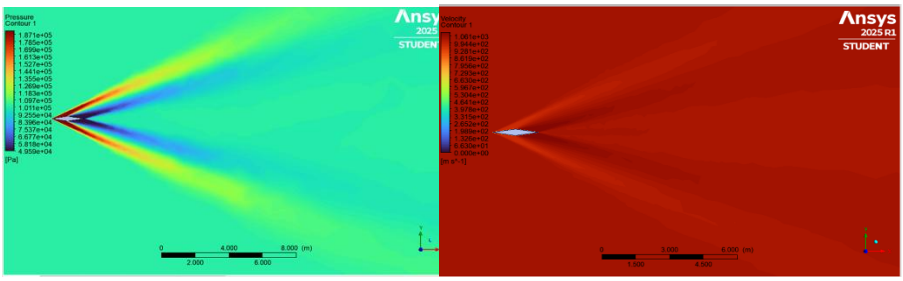

(a) **(b)**

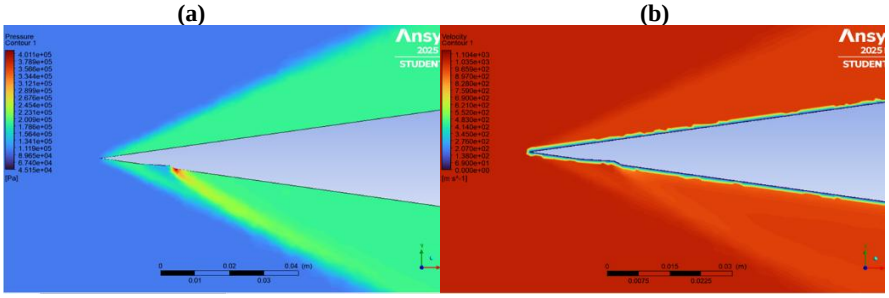

(c) **(d)**

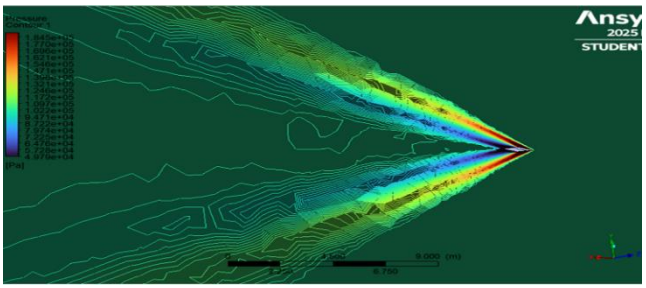

(e)

Fig. 5. (a) pressure contour of baseline airfoil, (b) velocity contour of baseline airfoil, (c) pressure near dimple area (case 6),
(d) velocity around dimple area (case 6), (e) pressure contour of (case 2)

4 Conclusions

This study completely explored the aerodynamic impact of symmetric and non-symmetric dent holes on airfoils under subsonic and supersonic flow. 54 subsonic CFD runs on a 3D NACA 0012 airfoil with variation of dent shape, size (diameter and depth), and location along the chord were conducted. In the supersonic regime, nine 2D runs on a double-wedge airfoil at Mach number 3 examined the impact of corresponding geometric perturbations on shockwave formation and aerodynamic coefficients. The results confirmed that some of the dent configurations could enhance lift-to-drag ratio (L/D), verifying the aerodynamic potential of passive geometric control. The best performing subsonic case 15 with half spherical mid-chord dimple registered a Cl/Cd ratio of 49.6, while Case 26 (an asymmetric half-spherical dimple at lower leading edge) registered a ratio of 44.5. Supersonic computation also showed encouraging performance improvement, especially in Case 7, which significantly enhanced L/D ratio double over the baseline.

These findings validate that localized, shallow surface dents especially those positioned near the leading or mid-chord locations can have beneficial effects on flow behavior independently of active control mechanisms. The research hence advocates for the application of non-symmetric dimples as a passive approach to enhancing aerodynamic efficiency under both low-speed and high-speed flight conditions. Current and future work ought to advance viscous supersonic simulations, wind tunnel tests, and multi-objective optimization of dent geometries for practical applications in aerospace engineering.

References

1. E. Livya, G. Anitha and P. Valli, Aerodynamic Analysis of Dimple Effect on Aircraft Wing, International Journal of Aerospace and Mechanical Engineering, 9(2), pp. 350-353, 2015.
2. V. Kaushik, M. Mahore and S. Patil, Analysis of Dimpled Wing of an Aircraft, International Journal of Engineering Development and Research, 6(3), 2018.
3. D. Srivastav, Flow Control over Airfoils using Different Shaped Dimples, International Conference on Fluid Dynamics and Thermodynamics Technologies, Singapore, 2012.
4. A. K. Saraf, M. P. Singh, T. S. Chouhan, Effect of Dimple on Aerodynamic Behaviour of Airfoil, International Journal of Engineering and Technology, 9(3), pp. 2268-2277, 2017.
5. D. Singh, R. H. Gajghat, M. K. Manik, Experimental Investigation to Examine the Effect of Shape and Size of Dimple at Suction Surface of Aerofoil, International Journal of Scientific & Technology Research, 8(12), pp. 521-534, 2019.
6. L. Binci, G. Clementi, V. D'Alessandro, S. Montelpare and R. Ricci, Study of the flow field past dimpled aerodynamic surfaces: numerical simulation and experimental verification, 35th UIT Heat Transfer Conference, Ancona, Italy, 2017.
7. A. J. Stolt, A. H. Ullah and J. Estevadeordal, Study of Leading-Edge Dimple Effects on Airfoil Flow Using Tomographic PIC and Temperature Sensitive Paint, Fluids, 4(4), 2019.
8. N. F. Zulkefli, W. K. F. W. Samsudin and N. M. Nur, Dimples Effectiveness on Naca4415 Airfoil, International Journal of Advanced Science and Technology, 29(6), pp. 203-207, 2020.
9. R. Mustak, N. Uddin, MD. and M. Mashud, Effect of different shaped dimples on airfoils, Proceedings of the International Conference on Mechanical Engineering and Renewable Energy, Chittagong, Bangladesh, 2015.
10. G. R. Tej, B. Rajasai and S. Anurang, Variation of Behaviour of Dimples on Aircraft Wings, IEEE Aerospace Conference, Big Sky, Montana, 2016.
11. Attenuation of Shock Induced Separation, Int. J. Appl Sci Technol, 2(3), pp 34-52, 2012.
12. W. L. Siauw and J. P. Bonnet, Transient phenomena in separation control over a NACA 0015 airfoil, Int.J. Heat Fluid Flow, 67, pp 23-29, 2017.
13. J. Niu, J. Lei, T. Lu, Numerical research on the effect of variable droop leading-edge on oscillating NACA 0012 airfoil dynamic stall, Aerospace Science and Technology, 72, pp 476–485, 2018.
14. S. Mahon, X. Zhand, Computational analysis of pressure and wake characteristics on an aerofoil in ground effect, ASME, 127, pp 290-298, 2005.
15. J. D. Hodson, A. P. Christopherson, J. D. Deaton, A. M. Pankonien, G. W. Reich, P. S. Beran, Aeroelastic topology optimization of a morphing airfoil in supersonic flow using evolutionary design. AIAA Scitech Forum, 2019.
16. N. Hari, J. A. Schetz, R. K. Kapania, Numerical prediction of interference drag of a strut-surface intersection in supersonic flow, AIAA Scitech Forum, 2019.

17. [17] Manshadi MD, Aghajanian S (2018) Computational aerodynamic optimization of wing-design concept at supersonic conditions by means of the response surface method. J Braz Soc Mech Sci Eng 40(5):254–265
18. A. Varma, Aerodynamic Analysis Over Double Wedge Airfoil, IOP Conference Series Materials Science and Engineering, 197(1):012076, 2017.
19. Aminjan, Aerodynamic Analysis of Double Wedge Airfoil in Different Angle of Attack at Supersonic Flow, Solid State Technology, 63(6):14417-14428, 2020.
20. C. Ferrari, Analytical prediction of wave drag for double-wedge airfoils. Journal of the Aeronautical Sciences, 25(10), pp.662–664, 1958.

3rd International Engineering Research Symposium 2025 (IERS 2025)
Colombo, Sri Lanka

Assess the Technical Applicability of Piezoelectric Floor Tile Energy Harvesting as a Renewable Energy Source for Public Buildings in Sri Lanka

J. A. D. V. S. W. Jayasundara[1*], W. N. Kawmudi[1], U. M. Samararathne[1] and I. U. Atthanayake[2]

[1]Department of Quantity Surveying, Faculty of Built Environment and Spatial Sciences (FBESS),General Sir John Kotelawala Defence University, Sri Lanka
[2]Department of Mechanical Engineering, Faculty of Engineering (FOE), Open University Sri Lanka
[*]38-bqs-0015@kdu.ac.lk

Abstract **-** With rising energy demands and diminishing fossil fuel resources, there is an urgent need for sustainable and alternative energy solutions, especially in developing countries like Sri Lanka. High-traffic public buildings present an untapped opportunity to harness human kinetic energy through piezoelectric floor tiles, offering a supplementary renewable energy source. Piezoelectric energy harvesting systems convert mechanical pressure into electrical energy, and when integrated into pedestrian zones of public spaces, they can contribute to localized energy needs. However, challenges such as low energy conversion efficiency, system durability, maintenance concerns, and limited public awareness hinder their widespread adoption. Addressing these concerns, this research evaluates the technological feasibility of implementing piezoelectric floor tiles in Sri Lanka public buildings, using the Colombo Fort Railway station as a case study. Employing a mixed-method approach, including energy output estimations, performance simulations, and stakeholder surveys. The study assessed the potential of piezoelectric flooring to contribute to the daily energy demands of low-power appliances in high-traffic public spaces. The analysis estimates that approximately 83Wh/day could be generated from 200,000 pedestrian footsteps, which is sufficient to power low-consumption devices such as LED, CCTV cameras or smart panels. Comparative analysis reveals piezoelectric floor tiles' unique advantage for indoor applications, maintaining consistent output regardless of sunlight conditions. Environmental assessments demonstrate significant reductions in indirect carbon emissions compared to conventional power generation methods. When combined with other renewable energy sources like solar power, this technology shows great potential as an additional solution,

even though it is insufficient as a stand-alone energy source. The stakeholder analysis also revealed a gap in awareness, emphasizing the importance of education and engagement initiatives to support future adoption. As a conclusion, the study highlights the technical viability of piezoelectric floor tiles as a supplementary renewable source for Sri Lankan public infrastructure and recommends pilot projects and further research and development to test feasibility and performance. The finding contributes to the foundational knowledge and policymaking efforts required to support innovative energy solutions like piezoelectric energy harvesting in the Sri Lanka context.

Keywords: Piezoelectric floor tile, Energy harvesting, Sustainable energy, Technological feasibility, Sri Lanka

1 Introduction

The growing global demand for renewable energy is driven by limited fossil fuel reserves and the urgent need to reduce environmental impacts. According to the International Energy Agency (IEA), global power consumption is expected to increase by nearly 80% between 2012 and 2040, emphasizing the necessity for a clean energy revolution to improve energy security, sustain economic growth, and mitigate climate change (Hybrid & Graphics, 2023). In Sri Lanka, over 50% of electricity generation relies on fossil fuel imports, imposing a significant economic burden due to limited indigenous resources (Development Bank, 2017). Consequently, Sri Lanka must prioritize renewable energy development to meet rising demand and reduce dependence on imports.

Piezoelectric energy harvesting, which converts mechanical pressure from human movement into electrical energy, presents a promising yet underutilized renewable source, especially in public spaces where foot traffic is high (Solban & Moussa, 2019). Research indicates that piezoelectric floors could power electrical devices like lighting and display systems in public infrastructure, with potential applications extending to indoor environments (Elhalwagy et al., 2017); (Yingyong et al., 2021). Despite its potential, this technology remains largely unexplored within Sri Lanka's public building sector.

This study assesses the technological feasibility and technical performance of integrating piezoelectric energy harvesting floors in Sri Lankan public buildings, comparing them with traditional renewable sources like solar energy. The research highlights the, potential and resilience that piezoelectric systems could offer, promoting sustainable energy solutions aligned with global goals such as the United Nations' "Affordable and Clean Energy" initiative (United Nations Development Programme, 2023).

2 Literature review

Energy harvesting converts wasted ambient energy like vibrations, heat, and human movement into usable electricity (Du et al., 2023); (Song et al., 2020). Mechanical energy is ideal due to its availability and density. Piezoelectric harvesting offers high efficiency, durability, and simplicity, making it practical for real-world use (Ahmed et al., 2020); (Rashmi et al., 2023); (Song et al., 2017).

The process of piezoelectric energy harvesting typically encompasses three main phases of energy transformation, as illustrated in the Fig. 1. energy flow diagram. These stages represent the fundamental steps through which mechanical energy is captured and converted into usable electrical power using piezoelectric materials and devices.

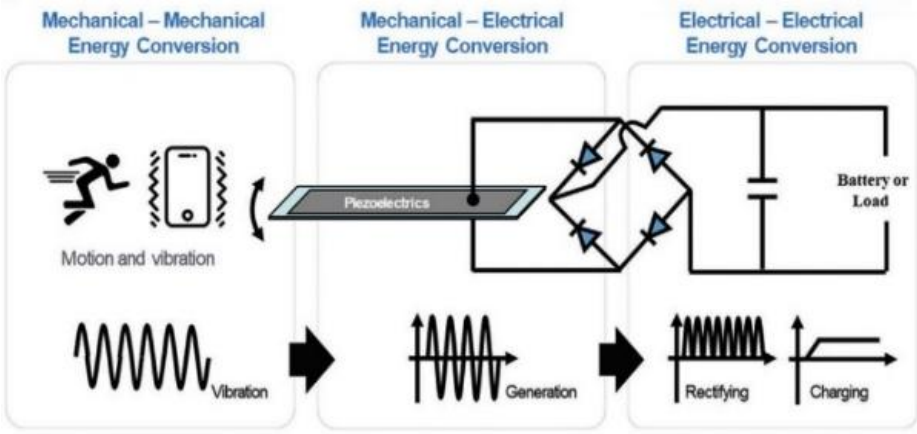

Fig. 1. Energy Conversion and Flow Diagram of Piezoelectric Energy Harvesting
Source: (Song et al., 2020)

Several global case studies highlight the practical applicability and efficiency of piezoelectric tiles in generating clean energy from foot traffic while reducing dependency on non-renewable energy sources. At Macquarie University, tiles installed in only 3.1% of the library floor space generated up to 9.9 MWh/year, showcasing their potential in high-traffic zones despite high costs (Li & Strezov, 2014). KLIA explored adoption factors using the TEMIF model (Chew et al., 2017), while installations in Portugal, Japan, and the Netherlands demonstrated energy savings up to 65% in bridges and clubs (Solban & Moussa, 2019) in Kuwait, 209.9 kWh/week was generated on sports tracks (Khalil, 2020).

Egypt's Rod El-Farag Metro station achieved 99.9% savings, with Wayenergy tiles generating 4560 kWh/day (Moussa et al., 2022). These examples support the study's objectives: evaluating piezoelectric tiles' potential to produce renewable energy and assessing their effectiveness as an alternative to traditional energy methods in high-footfall urban interiors. There are several varieties of piezoelectric tiles, as illustrated in Table 1.

Table 1. Piezoelectric Floor Manufacturers

	Company	**Average generating Power**
1	Pavegen	5W continuous power for footstep
2	Wayenergy	10W per step
3	Energy floors	35W/315W

Source: (Elhalwagy et al., 2017a); (Sharma et al., 2022)

This summarizes piezoelectric tile types based on their technical features and summarizes data from worldwide firms' product specifications for piezoelectric tiles. Also, shows the characteristics of different types of piezoelectric tiles, including size, energy output. (Solban & Moussa, 2019).

Public buildings in Sri Lanka serve as key spaces for public engagement, cultural expression, and social cohesion, blending colonial and modern architectural styles with climate-responsive features like high ceilings and verandas. Despite traditional materials, modernization has led to increased use of mechanical systems such as air conditioning (Gang et al., 2015). Efficient energy management remains a challenge, with studies highlighting the need for balance between environmental, social, and economic factors (Ozgun, 2020). Adaptive reuse of historic buildings offers sustainable solutions by reducing energy consumption, emphasizing user engagement amid global energy concerns (Ariyarathna et al., 2023); (Fouda et al., 2021).

Sri Lanka's public buildings face increasing energy demand due to modernization yet lack context-specific research. A comprehensive strategy addressing social, economic, and environmental factors is essential. Global studies (Alahakoon et al., 2022); (Catrini et al., 2020); (Pavlović et al., 2021) highlight the need to explore innovative renewable energy solutions locally.

3 Methodology

This study presents a mixed-methods approach to assess technical feasibility of piezoelectric energy harvesting in Sri Lankan public buildings. It involves analyzing energy needs, foot traffic data, product specifications, and stakeholder input through qualitative and quantitative methods. Using purposive sampling, the study adopts a pragmatic philosophy, combining technical and social analyzes for feasibility assessment.

Population and sample assessed piezoelectric energy harvesting in Sri Lankan public buildings including schools, universities, libraries, transport hubs, and museums – a representative sample of industry professionals, suppliers, and stakeholders from Sri Lanka and abroad will be surveyed. Respondents will be randomly selected from the industry.

a. Data Collection Methods

Evaluate the feasibility and effectiveness of piezoelectric energy harvesting in Sri Lankan public buildings, the study utilized two main data collection methods to gather comprehensive and reliable information. These methods ensured both practical field insights and theoretical background data for analysis.

In this study, a structured questionnaire was distributed to academic and industry professionals in Sri Lanka's building services sector to assess the technological feasibility of piezoelectric energy harvesting [Refer annexure A]. It was designed for clarity and accessibility, incorporating input from both groups to accommodate varying levels of prior knowledge. 50 questionnaires were distributed via Google Forms and in person, targeting 30% industry experts and 20% academic professionals. As above-mentioned this survey aimed to assess the technological feasibility, compared to solar energy, and implementation potential of piezoelectric floor tiles in Sri Lanka. It included open- and close-ended questions across two sections: respondent background and topic-specific insights, tailored to academic and industry groups.

Semi-structured interviews were conducted with renewable energy experts using purposive sampling, both in person and online. Open-ended questions covered two sections, similar to the questionnaire. Interviews with piezoelectric tile suppliers focused on the legal, and social feasibility of implementing such systems in Sri Lanka. Sessions were recorded for accuracy and reference.

Document review of existing academic literature, technical reports, case studies, and government policies related to renewable energy technologies, including piezoelectric floors and solar. Furthermore, include technical data on energy output, efficiency, and cost

from existing piezoelectric projects and compare it with other renewable technologies (ex: solar).

There is a need to select the most suitable public building to validate this research subject and findings. Transportational hubs were the best option to validate this research according to higher foot traffic volume. Within the proportional number of buildings from each group, using purposive sampling evaluated the applicability of this piezoelectric energy harvesting technology.

Colombo Fort Railway Station, established in 1908, is the central transit hub in Sri Lanka's capital, featuring 10 platforms, waiting areas, utility rooms, and accessible facilities (Colombo Fort Railway Station, 2024). As a key public space, it functions beyond transportation serving as a commercial and social hub with diverse patterns, including daily commuters during peak hours and leisure travellers on weekends. Serving nearly 200,000 passengers daily, the station reflects high public usage (Colombo Fort Railway Station, 2024). Factors such as city population, tourism, economic activity, and transport accessibility influence its foot traffic. This high traffic volume poses challenges in management but also presents strong potential for sustainable innovations like piezoelectric energy harvesting through floor tiles (Gang et al., 2015).

b. Data Analysis Methods

Content analysis was used to examine qualitative data from interviews and questionnaires, supporting the study's goal of exploring piezoelectric energy implementation in Sri Lanka, while also contributing to assessing its technological feasibility. Some analysis was based on assumptions due to limited practical evaluation during data collection. Technological possibility, was conducted using Sri Lankan government frameworks and a case study at Colombo Fort Station to assess implementation feasibility. Below energy calculation establish a framework to estimate piezoelectric energy generation in Sri Lankan public buildings using foot traffic data, energy per step, and system efficiency.

-Footsteps = Number of average pedestrian steps per day
-Energy per steps = Average joules harvested per step (J)
-Efficiency = System efficiency
-1Wh = 3600J

$$\text{Daily energy (Wh)} = (\text{Footsteps} \times \text{Energy per step} \times \text{Efficiency}) / 3600 \quad (1)$$

Source: Rumman & Elnaklah, (2024); Selim et al., (2024)

Equation 1, assumes a linear foot traffic-energy harvesting relationship, which is that the energy generation increases proportionally with the number of footsteps (Elhalwagy et al., 2017b). And the average steps in Colombo fort railway station was obtained by primary and secondary resources in accordance with the studied time period. For the average energy generated per step has obtained from research studies & real-time suppliers' interviews (Azmi & Adnan, (2024); Pavegen, (2025)). Efficiency is included to account for electrical losses in rectification, storing and transferring (Yue & Du, 2024).

This simulation results were compared against available real-world implementations, such as the piezoelectric pilot project at Japan-Tokyo station. Which reported average outputs 10-15Wh/day per m^2 under heavy foot traffic [(C et al., 2017; S et al., 2024; Thanach-Issarasak et al., 2021). However, the model outputs for this case study project fall within a similar scope order of magnitude, thereby providing this extracted equation for this study validation.

4 Data Analysis

a. Analysis Of Technological Feasibility by Validation Using Public Buildings in Sri Lanka

A simulated example was created based on important criteria, including densely populated, high-traffic regions (the Colombo Railway Station in particular) and other carefully chosen public areas, in order to verify the technological viability of this study.

The following assumptions were made:

- Average energy output per Footstep: 2 – 5 joules (Selim et al., 2024)

  Assumed minimum footsteps are equal to passenger count.
- Energy tile efficiency: 50% (Selim et al., 2024)

  Assumed 50% energy loss to storage and conversion procedures.

  According to actual parameters and above assumptions,

The estimated daily energy output is:

[Please note that 3J/step at 50% efficiency chosen as conservative midpoint to avoid overestimation in the feasibility analysis]

Daily energy output = 200,000 x 3 J x 0.5/3600

= 300,000 J (or 83.33 Wh)

- Daily footsteps: 200,000 (Colombo Fort Railway Station, 2024)

Fig. 2. Proposed Piezoelectric Flooring for Fort-Railway station
Source: Assumptions and interviewee data

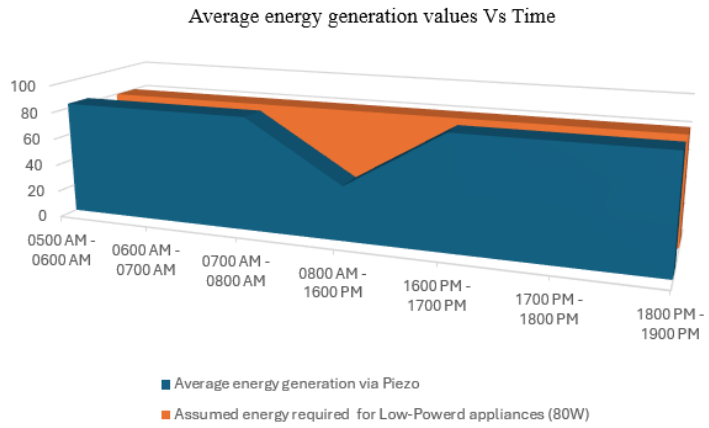

Fig. 3.

Technically, by evaluating the above simple analysis and graph detail, energy generation fluctuates across the day, with peaks corresponding to morning and evening rush hours (05:00am-08:00am and 16:00pm-19:00pm). This trend aligns with Colombo Fort commuter inflows, indicating that piezo harvesting may provide a predictable daily energy curve useful for low-power appliances load planning. So, using this technology some amount of energy can be harvested to cover up targeted energy demand. Following table will provide a summary for projected energy yields against some potential devices that can compatible.

Table 2. Projected energy yields & device compatibility

Device	Typical Power Rating	Operating hours Supported (Per day) with 83.33Wh
Ceiling Fan (60W)	60 W	~1.4 hours
LED Tube Light (15W)	15 W	~5.5 hours
CCTV Camera (10W)	10 W	~8.3 hours
Mobile Charging (5W)	5 W	~16.6 hours

b. Comparison with Solar Energy

Energy generation from a solar PV panel under Colombo's average solar irradiance of ~5.0kWh/m^2/day(SLSEA, 2022). Assuming a commercial panel efficiency of 18%, and this would yield ~900Wh/day per m^2, which is an order of magnitude higher than piezoelectric tiles. Nevertheless, unlike solar panels, piezo systems can independently work on any weather conditions and directly from foot traffic.

The above bar chart shows that general comparison between both systems, main concern of this chart is to demonstrate the applicability of this piezoelectric floor tile against solar systems. While solar panels currently offer higher efficiency due to more advanced technology, piezoelectric systems have a lower environmental impact, suggesting future potential as technology improves, according to expert opinions. Interviewees noted major practical challenges for the technological feasibility of piezoelectric tiles:

- Lack of skilled engineers
- Limited material availability
- Low energy conversion efficiency

Maintenance issues due to unawareness; are the main challenges when implementing this technology into Sri Lanka

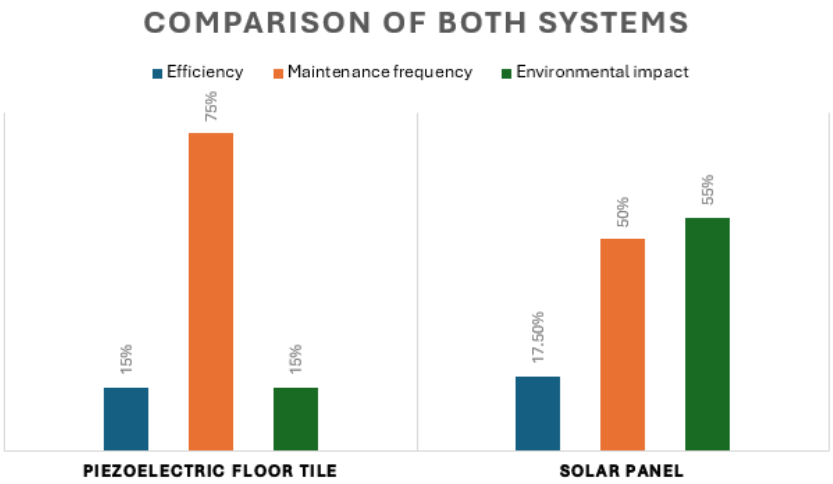

Fig. 4. General comparison between Solar and Piezo
Source: Ambrożkiewicz et al., (2023); Antwi et al., (2024); Verma et al., (2022); Zhang et al., (2024)

As previously mentioned, piezoelectric tiles have several long-term benefits as well. Environmental Benefits (Reduction of using fossil fuels) (Mohammed et al., 2024), Energy independence (Innovative energy contribution for country demands) (Uvaraj Mane et al., 2024), Public awareness (Innovative energy awareness) (Padmanegara Putra et al., 2024).

Piezoelectric tiles can power low-energy appliances but face durability and efficiency challenges in tropical climates; hybrid integration with solar panels is recommended for better energy reliability.

c. Technological Feasibility Analysis Based on Interview and Questionnaire Findings

Awareness and Understanding

About more than 50% of academics and industry professionals are already familiar with the concept, showing moderate readiness. However other remaining parties still remain

unfamiliar, indicating that for public-scale deployment such as Fort station, awareness campaigns and pilot demonstrations would be essential to build this stakeholder trust.

Challenges Identified
Higher initial cost woold be the most significant matter for these kinds of projects. Most of professionals have suggested to have this as research & development project or PPP funding. Lack of expertise, 65% of respondents have less expertise on this technology, therefore training programs, campaigns or some introduction courses would be more effective on this. Maintain difficulties also raised challenge throughout the interviews, so the suggested way is to have more durability testing and integrated ways to implement with this technology.

Applicability by Building Type
Public buildings like railway stations allocated as moderated benefited as per the respondent responses, while commercial spaces may show faster returns, fort station's symbolic visibility and very high pedestrian density make it strong candidate for piloting as well.

Academic Options
Researchers noted that data and prior studies are limited also making large -scale adoption challenging as well. Fortunately, they emphasized research contributions, new material development and academia-industry collaborations as crucial benefits.

Feasibility Outlook for Fort Station
As per most respondents' technological feasibility is positive, given the heavy consistent foot flow as mentioned and evaluated earlier in the study. Challenges like upfront cost, durability and skilled expertise remain but these may mitigate by implementing this technology as integrated model with solar. Ultimately implementing this project at heavy crowded area like fort station will serve as demonstration project, also it will cover the awareness gap and attract new stakeholders or investors for government support.

5 Conclusions

This study explored the technical applicability of piezoelectric energy harvesting in Sri Lankan public buildings, addressing technology, and social acceptance facts. Furthermore, this analysis indicates that a energy harvesting piezoelectric tile could generate approximately 83.33Wh/day in accordance to assumed foot print in Colombo fort railway station

at assumed parameters. While modest compared to solar, this generated output significantly enough for low-power consumption applainces such as LED, CCTV cameras or smart panel boards. Though the lack of suitable engineering, long-term benefits such as reduced fossil fuel use and lower environmental impact are promising [(Pasindu et al., 2017); Farnoosh, 2002)]. These findings are aligning with Sri Lankan national renewable energy vision, which target as 70% renewable energy sourced by 2030 and also net-zero pathway by 2050 as well (SLSEA, 2022). Integration with solar power is recommended for efficiency. Key barriers include harvesting engineering method, limited expertise, and maintenance challenges (Chew et al., 2017), but these can be overcome through strategic implementation and stakeholder engagement, making the technology viable for Sri Lanka.

6 Recommendations

To support piezoelectric energy adoption, pilot or R & D projects should test real-world feasibility. Hybrid systems combining piezo tiles with solar are recommended for better energy efficiency. Government incentives, like tax exemptions (Pasindu et al., 2017), can reduce initial costs and encourage stakeholder adoption. Awareness campaign and academic-industry collaborations are vital to build knowledge and promote implementation through universities and training programs (Farnoosh, 2002)

7 Research Limitations and Future Research Directions

This study focused solely on technological aspects in according to Sri Lankan context. The time frame of the investigation was confined to the recent years coinciding with the onset of the digital collapse in Sri Lanka. The recommendations that put forth in this study purely based on insights and expertise provided by industry or academic professionals within the industry.

This study establishes the adoption of piezoelectric energy technology in Sri Lanka; it is essential to explore the most suitable implementation methods and study its long-term impact on local energy demand and weather conditions. Further research is needed to identify the most efficient energy harvesting techniques, and establishing local production is a crucial direction to improve accessibility and reduce costs.

References

1. B. Ambrożkiewicz, Z. Czyż, P. Stączek, J. Anczarski, & M. Jachowicz, Enhancing Power Generation Efficiency of Piezoelectric Energy Harvesting Systems: A Performance Analysis. In M. Pawelczyk, D. Bismor, S. Ogonowski, & J. Kacprzyk (Eds.), Advanced, Contemporary Control, pp. 261–268, Springer Nature Switzerland, 2023.
2. V. Antwi, M. Gyan, D. Appiah, I. K. Acquah, F. A. Wuver & C. Jebuni-Adanu, Theoretical study of the strong piezo-phototronic effect in 2D monochalcogenides for multi-junction solar cells. Physica Scripta, 99(11), 115906, 2024. https://doi.org/10.1088/1402-4896/ad7cdc
3. M. Z. Azmi & S. F. S. Adnan, Energy Generating from Footsteps on Piezoelectric Module. IEEE Industrial Electronics and Applications Conference (IEACon), pp. 152–156, 2024. https://doi.org/10.1109/IEACon61321.2024.10797263
4. C. Ndungu, J. Nderu, L. Ngoo, & P. Hing, Reinforcing Kenya Power National Grid Using Statcom Devices. Review of Energy Technologies and Policy Research, 3(1), pp. 17–23, 2017. https://doi.org/10.18488/journal.77.2017.31.17.23
5. P. Catrini, D. Curto, V. Franzitta & F. Cardona, Improving energy efficiency of commercial buildings by Combined Heat Cooling and Power plants. Sustainable Cities and Society, 60, 102157, 2020. https://doi.org/https://doi.org/10.1016/j.scs.2020.102157
6. B. C. Chew, H. S. Loo, I. A. Bohari, S. R. Hamid, F. H. Sukri & R. Kusumarwadani, Feasibility of piezoelectric tiles adoption: A case study at Kuala Lumpur International Airport (KLIA) Malaysia. AIP Conference Proceedings, 1818(1), 020009, 2017. https://doi.org/10.1063/1.4976873
7. Colombo Fort Railway Station. (2024, July). Colombo Fort Railway Station. https://www.railway.gov.lk/web/index.php?option=com_content&view=article&id=568%3Ahappy-new-year-2024&catid=48%3Aslideshow&lang=en#:~:text=This%20is%20the%20main%20railway,caters%200.2%20million%20passengers%20daily.
8. A. M. Elhalwagy, M. Y. M. Ghoneem & M. Elhadidi, Feasibility Study for Using Piezoelectric Energy Harvesting Floor in Buildings' Interior Spaces. Energy Procedia, 115, pp. 114–126, 2017a. https://doi.org/10.1016/j.egypro.2017.05.012
9. A. M. Elhalwagy, M. Y. M. Ghoneem & M. Elhadidi, Feasibility Study for Using Piezoelectric Energy Harvesting Floor in Buildings' Interior Spaces. Energy Procedia, 115, pp. 114–126, 2017b. https://doi.org/https://doi.org/10.1016/j.egypro.2017.05.012
10. O. D. Mohammed, S. Alzaher, I. Bubshait, R. Alhussain, K. Almenayan, & R. AlQahtani, A Developed Design of Power Generating Tiles. Prognostics and System Health Management Conference (PHM), pp. 127–131, 2024. https://doi.org/10.1109/PHM61473.2024.00032
11. R. R. Moussa, W. S. E. Ismaeel & M. M. Solban, Energy generation in public buildings using piezoelectric flooring tiles; A case study of a metro station. Sustainable Cities and Society, 77, 2022. https://doi.org/10.1016/j.scs.2021.103555

12. A. Padmanegara Putra, N. Fahmi, A. Hakim, E. Haritman, S. Ath, T. Al Azhima, M. Al Qibtiya, & A. P. Putra, Application of Piezoelectricity on Running Tracks: A Prototype for the Realization of Sustainable and Efficient Energy, Journal of Universal Studies, 4(7), 2024. http://eduvest.greenvest.co.id
13. B. M. C. Pasindu, K. T. M. U. Hemapala & K. K. W. Siriwardena, A Least Cost Long -Term Energy Supply Strategy for Sri Lanka using Petroleum, Coal and Natural Gas. Engineer: Journal of the Institution of Engineers, Sri Lanka, 50(3), 55, 2017. https://doi.org/10.4038/engineer.v50i3.7265
14. Pavegen. (2025). https://www.pavegen.com/faq. FAQs. https://www.pavegen.com/faq
15. B. Pavlović, D. Ivezić & M. Živković, A multi-criteria approach for assessing the potential of renewable energy sources for electricity generation: Case Serbia. Energy Reports, 7, pp. 8624–8632, 2021. https://doi.org/https://doi.org/10.1016/j.egyr.2021.02.072
16. S. A. Rumman & R. Elnaklah, Investigating the Energy Generation Potential of Piezoelectric Flooring in Educational Buildings. 2024 International Conference on Electrical, Computer and Energy Technologies (ICECET, pp. 1–7, 2024. https://doi.org/10.1109/ICECET61485.2024.10698071
17. S. Hari Prasadh, K. Mukeshkanna, K. Mohankumar, S. Mohamed Halith, Design and Fabrication of inTouch Power Generation Tiles. International Conference on Distributed Computing and Optimization Techniques (ICDCOT), pp. 1–8, 2024. https://doi.org/10.1109/ICDCOT61034.2024.10515896
18. K. K. Selim, H. M. Yehia & D. A. Saleeb, Energy Harvesting Floor Tile Using Piezoelectric Patches for Low-Power Applications. Journal of Vibration Engineering and Technologies, 2024. https://doi.org/10.1007/s42417-024-01379-z
19. S. Sharma, R. Kiran, R., P. Azad & R. Vaish, A review of piezoelectric energy harvesting tiles: Available designs and future perspective. Energy Conversion and Management, 254, 115272, 2022. https://doi.org/https://doi.org/10.1016/j.enconman.2022.115272
20. SLSEA. (2022). SLSEA. Https://Www.Energy.Gov.Lk/En/. https://www.energy.gov.lk/en/
21. M. M. Solban & R. R. Moussa, Piezoelectric Tiles Is a Sustainable Approach for Designing Interior Spaces and Creating Self-Sustain Projects. IOP Conference Series: Earth and Environmental Science, 397(1), 2019. https://doi.org/10.1088/1755-1315/397/1/012020
22. H. C. Song, S. W. Kim, H. S. Kim, D. G. Lee, C. Y. Kang & S. Nahm, Piezoelectric Energy Harvesting Design Principles for Materials and Structures: Material Figure-of-Merit and Self-Resonance Tuning. Advanced Materials, 32(51), 2002208, 2020. https://doi.org/https://doi.org/10.1002/adma.202002208
23. N. Thanach-Issarasak, S Jayasvasti, P. Yingyong & D. Isarakorn, Potential of Piezoelectric Floor Tile for Harvesting Energy from Human Footsteps. International Conference on Power, Energy and Innovations (ICPEI), pp. 119–121, 2021. https://doi.org/10.1109/ICPEI52436.2021.9690688
24. United Nations Development Programme. (n.d.).

25. U. Mane, O. Sakpal, A. Shetye, & Y. Lale, Generate Electricity from Pizoelectric. International Journal of Advanced Research in Science, Communication and Technology, pp. 228–233, 2024. https://doi.org/10.48175/ijarsct-17441
26. R. Verma, A. Chauhan, R. Kalia, R. Jasrotia, M. Sharma & R. Kumar, A comprehensive study on piezo-phototronic effect for increasing efficiency of solar cells: A review. Optics & Laser Technology, 149, 107779, 2022. https://doi.org/https://doi.org/10.1016/j.optlastec.2021.107779
27. P. Yingyong, P. Thainiramit, S. Jayasvasti, N. Thanach-Issarasak & D. Isarakorn, Evaluation of harvesting energy from pedestrians using piezoelectric floor tile energy harvester. Sensors and Actuators A: Physical, 331, 2021. https://doi.org/10.1016/j.sna.2021.113035
28. X. Yue & S. Du, A Single-Stage Bias-Flip Regulating Rectifier with Fully-Digital Fast-MPPT for Piezoelectric Energy Harvesting Achieving 9.3X Power Enhancement and 92.5% End-to-End Efficiency. IEEE Custom Integrated Circuits Conference (CICC), 1–2, 2024. https://doi.org/10.1109/CICC60959.2024.10528996
29. T. Zhang, et al., Piezo-photocatalysis synergy in γ-GeSe for highly efficient oxygen evolution reaction. Journal of Applied Physics, 136(11), 114302, 2024. https://doi.org/10.1063/5.0217893

3rd International Engineering Research Symposium 2025 (IERS 2025)
Colombo, Sri Lanka

Assessing the Compound Impacts of Climate Change and Land Use Dynamics on Future Groundwater Availability in Dry Land Areas of Sri Lanka

K. R. H. M. O. N. Herath[1] and H. G. L. N. Gunawardhana[1,2]

[1]Department of Civil Engineering, University of Moratuwa, Moratuwa, Sri Lanka
[2]UNESCO-Madanjeeth Singh Centre for South Asia Water Management, University of Moratuwa, Moratuwa, Sri Lanka
herathkrhmon.24@uom.lk

Abstract. Climate change and land use and land cover (LULC) change are the primary challenges that disrupt groundwater availability. While numerous studies have examined their individual impacts, a critical gap exists in understanding their combined impact on groundwater availability. To address this gap, the present study assesses the compound impacts of climate change and LULC change in the Kumbukkan Oya catchment, a dryland area in southeastern Sri Lanka. The analysis uses hydrometeorological data, groundwater levels, borehole logs, and catchment characteristics such as land use, soil type, and elevation. Climate data were obtained from 1989 to 2011, while the groundwater level data and hydrological data were used from 2022 to 2024 at a mostly daily time step. Groundwater flow was then numerically modeled with MODFLOW. Projected future climate was obtained from the CNRM-CM6-1-HR General Circulation Model (GCM) and downscaled to the local scale using a stochastic Random Forest (RF) machine learning algorithm. Land-use data of 2018 and projected for future conditions were employed in assessing LULC dynamics. According to the result, the model captures the seasonal patterns of decline and recovery, particularly in the upstream, although some overestimation occurred in mid-catchment areas. Future projections indicate a decrease in seasonal rainfall compared to the baseline period, with reduced average rainfall but still frequent extreme events. The future period total rainfall will be 1,552 mm, and the observed total of 1,733 mm. Based on the projected results, groundwater levels are expected to decline by approximately 0.43 m to 0.65 m compared to observed conditions. Therefore, simulation reveals that the Kumbukkan Oya catchment has some extent of resilience in the groundwater level relative to the projected climate and land use change. However, localized tendencies in the fall in groundwater levels suggest the need for site-specific adaptation responses, particularly over vulnerable recharge zones.

Keywords: Climatic alterations, Compound Impacts, Land use changes.

1 Introduction

Groundwater is one of the most important natural resources on Earth, offering several advantages over surface water, such as better quality, lower risk of contamination, and more stable availability throughout the year. Groundwater is essential for global water needs, especially agriculture, which uses 69%. In Asia, 76% of groundwater supports irrigation, underscoring its role in food security. Additionally, groundwater supports domestic and industrial uses and helps sustain ecosystems, making it essential for both human and environmental well-being [1].

Groundwater depletion is a growing global concern, with many regions experiencing sharp declines in groundwater levels (GWLs), evident from well data and Gravity Recovery and Climate Experiment (GRACE) satellite observations [2]. However, this use is not evenly distributed—nearly two-thirds was withdrawn in Asia, particularly in South and East Asia, where dependence on groundwater is especially high [1].

Groundwater depletion is primarily caused by climate change and land use changes[3,4]. Land Use and Land Cover (LULC) changes, such as deforestation or urbanization, affect land surface characteristics, which in turn impact infiltration and runoff. Meanwhile, climatic variations, including shifts in precipitation and temperature, directly influence groundwater recharge. Understanding climate change along with incremental LULC changes is synergistic, as these factors operate in complex interdependent ways. Therefore, studying the combined consequences of these factors on groundwater availability is more rational than assessing the impacts one at a time [5].

While several studies have examined the compound effects of climate change and LULC change on surface water [6,7], relatively few investigations have critically examined their effects on groundwater [4,5]. This gap highlighted the need to investigate the compound impacts of climate change and LULC change on the availability of groundwater. Additionally, this assessment is crucial in the development of long-term water management practices that contribute to mitigating the effects of drought by providing a constant groundwater supply.

As indicated by the latest assessment report from the Intergovernmental Panel on Climate Change (IPCC), Assessment Report [8], South Asia is one of the hotspots in the world for climate-induced hazards. Within this context, Sri Lanka, particularly its dry zone, is increasingly vulnerable. This region has experienced a significant reduction in rainfall and heightened rainfall seasonality, impacting groundwater recharge. Since over 60% of Sri Lanka's population depends on agriculture, mainly in the dry zone, groundwater remains a vital resource for sustaining livelihoods. However, the Water Resources Board (WRB) data in 2017 show that much of the dry zone has low groundwater yields

(0–50 lpm), underscoring the scarcity and vulnerability of water resources in these areas [9]. Also, to date, no studies in Sri Lanka have assessed the compound impacts of climate change and land use dynamics on groundwater using Coupled Model Intercomparison Project (CMIP) 6 data.

Therefore, this study focuses on the Kumbukkan Oya catchment to investigate the compounded impacts of climate change and LULC changes on groundwater resources in Sri Lanka's dry zone. The main objective of this study is to evaluate the effects of climate change and potential LULC changes on groundwater aquifers using an integrated approach. This involves combining a process-based physical model with machine learning (ML) techniques to simulate and predict groundwater responses under different future scenarios.

2 Study Materials

a. Study Area

Kumbukkan Oya catchment, which is shown in **Fig.** is in Sri Lanka's Uva and Eastern provinces, with most of it located in the Monaragala District. Covering 1,227 km², the catchment has an elevation range from the mean sea level to 1,400 m above sea level. The Kumbukkan Oya River flows for 116 km, supporting the largest irrigation system in Monaragala. Located at approximately 6.8°N and 81.5°E, the catchment is essential for agriculture and water resources in the region. It irrigates about 2,000 acres of cultivated land and plays a vital role in agriculture and water management in the areas surrounding it [10].

Borehole data reveal a layered subsurface of topsoil, sand, clay, gravel, weathered rock, and bedrock. The catchment receives an average annual rainfall of about 1,700 mm, with distinct seasonal patterns: the Northeast Monsoon (35.2%) and Second Inter-Monsoon (21.3%) contribute the highest rainfall, while dry spells prevail mid-year. The region experiences an average annual temperature of 23°C and a pan evaporation of approximately 1,100 mm, both key factors affecting the hydrological balance. GWLs mostly range from 80 to 400 m, with higher values at elevated terrain, influenced by topography and aquifer properties.

According to the 2018 land use map, forest land is the dominant class in the catchment, covering 62% of the area. Agricultural land accounts for 26%, underscoring the catchment's critical role in supporting local farming. Built-up areas comprise 6%, indicating limited urban development. The remaining land consists of rocky terrain (4%), water bodies (1%), and a small portion (0.8%) classified as wetlands, bare lands, and sandy areas.

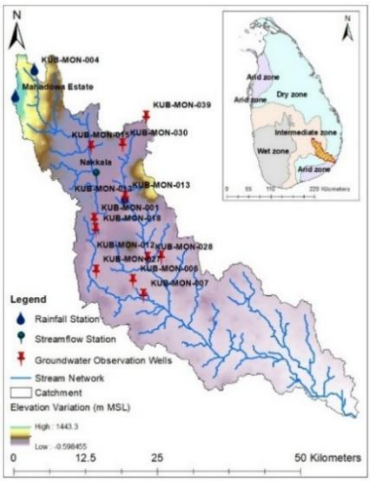

Fig. 1. Kumbukkan Oya catchment and the locations of the rainfall, streamflow, and groundwater monitoring stations

b. Data Collection

Various datasets were collected from both national and global sources. A 30 m × 30 m resolution Digital Elevation Model (DEM) was obtained from the Shuttle Radar Topography Mission (SRTM). GWLs and borehole data from 2022 to 2024 were collected from the WRB. Daily rainfall data for the periods 1989–2011 and 2022–2024 were obtained from the Department of Meteorology and the WRB. Daily streamflow data (2020–2024) were sourced from the Irrigation Department. Temperature data for the same periods were acquired from the Department of Meteorology and NASA POWER (https://power.larc.nasa.gov/data-access-viewer/). Pan evaporation data (monthly) for 2019/2020 were taken from the Hydrological Annual published by the Ministry of Irrigation. 2018 land use data (scale 1:100,000) were collected from the Survey Department. Climate data from Global Climate Models (GCMs) for 1989–2011 and 2030–2049 were sourced from the IPCC data portal (https://www.ipcc-data.org/).

3 Methodology

The groundwater model was developed using MODFLOW to simulate the aquifer response [11,12]. Parameter optimization was carried out by optimizing hydraulic properties

to match observed GWLs. To assess future groundwater responses to climate variability, climate projections were introduced from the CNRM-CM6-1-HR model, a high-resolution GCM under the CMIP6 framework [13]. This model was selected for its demonstrated capability in accurately representing South Asian monsoonal rainfall and its fine spatial resolution (0.5° × 0.5°), making it suitable for small island nations like Sri Lanka [14]. The SSP5-8.5 scenario was employed to simulate potential future extremes. Climate data for the baseline period (1989–2011) and the future projection period (2030–2049) were used for comparison and scenario analysis.

a. Development of the Groundwater Flow Model

A groundwater flow model was developed for a 1,227 km² area using MODFLOW, incorporating lithology, GWLs, and recharge data. The model domain was discretized into a single-layer finite difference grid with 266 columns, 280 rows, and a cell size of 250 m. The DEM was used to define the model top. Boundary conditions included a constant head of 0 m at the coastal boundary to represent mean sea level, and a time-varying constant head at the upstream boundary based on GWL observations from nearby monitoring wells during the simulation period. No-flow boundaries were assigned to the eastern and western sides. Recharge was applied using a recharge-to-rainfall ratio of 0.22, with daily rainfall data used to generate time-series recharge inputs across the model domain. Initial heads for the transient simulation were taken from steady-state results, and the model was run using daily time steps over 164 stress periods from 1 July to 12 December 2023.

b. Development of the ML Model for Climate Data Downscaling

Due to the coarse resolution of GCMs, statistical downscaling is preferred over dynamic methods for its computational efficiency and ability to apply bias correction. Among statistical techniques, ML methods like Random Forest (RF) are most effective due to their robustness, ability to model non-linear relationships, and minimal preprocessing needs [15]. Therefore, RF was chosen for downscaling GCM precipitation data in this study.

The downscaling process involved preparing both observed and GCM-predicted precipitation datasets, where input variables included the GCM-derived precipitation along with time-related attributes such as year, month, and day. The target variable was the observed precipitation, representing the actual measured values. Both datasets were merged by date, and temporal features were extracted to enhance model performance. The combined dataset was then split into training and testing sets using an 80/20 ratio, with 80% allocated for training and 20% for testing. An RF model was trained using 100 trees to ensure robust performance while maintaining computational efficiency. The trained model

was later applied to correct the future GCM projections, ensuring improved accuracy for climate impact assessments.

4 Results and Discussion

a. Results and Analysis of Transient Groundwater Flow Simulation

The transient groundwater flow model simulated the seasonal fluctuation from June 2023 to January 2024. The declining trend in GWLs from June to October and the increasing trend during October to January followed a uniform pattern in all the wells. **Fig.** shows the hydrograph in well KUB_MON_004 from the upstream area. The model accurately captures both the declining and recovery phases, with some slight overestimation of peak, and the residual of nearly -0.8 m.

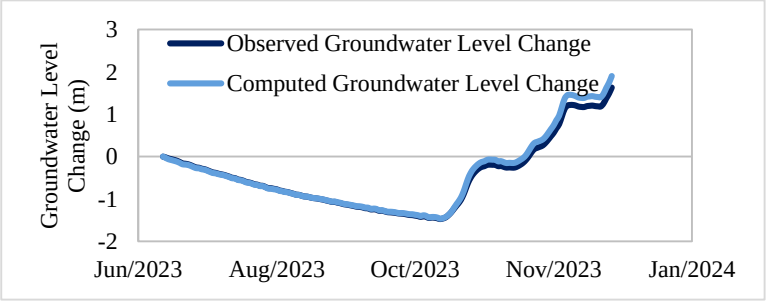

Fig. 2. GWL Change at the monitoring well KUB_MON_004 (Upstream) throughout the transient simulation period

The mid-catchment well KUB_MON_015 (**Fig.**), however, exhibited systematic overestimation of GWLs with the residual of -1.0 m. Overall, the model reproduced seasonal dynamics at upstream wells quite well, while mid-catchment performance could be enhanced. The results indicate that the model is well calibrated for general trend and seasonal variation prediction, but further refinement may be needed to distinguish site-specific recharge and flow processes.

These types of disparities between the computed and observed GWLs appear because of the site-specific conditions. Among the likely causes are groundwater pumping, which was not accounted for because the data were limited. The annual amount of groundwater abstraction of the Monaragala District is estimated to be 4000 m^3/day [16], excluding the extraction from the private individual wells. If the drawdown is calculated using a model cell size of 250 m x 250 m and assuming an assigned specific yield value of 0.1 for sandy

soil, the estimated drawdown would be approximately 0.7 m/day. This rate of abstraction is also consistent with the disparity reported between computed and observed groundwater heads in the downstream region. Therefore, incorporation of this abstraction in the model could significantly reduce the disparity and improve computed GWL precision.

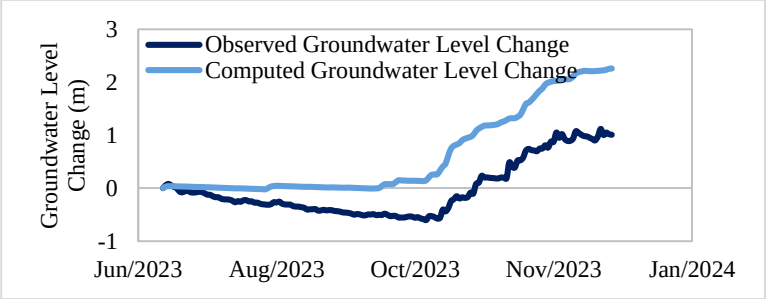

Fig. 3. GWL change at the monitoring well KUB_MON_015 (midstream) throughout the transient simulation period

Also, this overestimation can be attributed to the impact of nearby land cover categories. In agricultural areas such as those around KUB-MON-015, large abstraction of groundwater for irrigation can reduce actual water levels. If such land–use–specific pumping effects are not adequately simulated by the model, it may cause computed GWLs that are higher than the true field observed levels. In the model, the entire catchment is considered as a single recharge zone. Except for the upstream and downstream parts, no-flow boundaries have been given to the other two sides. But additional complexity can be introduced in the middle of the catchment due to the change in land use and varying recharge rates. Additionally, the influence of lateral outflows and inflows cannot be efficiently modeled, supporting further overestimation of GWLs.

Moreover, model assumptions and simplifications can also be the cause of these deviations. For example, MODFLOW assumes that aquifer properties, including hydraulic conductivity and storativity, are homogeneous. Aquifers in the real world are usually heterogeneous, and ignoring local variations in properties can lead to incorrect simulations. Also, boundary conditions such as no-flow boundaries may not be representative of actual conditions, especially when there are lateral inflows or outflows, which are not accounted for by the model. These assumptions might cause the model to overpredict GWLs.

b. Results of Downscaled Climate Projections and Precipitation Pattern Analysis

Due to limited data, the precipitation from both GCM and the single observation point was compared over time. **Table** shows the long-term average monthly rainfall variation during a monsoon cycle. According to the data in the table, there is a clear declining pattern of seasonal rainfall during all phases of the monsoon. A closer examination of the monsoon-specific trends suggests that the Second Inter-Monsoon (October-November) and South-west Monsoon (May-September) periods, which used to get the maximum rainfall in the past, will experience a significant decline in the future. By comparison, the Northeast Monsoon (December-January) and First Inter-Monsoon (March–April) phases, which are historically lower rains, also experience a slight reduction in future rain, following the trend of becoming progressively drier across all the seasons.

Table 1. Long-term monthly average rainfall data during a monsoon cycle

Long-Term Average Monthly Precipitation (mm) [Based on the data from 1989 to 2011]			Long-Term Average Monthly Future Precipitation (mm) [Based on the data from 2030 to 2049]
Month	Observed	GCM	GCM
October	277.4	299.1	255.5
November	271.6	276.5	228.1
December	229.1	238.2	144.7
January	114.1	116.3	89.7
February	115.4	117.8	114.4
March	90.6	94.6	99.3
April	133.3	141.6	121.1
May	130.1	141.6	146.1
June	51.6	57.9	50.4
July	65.2	69.7	41.7
August	96.0	99.1	100.5
September	147.9	156.7	160.1

c. Compound Impacts Assessment

This section aims to assess the compound impacts of climate change and potential LULC changes on fluctuations in GWLs. Following the United Nations Population Division's

World Urbanization Prospects, World Bank staff estimates have projected a steady increase in the rural population from 1960 to 2023 [17]. Additionally, according to a study by Dey et al. (2024) [18], the population of Sri Lanka is projected to increase between 2030 and 2060, based on the logistic growth model. As the population grows, pressure on food production, shelter, and infrastructure is likely to mount, particularly in developing regions such as the Monaragala District. This will result in the conversion of forests to agricultural land and built-up areas. Therefore, assessment assumes that, in the future, population growth will drive land use transformations characterized by a reduction in forest cover, an expansion of agricultural land, and an increase in built-up areas. Incorporating these transformations within the groundwater model, the analysis accounts for the interactive influence of both drivers, giving an integrated picture of their potential influences on groundwater resources.

GWL fluctuation estimation under the compound impacts of climate change and LULC change indicates a generally moderate hydrological response in the catchment. Despite the reduction in all the phases of rainfall in the seasons and extensive land transformation, the varying GWLs were nearly within a narrow range. Overall, the mean average GWL decreased by approximately 0.65 m and the maximum GWL by approximately 0.43 m across the catchment. These reductions are hydrologically consistent with decreased infiltration caused by increased impervious surfaces and loss of vegetation cover, and greater groundwater pumping for irrigation. Lower monsoonal rains also contribute to the decreased opportunity for recharge, further diminishing the demand on groundwater resources.

5 Conclusions and Recommendations

a. Conclusion

This study was carried out to analyze how climate change-induced LULC changes can affect groundwater availability in the arid zone of Sri Lanka, namely the Kumbukkan Oya catchment. To achieve this, the study aimed to develop a numerical groundwater flow model using MODFLOW and apply ML techniques to downscale climate projections to the local scale.

Generally, on all observation wells, there was a decrease in GWL between June and October 2023, followed by a sharp rise up to January 2024. Overall, the model performed well in upstream areas; its lower accuracy in midstream regions highlights the need for localized parameter refinement, better treatment of recharge uncertainty, and enhanced calibration using additional field data. The total annual rainfall during the baseline period

(1989-2011) was approximately 1,733 mm, while projections for 2030-2049 show a decrease to about 1,552 mm. This is important to groundwater recharge, surface water supply, and agriculture planning within the catchment.

However, the compound impact assessment of climate change and LULC change shows an average GWL decline, suggesting that the catchment is sufficiently resilient to these compound stressors. This may be because there are deeper aquifers, larger storage capacity in the aquifers, and spatially heterogeneous areas of recharge that buffer the effects of declining rainfall and increasing land use intensity. Additionally, the low degree of change is an indicator that the system can still be below critical groundwater stress levels. However, while aquifer response has so far been steady, accelerating land use intensification and long-term climate variability can push the system beyond its buffering capacity.

Results of this study benefit the efficient management of Sri Lanka's dry zone groundwater resources, in the case of the Kumbukkan Oya catchment. The study provides a scientific basis for better planning and water allocation. An understanding of how GWLs can reduce, especially during droughts, empowers governments to formulate effective water use plans, allocate priority uses such as drinking and irrigation, and implement recharge enhancement practices such as artificial recharge and soil conservation. Moreover, an understanding of how deforestation and urbanization affect groundwater recharge guides land use zoning and policy guidelines. These results also justify the construction of early warning systems by establishing thresholds for initiating water conservation actions at key times.

b. Recommendations

To improve the enhancement of future studies, it is necessary to address the shortcomings of this study. These are mainly data deficiencies, simplifications in model assumptions, and environmental and human influences are not accounted. The following are suggested to reduce such limitations and enhance the performance of future groundwater models.

- Future research should include the effects of socio-economic factors, e.g., population growth and land demand, on groundwater use.
- It is recommended to investigate the use of coupled climate-hydrology-socioeconomic models for more integrated impact analysis.
- More comprehensive soil and geology information in models can be utilized to refine model accuracy, especially in mid-catchment regions.
- Also, the use of multiple GCMs and several SSP scenarios can be recommended.

References

1. UNESCO, Groundwater Making the invisible visible, 32(19). 2022. doi: 10.12968/bjon.2023.32.19.922.
2. L. Longuevergne, B. R. Scanlon, and C. R. Wilson, GRACE Hydrological Estimates for Small Basins: Evaluating Processing Approaches on the High Plains Aquifer, USA, Water Resour. Res., 46(11), pp. 1–15, 2010, doi: 10.1029/2009WR008564.
3. J. Sha, Y. Zhao, X. Li, and Z. L. Wang, Assessing impacts of Future Climate Change on hydrological processes in an urbanizing watershed with a Multimodel Approach, J. Water Clim. Chang., 12(4), pp. 1023–1042, 2021, doi: 10.2166/wcc.2020.142.
4. R. P. Neupane and S. Kumar, Estimating the effects of potential climate and Land Use Changes on Hydrologic Processes of a Large Agriculture Dominated Watershed, J. Hydrol., 529, no. P1, pp. 418–429, 2015, doi: 10.1016/j.jhydrol.2015.07.050.
5. Z. Hao, V. P. Singh, and F. Hao, Compound Extremes in Hydroclimatology: A Review, Water (Switzerland), 10(6), pp. 16–21, 2018, doi: 10.3390/w10060718.
6. M. I. Faridatul, A Comparative Study on Precipitation and Groundwater Level Interaction in the Highly Urbanized Area and Its Periphery, Curr. Urban Stud., 6(2), pp. 209–222, 2018, doi: 10.4236/cus.2018.62012.
7. X. Tan et al., Impacts of Climate Change and Land Use/Cover Change on Regional Hydrological Processes: Case of the Guangdong-Hong Kong-Macao Greater Bay Area, Front. Environ. Sci., 9, pp. 1–16, 2022, doi: 10.3389/fenvs.2021.783324.
8. IPCC, Climate Change 2023 Synthesis Report, 2023. doi: 10.59327/IPCC/AR6-9789291691647.
9. W. R. Board, Water Resources Board. [Online]. Available: Water Resources Board
10. K. Rathnayaka, A Study on Identifying Land Use Changes and the Causes Affected to Changes of Land Use Pattern in Monaragala City Area, Int. J. Sci. Res., 10(3), pp. 429–433, 2021, doi: 10.21275/SR21304165115.
11. M. Basharat and M. Jawad, Building MODFLOW Model in ModelMuse GUI For Bari Doab, J. Anesth. Pain Med., 8(5), pp. 194–203, 2023, doi: 10.33140/japm.08.05.01.
12. A. Akter and S. Ahmed, Modeling of Groundwater Level Changes in an Urban Area, Sustain. Water Resour. Manag., 7(1), pp. 1–20, 2021, doi: 10.1007/s40899-020-00480-x.
13. M. Almazroui, S. Saeed, F. Saeed, M. N. Islam, and M. Ismail, Projections of Precipitation and Temperature over the South Asian Countries in CMIP6, Earth Syst. Environ., 4(2), pp. 297–320, 2020, doi: 10.1007/s41748-020-00157-7.
14. C. Jayaminda, L. Gunawardhana, and L. Rajapakse, Rating Performances of Global Climate Models in Capturing Monsoon Rainfall Patterns in Sri Lanka, Moratuwa Eng. Res. Conf.

MERCon, pp. 264–269, 2023, doi: 10.1109/mERCon60487.2023.10355390.

15. C. Hutengs and M. Vohland, Downscaling Land Surface Temperatures at Regional Scales with Random Forest Regression, Remote Sens. Environ., 178, pp. 127–141, 2016, doi: 10.1016/j.rse.2016.03.006.

16. K. G. Villholth and L. D. Rajasooriyar, Groundwater Resources and Management Challenges in Sri Lanka-an Overview, Water Resour. Manag., 24(8), pp. 1489–1513, 2010, doi: 10.1007/s11269-009-9510-6.

17. Word Bank, Rural population - Sri Lanka. [Online]. Available: https://data.worldbank.org/indicator/SP.RUR.TOTL?end=2023&locations=LK&start=1960&view=chart

18. P. Dey et al., Qualitative Analysis of Demographic Perspective and Human Population Model Within Bangladesh and Sri Lanka, J. Mech. Contin. Math. Sci., 19(12), pp. 139–158, 2024, doi: 10.26782/jmcms.2024.12.00009.

3rd International Engineering Research Symposium 2025 (IERS 2025)
Colombo, Sri Lanka

Comparative Analysis of Deep Learning Models for Software Defect Prediction in Agile Environments

P. U. N. Pathirana[1] and W. V. S. K. Wasalthilaka[2]

[1]Department of Computing and Information Systems, Faculty of Computing, Sabaragamuwa University of Sri Lanka, Sri Lanka.
[2]Department of Software Engineering, Faculty of Computing, Sabaragamuwa University of Sri Lanka, Sri Lanka.
uthpalanp@gmail.com

Abstract. Software defect prediction is a critical part of development, identifying mismatches between expected and actual outcomes as detected by developers or end users. The main purpose of agile defect prediction is identifying defects in timely manner. But the iterative and fast paced nature of agile environments raises several challenges for defect prediction such as handling code changes, managing limited development time and addressing dynamic and evolving project requirements. So, there is a notable gap related to the research studies of agile defect prediction. Traditional defect prediction methods frequently struggle to identify dynamic and complex data patterns. This study performed a comparative analysis between deep learning models to identify the most effective model with the highest defect prediction accuracy. For the research, Convolutional Neural Network (CNN), Recurrent Neural Network (RNN), Long Short-Term Memory (LSTM) and Deep Belief Network (DBN) models are used which can identify complex data patterns and relationships by extracting the meaningful features automatically. Jira defect dataset was used and cleaned using data pre-processing and feature selection techniques, and processed dataset was divided into training and testing sets. The trained models were evaluated using metrics like accuracy, precision, recall and f1-score. The study exposes RNN outperforms other models with 80.78% accuracy, processing sequential data and predicting future risks by analyzing past defects effectively. The findings of the research emphasize the effectiveness of using deep learning models in agile software defect prediction for high-quality, reliable real-world agile development practices.

Keywords: Agile, Deep Learning, Software Defect Prediction, Software Development, Software Quality

1 Introduction

a. Background

Software systems have now become an indispensable part of our day-to-day lives. Almost every field such as education, health care, communication, transportation and also entertainment, is getting the benefits from using software systems. Due to the strong dependency on the software, the quality of the software is very crucial part to be necessarily considered. With its usage, growing size and complexity, it has become a major problem to be always concerned about how to improve the quality of software by reducing the software defects as much as possible [1].

Quality of the software is one of the crucial concerns of the software development process. Software quality is the process of measure how it is designed and how well the software conforms to that design. To build a standard quality software, testing is essential. If there is not proper testing of the software, it can include many defects which causes the system fails to perform its required functions.

IEEE standard defines a defect as "the lack to perform the tasks and system requirements that are provided by developers and customers" [2]. For the question of why the defects should be identified in the software projects, the answer can be provided with three major considerations: quality, performance and costs. A project with defects is normally a low-quality software due to poor performance and high maintenance costs. But if the project teams can develop a defect-free software, it can always increase the quality, improve its performance and reduce the maintain costs. Therefore, software defect prediction has become one of the most important part of the software engineering field.

Agile methodology is now gained more attention in many industries as most of the organizations are moving towards the adaptation of agile methodologies. Among all other software development methodologies, agile has become most effective and useful since it focuses to develop high quality software products with minimum defects and the defect management of agile environment should be involved in every development stage to gain the full confidence of the customer satisfaction [3].

Deep learning (DL) models are known for their specialties in software defect predication (SDP). They can automatically extract the features for the source code effectively by reducing the reliance on the manual feature engineering. And they can improve the prediction accuracy by outperforming the traditional machine learning methods. Deep learning models are famous for capturing the structural and semantic information from the code to handle complex data. Also, they are successfully address the challenges in cross project defect prediction by learning the transferable features efficiently.

b. Problem Statement and Objectives

Even though, different types of traditional techniques and methods have been used for SDP, there are still lack to handle complex data and frequent code changes which the DL models can easily do. Due to the iterative and fast-moving nature in agile environments, rapid changes in the system is done frequently, so it brings a significant challenge to test the system and find the defects in timely manner.

Therefore, an effective SDP is crucial point to maintain the quality of the software and reducing the cost which are associated to fix the defects late in the development life cycle. Even though, different types of DL approaches have been proposed, there is a lack of comprehensive comparative studies evaluating the performance of deep learning models in agile software defect prediction contexts. Therefore, the question of the research to address is which DL model for the SDP will be provided high accuracy in agile environments are arisen.

So, the main objective of the research is to compare different DL models to find which model is high accurately predicted the software defects in agile environments. To achieve the main objective, there are sub-objectives which are made to organize the research path in step-by-step manner. The first sub objective is, analyzing the effectiveness of DL models and traditional approaches in agile SDP by comparing both under same criteria. Second one is developing DL models using, CNN, RNN, DBN and LSTM algorithms to predict software defects. And third one is evaluating and comparing the accuracy of DL models and select the best performance model.

c. Significance of the study

Agile development is an environment where the frequent releases, quick iterations, and continuous integrations are happened. Because of these characteristics, it is crucial to identify software defects in timely manner to maintain the software quality and efficiency. This early identification of defects gives more benefits to the agile team such as, enhance task prioritization, efficient resource allocation, strengthen continuous delivery etc.

For the agile SDP, DL models contribute with the real-time defect prediction which accomplished the purpose of the agile defect prediction. Using DL can benefit in agile SDP as: early and accurate defect detection, reduce the manual effort, adaptability to evolving codebases etc. The research study is brought out the importance of the agile SDP by emphasizing the benefits of using DL for an effective prediction process.

2 Literature Review

Software defect prediction is one of the most popular research areas in software engineering field. Various number of research studies have been done by the researchers all around the world as it is now getting a more considerable and valuable area.

Hoang et al. [4] described that the software systems as the backbone of the economy and society, so the defects of those systems may substantially affect the businesses and people's lives in different ways. They suggested that it is best to identify and fix the defects early as possible because it would be difficult and costly as software grows in both size and complexity. Moreover, P. Deep Singh and A. Chug [5] emphasized that the quality is the most important aspect of a software as SDP can directly affect to the software quality which can glorify or ruin of the brand image of a company and deviation of time, cost and budget.

Recent research studies explore the different DL approaches for the SDP. According to S. Omri and C. Sinz [6], Convolutional Neural Network (CNN), Recurrent Neural Networks (RNN), Deep Belief Networks (DBN) and Long Short-Term Memory (LSTM) based models are widely used and outperform traditional methods by which automates feature generation from source code. They emphasized that those models outperform traditional models by learning specific characteristics straight from the code.

M. Nevendra and P. Singh [7] proposed enhanced CNN model for SDP to enhance prediction accuracy and reduce overfitting compared to the traditional Machine Learning models, by emphasizing that CNN captures non-linear patterns and automates feature extraction. And Qiu et al. [8] also addressed the challenge of traditional cross project defect prediction (CPDP) methods neglect the semantic code patterns in favor of handcraft features. Therefore, they used the Transfer CNN which extracts the semantic feature.

E. Borandag [9] emphasized that RNNs are highly effective for the software fault prediction due to its ability to capture sequential dependencies in the code to learn from both structured and unstructured patterns, and to perform well on large datasets. And Fan et al. [10] proposed a DL framework to enhance the defect prediction by leveraging semantic and syntactic features from the source code.

Wang et al. [11] proposed a DL-based approach, to learn semantic features from the source code automatically to improve software defect prediction. They used DBN to extract semantic features from Abstract Syntax Trees (ASTs) and code changes. Because traditional defect prediction features fail to capture semantic differences between the programs, which leads to suboptimal performance.

Liang et al. [12] used a semantic LSTM model for defect prediction which processes token sequences in order to predict software defects, leveraging pooling layer to handle the variable-length inputs. Timperley et al. [13] also found that temporal dynamics of code

changes are omitted by the traditional approaches. They gave a solution as "AttentiveLSTM" which is an enhanced LSTM model that can learn long-term dependencies and automatically focus on the defect-prone commits.

Louis F and Saleh M [14] emphasized the nature of agile development environment as the iterative and fast-paced, so it often leads rapid changes in the code, making it challenging to find and address defects in timely manner. They described that the agile defect prediction becomes very crucial as it helps teams to anticipate the potential issues early in the development process. They also exposed that the agile teams can allocate resources more efficiently and streamline their testing efforts to deliver high quality software product.

This review of related research studies emphasizes the significance of SDP, precisely in agile environments. Many studies expose the importance of agile SDP and how DL models outperform traditional SDP techniques by adopting to special nature of agile. Therefore, this comprehensive literature review helped to identify the gap of the research area of lack of agile SDP studies using DL models which can be more beneficial in the software development industry.

3 Methodology

The research methodology includes several steps as it is represented through the following diagram (see Fig. 1).

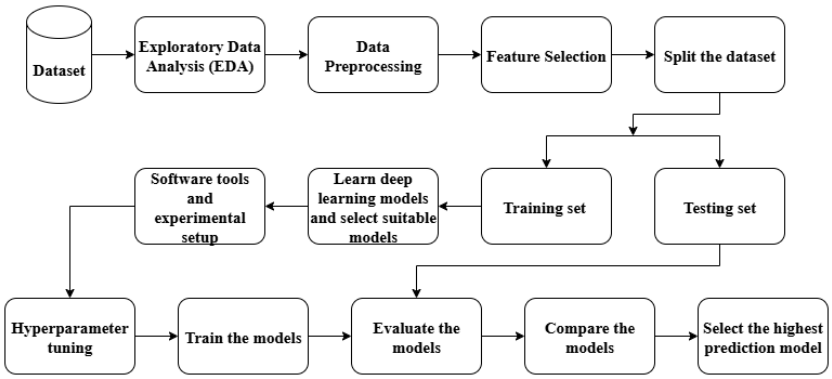

Fig. 1. Research Methodology

1) **Dataset:** A publicly available "Jira Defect Dataset" dataset from "Rnalytica" repository which can access via GitHub was used for the research study.

2) **Exploratory Data Analysis (EDA):** An extensive EDA was conducted to understand the structure, quality and underlying patterns of the dataset. For this, data size, defect distribution and the feature types were analyzed. Each data point includes code complexity metrics, code volume metrics, code churn metrics, commit activity metrics and defect labels. Each data record is labeled as either defect (1) or non-defect (0). A significant class imbalance was identified and, boxplots were used to identify the outliers and trends.
3) **Data Preprocessing:** Cleaned the dataset to get a high accurate prediction accuracy, data preprocessing part was done with several techniques such as handling missing values and duplicate data, handling outliers and reshaping the data for the models.
4) **Feature Selection:** Among 70 total columns of the raw dataset, 15 most relevant attributes were selected for prediction process (like AvgCyclomatic, CountLineCode, Added_lines, COMM, RealBug etc.) to reduce the redundancy of features and improve the performance.
5) **Split the dataset:** Dataset was divided into 2 sets as; training set and testing set.
6) **Learn the DL models and select suitable models:** By reviewing existing related studies, CNN, RNN, LSTM and DBN models were selected for the research.
7) **Software tools and experimental setup:** All the DL models were implemented using Python in Google Colab environment with TensorFlow and Keras libraries. Data preprocessing and analysis were performed using Pandas and NumPy. Matplotlib and Seaborn were used to generate visualizations. Evaluation metrics were computed using scikit-learn. Each model was designed with relevant standard setups: CNN with 1D Convolutional layers (ReLU and Sigmoid activations), DBN with Pretraining RBMs (Sigmoid activation), LSTM with two LSTM layers (ReLU and Sigmoid activations), and RNN with two SimpleRNN layers (tanh, ReLU and Sigmoid activations).
8) **Hyperparameter tuning:** To train the models, key hyperparameters were tuned as following to optimized the model performance:
    - Data Split (Train, Test): (85%, 15%), (80%, 20), (75%, 25%), (70%, 30%), (65%, 35%), (60%, 40%)
    - Batch sizes: 16, 32, 64, 128
    - Epoch count: 50, 100, 150, 200
    - Learning rate was tuned as 0.001, 0.0001, 0.0003 and 0.0005
9) **Train models:** All selected DL models were trained using training dataset.
10) **Evaluate models:** All the trained DL models were evaluated using testing dataset with accuracy, precision, recall and f1-score metrics.
11) **Compare the models:** All the models were compared with evaluation metrics wise.

12) **Select the highest prediction model:** After comparing the models, the model with highest accuracy was selected as the best prediction model.

4 Results and Findings

a. Effectiveness of Deep Learning vs Traditional approaches in Agile SDP

The research study compared the effectiveness of DL models with traditional SDP methods, as pointed out in the literature review part. This comparison was followed by the criteria which were derived from the categories mentioned in the existing related studies such as; challenges for agile SDP, the limitations of the traditional methods and the strengths of DL models. By analyzing these categories, four criteria for the comparison was identified. The following Table 1 gives the summary of the comparison.

Table 1. Comparison between the effectiveness of DL models vs Traditional models

Criteria	Deep Learning Approaches	Traditional Approaches
Feature Engineering	Automatic (learns raw code/commit data)	Manual (require expertise and time consuming)
Adaptability	Handles frequent changes via incremental learning	Struggle with dynamic requirements of agile projects
Sequential data	Specializes in temporal pattern recognition	Cannot model temporal dependencies effectively
Class imbalance mitigation	Provides data augmentation techniques to improve the prediction of minority (defective) class	Often resulting in poor minority class prediction due to bias towards the majority (non-defective) class

b. Model Performance Evaluation

The performance of each DL model can be presented according to the train-test split, in the Table 2 to Table 5.

The analysis shows that CNN model achieves its highest accuracy as 79.20% with an

60%-40% train-test split, in batch size 128 and 200 epochs using ReLU and Sigmoid activation functions (learning rate 0.0003).

Table 2. CNN Model's Performance

Train - Test Split	Batch Size	Epochs	Accuracy	Precision	Recall	F1-Score
85%-15%	16	150	74.80%	74.10%	76.27%	75.17%
80%-20%	64	200	77.73%	76.90%	79.29%	8.08%
75%-25%	64	200	78.58%	76.56%	82.38%	79.37%
70%-30%	128	200	78.26%	76.75%	81.07%	78.85%
65%-35%	64	200	77.70%	76.57%	79.82%	78.16%
60%-40%	128	200	**79.20%**	76.43%	84.45%	80.24%

Table 3. DBN Model's Performance

Train - Test Split	Batch Size	Epochs	Accuracy	Precision	Recall	F1-Score
85%-15%	16	100	**74.22%**	73.61%	75.51%	74.55%
80%-20%	64	150	73.19%	78.44%	63.96%	70.47%
75%-25%	64	50	73.84%	78.71%	65.38%	71.43%
70%-30%	128	150	73.53%	78.99%	64.13%	70.79%
65%-35%	64	200	73.44%	73.45%	73.42%	73.43%
60%-40%	64	200	73.83%	73.82%	73.82%	73.82%

The analysis shows that DBN model achieves its highest accuracy as 74.22% with an 85%-15% train-test split, in batch size 16 and 100 epochs using Sigmoid activation (learning rate 0.0005).

Table 4. LSTM Model's Performance

Train - Test Split	Batch Size	Epochs	Accuracy	Precision	Recall	F1-Score
85%-15%	128	200	73.48%	73.41%	73.65%	73.53%
80%-20%	128	100	75.06%	75.01%	75.15%	75.08%
75%-25%	64	200	74.63%	75.13%	73.65%	74.38%
70%-30%	128	200	75.30%	74.99%	75.92%	75.46%
65%-35%	16	200	76.61%	74.87%	80.11%	77.40%
60%-40%	128	200	**79.42%**	79.38%	79.48%	79.43%

The analysis shows that LSTM model achieves its highest accuracy as 79.42% with an 60%-40% train-test split, in batch size 128 and 200 epochs using ReLU and Sigmoid activation functions (learning rate 0.0005).

Table 5. RNN Model's Performance

Train - Test Split	Batch Size	Epochs	Accuracy	Precision	Recall	F1-Score
85%-15%	64	200	73.86%	72.93%	75.88%	74.38%
80%-20%	64	200	78.83%	78.32%	79.71%	79.01%
75%-25%	32	50	79.08%	77.56%	81.84%	79.64%
70%-30%	128	200	80.68%	79.25%	83.13%	81.14%
65%-35%	128	200	79.33%	79.17%	79.63%	79.39%
60%-40%	32	200	**80.78%**	78.51%	84.77%	81.52%

The analysis shows that RNN model achieves its highest accuracy as 80.78% with an 60%-40% train-test split, in batch size 32 and 200 epochs using tanh, ReLU and Sigmoid activation functions (learning rate 0.0003).

c. Comparison of the models

In order to provide a comprehensive assessment of the established DL models, performance of above DL model architectures was evaluated. By analyzing each performance, following graph shows the comparison of highest accuracy of each model (see Fig. 2.). **RNN model achieves an accuracy of 80.78%, outperforming all other models.** Following that, LSTM gave 79.42% accuracy, and CNN and DBN models followed 79.20% and 74.22% accuracy respectively.

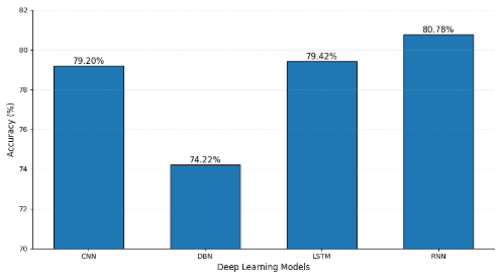

Fig. 2. Accuracy Comparison

The Fig. 3 to Fig. 5 show the Precision, Recall and F1-Score comparison between each model. It displays that LSTM achieve the highest precision value, and RNN achieve highest values for both recall and f1-score metrics.

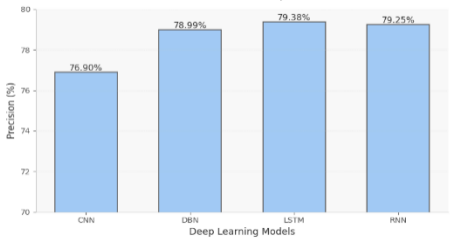

Fig. 3. Precision Comparison

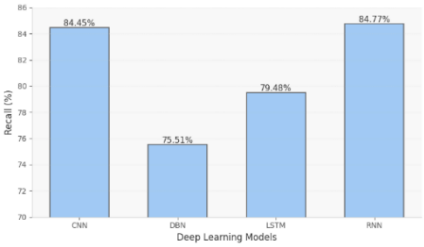

Fig. 4. Recall Comparison

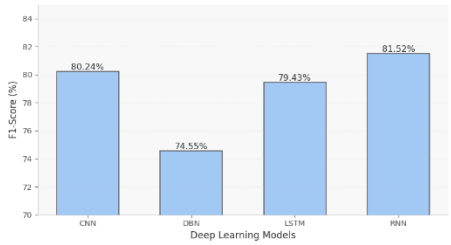

Fig. 5. F-Score Comparison

5 Discussion and Conclusions

The research study is conducted for a comparative analysis of DL models to identify their performance at SDP in agile environments. The research exposed the significance of using DL approaches to bridge the gap of lack of studies related to SDP in agile environments. During the research, class imbalance challenge was prevented by using data augmentation methods and overfitting was reduced by hyperparameter tuning over the models.

Research findings exposes that DL models performed noticeably better in agile environments compared to the traditional defect prediction methods. DL models have the ability to automatic feature engineering and they specialize in temporal pattern recognition.

They can handle frequent changes via incremental learning, and also handle class imbalance issues using data augmentation techniques. It reveals that these are hard to perform by traditional SDP methods in agile environment. Parallel to that, RNN model achieved 80.78% of its highest accuracy among all other models, emphasizing its outstanding ability to analyze the sequential data and predict the future defects risks by using historical patterns, which is crucial in fast-paced nature of agile environments.

Due to the special nature of agile environment, using DL models brings more advantages to the agile teams to identify defects in timely manner. This helps teams to prioritize tasks, allocate resources to the riskiest parts of the code, enhance sprint planning and improve software quality by supporting effective continuous development. In practically, these findings can be implemented into the issue tracking or CI/CD workflows of agile teams to enable the early detection of defects during sprints cycles, by integrating the selected DL model. To enhance the SDP accuracy, future research may focus on integrate project-level data and applying advanced architectures such as transformer-based models.

References

1. 2019 IEEE 5th International Conference on Computer and Communications (ICCC). IEEE, 2019.
2. M. Fokrul, I. Khan, A. Kader, and M. Masum, Predictive Analytics And Machine Learning For Real-Time Detection Of Software Defects And Agile Test Management, Theory And Practice, 4, pp. 1051–1057, 2024, doi: 10.53555/kuey.v30i4.1608.
3. R. Noor and M. Fahad Khan, Defect Management in Agile Software Development, International Journal of Modern Education and Computer Science, 6(3), pp. 55–60, Mar. 2014, doi: 10.5815/ijmecs.2014.03.07.
4. T. Hoang, H. Khanh Dam, Y. Kamei, D. Lo, and N. Ubayashi, DeepJIT: An end-to-end deep learning framework for just-in-time defect prediction, in IEEE International Working Conference on Mining Software Repositories, IEEE Computer Society, May 2019, pp. 34–45. doi: 10.1109/MSR.2019.00016.
5. P. Deep Singh and A. Chug, Software Defect Prediction Analysis Using Machine Learning Algorithms. IEEE, 2017.
6. S. Omri and C. Sinz, Deep Learning for Software Defect Prediction: A Survey, Proceedings - 2020 IEEE/ACM 42nd International Conference on Software Engineering Workshops, ICSEW Association for Computing Machinery, 2020, pp. 209–214. doi: 10.1145/3387940.3391463.
7. M. Nevendra and P. Singh, Software defect prediction using deep learning, Acta Polytechnica Hungarica, 18(10), pp. 173–189, 2021, doi: 10.12700/aph.18.10.2021.10.9.

8. S. Qiu, H. Xu, J. Deng, S. Jiang, and L. Lu, Transfer convolutional neural network for cross-project defect prediction, Applied Sciences (Switzerland), 9(13), 2019, doi: 10.3390/app9132660.
9. E. Borandag, Software Fault Prediction Using an RNN-Based Deep Learning Approach and Ensemble Machine Learning Techniques, Applied Sciences (Switzerland), 13(3), Feb. 2023, doi: 10.3390/app13031639.
10. G. Fan, X. Diao, H. Yu, K. Yang, and L. Chen, Software Defect Prediction via Attention-Based Recurrent Neural Network, Sci Program, 2019, doi: 10.1155/2019/6230953.
11. S. Wang, T. Liu, J. Nam, and L. Tan, Deep Semantic Feature Learning for Software Defect Prediction, IEEE Transactions on Software Engineering, 46(12), pp. 1267–1293, Dec. 2020, doi: 10.1109/TSE.2018.2877612.
12. H. Liang, Y. Yu, L. Jiang, and Z. Xie, Seml: A Semantic LSTM Model for Software Defect Prediction, IEEE Access, 7, pp. 83812–83824, 2019, doi: 10.1109/ACCESS.2019.2925313.
13. C. S. Timperley, L. Herckis, C. Le Goues, and M. Hilton, Understanding and improving artifact sharing in software engineering research, Empir Softw Eng, 26(4), Jul. 2021, doi: 10.1007/s10664-021-09973-5.
14. L. Frank and S. Mohamed, Training Machine Learning Models for Software Defect Prediction in Agile Development, 2024. [Online]. Available: https://www.researchgate.net/publication/380288702

3rd International Engineering Research Symposium 2025 (IERS 2025)
Colombo, Sri Lanka

Design of a Carton Box Orientation Changing Machine for an Industrial Cologne Packing Process

K. H. A. C. Kavindi, H. K. Shalinda, W. A. U. I. S. Wickramasingha, V. Lalith Kumar, K. C. Wickramasinghe* and K. T. K. M. De Silva

Department of Mechanical and Manufacturing Engineering, University of Ruhuna, Sri Lanka
* krishan@mme.ruh.ac.lk

Abstract. The cologne packing process presents considerable challenges due to the flammable nature of the liquid and the fragility of the glass bottles. Cologne packing typically involves two primary stages: packing individual cologne bottles into carton boxes and subsequently packing carton box stacks into corrugated boxes. This research specifically addresses the second stage, focusing on the design of a simple, efficient carton box orientation changing machine that can be integrated into existing automated packing lines. The proposed mechanism is capable of changing the orientation of carton boxes at a rate of 60 pieces per minute without causing bubble formation inside the cologne bottles. It is designed to handle three common bottle sizes: 50 ml, 100 ml, and 200 ml and change the orientation of carton boxes by 90 degrees. Currently available systems face persistent challenges related to product quality and operational efficiency, particularly in the carton box orientation changing process. Frequent misalignment, jams and manual handling reduce product quality and throughput, while rigid mechanisms cause high maintenance and downtime. Moreover, limited adaptability to varying carton sizes restricts their use in flexible production environments. These shortcomings highlight the need for a more efficient, reliable, and adaptable design solution. Existing mechanisms frequently damage carton boxes or deform the packaging and form bubbles inside the bottle, leading to increased product rejection rates and reduced customer satisfaction. This paper provides a comprehensive review and critical evaluation of current orientation changing methods, identifying their key limitations. The newly proposed mechanism offers a solution that minimizes physical damage to the packaging, enhances the overall quality of the packed product, and improves system efficiency. Furthermore, integrating this mechanism into the existing packing lines has the potential to replace three manual labor positions, contributing to labor cost reduction and process optimization.

Keywords: Carton box, Corrugated box, Orientation changing mechanism

1 Introduction

In modern manufacturing industries automation processes play a significant role. Through automation process can achieve consistent product handling and reduce operational cost. When considering the cologne packing process there are two main stages. Those are carton box packing process and the corrugated box packing process. At the first stage final product is packed into carton boxes. Most of the industries use automated packing machines for this process [1]. The next step is to pack those carton boxes in large corrugated boxes for easy handling and transportation. This process is more complex than the first step. Most of the methods currently used in the industry for changing the orientation of the carton boxes such as twist conveyor, box flipping mechanism may damage the carton boxes. This will affect to the appearance of the final output and therefore these items will be rejected in the quality checking process.

For packing carton boxes in corrugated boxes first need to change the orientation of the output of the automated carton box packing machine. Then need to form a stack of carton boxes. After that need to pick and place this stack. The most common industrial use for this pick and place method is a collaborative robot arm [2]. Finally place those carton box stack in a corrugated box and tap.

This research mainly focuses on the changing orientation of the carton boxes which gives as the output of automated carton box packing machine. Here mainly consider the quality of the final output, cost effective method and easy mechanism which reduce the generation of form. In literature review explores existing methods and technologies used in the industry to change the orientation of the carton boxes.

Twist conveyors are the most common method to change the orientation of the product. There are different types of twisted conveyors in the market. The most common type is the twisted chain conveyor. In this method change the orientation without the use of any external devices. These are commonly used for foolproof product reorientation and reoriented by any angle up to 90˚ degrees. Main features of this product are can rotate the product 90˚ degrees in 60 linear inches and all within a 96 inches footprint, no need any additional automation or no disruption in conveyance and can be used for slight incline and decline applications. However, these conveyors required more space for the installation process [3].

Box flipping mechanism is another most commonly used mechanism for changing the orientation of boxes. In this method box automatically flip and rotate products when the product travels along the conveyor belt. By using this method can flip boxes 90˚or 180˚ degrees. In here, grip the box by frame with fingers and by using linear actuators rotate it. However, this mechanism can only flip one box at a time [4].

The twisting plate is the simplest way that can be used to change the orientation of boxes. These plates include two twisted guide plates along the conveyor. The length of the twisted plate changes because of the size and weight of the carton box. When the box is moved forward this twisted plate applies force on it to rotate. After carton boxes are entered to the twisted plate on conveyor these conveyors will be guide by plates. Plates gradually twist and this twisting angle can be adjusted to 90˚or 180˚ degrees. While using this method need to consider the space requirement because it requires a longer conveyor section for smooth rotation and for the friction of boxes [5].

The turning table method mostly uses a rotating hammer or plates to change the orientation of boxes. While using a rotating hammer it strikes the side or edge of the box. That force will impact while the conveyor continues moving. Advantages of this method are can be used for high-speed production lines; hammer speed and impact force can be adjusted for different orientations and it only requires less space. However, it is not suitable for fragile items due to impact force [6].

2 Methodology

The proposed design focuses on automating the carton box handling process in cologne packing lines, specifically addressing the challenges in orientation change and stacking for final packaging.

A detailed study of the existing manual and semi-automated packing processes was conducted to identify inefficiencies in orientation change, stacking, and final packing. Performance requirements such as throughput 60 cartons/min, gentle handling to avoid bubble formation, and seamless integration with the upstream carton packing machine were established.

The overall system was divided into four functional subtasks which are receiving cartons, orientation change, stack formation, and pick-and-place transfer. For each subtask, alternative mechanisms were explored such as roller conveyors, belt conveyors for transfer, mechanical and pneumatic orientation systems, and the most feasible solutions were selected through a morphological chart and evaluation matrix.

The methodology is structured around four key sub-tasks essential for the development of the new system as follows:

Receiving Cartons from the Automated Carton Packing Machine: The system is designed to receive individual carton boxes directly from the automated carton packing machine. A conveyor mechanism ensures the smooth transfer of cartons to the orientation changing unit while maintaining continuous flow and synchronization with upstream processes.

Changing the Orientation of the Carton Box: An orientation changing mechanism is developed to reorient 90 degree each carton box to the required position for efficient stacking and packing. The system ensures the reorientation is completed without causing internal agitation that could lead to bubble formation within the cologne bottles.

Forming a Stack: After orientation, the cartons are sequentially arranged and stacked into predefined configurations suitable for placement into corrugated boxes. The stacking process is carefully controlled to prevent misalignment and to ensure stability during subsequent handling.

Picking and Placing the Stack into Corrugated Boxes: The final sub-task involves transferring the formed stack into a corrugated box using a pick-and-place system. This step is automated using collaborative robot arm to minimize manual intervention and maintain the required packing speed of 60 pieces per minute.

Finally, the selected mechanisms were modeled using CAD (SolidWorks) to ensure dimensional compatibility, smooth flow, and structural stability. The orientation unit was designed with synchronized motion control to achieve 90° re-orientation without disturbing bottle contents. The stacking system was designed for alignment accuracy, while the collaborative robot arm was programmed to achieve reliable pick-and-place operations.

a. Design Specifications

The proposed carton box orientation changing mechanism is designed to meet specific operational and performance requirements suitable for integration into an automated cologne packaging line. The system is expected to handle a maximum output of 60 pieces per minute, ensuring compatibility with high-speed industrial production lines because the conveyor is configured to deliver cartons at a rate compatible with the upstream packing machine, ensuring continuous flow without bottlenecks and the orientation change is achieved within a fraction of a second using high-speed MJ linear actuators, which provide fast and precise movement. Also, these actuators can be configured as required through PLC modules, enabling optimization of stroke length and speed to minimize cycle time. During stacking, actuator speeds are synchronized with conveyor motion to prevent accumulation delays. The collaborative robot used for pick-and-place operations has a high joint speed and repeatability accuracy, ensuring that the formed stack can be transferred reliably into corrugated boxes within the required cycle time. This machine operates on a standard three-phase power supply with an electrical requirement of 400 V, 50 Hz. The mechanism is designed to achieve a precise rotation angle of 90 degrees, enabling accurate orientation of the carton boxes without causing damage or misalignment. The system must be capable of handling carton box stacks with a weight range between 1.08 kg (for 50 ml

box single layer) and 2 kg (for 100 ml box single layer), ensuring stability and consistent performance across various product sizes.

weight of single layer of 50 ml boxes= weight of one box x number of boxes in one stack
= (6.5/48) * 8
= 1.08 kg

weight of single layer of 100 ml boxes= weight of one box x number of boxes in one stack
= (12/48) * 8
= 2 kg

Table 1 shows the specifications for three different cologne bottle sizes:50ml, 100ml and 200 ml. For both the 50 ml and 100 ml bottles, 48 individual carton boxes are packed into a single corrugated box. In contrast, due to their larger size, only 12 cartons of the 200 ml bottles can be accommodated per corrugated box. The input feeding speed of the carton boxes into the system is maintained at 60 pieces per minute for the 50 ml and 100 ml bottles, whereas the speed is reduced to 25 pieces per minute for the 200 ml bottles to facilitate careful handling and prevent potential damage during processing.

Table 1. Details of packing boxes

Size	Number of cartons in one corrugated box	Input carton speed(pcs/min)	Corrugated box weight(kg)
50 ml	48	60	6.5
100 ml	48	60	12
200 ml	12	25	5

b. Components of Design

Flexible conveyor

The output of the cartooning machine is delivered into the flexible conveyor, where the boxes are aligned horizontally and transported cartoon boxes forward.

Pushers

There are two pushers used in the system, pusher number 1 is used to change the orientation of the boxes horizontally to vertically and the other one is used to place the boxes

frequently vertically in the stacking stable. One movement of the pusher can place of carton boxes vertically in the stacking table. The pushers are actuated by help of the linear actuators.

Stack stopper

Stack stopper act as a gate and help to form a set of carton boxes and pushes them into the Stack stable.

Angle plate

The angle plate helps guide the boxes down smoothly into the pocket. The cartoon boxes move slides in the angle plate and place them vertically in the pocket.

Linear actuators

There are four actuations in the system, those are pusher number 1, pusher number 2, stack stopper and pocket actuations. Linear actuators play a critical role in the pick-and-place operation. Specifically, an XY linear actuator system from MJ Unit is employed to handle the precise movement of the prepared carton stacks. This actuator system is equipped with a suction pad mounted on the Y-axis actuator, which securely grips the carton stacks during transfer. The XY linear actuator enables controlled, accurate motion in both the horizontal (X-axis) and vertical (Y-axis) directions, facilitating the smooth transfer of the carton stacks from the stacking table into the corrugated boxes positioned on the roller conveyor. The use of this actuator ensures high positioning accuracy and reliable handling of the product, contributing to the overall efficiency and consistency of the packing process.

Pocket

The function of the pocket is to collect vertically and stabilize the cartoon boxes, after that process pocket moves away to form the stacks.

Stacking table

This is the final resting place of the stacked boxes. In here, carried out the boxes next pick and place process.

c. Specifications of components

Roller conveyor

The effective length of conveyor roller is 450 mm and the maximum corrugated box width is 320 mm.

Pneumatic actuators

The system uses two pneumatic actuators, a stack stopper actuator with a 16 mm bore and 80 mm stroke, and a tightening actuator with a 16 mm bore and 10 mm stroke.

Pusher

The system considers surface contact coefficients of 0.2–0.6 (plastic–cardboard) and 0.2–0.45 (SS–cardboard). Actuation is achieved using an MJ 50M with 400 W servo motor for stack forming, an MJ 50 with 400 W servo motor for the pocket holder, and MJ 70 + MJ 70M with 750 W servo motors for pick-and-place.

3 Results and Discussion

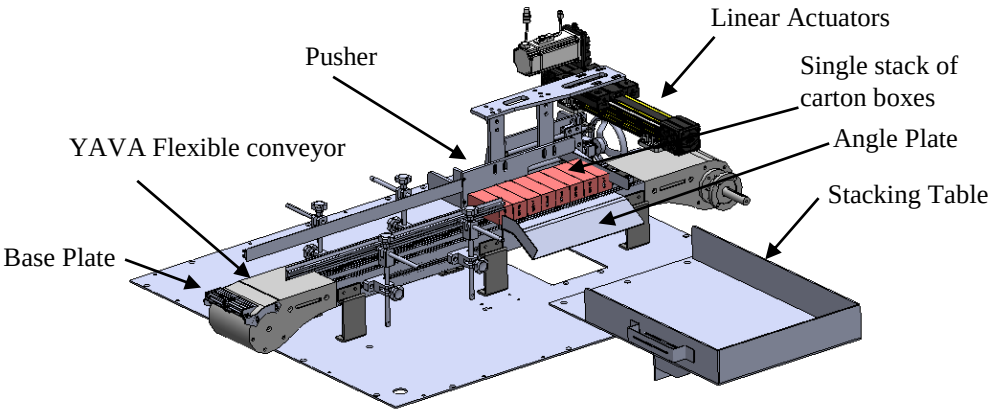

Fig. 1. Solid model of the design

Horizontally oriented carton boxes are discharged from the end of the cartoning machine and transferred to the YAVA flexible conveyor, which has an operating width of 180 mm. These cartons are sequentially received by the conveyor and guided toward a stopper positioned at the end of the conveyor to form linear stacks. The quantity of cartons within each stack is monitored and controlled using proximity sensors installed along the conveyor.

Once the required number of cartons is accumulated, pusher 1 is actuated to transfer the linear stack toward an angled plate. As the stack moves along the angled plate, the orientation of the carton boxes is changed from horizontal to vertical. To prevent the carton boxes from toppling during this transition, the stack is directed into a specially designed pocket that temporarily holds the cartons in position. Following stabilization, the pocket

is actuated backward, releasing the vertical stack onto the next stage. Subsequently, pusher 2 is actuated to transfer the oriented stack onto the stacking table for further processing.

Simultaneously, corrugated boxes are formed using a Fairinon FR5 collaborative robot (cobot) equipped with a suction pad. The cobot assembles the corrugated boxes and places them onto a roller conveyor. The availability of a box in the correct position is detected using proximity sensors, which signal two tri-rod pneumatic cylinders to stop the box accurately at the designated location.

While the box is stationary, a pick-and-place system is engaged to transfer the prepared carton stacks into the corrugated box. This operation is performed using an XY linear actuator from MJ Unit, equipped with a suction pad mounted on the Y-axis actuator to securely handle the stacks.

Once the carton stack is successfully placed into the corrugated box, the pneumatic stoppers are released, and the fully packed box is conveyed to the top flap forming and taping station, completing the packing process.

a. Efficiency

Table 2. Efficiency calculation

Packing rate (Manual)	40 pieces /min
Packing rate (Automated system)	60 pieces /min
Increased packing rate	33.33 %

b. Return of Investment (ROI) Analysis

Table 3. ROI calculation

Allocated budget	LKR 10,000,000.00
Expected cost	LKR 10,000,000.00
Amount of the salary for the employee per month	LKR 60,000.00
Number of employees per shift	3
Number of shifts per day	1
Total number of employees per day	3
Monthly employee cost	LKR 180,000.00
Yearly employee cost	LKR 2,160,000.00
Pay Back Period (Years)	4.6

By integrating the proposed automated system, these three manual positions can be fully eliminated from the packing process, leading to significant annual labor savings. Based on the total investment and the yearly cost reduction, the payback period is calculated to be approximately 4.6 years. This indicates that the initial investment in the new automated system will be recovered through labor cost savings within this period.

The return on investment (ROI) analysis demonstrates that the project is financially justifiable, as it offers long-term cost benefits, increased operational efficiency, and reduced dependency on manual labor, while simultaneously improving product handling quality and process consistency.

4 Conclusions

The cologne packing process presents unique challenges due to the fragility of glass bottles and the flammable nature of the liquid product. This research successfully addressed these challenges by developing a simple, efficient, and cost-effective carton box orientation changing mechanism that can be integrated into existing automated packing lines. By automating the manual process, the system establishes a continuous flow operation, eliminating inconsistencies associated with human handling. The use of high-speed MJ actuators with PLC control and a collaborative robot for pick-and-place ensures reliable performance and enables the system to achieve the target throughput of 60 pieces per minute.
In addition, the system is designed with food-grade stainless steel (SS) to meet hygiene and safety requirements, while the adoption of higher GSM cartons provides improved strength, reducing the risk of bubble formation and physical damage to packaging during handling. The modular design also allows adjustment for multiple carton sizes, enhancing the flexibility of the packing process.

Beyond technical performance, the design offers substantial operational benefits by reducing manual labor, achieving significant cost savings, and providing an estimated payback period of 4.6 years. Overall, this solution not only mitigates the existing limitations in cologne packing but also delivers a sustainable, safe, and economically viable advancement for modern automated packaging lines. Future work may focus on further enhancing flexibility and incorporating advanced control technologies to accommodate an even wider range of packaging configurations.

References

1. A. A. Algitta, S. Mustafa, F. Ibrahim, N. Abdalruof and M. Yousef, Automated Packaging Machine Using PLC, IJISET - International Journal of Innovative Science, Engineering & Technology, 2(5), pp. 282-288, 2015.

2. N. M. Gomes, F. N. Martins, J. Lima, H. Wörtche, Reinforcement Learning for Collaborative Robots Pick-and-Place Applications: A Case Study, Automation, 3(1), pp. 223 -241, 2022.
3. SpanTech, spantechconveyors.com, 2024. [Online]. Available: https://spantechconveyors.com/conveyors/standard-conveyors/twisting-conveyor/. [Accessed 10 06 2025].
4. "Youtube.com," [Online]. Available: https://youtu.be/iKzjGKQHVhc?si=Bef2qLzVCo5EHbuo.. [Accessed 11 06 2025].
5. youtube.com, [Online]. Available: https://youtu.be/UZdSjqgbrLo?si=J894s_xs5AFA_GJ1.. [Accessed 11 06 2025].
6. "wsiglobal.com," WSIGLOBAL, [Online]. Available: https://wsiglobal.com/mitt-packing/. [Accessed 11 06 2025].

3rd International Engineering Research Symposium 2025 (IERS 2025)
Colombo, Sri Lanka

Design of a Reusable Pen Assembling and Dispensing Unit

I. A. Wijayaratne, H. W. Thilanka, K. K. S. B. Kodithuwakku, W. B. N. N. Bandara and K. M. T. M. De Silva

Faculty of Engineering, University of Ruhuna, Galle 80000, Sri Lanka
muthumali@mme.ruh.ac.lk

Abstract. The paper discusses a reusable pen assembly and dispensing unit designed to meet the growing need for a sustainable and cost-effective alternative to single-use pens. This system automates key operations such as blind cap removal, ink tube replacement, and pen reassembly through a series of electromechanical actuators, sensors, and limit switches, thereby retaining proper alignment and operational precision. In addition to promoting sustainability, the design focuses on the reuse of pen components such as pen barrels and blind caps, reducing plastic waste. Also, it encourages environmentally responsible behavior, especially among younger users, by promoting the reuse of disposable pens. This initiative supports the global shift toward circular economy solutions in everyday consumer products. The machine features a compact footprint of 610 mm × 650 mm × 350 mm and completes a full pen reassembly cycle in just 48 seconds, making it suitable for educational institutions and small-scale applications. Performance evaluation will be carried out after fabrication to assess assembly accuracy, reliability, and cycle efficiency. Overall, the system contributes to green behavior on the consumer side and reinforces the concept of the circular economy in daily life.

Keywords: Reusable pen assembling unit, Automation, Plastic Waste Reduction

1 Introduction

Plastic disposable pens have turned out to be a major form of plastic pollution due to their wide use and short lifespan. Most consumers discard the entire pen when its ink runs out, even though only the refill is exhausted. Disposable pens are made of non-biodegradable plastic material and usually contain metallic components, which cannot be recycled easily. As a result, billions of used pens reach landfills and the environment annually, incurring long-term environmental damage, as shown in

Fig.. Waste minimization is needed to promote sustainable consumption and minimize environmental footprints [1].

Millions of disposable plastic pens are cast aside annually, causing plastic pollution and an environmental menace of sorts. Despite their small size, the cumulative impact of discarded pens is significant. These pens are typically made from non-biodegradable plastics such as polypropylene (PP), acrylonitrile butadiene styrene (ABS), and polyethylene (PE), which can persist in the environment for centuries [2].

Fig. 1. Environmental impact of plastic pens

A majority of pens are thrown away after the ink has dried out, rendering reusable parts like plastic barrels and metal tips useless. This creates unnecessary plastic waste and higher production costs [3]. Though replacing only the ink chamber is ecologically friendlier and cheaper, the lack of simple refilling mechanisms deters the use of reusing. A semi-automatic machine is proposed to simplify pen disassembly and assembly, rendering replacement of ink convenient and promoting sustainable writing in schools, offices, and stores.

A standard ballpoint pen consists of various necessary components that work together to draw ink smoothly on paper, as shown in Fig.. These are the pen barrel, which is the body, the ink chamber in which the ink is held, the metal tip through which the ink is expelled by a rolling ball, the blind cap which caps the rear of the pen, and the pen cap which covers the tip when not being used [4].

Among all of these, only the ink chamber can be consumed, while the rest of the parts still retain their structure even when the ink is exhausted. This indicates the potential for designing reusable systems to replace only the ink chamber and reuse other components of the disposable pen.

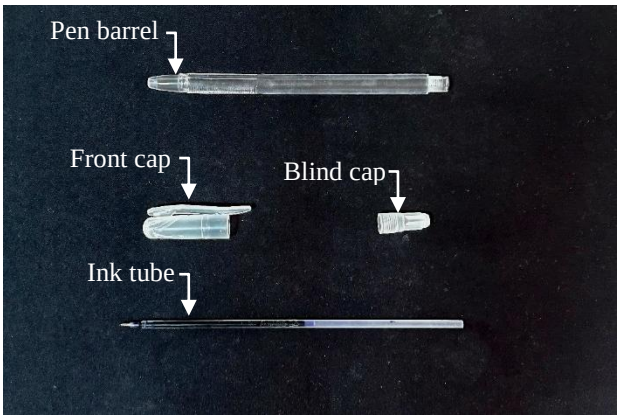

Fig. 2. Main parts of the pen

By enabling users to replace only the ink tube while reusing the pen's plastic body and caps, the proposed system directly reduces plastic waste at source. Based on measured part masses, each refill keeps approximately 5.30 g of plastic in circulation, which includes the pen barrel weighing 3.86 g, the front cap weighing 1.15 g, and the end cap weighing 0.29 g, instead of discarding the entire 5.90 g pen. This saving highlights the role of the machine in supporting sustainability by reducing plastic waste and improving resource efficiency.

2 Methodology

Developing an effective automated system in which pen reuse is easily accessible to small-scale businesses and educational institutions helps promote environmentally sustainable practices that counter a culture dominated by single-use pens.

Mainly, there are two types of ballpoint pens which are back-loading pens and front-loading pens. Back-loading pens are designed so that the ink tube is inserted from the rear end of the pen barrel, typically secured with a threaded blind cap while front-loading pens allow the ink tube to be inserted from the front. An initial survey was conducted among users to identify the most commonly used pen type and the machine was designed to accommodate this model mechanism as an initial step. The survey results indicate that Atlas Max is the most commonly used pen in Sri Lanka, featuring a back-loading mechanism (Fig. 3).

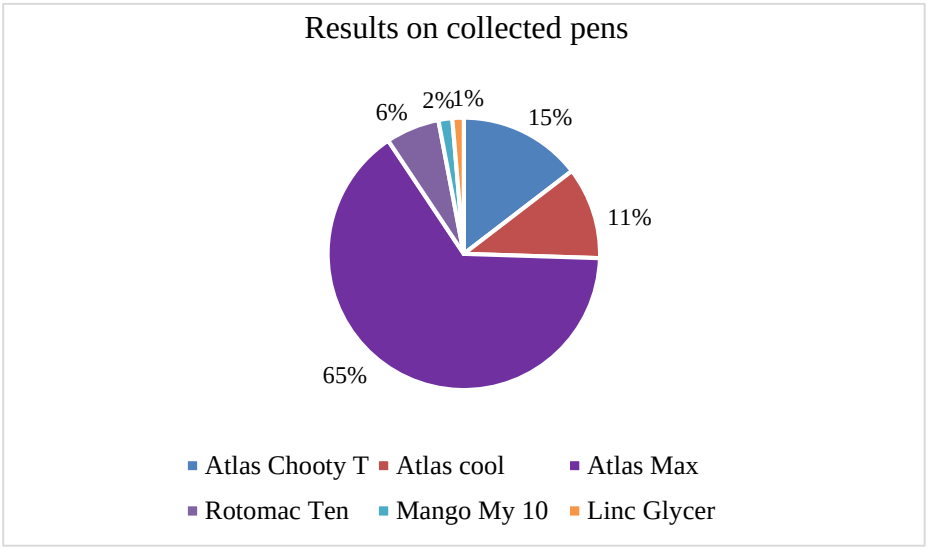

Fig. 3. Results of the initial user survey

In back-loading pens, the ink tube is inserted and secured from the rear end of the pen barrel. During testing with this type of pen, it was found that, in most cases, for back-loading pens, the ink tube tends to stay attached to the blind cap. As a result, when the blind cap is removed, the ink tube is often removed along with it, as shown in Fig. 4. Careful attention was given to this aspect during the design of the system.

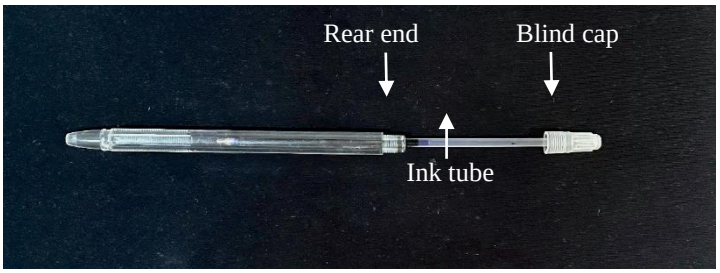

Fig. 4. Removing blind cap of the back-loading pen

The key processes are as follows. First, the user manually removes the pen clip and inserts the pen into the machine. The pen is clamped and transferred for blind cap removal,

where the blind cap is unscrewed and removed using a rotary mechanism. The blind cap removal mechanism then moves backward while holding the cap. The system separates the ink tube from the pen barrel. If the ink tube is not attached to the blind cap, it is removed directly from the pen barrel. The used ink tube is transferred to the disposal unit, where it is collected, and the pen is moved to the next station for a new ink tube insertion, which is supplied from the new ink tube storage unit. Once a new ink tube is inserted into the pen barrel, the blind cap is brought back to the front, and the pen is transferred again to the place where the blind cap removal removed. The blind cap is reattached to the pen, completing the assembly process. Finally, the pen returns to the initial position, the clamp is released, and the user retrieves the pen.

In addition to that, the machine should be compact and lightweight, making it suitable for portable use. Also, the mechanism should be simple to allow easy maintenance and user-friendly operation for all users.

3 System design and development

a. Design consideration

The following design criteria were taken in the designing process
Pen dimensions:

Table 1. Basic dimensions of Atlas max pen

Total pen length	135.95 mm
Ink barrel length	118.95 mm
Number of threads	6
Thread pitch	1.06 mm
Thread diameter	6.39 mm
Blind cap length	19.25 mm
Ink tube length	133.34 mm
Ink tube diameter	3.00 mm
Total pen length	135.95 mm
Ink barrel length	118.95 mm
Weight of the full pen	5.90 g
Weight of the end cap	0.29 g
Weight of the pen barrel	3.86 g
Weight of the front cap	1.15 g

- Nominal Cycle Time: 48 seconds per pen

Table 2. Nominal cycle time

1	Machine Start and Pen Clamp	2 S
2	Pen travelling to station 2	3 S
3	Main rack and pinion travelling forward (15 cm)	5 S
4	2 DOF clamp the end cap	1 S
5	Main rack and pinion travelling back (3 cm)	1 S
6	Clamp the pen tube	2 S
7	Main rack and pinion travelling back (12 cm)	4 S
8	Upper rack and pinion mechanism moves forward (2 cm)	2 S
9	Release the pen tube	1 S
10	Upper rack and pinion mechanism moves backward (2cm)	2 S
11	Pen travelling from station 2 to station 3	3 S
12	Scotch Yoke	3 S
13	Pen travelling from station 3 to station 2	3 S
14	Main rack and pinion travelling forward (15 cm)	5 S
15	Unclamp the end cap and refix it	1 S
16	Main rack and pinion travelling backward (15 cm)	5 S
17	Pen travelling station 2 to the initial position	3 S
18	Unclamp the pen	2 S
Total time		48 S

- Control System: Micro controllers with sensors and limit switches
- Size and Portability: Compact design (610 mm × 650 mm × 350 mm)
- Power Supply : Powered by 12 V DC

b. Key Mechanisms Used in the Machine

The described pen assembling and dispensing machine has several main mechanical systems to accomplish its tasks effectively. To maintain simplicity and quick performance, motor actuators are used for all main operations. The method of smooth, precise motion between stations is facilitated through a belt-driven linear actuator shown in Fig..

Limit switches are built into the system to detect part positions and assist in control throughout each step. Rotary to linear motion conversion for the insertion of the ink tube is facilitated through the reciprocating mechanism.

To keep the pen barrel in a fixed state for operations, a clamp system should be used. Also, another two-arm clamp is used to hold the used ink tube. In addition to that, a two-degree-of-freedom (DOF) robot arm is used to hold and rotate the blind cap, allowing it to be unscrewed or tightened as required. The linear movement of this robotic arm is achieved by a rack and pinion mechanism.

Fig. 5. Belt-driven linear actuator

c. CAD Design

A complete CAD model was developed to visualize the design arrangement. Refer to Fig.6 and Fig. 7 for the overall CAD model.

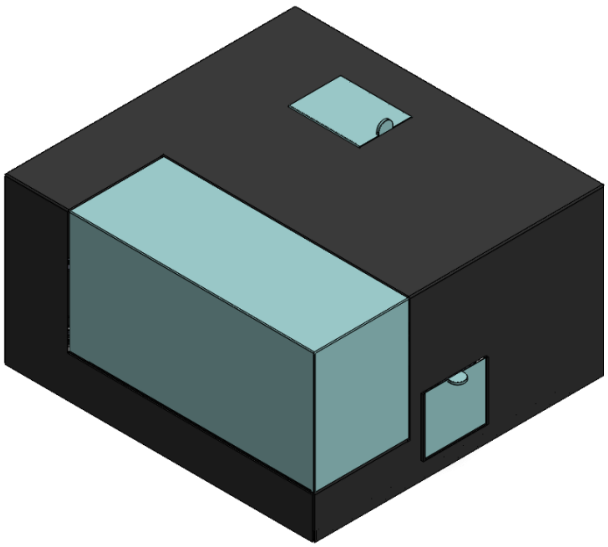

Fig. 6. CAD model

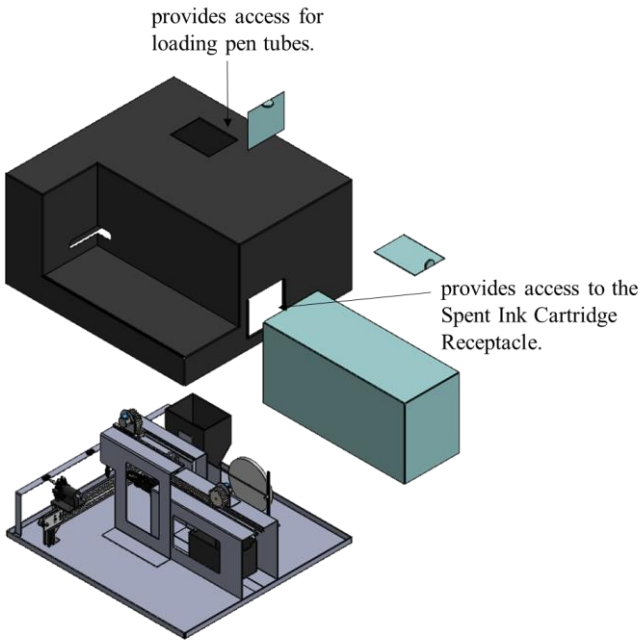

Fig. 7. With easy access to load and unload pen tubes

Fig. 8 illustrates the same design without the outer cover, with individual components labeled.

Then the belt conveyor moves the pen to station 3. Upon reaching station 3, the presence of the pen barrel is detected by a limit switch, and again, the conveyor is stopped. Here, using a reciprocating mechanism, a new ink tube is inserted into the pen barrel from the pen tube holder. A sensor placed in front of the pen can detect the presence of the tip of the new ink tube, and it confirms the end of the process.

The conveyor again becomes active, returning the pen to station 2. At the same time, the robot arm brings the old blind cap to the front using the rack and pinion mechanism. After the pen reaches the station, the system halts, and the robot arm reattaches the blind cap. Finally, the conveyor moves the pen back to the station 1 where it is released.

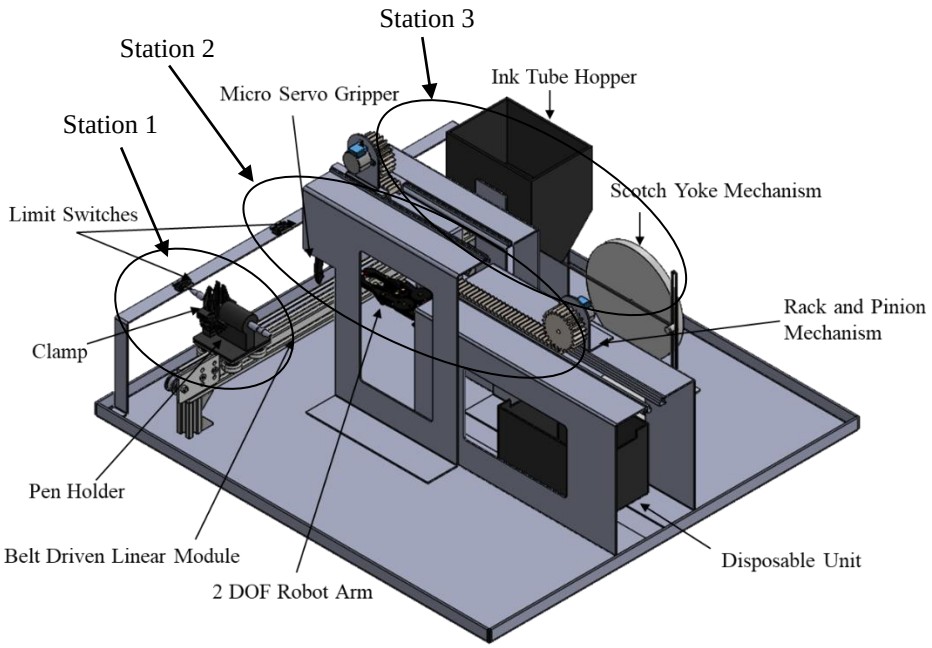

Fig. 8. Design without Outer Cover

4 Conclusions and Future work

a. Conclusions

The production of the reusable pen assembling and dispensing machine presents an alternative way of reducing plastic waste caused by disposable pens. Since the machine only replaces the ink chamber, it encourages an environmentally friendly use of pens without compromising on functionality and ease of use. Usage of mechanisms such as the belt-driven linear actuator, reciprocating mechanism, limit switches, clamp mechanism, and rack-and-pinion assembly ensures precise and automatic assembly of pen parts. The device is easy to use, occupies minimal space, and can be easily implemented in schools, bookstores, and shopping stores. Overall, this project offers a utilitarian and sustainable alternative to traditional pen usage, promoting environmental sustainability as well as longer-term economic returns.

b. Limitations and Future Work

The current design also has certain limitations. It is only compatible with back-loading pens, and manual removal of the pen clip is required, which limits the level of full automation.

Future work may include:

- Completing fabrication and conducting experimental testing to validate the system's reliability, success rate, and efficiency.
- Developing a coin-based operation system to enable automated payment and dispensing in public spaces.
- Incorporating a damaged component identification mechanism to detect worn-out or defective pen parts and replace them automatically.
- Extending compatibility to different pen types through adaptive clamping and modular gripper designs.
- Automating clip removal to achieve full automation.
- Optimizing mechanism design for higher speed, throughput, and energy efficiency.

References

1. Environmental Impact of Disposable Pens and Their Eco-Friendly Rivals. Accessed: Jun. 22, 2025. [Online]. Available: https://www.printedpens.com.au/blog/environmental-impact-of-disposable-pens-their-eco-friendly-rivals.htm
2. The Problem of 50 Billion Plastic Ball Pens - No Offence To Earth. Accessed: Jun. 22, 2025. [Online]. Available: https://thenote.earth/plastic-ball-pen-pollution-note-pen-no-offence-to-earth/
3. How Are Pens Made? Unveiling the Ballpoint Pen Creation Process – Dayspring Pens. Accessed: Jun. 22, 2025. [Online]. Available: https://www.dayspringpens.com/blogs/the-jotted-line/how-ballpoint-pens-are-made
4. What Are the Key Parts of Pen Anatomy? Accessed: Jun. 22, 2025. [Online]. Available: https://www.penfinder.com/pen-anatomy/what-key-parts-pen-anatomy/

3rd International Engineering Research Symposium 2025 (IERS 2025)
Colombo, Sri Lanka

Feasibility of Utilizing Rice Husk Biochar as a Supplementary cementitious material in Concrete Blocks

T. Vidushi Anjana[1] and S. M. V. P. D. Senanayake[2]

[1]Department of Biosystems & Biotechnology, Sri Lanka Technology Campus, Meepe, Sri Lanka
[2]Technology Incubator, National Engineering Research & Development Centre, Ja-Ela, Sri Lanka
vidushianjana0@gmail.com

Abstract. Rice husk is one of the major byproducts of agriculture. This research is conducted to evaluate the feasibility of rice husk biochar (RHB) integrated concrete blocks and normal M30 grade concrete blocks through compressive strength test performance. RHB is used in this research as a supplementary cementitious material (SCM) in concrete blocks. The rice husk was pyrolyzed by burning in a muffle furnace with limited or no oxygen conditions under 700°C temperature. Blocks with the dimensions of 150mm×150mm×150mm were made according to the BS 1881-108 1983 standard. The RHB integrated blocks were made by replacing 1 wt.% of the weight of cement with RHB. Three RHB integrated blocks and three normal concrete blocks (as control blocks) were made. The concrete blocks were made using M30 Grade with a volume ratio of cement: sand: coarse aggregate, 1:1:2 accordingly, and the cement to water weight ratio was taken as 1:0.5. One of each control concrete block and RHB integrated concrete block were put into a water bath to cure for 7, 14 and 28 days accordingly. Then the compressive strength test was performed on each block. Although the compressive strengths of RHB integrated blocks were lower compared to normal concrete blocks, the compressive strength of 7, 14 and 28 days cured blocks had acceptable compressive strength above 30MPa.

Keywords: Supplementary cementitious material (SCM), Rice husk Biochar (RHB), Concrete blocks, Pyrolysis, Ordinary Portland Cement (OPC)

1 Introduction

Cement is considered a highly sought-after material in development and infrastructure due to its accessibility, reasonable price, and strength. According to research, the global cement production has reached approximately 4.28 billion tons [1]. Although it is found that

the cement industry directly represents 7-8% of the CO_2 emissions associated with human activities [2]. CO_2 is a major greenhouse gas (GHG) which contributes to climate change due to its ability to trap heat in Earth's atmosphere. Demand for cement is increasing due to economic growth, rapid industrialization, and urbanization in the world. Therefore, the cement industry is actively working to reduce its carbon footprint, aligning with the UN's sustainable development goals (SDGs), particularly SDG 12 (responsible consumption & production) and SDG 13 (Climate action), through various policies, regulations and initiatives focused on sustainability [3]. Therefore, complying with SDG 13 (Climate Action), the industry is acknowledged to decarbonize processes, including reducing CO_2 emissions per ton of cement by 30% by 2030 and to achieve net-zero emissions by 2050 according to the Global Cement and Concrete Association (GCCA) [4]. To mitigate this issue, several solutions have been suggested in the literature, such as the addition of biomass and waste materials, ashes to replace cement products and the development of alkali-activated materials to get rid of Portland cement in concrete and mortars. Cost-effective, sustainable solutions can be limited to the use of bio-based materials (as raw or ash) the main composition of mortar or concrete.

a. Biochar

Biochar is a unique carbon-neutral solution among bio-renewable materials has recently gained much attention in the construction field as a supplementary cementitious material (SCMs) for Portland cement as it can reduce CO_2 emissions from cement production [5]. Biochar is a carbon-rich, porous material which is produced by pyrolyzing agricultural waste residues (bagasse, corn husk, rice husk ash, etc.) using a muffle furnace under zero or reduced oxygen conditions. The qualities of the biochar, such as the yield, physico-chemical and microstructural properties, are dependent upon conditions of biochar production, which are;

- Temperature range
- Heating rate
- Residence time.

High temperature pyrolysis (500-700°C), Biochar undergoes thermal cracking, which releases volatiles from its pores and leaves behind a carbon skeleton [6]. Also, pyrolysis performed at a temperature higher than 500°C produces hydrophilic biochar due to the removal of labile aliphatic functional groups existing on the surface of biochar, resulting in the formation of high porosity [7].

There are two types of pyrolysis types that can be separated according to the heating rate they are slow pyrolysis and fast/flash pyrolysis. Slow pyrolysis, which is usually performed over several hours, is normally associated with higher yield of biochar and low

flammability of the produced char compared with fast and flash pyrolysis, which are typically performed over seconds [8].

b. Rice Husk Biochar

The annual production of rice is more than 750 million tons of rice grain, according to research conducted in 2024. Rice husk is a predominant agricultural waste residue generated by rice mills in rice-cultivating countries. The elemental composition of Rice husk has been tested in research using energy dispersive X-ray analysis and found to be include 9.55- 18.74% Carbon, 30.90 -35.51% Oxygen, 43.17-58.19% silica and 1.36-1.66% Potassium by weight. Also, in 2022 Chen found that rice husk comprises 25-33% cellulose, 25-31% lignin, 18-21% hemicellulose, 15% pentosans, and minerals with 16% silica compositions [9].

Rice husk biochar (RHB) is generated by pyrolyzing the rice husk using a muffle furnace at limited or zero oxygen conditions. RHB is found to consist of 87-97% silica in the form of non-crystalline or amorphous silica with small quantities of inorganic salts [10], [11]. The amorphous portion is a crucial factor in determining the contribution of a particular biochar in the pozzolanic reaction. Pozzolanic materials react with Calcium Hydroxide during cement hydration, which results in the formation of calcium silicate hydrate (C-S-H) gel, which is a key component responsible for the strength and cohesion of cementitious structures [12]. The amorphous nature of silica enhances the surface area and increases contact points, which facilitates the formation of C-S-H gel and promotes the densification of the material microstructure [13], [14].

According to ASTM 2019, a pozzolan must be a siliceous or aluminous material that reacts chemically with calcium hydroxide $Ca(OH)_2$ at ambient temperatures. Natural pozzolan should have a combined total of at least 70% silica (SiO_2), alumina (Al_2O_3), and iron oxide (Fe_2O_3), while the magnesium oxide (MgO) content should not exceed 5% [15]. RHB meets this requirement, because it has a combined total of SiO_2, Fe_2O_3 and Al_2O_3 greater than 70%. Therefore, RHB can be considered a good natural pozzolan that can be used to replace cement.

c. RHB as a Supplementary Cementitious Material

Due to pozzolanic properties and environmental benefit, RHB has gained attention as a potential SCM. Supplementary cementitious materials (SCMs) are materials that contribute to the hydration process and enhance the mechanical and durability properties of concrete.

The proximate analysis of rice husk biochar has shown an increased fixed carbon when the temperature was increased to 400°C to 700°C [16]. The amorphous nature of SiO_2

content in RHB at 450°C (33.50%) and 650°C (41.30%) shows higher potential for pozzolanic reactivity compared to crystalline silica [15], [17]. It was found that RHB at 700°C has the highest pozzolanic reactivity, resulting in the highest hydration degrees and highest compressive strength of RHB incorporated cement materials [18].

It was stated in [19] that Biochar pyrolyzed at 700°C had improved the compressive strength of the concrete sample more than that pyrolyzed at 500°C because of the high porosity and large surface area, which facilitates cement hydration. But in contrast, the research conducted by Gupta and Kua in 2018 highlights that the optimum temperature range highly depends on the biomass selection [19].

Incorporation of RHB as an SCM was found to be optimal within the range of 0.085 – 5 wt.%, which has resulted increased strength and enhancement of other properties, and also the same authors have stated that the addition of 1-2 wt.% RHB has significantly reduced water permeability compared to the control mortar, resulting in a 15-18% increase in strength of the cement mortar after 7,42, and 120 days [20]. The same authors also stated that 1 wt.% of RHB increased the hydration rate due to the high specific surface area and smaller particle size of the biochar compared to cement. Another study has reported that incorporating 1wt.% of RHB increased the compressive strength of concrete by 8.9% [21].

2 Methodology

According to the Literature review, the optimal temperature to produce RHB that was used as an SCM in this study was found to be 700°C, and the concrete mixture was determined to be made by replacing 1% of the weight of the ordinary Portland cement (OPC) with RHB.

a. Material preparation

Rice Husk was collected from a rice mill and pyrolyzed to produce RHB at 700°C at Sri Jayawardhanapura University of Sri Lanka. The pyrolyzing conditions are mentioned in Table 1.

Then produced RHB was granulated and sieved to a size between 0.063mm and 2mm. Ordinary Portland Cement (OPC) with SLS 107 has been purchased from a local hardware store. River sand (0.063mm – 2mm) was used as the fine aggregate for the concrete. In this research, 1 wt.% of OPC was replaced with RHB pyrolyzed at 700°C.

Then 10g of river sand was taken to an evaporating dish with a known mass and put into the oven at 105°C and kept for 24 hours. Next, the sample with the evaporating dish was taken out and kept inside a desiccator until it came to the room temperature. Next, it was weighed using an electronic balance. Then it was again put inside the oven at 105°C

for 2 hours and was taken out and weighed again. This process was repeated until the sample achieved a constant weight. The moisture content of the river sand was calculated as a percentage, and the amount of water was adjusted using the moisture content accordingly.

Table 1. Pyrolysis Conditions of RHB.

Pyrolysis Conditions	Example
Temperature (°C)	700
Residence Time (hour)	1
Temperature ramp (°C/minutes)	10
Oxygen condition	Low/ Zero

According to BS 1881-108:1983 standard, should incorporate coarse aggregates having a nominal maximum size not exceeding 40mm should be incorporated to build the concrete blocks of 150mm. Gravel was used as the coarse aggregate.

Standard concrete test cube moulds of 150mm×150mm×150mm size were taken from the Civil Engineering Department of the National Engineering Research and Development Centre.

b. Experimental Procedure

According to BS 1881-108:1983 standard, before assembly of the mould, the joints between the sides of the mould, between the sides of the mould and the base plate were thinly coated with oil and grease to prevent water loss. Then the mould was assembled in a manner where the sides of the mould were positively located, and the whole assembly was held rigidly together to prevent leakages from the mould (Fig. 1). The internal faces of the assembled mould were then thinly coated with release agent to prevent adhesion of concrete.

Fig. 1. Oil & grease applied (150×150×150mm) mould

The concrete mixture for 150mm test cubes was made by blending OPC, River sand, and RHB 1wt% from OPC according to the M30 grade volume and weight ratios. The

volume ratio between OPC cement, sand, coarse aggregate is 1:1:2 and cement-to-water weight ratio was taken as 1: 0.5. The moisture content of sand should be considered in determining the water amount needed to add to the mixture.

According to the standard, after mixing OPC, sand, RHB, and coarse aggregates, water was added and mixed well. Then the mixture was thoroughly mixed by shoveling it to form a cone on the sampling tray, and then it was turned over with a shovel to form a new cone. This was done three times. When forming the cones, each shovelful of material on the apex of the cone was deposited so that the portions that slides down the sides were distributed evenly, and the Centre of the cone was not displaced.

Fig. 2. Compacting each 50mm layer with a compact bar

Then the 150mm× 150mm × 150mm moulds were placed on a rig of horizontal surface rig and the concrete was filled in a way to remove entrapped air as much as possible. To produce full compaction of the concrete with neither excessive segregation nor laitance, the concrete was placed in layers of approximately 50mm deep and compacted each layer using a compact bar as shown in Fig. 2. Each layer was compacted with evenly distributed 25 strokes as mentioned in the BS 1881-108:1983 standard. After the top layer was compacted, leveled the top surface by using a mason trowel and the outside of the moulds were wiped to clean.

Three 150mm× 150mm × 150mm test cubes were made using this method (Fig. 3). Then the mould with the sample was kept to dry for 24 hours, and then after dried, it was named and transferred to a water bath to cure. One block is kept for 7 days, another for 14 days, and the last test cube for 28 days.

(a)

(b)

Fig. 3. (a) Dried RHB 1wt% integrated concrete blocks with mould; (b)Curing water bath.

The same steps that were used to develop the RHB integrated concrete blocks were followed to make the normal concrete block according to the standard of M30 grade concrete blocks without replacing 1% of the weight of cement with RHB.

Compressive strength test

After 7,14, and 28 days, each block was taken out of the water bath and kept until the water dried off. Then the weight of the test cube was measured the weight using an electronic balance. Next, the uniaxial compressive strength of the block was examined using the standard testing instrument (Compression Testing Machine: CTM) with a pace of 6.8 kN/s at the National Engineering Research & Development Centre (Fig. 4).

A few samples of each test cube cured for 7, 14 and 28 were collected and stored in a waterproof bag to test under a Scanning electron microscope (SEM) and a Transmission electron microscope (TEM).

Fig. 4. Compression Testing Machine (CTM)

3 Results and Discussion

Table 2. Compressive Force of Control Concrete Block and RHB 1% incorporated concrete block.

Curing Period	Compression Force (kN)	
	RHB 1% integrated Concrete Block	Control concrete blocks
7	916.5	1015.3
14	968.1	1035.5
28	814.11	1066.2

The 1 wt% RHB replaced test cubes and control test cubes built for M30 grade, which had been cured for 7, 14 and 28 days respectively were subjected to compressive strength test. Table 2 shows the results of the compressive force.

The compressive strength of the concrete blocks was calculated by dividing the compressive force by the area of one concrete cube (0.15m×0.15m). Table 3. shows the compressive strength according to the compression force in Table 2.

Table 3. Compressive strength of Control Concrete Block and RHB 1% incorporated concrete block.

Curing Period	Compressive Strength (MPa)	
	Control Concrete Block	RHB 1% integrated Concrete Block
7	45.12	40.73
14	46.02	43.03
28	47.39	36.18

Compressive strength of RHB incorporated samples is illustrated in Fig. 5. The graph shows that the compressive strength of Biochar incorporated blocks are less than the control concrete test cubes. The blocks are made in accordance with M30 grade. According to the standard, Concrete cubes of M30 grade should have a minimum compressive strength of 30 MPa. When comparing data of the compressive strength test, all compressive strengths were over 30MPa, which is the standard of the M30 grade concrete block. Compared to the RHB 1wt.% integrated block that was cured for 7 days was above 40 MPa, and the compressive strength had increased gradually. However, the compressive strength of the RHB 1wt.% integrated block that was cured for 28 days was decreased. According to research, there can be several reasons that cause this deviation. The three blocks were made by using 1 concrete mixture and therefore, RHB might not have been distributed equally through the mortar mixture. The microstructure analysis of the scanning electron microscope has shown that a homogenous matrix of the test concrete cube is important for the compressive strength, and strength changes could occur due to mechanical interlocking or altered crack patterns [22]. The porous nature of RHB has relatively low load-bearing capacity creating weak zones (like voids) in the concrete, which significantly reduce the mechanical strength of the hardened concrete. While the internal curing nature of RHB can promote cement hydration and increase the formation of hydration products, it is minimal compared to the weakening effect caused by the biochar [23].

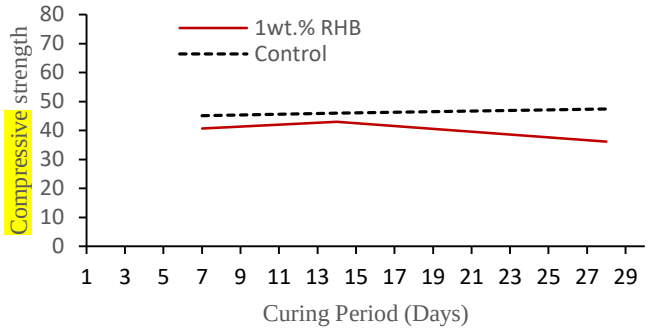

Fig. 5. Compressive strength of Control Concrete block and RHB 1% incorporated concrete block after 7,14 and 28 days of curing

In another research, it has been found that the lower envelope density of RHB, which is lower than cement and sand, results in an overall decrease in the density of the composites. Furthermore, the incorporation of biochar into Ultra-high-performance concrete (UHPC) matrix led to the generation of porosity surrounding its particles, resulting in a decrease in the density of UHPC composites [24].

This research could be further improved to achieve accuracy by building 3 blocks from both control and RHB 1wt% integrated concrete for each 7, 14, and 28 days of curing period. Once the research was done in this way, the random errors will be minimized.

4 Conclusions

This study investigated the potential of rice husk biochar (RHB) as a supplementary cementitious material for 150×150×150mm concrete blocks. Results have shown that concrete blocks with 1wt% of cement replaced with RHB has a compressive strength above 30MPa, which is acceptable for M30 grade concrete blocks. Although the compressive strength of RHB incorporated blocks cured for 7, 14 and 28 days were above 30MPa, the 28-day cured block had a lower compressive strength than the others. The research revealed this deviation might have occurred due to reasons such as significant inconsistencies in the reinforcement properties of RHB due to the unequal distribution throughout the matrix, high porosity, and low load-bearing strength of RHB. This research underscores the importance of homogeneity of matrix, and determining the optimum value of pyrolyzing temperature and weight percentage of specific biochar on material performance. These

inconsistencies could be avoided by using at least 3 samples from each block for curing days in future studies.

References

1. Y. Wang, M. Xu, X. Lv, Z. Wen, and C. Chen, The eco-efficiency evaluation in China's cement industry: A city-level study, Science the Total Environment, 865, p. 161132, Mar. 2023, doi: 10.1016/j.scitotenv.2022.161132.
2. B. Massoumi Nejad, S. Enferadi, and R. Andrew, A comprehensive analysis of process-related CO2 emissions from Iran's cement industry, Cleaner Environmental Systems, 16, p. 100251, Mar. 2025, doi: 10.1016/j.cesys.2024.100251.
3. X. Lin, W. Li, Y. Guo, W. Dong, A. Castel, and K. Wang, Biochar-cement concrete toward decarbonisation and sustainability for construction: Characteristic, performance and perspective, J Clean Prod, 419, p. 138219, Sep. 2023, doi: 10.1016/j.jclepro.2023.138219.
4. Global Cement and Concrete Association, Global Cement and Concrete Industry Announces Roadmap to Achieve Groundbreaking 'Net Zero' CO2 Emissions By 2050,
5. Z. Zhao, A. El-Naggar, J. Kau, C. Olson, D. Tomlinson, and S. X. Chang, Biochar affects compressive strength of Portland cement composites: a meta-analysis, Biochar, 6(1), p. 21, Mar. 2024, doi: 10.1007/s42773-024-00309-2.
6. F. Ronsse, S. van Hecke, D. Dickinson, and W. Prins, Production and characterization of slow pyrolysis biochar: influence of feedstock type and pyrolysis conditions, GCB Bioenergy, 5(2), pp. 104–115, Mar. 2013, doi: 10.1111/gcbb.12018.
7. R. Zornoza, F. Moreno-Barriga, J. A. Acosta, M. A. Muñoz, and A. Faz, Stability, nutrient availability and hydrophobicity of biochars derived from manure, crop residues, and municipal solid waste for their use as soil amendments, Chemosphere, 144, pp. 122–130, Feb. 2016, doi: 10.1016/j.chemosphere.2015.08.046.
8. M. Senath and H. Karunanayake, Feasibility of Utilizing Rice Husk Ash as a Reinforcement Material for Soil-Based Roofing Sheets, 2024.
9. R. S. Chen, S. Ahmad, S. Gan, and M. A. Tarawneh, High loading rice husk green composites: Dimensional stability, tensile behavior and prediction, and combustion properties, Journal of Thermoplastic Composite Materials, 33(7), pp. 882–897, Jul. 2020, doi: 10.1177/0892705718815536.
10. Y. Zhang et al., Comparison of the Physicochemical Characteristics of Bio-char Pyrolyzed from Moso Bamboo and Rice Husk with Different Pyrolysis Temperatures, Bioresources, 12(3), May 2017, doi: 10.15376/biores.12.3.4652-4669.

11. R. P. Jaya, M. A. A. Muhamad Nor, Z. A. Ahmad, and Z. Mohd Amin, Properties of mortar containing rice husk ash at different temperature and exposed to aggressive environment, Advanced Materials Research, 2013, pp. 87–93. doi: 10.4028/www.scientific.net/AMR.620.87.
12. K. H. Tan, T. Y. Wang, Z. H. Zhou, and Y. H. Qin, Biochar as a Partial Cement Replacement Material for Developing Sustainable Concrete: An Overview, Journal of Materials in Civil Engineering, 33(12), Dec. 2021, doi: 10.1061/(asce)mt.1943-5533.0003987.
13. K. H. Tan, T. Y. Wang, Z. H. Zhou, and Y. H. Qin, Biochar as a Partial Cement Replacement Material for Developing Sustainable Concrete: An Overview, Journal of Materials in Civil Engineering, 33(12), Dec. 2021, doi: 10.1061/(ASCE)MT.1943-5533.0003987.
14. J. G. S. P. P. Gunawardana, Development of Biochar-Reinforced Low-Cost Roofing Sheet Using Earth Soil & Cement, 2024.
15. N. Claoston, A. Samsuri, M. Ahmad Husni, and M. Mohd Amran, Effects of pyrolysis temperature on the physicochemical properties of empty fruit bunch and rice husk biochars, Waste Management & Research: The Journal for a Sustainable Circular Economy, 32(4), pp. 331–339, Apr. 2014, doi: 10.1177/0734242X14525822.
16. A. Uroić Štefanko and D. Leszczynska, Impact of Biomass Source and Pyrolysis Parameters on Physicochemical Properties of Biochar Manufactured for Innovative Applications, Front Energy Res, 8, Jul. 2020, doi: 10.3389/fenrg.2020.00138.
17. T. M. Myint and N. Tuntiwiwattanapun, Evaluation of pozzolanic activity in rice husk biochar and ash activated by ball milling for enhanced cement-based composites, IOP Conf Ser Earth Environ Sci, 1500(1), p. 012081, May 2025, doi: 10.1088/1755-1315/1500/1/012081.
18. G. Huang et al., Upcycling rice husk biochar into carbon-negative composites, Constr Build Mater, 470, p. 140459, Apr. 2025, doi: 10.1016/j.conbuildmat.2025.140459.
19. S. Gupta and H. W. Kua, Effect of water entrainment by pre-soaked biochar particles on strength and permeability of cement mortar, Constr Build Mater, 159, pp. 107–125, Jan. 2018, doi: 10.1016/j.conbuildmat.2017.10.095.
20. A. M. N. Aman, A. Selvarajoo, T. L. Lau, and W. H. Chen, Biochar as Cement Replacement to Enhance Concrete Composite Properties: A Review, Oct. 01, 2022, MDPI. doi: 10.3390/en15207662.
21. L. Wang et al., Biochar as green additives in cement-based composites with carbon dioxide curing, J Clean Prod, 258, p. 120678, Jun. 2020, doi: 10.1016/j.jclepro.2020.120678.
22. A. Alagesan, V. B. Raju, M. Veerapathran, and P. Arunachalam, Investigation the effects of adding biochar to concrete mixture experimentally on performance properties, Matéria (Rio de Janeiro), 30, 2025, doi: 10.1590/1517-7076-rmat-2024-0965.
23. D. Wang, A. Jantwal, E. Kaynak, G. Sas, and O. Das, Promoting internal curing in concrete by replacing sand with sustainable biochar, Case Studies in Construction Materials, 22, p. e04542, Jul. 2025, doi: 10.1016/j.cscm.2025.e04542.

24. Q. Zhang et al., Investigation of the macro performance and mechanism of biochar modified ultra-high performance concrete, Case Studies in Construction Materials, 21, p. e03595, Dec. 2024, doi: 10.1016/j.cscm.2024.e03595.

Fundamental Study of the Magnetic Fields Applied for Efficient Rotor Drone Thrust Selection

P. F. S. Perera

National Engineering Research and Development Centre, Jaela, Sri Lanka

Abstract:
Energy-efficient design has become a priority research area in drone technology, with motor and aero foil selection playing a critical role in optimizing performance. This study develops a simulation-based framework that integrates magnetic field analysis and aerodynamic modelling to improve rotor drone efficiency. The primary research problem addressed is the need for aero foil pilot testing under real environmental conditions to identify the most suitable aero foil type for drones. Secondary and dependent problems, such as pilot test selection, test machine design, power supply, and payload capacity, are also considered. The methodology involves three key stages: (i) applying magnetism fundamentals to develop a complex magnetic field simulator for motor efficiency analysis, (ii) conducting aerodynamic simulations and benchmarking thrust performance across different aero foil designs, and (iii) integrating simulation results with pilot tests to validate drone performance. The outcomes enabled the selection of a high-efficiency motor–aero foil configuration. A prototype drone was subsequently developed and tested for coconut plucking applications, demonstrating the practical viability of combining magnetic and aerodynamic simulations for energy-efficient drone design.

Keywords—drone motor, magnetic field simulator, aerodynamics, energy-efficient UAV, coconut harvesting

1 Introduction

Motor Selection for Drone Applications with Coconut Plucking Device

As a practical application, this study also considers the development of a coconut-plucking device. Traditionally, coconut harvesting is carried out using labour-intensive methods that consume significant time, energy, and manpower. The proposed device leverages optimized drone motor technology to assist in plucking coconuts efficiently. Such a system

can reduce health risks, save money and time, conserve energy, and improve overall productivity. From an industrial perspective, this approach offers a scalable and systematic solution that can enhance economic outcomes and promote sustainable agricultural practices.

2 Literature Review

a. Problem Analysis

The primary problem is the design of an efficient rotor drone for harvesting coconuts, aiming to select the most suitable type of drone under real environmental conditions. Secondary problems include evaluating design types, identifying current drawbacks, and selecting appropriate methods. Dependent problems involve deeper ethical considerations related to implementation.

Magnetism

Magnetism was first observed in ancient times with lodestones—naturally magnetized pieces of magnetite—that could attract iron. The first scientific discussion is attributed to Thales of Miletus (c. 625–545 BCE), and by 1187, Alexander Neckam described the compass in Europe. Significant advances followed: Niccolò Cabeo (1629) expanded earlier studies, Ørsted, Biot, and Savart (1819–1820) explored the link between electricity and magnetism, and André-Marie Ampère analyzed forces between current loops. Faraday (1831) discovered that a changing magnetic flux induces voltage, and Gauss, Weber, and Maxwell (1861) formalized electromagnetism, later applied by Einstein in 1905.

Magnetism is central in engineering, with applications in motors, relays, transistors, and more. In drones, Brushless DC (BLDC) motors are widely used for their efficiency and reliability. Selecting the optimal motor is complex due to interactions between magnetic fields and aerodynamic forces, making the study of both essential for energy-efficient drone design.

Aerodynamics

Aerodynamics is the study of air motion, particularly when interacting with solid objects such as airplane wings. Fundamental concepts of continuum, drag, and pressure gradients date back to Aristotle and Archimedes. In 1726, Sir Isaac Newton developed the first theory of air resistance, followed by Daniel Bernoulli's *Hydrodynamica* (1738). Leonhard Euler (1757) published the general Euler equations for compressible and incompressible flows, later extended to include viscosity, resulting in the Navier–Stokes equations. In 1799, Sir George Cayley identified the four aerodynamic forces of flight. Francis Herbert Wenham constructed the first wind tunnel in 1871, allowing precise measurement of aerodynamic forces. Drag theories were developed by Jean le Rond d'Alembert, Gustav

Kirchhoff, and Lord Rayleigh. Charles Renard (1889) predicted the power required for sustained flight. Otto Lilienthal achieved successful glider flights, and the Wright brothers conducted the first powered flight in 1903. Frederick W. Lanchester, Martin Kutta, and Nikolai Zhukovsky independently developed theories connecting fluid circulation to lift.

3 Study Objectives

3.1. The main objectives of this project are, introduce a SMART agricultural mechanism for safe and efficient coconut plucking. Develop and implement an automated control system for the plucking process. Reduce labor dependency and improve operational visibility, addressing challenges of traditional harvesting. Conduct laboratory testing to identify potential failures, implement improvements, and finalize an optimized system.

3.2. Sub-objectives for this sub-study include:

- Develop a high-efficiency motor.
- Develop an empirical estimation tool to measure magnetic fields (currently using iron dust tests), aerodynamics, and buoyancy.
- Explore philosophical and parametric analyses of magnetism, aerodynamics, and thrust, justifying the validity of complex particle interactions in relation to ontology and near-shape functions.

4 Methodology:

In this project, the literature review focuses on fixtures suitable for agricultural harvesting and available. The research involves designing and developing a machine, selecting and applying appropriate motors, and creating a high-efficiency motor. The study also includes deep metaphysical modeling of magnetism and the development of empirical and conceptual frameworks for magnetic systems. A simulator will be created and tested under actual operating conditions to analyze forces in complex magnets and evaluate drone motor efficiency. Aerodynamic simulations will also be conducted to benchmark thrust and optimize the propulsion mechanism. The device is intended for industrial coconut harvesting, where it can reduce energy consumption, costs, time, and health risks compared to manual plucking.

Magnetism Fundamentals:

- Magnetism is the force exerted by magnets when they attract or repel each other.
- The motion of electric charges generates magnetism.

- Every atom contains electrons, whose movement generates electric currents and causes each electron to act like a microscopic magnet.
- In most substances, equal numbers of electrons spin in opposite directions, canceling out magnetism.
- In substances such as iron, cobalt, and nickel, most electrons spin in the same direction, making the atoms strongly magnetic, though not yet permanent magnets.

a. Conceptual frame analysis for simulators

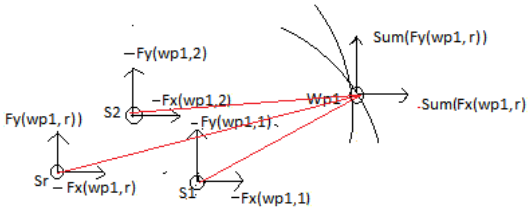

Fig. 1. Gauss and Reaction forces graphical analysis

Let,

Particle Sr force on the particle Wp1 $=$ $F1,r$; $Fr,1$ is a force vector on WP1 by Sr

Then Net force on the particle WP1 by whole particles Sr $=$ Sum($F1,r$)

$F1,r = Fx(wp1,r)\ i + Fy(wp1,r)\ j + Fz(wp1,r)\ k$

$Fr = \text{Sum}(Fx(wp1,r)\ i + Fy(wp1,r)\ j + Fz(wp1,r)\ k)$

F1,r=f(L ,m1, m2, uo) ;

L = distance between particle ; m1,m2 strength of particles ; uo space coefficient of relativity

m1 strength can be electrical or inertia or magnetic or other particle that have reactions force on m2 same or different particle.

5 Results

a. Preliminary and Pilot research of the appropriate motor for the drone. For a Coconut plucking drone effective motor selection pilot test.

Magnetism Fundamentals:

- Magnetism is the force exerted by magnets when they attract or repel each other.

- The motion of electric charges generates magnetism.
- Every substance is made up of atoms, each containing electrons that carry electric charges.
- The movement of electrons generates electric currents, causing each electron to act like a microscopic magnet.
- In most substances, equal numbers of electrons spin in opposite directions, canceling out their magnetism.
- In substances such as iron, cobalt, and nickel, most electrons spin in the same direction, making the atoms strongly magnetic, though they are not yet permanent magnets.

Considering these fundamentals, a simulator was developed to analyze forces in complex magnetic systems, allowing for detailed evaluation of drone motor efficiency. An aerodynamic simulator was also created to benchmark thrust and optimize the propulsion mechanism. Using these analyses, a high-energy-efficient drone was selected and implemented for coconut plucking.

b. **Pilot Magnetic motor test**

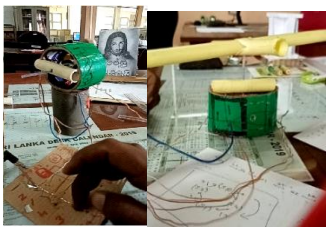

Fig. 2. Actual pilot test of the second BLDC Motor for rotor drone to high efficient (Preliminary study)

Fig. 2 shows the pilot-made motor at the NERD Centre, constructed using a copper coil, two permanent magnets, and cardboards (Picture 1). A 12V DC PWM power supply was applied to each coil, and the resulting movements were observed. After identifying the pattern for full rotation, a helicopter blade made of PVC was attached to the motor and tested for functionality.

c. Simulator development for magnetisms

To observe the magnetic field, a recently used tool involves spreading iron dust on a surface perpendicular to the field. However, no proper empirical methods exist for analyzing groups of magnetically induced solids. Magnetic fields are not linear across a surface, unlike light. This may be due to the need for sensory transformation to perceive magnetic

fields. Additionally, magnetic fields depend on ontological and spontaneous axiological dimensions, so near-shape dimensions must be estimated. This arises from the justified law of electron rate of change extended to magnetism measurements, with highly complex mathematical algorithms required to explain the observed coherencies. After a detailed study, the magnets and fields were analyzed using advanced calculations, and a simulator was developed to model the magnetic fields. In this simulator, magnets were considered as individual particles, with flux assigned to each particle. Complex curves were generated using the coordinates and flux at each point. To calculate forces and moments for other complex curves, the effects of each particle were taken into account. Figure 3 shows the coordinates, flux strength, and results represented in graphs. In these graphs, the components (Fx, Fy) were calculated and plotted at each point to scale.

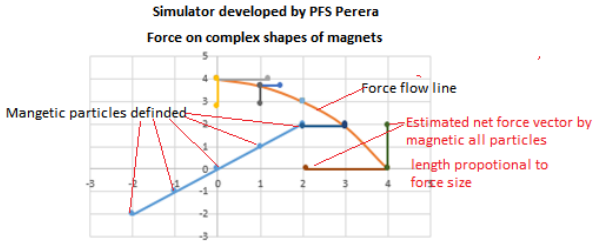

Fig. 3. One image of complex magnets curves simulator for force estimates

d. Actual benchmark of the simulator of excel by magnets and iron dust.

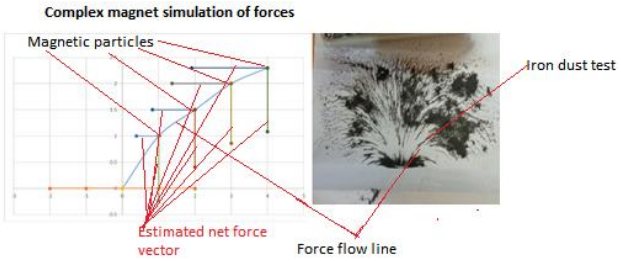

Fig. 4. One magnet field in flat surface simulation benchmark with the actual for force estimates

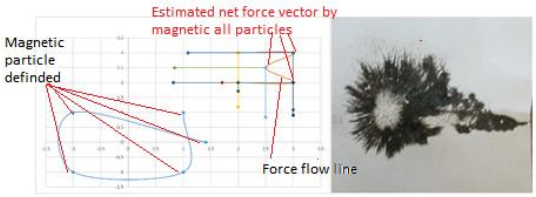

Fig. 5. Two magnet fields in flat surface simulation benchmark with the actual for estimates

Fig. 4 shows the actual test of a magnet using iron rust to visualize the field. A cylindrical magnet was placed tangent to a paper surface, and its magnetic field was observed. In the simulator, forces along two paths were calculated by placing a single magnetic particle, and the results were compared with near values on the graph.

Fig. 5 shows similar simulations performed with two cylindrical magnets. One magnet's flat surface was placed on the paper, while the other's rounded surface was placed on the paper surface. Using the concept of magnetic particles, the forces between the magnets were analyzed and benchmarked against the actual experimental results.

6 Further developed Simulations of the drone motor made at NERD Centre

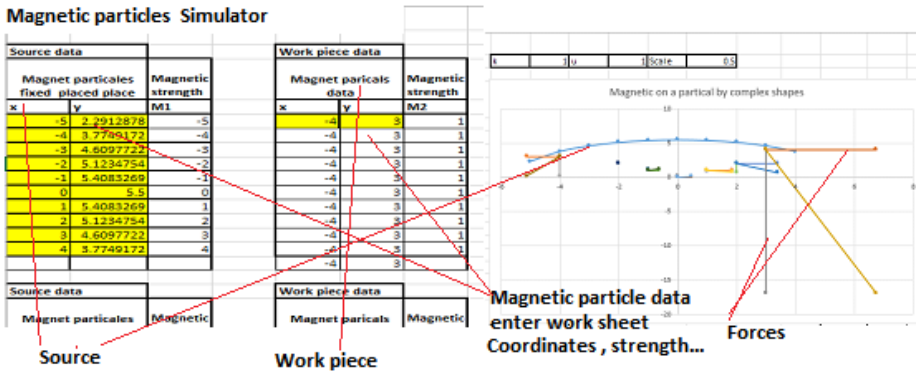

Fig. 6. Magnets simulator further developed.(Top left magnetic particles data and coordinates to enter and the right estimated force required points with magnetic strength). Bottom graph visual show of the values to scale

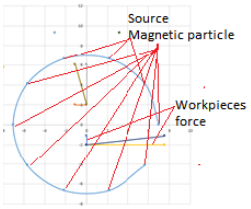

Fig. 7. Simulation of the magnetism made for forces estimates.

Fig. 6 indicates the calculated forces along with the resultant force. The calculations were performed using Excel, utilizing its mathematical, graphical, and modular capabilities. The results show that when magnetic particles are close to each other, the force is very high, regardless of the magnetic moment.

After developing the simulator, the motor shapes and magnet rotor were simulated and their values verified. The appropriate positions for placing the coils were then identified. Fig. 7 shows the motor simulations corresponding to the motor shown in Fig. 2.

7 Aero dynamics forces

a. Simulator tested by Excel worksheet.

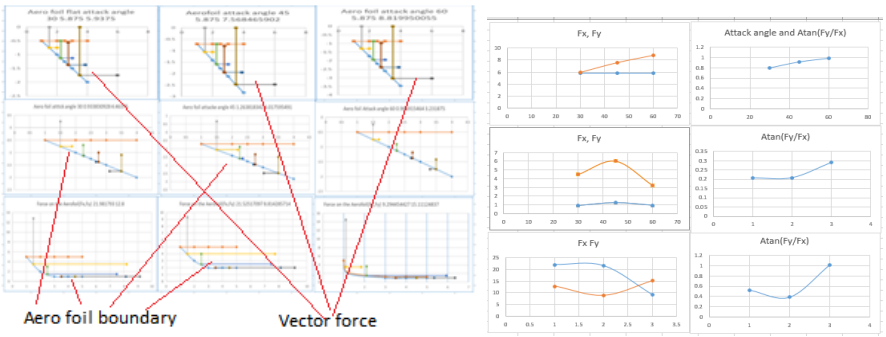

Fig. 8. Estimate of the aero foil for the drone by excel simulator made

The Excel sheet was used to obtain near values for different shapes, similar to the magnetic simulations. Fig. 8 shows the aerodynamic forces acting under constant airflow. In the first series, a flat surface was angled at 30°, 45°, and 60°. A similar procedure was followed for the second series. The third series involved a complex aero foil, showing the forces

acting on the complex surfaces. It is clear that the third row, third column configuration produces the highest lift. From Fig. 8, it can be observed that as the attack angle increases, both Fx and Fy increase with the aerofoil length. Using the arctangent of (Fy/Fx) versus the attack angle, it can be concluded that the ratio of forces along Fy increases with increasing attack angle. These calculations were simulated for a wind speed of 10 m/s.For the simulations, the wing length was set to 2.5 cm and the width to 2 cm. The graph corresponding to the maximum force shape was used to determine the optimal aerodynamic configuration. Per length the lift force on the wing = 1511 N,Per length the drag force on the wing = 929 N,Therefore, by the force analysis it is clear that,

$$Power\ need\ at\ the\ 10ms^{-1}\ speed\ per\ length\ =\ 929*10W\ =\ 9.29kW$$

$$Per\ 2.5cmx2cm\ blade\ power\ need\ at\ 10ms^{-1}\ speed = 929*10*\frac{2}{100}\ W$$

$$= 185.8\ W$$

By the graph, it is clear that under the uniform conditions force on the wings were constant. Ratio between the Fy/Fx = 1.626.

So the power need to lift the 2.5cm x 2 cm wings are without load at 10ms-1 = Fx*10 = 929*0.025*10 = 235.2W

Also, at this speed the total load can take 151.1 kg
So the motor types, Let the Motor coil properties as below,
Coil turns=N1, Wire dimeter=d1, Coil length= l1, Coil width=b1
Then;

$$V1 = I1*R1 = I1*pi*2*N*\frac{l1+b1}{\frac{d1^4}{4}}\ \text{---(1)}$$

$$I1 = V1/(\ pi*2*N*\frac{l1+b1}{\frac{d1^4}{4}})\text{---(2)}$$

$$B1 = U*\frac{I1}{2*pi*r1}\ \text{----(3)}$$

$$C1 = B1*I1*N1*A1*sin(a1)\ \text{-----(4)}$$

b. For a rubber balloon

The flying time of a rubber balloon was checked using a YouTube video as a reference. It was observed that under normal conditions, a rubber balloon could fly for approximately nine seconds when an additional paper cup weight was attached.

Fig. 9. H_2 balloon trust increase and energy efficiency increase methods [2]

This implies that without any battery power but only compressed air some materials can float in the air.

Inside pressure = Outside pressure + Rubber surface pressure

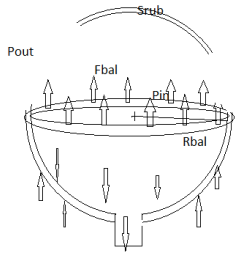

Fig. 10. Force analysis of the floating balloon strength

$$Fbal = Pout * Abalout - Pin * Ain \quad ----(5)$$

$$\frac{Fbal}{Abalout-Abalin} = \frac{Pout*Abalout-Pin-Abalin}{Abalout-Abalin} \quad ---(6)$$

$$Sbal = \frac{Pout * Abalout - Pin - Abalin}{Abalout - Abalin}$$

$$Fbal = k * Dx; \quad ---(7)$$

$$k * Dx = Pout * Abalout - Pin * Abalin \quad ---(8)$$

$$Pin = \frac{Pout*Abalout-k*Dx}{Abalin} \quad ---(9)$$

By the B'nule theory,

$$Pout + 0.5 * Dair * U^2 = Pin + Dh * Dair * g \quad --(10)$$

$$U = sqrt\left(\frac{Pout - Pin}{.5 * Dair}\right) \quad ----(11)$$

$$Moment\ change\ of\ the\ air\ inside = \frac{d(mv)}{dt} \quad --(12)$$

$$\frac{d(mv)}{dt} = Dair * Aoutmouth * (V^2 + x * a) --- (13)$$

So;

$$Balloon\ lift\ force\ by\ mouth = Dair * Aoutmouth * U^2 \quad --- (14)$$

$$Balloon\ lift\ force\ by\ mouth = Aoutmouth * \left(Pout * \left(1 - \frac{Abalout}{Abalin}\right) + k * \frac{Dx}{Abalin}\right) - - - (15)$$

$$Balloon\ power\ out = \frac{d(PV)}{dt} = \frac{(\frac{2}{3} * d(Pout * pi * \frac{Dbalout^2}{4} - k * Dx) * Dbalin)}{dt} \quad ----(16)$$

8 Excel Simulator for H_2 balloon lift estimates.

D mouth	0.002	m					
Amouth	0.001570796	m^2					
Pout	1000000	Pa					
Young modulas of the rub	10000000	Pa					
E=S/e=F/A/(dx/L)=FL/A/dx							
F=kdx							
E=kdxL/A/dx=kL/A							
A=2*pi()*r*t	1.5708E-05	m^2	r0 bal	0.025	m		
L0	0.1	m	to bal	0.0001	m		
k=EA/L	1570.796327						
Abal out	0.020106193	m2	Dbal out	0.16	m		
Abal in	0.020106168	m2	Dbal in	0.1599999	m	k1	0.001
Dx bal	0.1	m					
F lift	12.26989815	N	1.226989815	kg			

Balloon power out= (2/3)*d(Pout*pi()*Dbalout^2/4-k*Dx)*Dbalin)/dt			
per second energy need	2135.194418	J	

By the balloon forces analysis, excel calculations were done to find the energy consumption of the balloon to lift with the assumed values of the balloon shown.

Benchmark of the Positive displacement pumps and axial pump for drone lift.

Table 1. benchmark of the Pump efficiencies [3].

Pump Type	Overall Efficiency %
External gear	85
Internal gear	90
Vane	85
Radial piston	90
Bent axis piston	92
Axial piston	91

a. Positive displacement pump formulae

$$\text{Energy in} = (\text{Work done on the piston})$$
$$= (\&\text{Piston Friction loss}) + (\text{Internal energy rise in the air})$$

$$\text{Energy on air} = \text{Air kinetic energy increase}$$
$$\text{Energy efficiency} = \frac{\text{Air Kinetic energy increase}}{\text{Piston mechanical loss} + \text{Internal energy rise in the air}}$$
$$= 1 - \frac{\text{Mechancial losses}}{\text{Work done on the piston}}$$
$$\text{Mechanical losses} = (\text{Friction by piston}) + (\text{Friction by shafts}) + (\text{Friction by the air heat})$$

b. Axial pump

$$\text{Energy in} = \text{Work done on the blade}$$
$$= \text{Kinetic increase of the air} + \text{Internal energy increase in the air} + \text{mechanical losses}$$
$$\text{Energy on air} = (\text{Kinetic increase of the air} + \text{Internal energy increase in the air} + \text{Mechanical losses})$$
$$= 1 - \text{Mechcnial losses/Work done on the blades.}$$
$$\text{Mechanical losses} = \text{Blade drag Losses} + \text{shaft losses}$$

9 Discussion

From the magnetic study, it is clear that this simulator effectively models complex magnetic curves in practical cases, assisting in the selection of low-energy, efficient devices for rotor drones. It also aids in determining optimal magnet placement in motors and the design of other complex magnetic devices. Regarding energy efficiency, piston pumps are observed to be more efficient for drones due to the absence of mechanical losses in the flow. From the aerofoil design analysis, it is evident that lifting a payload of at least 5 kg requires the motor blade speed to satisfy Fy/Fx > 1. For example, if Fy/Fx = 1, Fx would need to be 5 kg. However, drag losses are present in aerofoil blades. Using compressor-type blades can eliminate these drag losses, implying that compressed air systems provide higher efficiency and longer flight times.

Overall, rotor blade-type drones consume more energy due to two main factors: energy losses in the motor and energy losses due to aerodynamic drag forces. The simulations show that drag and lift cannot be entirely eliminated for any blade shape due to air-material

interactions. However, for continuous operation, axial pumps in superheated airflow regions may improve efficiency by optimizing the drag coefficient.

10 Conclusions

From the magnetic study, it is evident that the simulator effectively models complex magnetic curves in practical scenarios, assisting in the selection of low-energy, efficient devices for rotor drones. It also helps determine optimal magnet placement in motors and guides the design of other complex magnetic devices. Regarding energy efficiency, piston pumps are observed to be more effective for drones due to the absence of mechanical losses in the flow. From the aero foil design analysis, it is clear that lifting a payload of at least 5 kg requires the motor blade speed to satisfy $Fy/Fx > 1$. For instance, if $Fy/Fx = 1$, Fx would need to be 5 kg. However, drag losses are present in aerofoil blades. Using compressor-type blades can mitigate these drag losses, suggesting that compressed air systems provide higher efficiency and longer flight times. Overall, rotor blade-type drones consume more energy due to two main factors: energy losses in the motor and energy losses caused by aerodynamic drag forces. The simulations indicate that drag and lift cannot be entirely eliminated for any blade shape due to air-material interactions. However, for continuous operation, axial pumps operating in superheated airflow regions may improve efficiency by optimizing the drag coefficient.

References

1. Anon., 2021. Magnetism. [online] Available at: https://en.wikipedia.org/wiki/Magnetism [Accessed 25 April 2021].
2. T. K. Art, 2021. Paper cup balloon helicopter, balloon plane, how to make flying balloon cup plane, amazing fly, new. [online] Available at: https://www.youtube.com/watch?v=ArVCQ-rsr2k [Accessed 15 February 2021].
3. B. Casey, 2021. Hydraulic pumps and motors: Considering efficiency. [online] Available at: https://www.machinerylubrication.com/Read/28430/hydraulic-pump-motors-maintenance [Accessed 2021].
4. W. Brookes, The effect of aerofoil design on aircraft performance, Faculty of Aerospace Engineering at the University of Sheffield, 2022.
5. K. Setty, T. van Niekerk and R. Stopforth, SPIBOT: Drone-tethered mobile gripper for autonomous object retrieval in dynamic environments. Procedia CIRP, 91, pp.486–488, 2020.

6. T. Yoshida, Y. Onishi, T. Kawahara & T. Fukao, Automated harvesting by a dual-arm fruit harvesting robot, Robomech Journal, 9, 19 (2022). https://doi.org/10.1186/s40648-022-00233-9

7. Y. Xu, M. Lv, Q. Xu and R. Xu, Gripper mechanism for fruit picking, Actuators, 13(9), 338, 2024. https://doi.org/10.3390/act13090338.

8. K. E. T. Giljarhus, A. Porcarelli and J. Apeland**,** Investigation of rotor efficiency with varying rotor pitch angle for a coaxial drone. Drones, 6(4), p.91, 2022. https://doi.org/10.3390/drones6040091 [Accessed 26 August 2025].

9. **A.** Bondyra, S. Gardecki, P. Gąsior, W. Giernacki, Performance of Coaxial Propulsion in Design of Multi-rotor UAVs. In: Szewczyk, R., Zieliński, C., Kaliczyńska, M. (eds) Challenges in Automation, Robotics and Measurement Techniques. ICA 2016. Advances in Intelligent Systems and Computing, 440. Springer, Cham, 2016. https://doi.org/10.1007/978-3-319-29357-8_46

10. S. Hoang, L. Marsh, A. Aliseda and I. Y. Shen, Analysis of high fidelity modeling of drone dynamics and aerodynamics for reduced energy consumption. In: ASME 2020 International Design Engineering Technical Conferences and Computers and Information in Engineering Conference, 2020. https://doi.org/10.1115/DETC2020-22481

11. P. Candeloro, D. Ragni and T. Pagliaroli**,** Small-scale rotor aeroacoustics for drone propulsion: A review of noise sources and control strategies. Fluids, 7(8), 279, 2022, https://doi.org/10.3390/fluids7080279

12. ANSI, 2024. *Gaps progress report available: ANSI UASSC*. [online] Available at: https://www.ansi.org/standards-news/all-news/3-20-24-gaps-progress-report-available-ansi-uassc [Accessed 26 August 2025].

13. Wikipedia, 2025. *Inertia*. [online] Available at: https://en.wikipedia.org/wiki/Inertia [Accessed 26 August 2025].

14. M. Hampson, 2020. Amaran the tree-climbing robot can safely harvest coconuts: The robot could one day reduce the need for humans to take on the risky job of climbing coconut trees. Available at: https://spectrum.ieee.org/amazon-ai-robotics [Accessed 26 August 2025].

15. A. Abraham, 2016. *Advanced remote-controlled coconut harvesting robot*. [online] 15 March. Sharjah, United Arab Emirates. Available at: https://contest.techbriefs.com/2016/entries/machinery-automation-robotics/6311-0315-104233-advanced-remote-controlled-coconut-harvesting-robot [Accessed 26 August 2025].

16. A. Dubey, S. M. Pattnaik, A. Banerjee and S. R. Kumar, Autonomous control and implementation of coconut tree climbing and harvesting robot. Procedia Computer Science, 85, pp.755–766, 2016. https://doi.org/10.1016/j.procs.2016.05.263 [Accessed 26 August 2025].

17. Wikipedia, 2025. *Energy storage*. [online] Available at: https://en.wikipedia.org/wiki/Energy_storage [Accessed 26 August 2025].
18. YouTube, 2019. *How to run salt water power car*. [video online] 10 April. Available at: https://www.youtube.com/watch?v=fUtDfb19itQ [Accessed 26 August 2025].
19. Wikipedia, 2025. *Electric motor*. [online] Available at: https://en.wikipedia.org/wiki/Electric_motor#:~:text=Before%20modern%20electromagnetic%20motors%2C%20experimental,now%20known%20by%20his%20name [Accessed 26 August 2025].

3rd International Engineering Research Symposium 2025 (IERS 2025)
Colombo, Sri Lanka

Predicting Snakebite Species Using Patient Clinical Data in Sri Lanka: A Machine Learning Approach

M. H. Mihiranga[1], R. L. W. Koggalage[1], N. K. A. Silva[2], B. Hettige[1]

[1]General Sir John Kotelawala Defence University, Sri Lanka
[2]Faculty of Medicine and Allied Sciences, Rajarata University, Sri Lanka
39-bce-0014@kdu.ac.lk, koggalage@kdu.ac.lk, anjana@med.rjt.ac.lk, budditha@kdu.ac.lk

Abstract. In Sri Lanka, snakebite envenomation poses a serious risk to public health, leading to more than 30,000 hospital admissions each year. However, in areas with limited resources, doctors often struggle to determine the species of snake based on bite site and patient history; incorrect identification can result in the use of antivenom incorrectly, which can have negative effects and waste important antivenom resources. This study addresses this problem by developing a hybrid artificial intelligence model based on text-based clinical data for accurate snakebite species classification, with a plan to combine image-based bite site analysis in future work. Anuradhapura Hospital and the Rajarata Medical Faculty provided data on patient demographics, bite location and context, and bite side images. We trained a machine learning classifier on the structured text features, with the image-based model remaining in development for future integration. The accuracy, F1-score, and preliminary validation on actual clinical cases were used to assess the performance of the text-based model. This is the first snakebite identification system in Sri Lanka that utilizes clinical metadata with planned expansion to include bite-side images. It is also available as a smartphone app that may be used in emergency situations. The results show enhanced clinical responses, reduced needless antivenom administration, and better diagnostic accuracy in identifying envenoming species. This approach has an opportunity to improve snakebite management in rural hospitals and is scalable for global implementation in other snakebite-endemic regions.

Keywords: Snakebite Envenomation, Hybrid AI Model, Machine Learning in Healthcare

1 Introduction

In many tropical countries, snakebite envenomation is a serious but often neglected public health concern. According to the World Health Organization (WHO), snakebite envenomation is a neglected tropical disease that causes thousands of deaths and permanent disabilities in millions of survivors each year [1]. The largest risk occurs in rural areas, especially for agricultural workers, who frequently come into engage with venomous snakes. Sri Lanka reports tens of thousands of snakebite cases annually, making it one of the countries that is most affected. In Sri Lanka, for instance, between 2004 and 2014, there were between 35,000 and 40,000 snakebite cases annually, with an average of 100 deaths [2]. Considering underreporting and rural cases that never make it to hospitals, epidemiological studies suggest that the true deaths may be even higher, reaching an estimated 400 deaths annually. The incidence of snakebite is high in all of Sri Lanka's provinces; a community-based study found that 695 bites (323 with envenomation) occurred in a sample of about 165,000 individuals over a period of a year. Given its extremely high incidence rate, snakebite envenomation is still a major public health issue in Sri Lanka. For the most effective therapy, especially the use of antivenom, prompt identification of the snake species is essential.

a. Statement of the problem

There is currently no reliable method in Sri Lanka for correctly identifying the snake species from the bite alone, despite the serious medical concerns. Doctors feel obligated to make informed predictions based on patient history and bite mark appearance, both of which can be highly inaccurate. Many misdiagnoses result from the lack of a sufficient classification system for snakebite. Incorrect diagnosis can lead to incorrect or delayed treatment; for instance, giving antivenom for a Ceylon krait bite when it has minimal effect might waste money and have negative side effects. On the other hand, it can be deadly to not administer antivenom when it is required because one underestimates the severity of the bite or mistakes it for a non-venomous species. In rural and resource-limited environments, where medical staff might not have much experience with rare snake species and may not have access to specialized consultation, the diagnostic confusion is increased. Snakebite envenomation is still a neglected clinical problem in Sri Lanka. Early and accurate identification of the snake is critical for health outcomes, but current manual identification methods are frequently insufficient. A major problem is the gap between the instruments available to primary healthcare workers and the requirement for accurate snake identification. Without treatment, patients will still be at higher risk of antivenom toxicity, preventable complications, and even death due to snakebite mismanagement. To improve

clinical decision-making in snakebite patients, a more reliable, data-driven solution is essential.

b. Aim

To improve diagnostic accuracy and guide suitable treatment in Sri Lanka by developing a hybrid AI-powered system that accurately identifies the species of snake using clinical data, with the long-term goal of extending the system to incorporate bite site image analysis.

c. Objectives

- To accurately identify snake species by classifying antivenom-indicated, non-venomous, and hump-nosed vipers' bite patterns.
- To use parametric data to identify relationships between snake species and clinical circumstances.
- To construct a real, structured dataset for model training and validation using actual patient records.
- To develop a machine learning model that classifies snake species based on clinical features.
- To develop a hybrid framework for that are integration of bite site image analysis within the system.
- To improve species prediction for bites which are indicated by antivenom using cosine similarity on clinical features as future integration.

This study presents a text-based machine learning model that uses patients' clinical data to identify snakebite species, with a roadmap for future incorporation of bite site image analysis to create a hybrid system. In Section 2, related works are reviewed. Section 3 covers the proposed solution. Results are presented and discussed in Section 4. Section 5 summarizes the main conclusion and includes future works.

2 Literature Review

2.1 Global and Regional Burden of Snakebite Envenomation

Each year, hundreds of thousands of people are envenomated by snakebite envenomation, which causes an enormous number of deaths for several million people globally. This public health problem has the greatest impact in South Asia and sub-Saharan Africa. With tens of thousands of cases reported each year and significant death rates in endemic areas, India is a prominent example of a country in South Asia where snakebites cause a serious health risk [3][4]. In India, epidemiological studies have identified high-risk areas and highlighted the role of farming techniques, population density, and climate in influencing the incidence of snakebite. For instance, snakebite death rates are high in some Indian states, with annual incidence rates exceeding 30 per 100,000 people [3]. The uneven distribution of snakebite burden and the necessity of focused preventative measures in hotspots are shown by this geographical information [4] [5]. Therefore, a significant amount of the world's snakebite deaths occurs in South Asian nations like India and Sri Lanka, highlighting the urgent need for better management and control techniques in these areas.

2.2 Epidemiology and Clinical Challenges in Sri Lanka

Approximately 40,000 snakebite cases and 400 snakebite deaths are reported annually in Sri Lanka, which makes it one of the countries with the highest snakebite prevalence rates around the world [6]. The island’s rich snake fauna includes several deadly venomous species responsible for most envenomation. The main medically important snakes that cause serious snakebite cases in Sri Lanka include the endemic Ceylon krait (Bungarus ceylonicus), saw-scaled viper (Echis carinatus), common krait (Bungarus caeruleus), Russell's viper (Daboia russelii), and cobra (Naja naja) [2]. Most venomous bites and the resulting hospitalizations are caused by these species. Furthermore, formerly thought to be just mildly venomous, hump-nosed pit vipers (Hypnale spp.) are now regarded as extremely significant because of their capacity to cause severe systemic envenomation, which includes severe renal damage and coagulopathy [7]. In Sri Lanka, the hump-nosed viper has been categorized as a medically significant mildly venomous snake due to reports of potentially fatal envenomation. In addition to contributing to the high rate of snakebite in the whole country, the wide variety of venomous snakes makes it difficult for healthcare providers to tell the difference between various envenomation. An incorrect diagnosis of snakebite is a problem in Sri Lanka because rural hospitals lack the necessary resources and knowledge. Inappropriate use of antivenom puts patient safety at risk and wastes resources, particularly when it comes to attacks from Ceylon kraits and hump-nosed vipers. Improved identification tools are urgently required to enable accurate identification and treatment [8] [7].

2.3 Difficulties in Snakebite Diagnosis and Fang Mark Identification

When the snake is not taken to the hospital, it can be challenging to identify the species of snake that bit the patient. Doctors are forced to rely on often-deceptive patient reports, bite marks, and symptoms. Vipers, for instance, produce coagulopathy and swelling [9], whilst cobras and kraits [10] cause neurotoxicity [5]; however, the early signs may be uncertain or delayed. Initially, a krait bite might appear harmless, which could cause a missed diagnosis until paralysis sets in. Anxiety may lead non-venomous bites to resemble venomous symptoms. Though fang marks are one of the few quick signs of a snakebite, they are not without limitations. Non-venomous snakes typically leave several shallow teeth marks, while venomous snakes typically leave one or two wide puncture wounds. For instance, non-venomous bites can have light scratches; cobras and kraits produce smaller paired markings, while vipers usually create two severe punctures (Fig 1). Fang mark analysis by itself is unreliable, though, because these patterns can be deceiving due to variables including bite angle, snake size, and skin thickness [11].

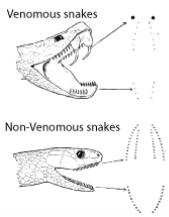

Fig. 1. Anatomical comparison of venomous vs non-venomous snake bite patterns

While non-venomous snake bites could resemble venomous ones, venomous snakes may leave marks that are confusing or unusual. Certain snakes with rear fangs produce patterns that are unclear. Because wound appearance alone often results in diagnostic confusion, fang mark analysis should always be supported by clinical observation [11]. The problem in Sri Lanka is made more difficult by the similarities in anatomy between some venomous and mildly venomous snakes (e.g., various viper species with similar fang arrangements or young cobras vs. mildly venomous snakes [12]). A significant gap in the management of snakebite is highlighted by these challenges with species determination and the unreliability of fang mark identification: the need for more reliable and accurate diagnostic tools to direct treatment.

2.4. Machine Learning and Deep Learning in Snake Classification

Research of machine learning (ML) and deep learning approaches to help with snakebite identification and classification has been encouraged by advancements in artificial intelligence. Convolutional neural networks (CNNs), a type of image recognition model, have shown significant potential in recent years for the classification of snake species from images of the snake. By using huge collections of snake images, researchers have shown that computer vision systems can be trained to identify snake species with high accuracy. Deep CNN models have actually been shown to be highly efficient at classifying snake species, even differentiating between venomous and non-venomous snakes by simply looking at images [13]. For instance, one study used a dataset of more than 1,700 snake images to develop a CNN-based model that classified snakes into "venomous" and "non-venomous" categories with an accuracy of over 90%. These findings show how deep learning may be used to recognize morphological characteristics that indicate dangerous snakes [14]. Simultaneously, natural language processing (NLP) methods have been used in healthcare for analyzing textual data; snakebite cases can benefit from this approach as well. To help in the identification of snakebites, prototype natural language processing (NLP) models can efficiently extract important features (e.g., described snake appearance, reported symptoms, timing of onset) that may point to a specific species from clinical notes, patient descriptions, and symptom reports. According to studies, text-based machine learning models could, for example, predict potential neurotoxic envenomation based on a patient's recorded symptoms and course, suggesting an elapid (cobra/krait) bite even in cases when the snake was not visible [15]. Using deep learning on bite mark images is a new approach in snakebite informatics. The bite mark pattern and local tissue damage were successfully evaluated as visual features in an initial study that used a deep learning model to classify the biting species from images of snakebite wounds. This approach aimed to differentiate between venomous and non-venomous snake bites solely based on the features of the wounds shown in images. According to initial results, CNNs can be used to identify small variations in bite geometry, fang mark spacing, and tissue changes brought on by envenomation that are associated with specific snake species [16]. Even though research in this field is still in its early stages, it could lead to an image-based diagnostic tool in situations where the snake is not visible. For determining the likely snake species, other researchers have focused on machine learning models that use structured clinical data, including patient demographics, bite location, timing, and symptom development. To discover statistical patterns that associate snakes with specific clinical profiles, these efforts frequently use algorithms trained on historical case data (for instance, Russell's viper bites frequently present with rapidly swelling and coagulopathy, whereas kraits present with delayed paralysis). However, most of the research to date has dealt with clinical data-based prediction and image-based identification in separate tracks. There is currently no fully integrated

framework that is considered standard in the treatment of snakebite, particularly in environments with limited resources. According to the research to date, there is still a gap between putting these methods together, even while CNNs can correctly detect snakes from images [13] [14] and NLP [15], or other ML models may evaluate clinical data to derive insights. This provides strong reasons to develop a hybrid system that can evaluate several data sources at once to improve snakebite diagnosis.

3 Methodology

3.1. Data Collection

This study compiled a comprehensive multi-source dataset that includes clinical, visual, and contextual information on snakebite incidents in Sri Lanka. At Anuradhapura Central Hospital, clinical parametric data was collected from patient records. This included details regarding the patient's demographics (age, gender, and Involvement in farming), the bite's situations (the location on the body, environmental location, date of the bite, and activities during the bite), and the season. In cooperation with the Rajarata Medical Faculty, images of snakebite wounds were collected for use as a visual foundation for pattern identification. These images show unique bite site patterns and local tissue effects related to several snake species. To ensure that the dataset contains important morphological and clinical characteristics reported in the literature, a thorough evaluation of papers was also carried out to choose significant characteristics of the region's most venomous snakes. Lastly, to gather data on snake distribution and public awareness on snakebite identification, a field survey was conducted across locals in snakebite-prone areas. The study created a large, comprehensive dataset for training and evaluating the snakebite identification models by combining these many sources.

3.2. Data Pre-Processing

Each element of clinical data that was gathered was carefully pre-processed to make sure it was suitable for machine learning analysis. After reviewing raw hospital parametric records, variables such as bite location, time of occurrence, patient activities, and demographics have been standardized to create an organized dataset. To deal with missing values, eliminate inconsistencies, and guarantee high-quality inputs for modeling, data cleaning techniques were used. To comprehend feature distributions and identify potential outliers, exploratory data analysis, or EDA, has been carried out. A Synthetic Minority

Oversampling Technique (SMOTE) was utilized to improve minority class samples without including artificial bias to address the issue of class imbalance, which is especially important in medical datasets. Algorithms like ADASYN were avoided because of their tendency to generate synthetic noise, which might compromise clinical relevance. The first machine learning model was trained using the dataset that had been generated after all categorical variables were encoded using label encoding methods and the one-hot encoding method. As part of the future work, preprocessing methods will be extended to incorporate an image-based component into the system. For this future development, images of snakebite injuries will specifically be pre-processed using normalization techniques such as resolution standardization, noise reduction, and contrast enhancement, and annotated with species-level data. To increase dataset variability and model durability, consider using image augmentation techniques such random flips and rotations. In preparation for the hybrid architecture, split the visual data streams into training, validation, and testing subsets. This image processing framework is a critical future improvement that will complement the current text-based method and result in a more reliable snakebite identification system.

3.3. Model Development (Text-based and Image-based)

While the image-based model is still a proposed future improvement, the machine learning model development in this study currently focuses on a fully functional text-based classification system. Structured parametric characteristics, such as bite site, bite location, patient activity, and demographic information, were used to train the text-based model. The dataset was balanced using SMOTE to reduce class imbalance, and all categorical attributes were encoded correctly. The model comparison plot shows the results of the evaluation of several supervised learning algorithms, including Random Forest, XGBoost, MLP Classifier, and a stacking ensemble combining Random Forest and XGBoost. The stacking ensemble provided the best results with an accuracy and F1-score of 0.970 (Fig. 2).

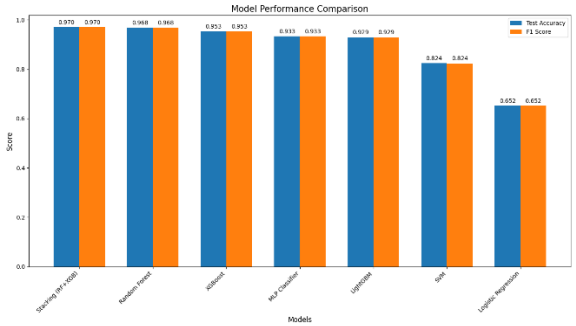

Fig.2. Performance comparison of machine learning models evaluated for snakebite classification

In addition, a neural network was built to evaluate the validity of deep learning; accuracy and loss curves over 80 epochs were used to show performance, confirming consistent convergence and generalization capability (Fig. 3).

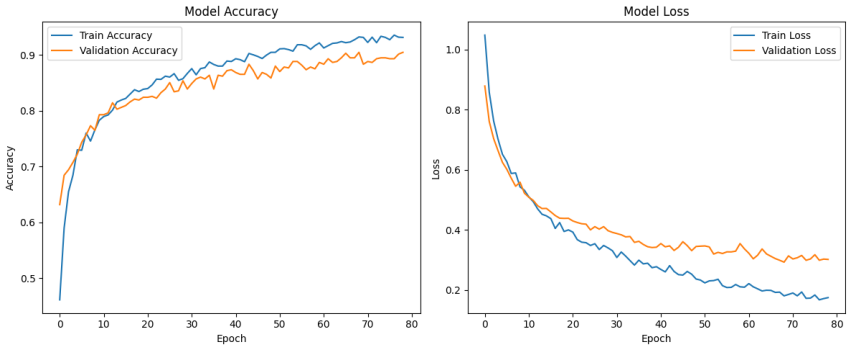

Fig. 3. Learning curves showing model accuracy (left) and loss function (right) over 80 training epochs.

While the classification performance for both antivenom-indicated and hump-nosed viper bites was encouraging, few cases were still incorrectly classified across categories, especially between antivenom-indicated and non-venomous bites, according to the final stacked model's confusion matrix (Fig. 4).

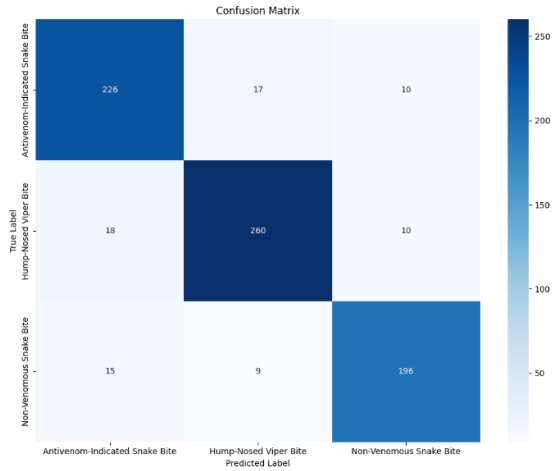

Fig. 4. Confusion matrix for the stacking ensemble model showing classification performance across three snakebite categories

This insight emphasizes how important it is to include a visual validation step to clear up any confusion that can result from using only text-based inputs. Therefore, a deep learning method will be used to create an image-based classifier as part of the suggested model development. Future research is going to concentrate on building a model from the ground up or using YOLOv8 [17] for bite-site pattern identification and wound detection.

3.4. Proposed Hybrid Decision System

As future work, a hybrid decision-making architecture will be developed as a proposed improvement to the current system to combine the results of the text-based and the soon-to-be image-based models. This future framework would combine the existing text-based model with a planned image-based model that has yet to be implemented. The envisioned workflow would begin with the current model, trained on structured parametric data, producing an initial prediction using clinical features. Subsequently, the proposed image-based model would cross-validate this classification by analyzing bite wound images, either supporting or contesting the initial forecast. The final decision will be made using a fusion technique, and the outcome will be accepted with high confidence if both models agree on the expected class (such as ‘Hump-Nosed Viper Bite’, ‘Antivenom-Indicated Bite’, or ‘Non-venomous Snake Bite’). When predictions based on images and text vary,

the system will either indicate the case for expert review or give priority to the model with the highest level of confidence. This hybrid approach reduces errors in diagnosis by utilizing the advantages of both data modalities, particularly in cases that are deceptive, such as bites from Ceylon kraits, when visual confirmation is critical. Additionally, the proposed approach would use clinical characteristics like swelling and blistering to determine that both models represent a bite that requires antivenom. The method can identify the most likely species by using cosine similarity to compare these characteristics to the symptom profiles of five medically important snakes. Targeted antivenom can be safely administered if Ceylon krait does not exist, increasing treatment accuracy and patient safety.

4 Result and Discussion

The developed text-based machine learning model evaluated strong predictive performance, with the stacking ensemble of Random Forest and XGBoost achieving a test accuracy of 96.98% and a weighted F1-score of 0.97. The value of epidemiology-based data, such as bite site, environmental location of bite, patient activity, and incident time, for identifying the general category of the snakebite was confirmed by this model's outstanding accuracy over other conventional classifiers and neural network techniques. But confusion matrix analysis represents serious misclassifications: 17 antivenom-indicated cases were misclassified as hump-nosed viper bites, 10 antivenom-indicated cases were incorrectly labeled as non-venomous, and 18 hump-nosed viper cases were misidentified as requiring antivenom. The Ceylon krait (Bungarus ceylonicus), a medically significant species that frequently confuses the model and shows minor local symptoms and does not respond to antivenom, was the subject of the most obvious mistakes, and the current model have several limitations: data imbalance despite SMOTE application, absence of complete visual bite characteristics, lack of temporal symptom progression data, regional variation in snake distribution, and limited exposure to rare venomous species. To address these limitations, future work will focus on developing a hybrid decision-making system that integrates the text-based classifier with an image-based model using bite-site images. In this system, the predictions provided by the text-based classifier will be verified by an image-based model, which may be implemented using YOLOv8. The approach aims to enhance species-level identification by integrating bite site analysis and employing similarity criteria to compare clinical symptoms with reference characteristics. It is expected that this layered architecture will greatly improve the accuracy of diagnosis and lower the possibility of misclassification, providing a more reliable and secure tool for medical judgment in the treatment of snakebite throughout Sri Lanka.

5 Conclusions

The findings of this study show that the text-based machine learning model to recognize snakebite patterns enhances clinical judgment. The model provided quick and accurate suggestions for treatment by correctly identifying most of Sri Lanka's venomous snake species. However, a few challenges were noticed, most notably the Ceylon krait's repeated misclassification, which was probably brought on by its rarity and similarity to other krait species. These challenges highlight the need for further development beyond the current text-based approach. In future work, plan to develop a hybrid method, which enhances overall identification accuracy by combining textual data analysis with image-based recognition. A multi-modal approach like this has a great chance to minimize misclassification problems and give doctors more reliable and strong decision support.

Future Development

- Develop an image-based bite site classification model using YOLOv8.
- Integrate text and image-based models into a hybrid decision system.
- Use cosine similarity on clinical features to identify the most likely snake species for accurate antivenom use.
- Test the complete system using real patient data in clinical settings.

References

1. World Health Organization: Snakebite envenoming: a strategy for prevention and control. World Health Organization, Geneva (2019).
2. Epidemiology-of-snakebite.pdf, https://slma.lk/wp-content/uploads/2017/11/2.Epidemiology-of-snakebite.pdf.
3. P. S. Salve, S. Vatavati, J. Hallad, Clustering the envenoming of snakebite in India: The district level analysis using Health Management Information System data. Clinical Epidemiology and Global Health. 8, pp. 733–738 (2020). https://doi.org/10.1016/j.cegh.2020.01.011.
4. D. N. Redewad, D. S. D. Bhaisare, D. Y. V. Bansod, Management and Outcome Study of Snake Bite Cases in Central India.
5. S. A. M. Kularatne, B. D. S. S. Budagoda, I. B. Gawarammana, W. K. S. Kularatne, Epidemiology, clinical profile and management issues of cobra (Naja naja) bites in Sri Lanka: first authenticated case series. Transactions of the Royal Society of Tropical Medicine and Hygiene. 103, pp. 924–930 (2009). https://doi.org/10.1016/j.trstmh.2009.04.002.

6. D. S. Ediriweera, A. Kasturiratne, A. Pathmeswaran, N. K. Gunawardena, B. A. Wijayawickrama, S. F. Jayamanne, G. K. Isbister, A. Dawson, E. Giorgi, P. J. Diggle, D. G. Lalloo, H. J. de Silva, Mapping the Risk of Snakebite in Sri Lanka - A National Survey with Geospatial Analysis. PLOS Neglected Tropical Diseases. 10, e0004813 (2016). https://doi.org/10.1371/journal.pntd.0004813.
7. K. Maduwage, G. K. Isbister, A. Silva, S. Bowatta, S. Mendis, I. Gawarammana, Epidemiology and clinical effects of hump-nosed pit viper (Genus: Hypnale) envenoming in Sri Lanka. Toxicon. 61, pp. 11–15 (2013). https://doi.org/10.1016/j.toxicon.2012.10.013.
8. U. Madhushani, G. K. Isbister, W. C. Hodgson, S. Siribaddana, A. Silva, Antivenoms for local effects of snake envenoming Ceylon Journal of Science. 52, (2023). https://doi.org/10.4038/cjs.v52i3.8209.
9. N. D. Abeyaweera, A. Sivaruban, A. Murugananthan, K. P. Amarasinghe, Russell's viper (Daboia russelii) in the Jaffna peninsula, Sri Lanka bears signatures of incipient genetic divergence from the South Indian population. Journal of the National Science Foundation of Sri Lanka. 52, (2024). https://doi.org/10.4038/jnsfsr.v52i2.11820.
10. C. Dalugama, I. Gawarammana, Confirmed Ceylon krait (Bungarus ceylonicus) envenoming in Sri Lanka resulting in neuromuscular paralysis: A case report. Journal of Medical Case Reports. 11, (2017). https://doi.org/10.1186/s13256-017-1503-0.
11. S. G. C. Cleuren, D. P. Hocking, A. R. Evans, Fang evolution in venomous snakes: Adaptation of 3D tooth shape to the biomechanical properties of their prey. Evolution: International Journal of Organic Evolution. 75, 1377–1394 (2021). https://doi.org/10.1111/evo.14239.
12. A. R. de Roodt, L. V. Boyer, L. C. Lanari, L. Irazu, R. D. Laskowicz, P. L. Sabattini, C. F. Damin, Venom yield and its relationship with body size and fang separation of pit vipers from Argentina. Toxicon. 121, pp. 22–29 (2016). https://doi.org/10.1016/j.toxicon.2016.08.013.
13. K. Ahmed, M. Alaa, A. Aboutabl, Snake species classification using deep learning techniques. Multimedia Tools and Applications. 83, pp. 1–42 (2023). https://doi.org/10.1007/s11042-023-16773-0.
14. N. I. Progga, N. Rezoana, M. S. Hossain, R. U. Islam, K. Andersson, A CNN Based Model for Venomous and Non-venomous Snake Classification. In: Mahmud, M., Kaiser, M.S., Kasabov, N., Iftekharuddin, K., and Zhong, N. (eds.) Applied Intelligence and Informatics. pp. 216–231. Springer International Publishing, Cham (2021). https://doi.org/10.1007/978-3-030-82269-9_17.
15. N. Rusli, A. Amir, N. A. H. Binti Zahri, R. B. Ahmad, Snake species identification by using natural language processing. Indonesian Journal of Electrical Engineering and Computer Science. 13, pp. 999–1006 (2019). https://doi.org/10.11591/ijeecs.v13.i3.pp999-1006.

16. R. Kamalraj, Deep Learning Model for Identifying Snakes by using Snakes' Bite Marks. In: 2020 International Conference on Computer Communication and Informatics (ICCCI). pp. 1–4. IEEE, Coimbatore, India (2020). https://doi.org/10.1109/ICCCI48352.2020.9104200.
17. M. Hussain, YOLO-v1 to YOLO-v8, the Rise of YOLO and Its Complementary Nature toward Digital Manufacturing and Industrial Defect Detection, https://www.mdpi.com/2075-1702/11/7/677, last accessed 2024/12/22.

3rd International Engineering Research Symposium 2025 (IERS 2025)
Colombo, Sri Lanka

Simulation-Based Evaluation of Cost-Effective Consensus Algorithms to Enhance Blockchain Scalability in Low-Resource Education Systems

W. A. Udeshika[1] and W. V. S. K. Wasalthilaka[2]

[1]Department of Computing and Information Systems, Faculty of Computing, Sabaragamuwa University, Sri Lanka.
[2]Department of Software Engineering, Faculty of Computing, Sabaragamuwa University, Sri Lanka.
ayomiudeshika19@gmail.com, subodhiwasalthilakeskw@gmail.com

Abstract. The use of blockchain technology in education credentialing schemes has strong po- tential for ensuring data integrity, transparency, and tamper resistance. Selecting the most suitable consensus mechanism according to the use case and making the system more sustainable is a challenge. The performance and efficiency of some consensus mechanisms selected through a strong literature review, Proof of Authority (PoA), Proof of Stake (PoS), Delegated Proof of Stake (DPoS), and Practical Byzantine Fault Tolerance (PBFT), have been evaluated here. A smart contract-enabled system of credentialing was deployed on a test private blockchain using different blockchain simulation environments, such as Ganache for no algorithms (base case), Hardhat for PoA, Geth for PoS, EOSIO for DPoS, and Hyperledger Fabric for PBFT, wherein all of the consensus mechanisms were given equal transaction loads. Performance metrics such as Transactions Per Second (TPS), latency, CPU usage, memory usage, and computational cost were compared and measured. Simulation indicated that DPoS achieved the highest throughput (~1200 TPS) with the lowest latency and was optimal for large-scale academic deployments. PBFT ensured high data consistency and ~300 TPS with the lowest gas usage but required huge computational resources. PoS and PoA ensured low resource usage and consistent scalable performance with ~0.95 TPS and are optimal for small to medium scale educational institutions with strict requirements on resources. The findings provide a helpful reference for educa- tional institutions and developers seeking to utilize efficient, scalable blockchain systems for the authentication of credentials. This research contributes to the grand vision of bringing blockchain technology within reach and accessible in the developing world.

Keywords: Academic Systems, Blockchain, Consensus Algorithms, Low-Resource Systems, Scalability

1 Introduction

1.1 Background

Blockchain technology has rapidly emerged as a revolutionary solution in many sectors, such as finance, healthcare, and supply chain management, due to its decentralized, secure, and tamper-proof nature. Its inherent properties, like immutability, decentralization, and auditability, have enabled the development of new applications in domains where trust, accountability, and data integrity are essential. Within education, blockchain has the ability to transform important processes such as credential verification, management of academic records, and secure exchange of educational data across institutions [1].

Although its potential is great, implementing blockchain technology in low-resource education systems in developing countries is also faced with many challenges. These systems are characterized by limited resources, weak infrastructure, and low technical capability. All these create scalability challenges in such settings. Most traditional consensus protocols, such as Proof of Work (PoW), are computationally demanding and do not effectively handle the large volume of transactions typically associated with academic operations such as processing of student information, certification, and record maintenance [2]

Furthermore, the computational and energy demands of such conventional mechanisms could make blockchain adoption unaffordable or even unsustainable in low-resource settings. Therefore, it becomes necessary to evaluate and identify cost-effective consensus algorithms that can make blockchain scalable while being suitable for low-resource education environments. By selecting the right algorithm, institutions can take advantage of blockchain without exceeding their financial or technical capacities, enabling them to implement a more efficient and inclusive transaction in education systems [3].

1.2 Problem Statement and objectives

Education institutes in developing countries often face issues with credential verification, data security, and administrative efficiency due to limited access to technological infrastructure and capital. Low-resource education system within this study refers to institutions without high-performance computing setup, with minimal financial ability to support energy-demanding technologies, and using low-cost or moderately powered facilities for digital-based solutions. These are public universities within developing countries that do not have the ability to support high-level blockchain but also require secure credentialing systems

Blockchain provides a feasible answer in its open, decentralized, and tamper-proof nature. However, the application of blockchain in resource-constrained environments is limited by the energy inefficiency and expense of traditional consensus algorithms like Proof of Work (PoW). Alternative algorithms like Proof of Stake (PoS), Delegated Proof of Stake (DPoS), and Practical Byzantine Fault Tolerance (PBFT) also show promise but have yet to be tested properly for use within educational environments that are resource- constrained.

This research aims at the evaluation of cost-effective, scalable, and deployable consen- sus algorithms in education institutes with less digital infrastructure and resources. By identifying proper mechanisms, this research aims to enable secure management of academic records and improve equitable access to trusted digital solutions in developing educational settings.

To meet the problem statement mentioned above, the research questions have been formulated. The research first aims to identify which consensus algorithms are most cost- effective and scalable in terms of low-resource education systems with limited financial and computational resources. It further explores the most significant variables that have the largest influence on the performance and scalability of these algorithms in the low- resource educational settings. The study also examines whether the selected algorithms can be effectively implemented in an emulated low-resource educational environment to evaluate their real-world functionality and confirm their scalability and affordability. Additionally, the research explores how well these algorithms perform regarding relevant performance metrics such as throughput, latency, and resource utilization, and how easily they can be tuned to meet the specific requirements of low-resource school networks.

1.3 Significance of the study

Growing demand for secure, transparent, and tamper-proof management of academic credentials and student data has driven international interest in using blockchain technology within the education sector. The inherited characteristics of blockchain technology, like decentralization, immutability, and auditability, place blockchain technology at the front of potential solutions for reducing legacy challenges to credential fraud, record-keeping inefficiencies, and administrative privacy.

The implementation of blockchain technology within low-resource education systems, particularly in developing countries, still has some barriers. This is primarily due to infrastructure expenses, high energy usage, and insufficient technical capacity. As a combination of these challenges, it tends to prevent the application of blockchain technology in low-resource settings from having a scalable and sustainable implementation.

The importance of this study is that it addresses such critical issues in a systematic examination of low-cost consensus algorithms that can assist in enhancing blockchain scalability without creating excessive financial or computational loads. Consensus protocols form the basis of any blockchain system, providing agreement and integrity among distributed nodes. Though security is offered by popular algorithms like Proof of Work (PoW), their power-intensive nature makes them unsuitable for low-resource systems. This work shifts the focus to alternative consensus algorithms like Proof of Stake (PoS), Delegated Proof of Stake (DPoS), and Practical Byzantine Fault Tolerance (PBFT), which could offer better performance at lower energy and operational costs.

The findings of this study aim at informing and empowering different stakeholders such as education administrators, IT managers, and blockchain programmers by providing evidence-

based guidelines for the deployment of blockchain technologies in low-resource environments. The findings will serve as a blueprint for the integration of blockchain into
learning processes such as student data management, issuance of certificates, and verification of credentials, thereby enhancing trust, eliminating fraud, and streamlining administrative processes in educational systems across the world.

2 Literature Review

With the potential to improve trust, security, and transparency in a variety of industries, including healthcare, supply chain management, banking, and education, blockchain technology has grown into a revolutionary invention [4, 5]. In recent years, excitement about the ability of blockchain to secure and upgrade educational organizations has increased. Blockchain has been increasingly emerging in the educational sector for use cases like quality assurance, academic transcript storage, enrolment management, and academic credential verification. Blockchain's transparency and immutability make it a valuable tool for solving problems like fraudulent enrolment, credential theft, and poor human verification processes [6].

Despite the potential they have, these applications provide some challenges. Due in substantial part to infrastructure limitations, a lack of finance, and low rates of digital literacy, especially in developing countries, the majority of blockchain solutions in education remain in the experimental phases [7]. Furthermore, blockchain-based applications are not practical in environments with low resources if they are implemented without optimized consensus protocols, which might end up with high costs and poor throughput for transactions [8]. These challenges emphasize how important it is to pick cost-effective, scalable consensus algorithms which suit the requirements and capacities of these types of settings. The base of blockchain technology is consensus algorithms that enable decentralized networks to achieve consensus on the distributed node's current state independently of a centralized authority. These algorithms ensure that only authorized transactions are recorded and that all participating nodes receive an identical representation of the blockchain while there is no trusted intermediary involved [9]. The consensus algorithm used by a blockchain system has an enormous effect on its security, decentralization, and scalability. Proof of Work (PoW) can be considered as the first and most well-known consensus protocol, which Bitcoin deploys. As a solution to the limitation of PoW, alternative mechanisms such as Proof of Stake (PoS), Delegated Proof of Stake (DPoS) and Practical Byzantine Fault Tolerance (PBFT) have been developed.

PoS is widely considered the energy-efficient alternative to PoW. Instead of being computation based, PoS grant validation rights on the basis of the amount of cryptocurrency "staked" by the user. PoS is an advancement of the efficiency of PoS using a vote-based process to enable token holders to vote in support of selecting a handful of representatives to approve transactions and produce blocks. roof of Authority (PoA) is a consensus mechanism widely

used in permissioned blockchains where pre-approved and trusted validators are utilized. Instead of computational work (PoW) or stake (PoS), PoA relies on the identity and reputation of validators to secure the network. PBFT and its variants are designed for permissioned blockchain networks, where nodes are partially trusted. Unlike PoW or PoS, PBFT does not require staking or extensive computation [10].

The selection of consensus an algorithm has a direct impact on blockchain energy efficiency, scalability, and usefulness in low-resource settings. In under-resourced learning environments, especially in developing countries, traditional power-consuming algorithms like Proof of Work (PoW) are barriers to entry [11]. This has led to the creation of lighter and less expensive solutions such as Proof of Stake (PoS), Delegated Proof of Stake (DPoS), Practical Byzantine Fault Tolerance (PBFT), and Proof of Authority (PoA).

This research addresses these particular deficiencies in a straightforward manner by proposing a comparison of PoS, DPoS, PBFT, and PoA with one and the same academic smart contract and dataset under controlled resource-constrained environments. In so doing, it aims to create practical evidence on throughput, latency, and cost-effectiveness of these consensus protocols, with a view to giving practical recommendations towards blockchain adoption within low-resource education systems. Study uses blockchain simulation environments like Ganache, Geth, Hardhat and EOSIO particular to each algorithm and also offers a reproducible foundation for future academic and institutional deployments.

3 Methodology

The research study uses a simulation-based evaluation method to compare the scalability and performance of various blockchain consensus algorithms in a low-resource academic context. The method consists of eight clearly defined stages, starting with data set generating and preprocessing, through algorithm selection and simulation, to performance eval- uation and proposing an optimal solution.

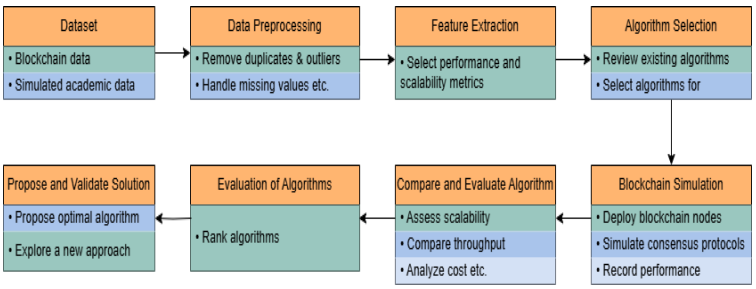

Fig.1. Methodology

- **Dataset**: Generated a synthetic dataset of 1000 records of data using Python faker

libraries since real credential data is sensitive in nature.

- **Data Preprocessing**: This included removal of duplicate records, identification and elimination of outliers, and handling of missing values.
- **Feature Extraction:** The crucial performance metrics were identified and extracted for evaluating the efficiency of consensus algorithms. They included key metrics such as throughput (transactions per second), latency (transaction confirmation time), cost-efficiency (resource and gas usage), and scalability (perfor- mance under additional load).
- **Algorithm Selection:** A thorough literature review was conducted to understand the strengths, weaknesses, and resource demands of the various consensus algorithms. Four algorithms—Proof of Stake (PoS), Proof of Authority (PoA), Delegated Proof of Stake (DPoS), and Practical Byzantine Fault Tolerance (PBFT)—were selected for simulation and analysis based on their suitability and potential in low-resource environments.
- **Blockchain Simulation:** A blockchain setup was simulated with the help of a separate blockchain simulation environment for each algorithm. All the selected algorithms were deployed and executed with the same setting for fair comparison. Performance metrics were recorded in a systematic manner to examine how each algorithm behaves in a simulated low-resource environment.
- **Compare and Evaluate Algorithms**: The performance metrics collected were compared to assess the scalability, efficiency, and overall suitability of each algorithm. Through the comparison of throughput, latency, resource consumption, and scalability, the strengths and weaknesses of each protocol were established in the context of academic credentialing.
- **Propose and Validate Solution:** Based on the simulation results and metric-based comparison, the most suitable consensus algorithm was proposed, along with practical recommendations on algorithm choice based on different levels of resource availability. The recommendations are designed to inform institutions in the choice of blockchain solutions that provide a good trade-off of performance, cost, and scalability.

4 Results and Findings

4.1 Experimental Setup

To assess the performance of various blockchain consensus algorithms, a test scenario was created in order to simulate a credentialing system that has a workload of 1000 credential transactions. Experiments were conducted on five various blockchain setups, as follows:

4.1.1 **No Consensus Algorithm**: This was chosen as a baseline model to observe how the system functions in the absence of any consensus mechanism used in the

Ganache blockchain simulation environment.

4.1.2 **Proof of Authority (PoA):** implemented according to the Hardhat framework, facil- itating authority-based consensus suitable for private blockchains.

4.1.3 **Proof of Stake (PoS):** Simulated in a private Ethereum network through Geth (Go Ethereum), replicating token-based verification.

4.1.4 **Delegated Proof of Stake (DPoS):** EOSIO platform used for DPoS.

4.1.5 **Practical Byzantine Fault Tolerance (PBFT):** Estimated based on published system behaviour and performance statistics of Hyperledger Fabric.

The tests were performed on an HP Laptop 15-da2xxx with an Intel Core i5-10210U CPU @ 1.60GHz (Turbo to 4.2GHz), 12 GB of RAM, Intel UHD integrated graphics, and 1.13TB storage, under Windows 11 (64-bit). All blockchain platforms were loaded in their respective simulation environment: Ganache v2.7.1, Hardhat v3.0.3, Geth v1.16.2, EOSIO 2.0 and Hyperledger Fabric v2.5. This is sufficient to facilitate controlled simulation of consensus protocols under low-resource settings with reproduciable outcomes.

4.2 Overall Performance Comparison

Table 1. Key Performance Indicators

Metric	**No Algorithm**	**PoA**	**PoS**	**DPoS**	**PBFT**
Transactions Per Second (TPS)	0.94	0.95	0.96	1200	300
Latency (sec)	0.018	0.0167	0.0167	0.0025	0.0032
PU Usage (%)	23.67%	7.54%	8.26%	12.45%	18.33%
Memory Usage (MB	9480.71	10185.53	9850.20	6432.00	11032.00
Transaction Finality (sec)	0.018	0.0167	0.0167	0.5	1.2
Gas Cost (ETH)	0.22836	1.452291	1.354672	0.0101	0.0018

4.3 Scalability Analysis

Scalability is a key factor in assessing the readiness of blockchain systems for real-world implementation, particularly in education systems where the number of transactions can be increased during peak periods. In this study, scalability was examined by incrementally increasing the number of credential transactions from 10 to 1000 and observing the impact on key performance metrics such as Transactions Per Second (TPS), latency, CPU usage, memory usage, and gas cost.

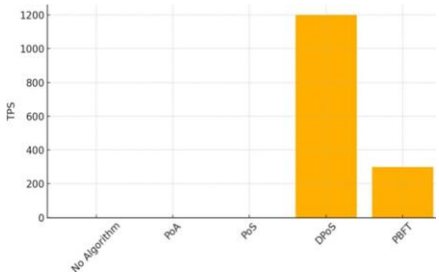

Fig.2. TPS comparison across consensus algorithms

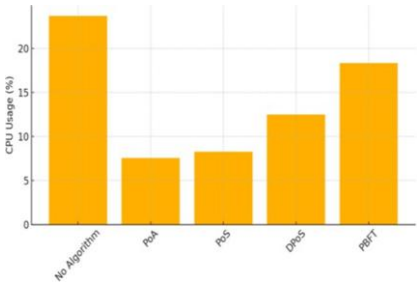

Fig.3. CPU consumption across algorithms during simulation

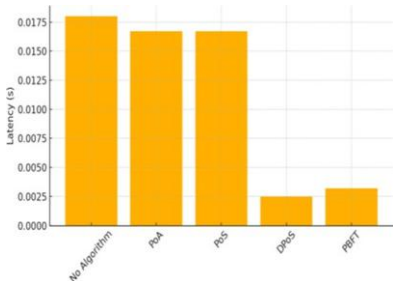

Fig.4. Average transaction latency across consensus algorithms

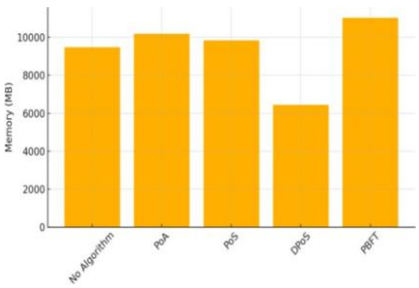

Fig.5. Memory usage comparison across consensus algorithms

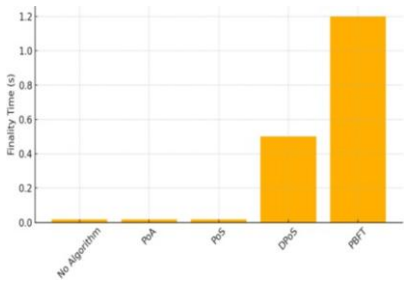

Fig. 6. Transaction finality times across algorithms

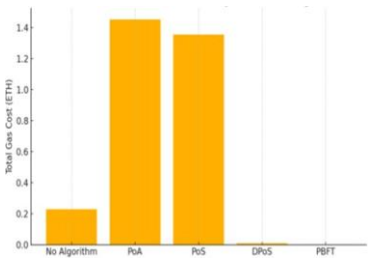

Fig. 7. Total gas cost for processing 1000 transaction

5 Discussion

This study is designed to evaluate the performance, scalability, and feasibility of block- chain consensus protocols, including Proof of Stake (PoS), Delegated Proof of Stake (DPoS), Practical Byzantine Fault Tolerance (PBFT), and Proof of Authority (PoA) for educational credentialing systems, particularly in low-resource learning environments. Through simulations, metric-based analysis, and noticeable findings were discovered.

DPoS also showed remarkable responsiveness and scalability with a high but consistent throughput of ~1200 TPS with low latency when transaction volume is up. Its performance is indicative that it is best-suited for use in national deployments or platforms responsible for large-scale academic data sets.

PoS and PoA showed minimal resource utilization, with low CPU and memory usage. Even with relatively lower throughput (~0.95 TPS), their latency and transaction cost con- sistency under growing loads indicate high potential for small to medium-sized institutions with small-scale infrastructure. Both algorithms walk along the performance-cost trade- off line.

PBFT was excellent at maintaining data consistency and accuracy of consensus, with good TPS (~300 TPS) and negligible gas usage. It also had significantly higher computa- tional and memory-intensive demands and is therefore less suitable for highly resource- constrained environments. However, it's still a good choice for systems requiring high trust
and consistency. The work contributes to understanding how consensus models impact blockchain scalability, cost, and energy use in educational use cases.

It can be observed from scalability testing that the DPoS is the most scalable solution, with the best throughput and responsiveness under load. PBFT has high integrity and pre- dictable performance but at increasingly more resources as transaction volume increases. PoS and PoA have low hardware pressure and consistent performance and are therefore viable in low-resource environments.

6 Conclusions

Consensus protocols are at the heart of making blockchain effective to use in low-resource education networks. The algorithm choice directly determines system scalability, transac- tion speed, and sustainability. According to the simulation results and analysis of metrics, PoS and PoA are the most practical options for re-

source-constrained education institutes. Their low operational overhead and reliability make them ideally suited for environments where high-end computational resources are not feasible. DPoS is especially suitable for scalability, offering a robust solution for broader deployments where transactional volume is great but moderate resources exist. PBFT, though resource-intensive, is high in trust and consistency and hence suitable for educational systems that value accuracy, integrity, and tamper resistance over performance. However, its suitability reduces in low-resource en- vironments.

7 Recommendations for Further Research

Investigating hybrid consensus models (e.g., PoS + PBFT) to achieve both scalability and strong consistency, examining how consensus algorithms solve security threats in aca- demic credentialing systems, checking how scalability solutions like rollups or sharing work in low-resource academic systems, and identifying sustainability along with compu- tational efficiency through power consumption and carbon footprint analysis can get the gaps identified further, and by filling these gaps, future research can further, refine block- chain-based academic credentialing to be robust, scalable, and inclusive in all education settings.

References

1. H. Xiong, M. Chen, C. Wu, Y. Zhao, and W. Yi, Research on Progress of Blockchain Consensus Algorithm: A review on recent progress of blockchain Consensus algorithms, Future Internet, 14(2), p. 47, Jan. 2022, doi: 10.3390/fi14020047.
2. A. K. Jain, N. Gupta, and B. B. Gupta, A survey on scalable consensus algorithms for blockchain technology, Cyber Security and Applications, 3, p. 100065, Jul. 2024, doi: 10.1016/j.csa.2024.100065.
3. Z. Hussein, M. A. Salama, and S. A. El-Rahman, Evolution of blockchain consensus algorithms: a review on the latest milestones of blockchain consensus algorithms, Cybersecurity, 6(1), Nov. 2023, doi: 10.1186/s42400-023- 00163-y
4. A. Reyna, C. Martín, J. Chen, E. Soler, and M. Díaz, On blockchain and its integration with IoT. Challenges and opportunities, Future Generation Computer Systems, 88, pp. 173–190, May 2018, doi: 10.1016/j.future.2018.05.046.
5. A. S. Kubeka, P-V criticality of a modified BTZ black hole in 2 + 1 dimensional intrinsic time quantum gravity, Journal of Modern Physics, 10(3), pp. 294– 301, Jan. 2019, doi: 10.4236/jmp.2019.103020

6. A. Grech and A. F. Camilleri, Blockchain in education, RePEc: Research Papers in Economics, Nov. 2017, doi: 10.2760/60649
7. I. Alnafrah and S. Mouselli, Revitalizing blockchain technology potentials for smooth academic records management and verification in low-income countries, International Journal of Educational Development, 85, p. 102460, Jul. 2021, doi: 10.1016/j.ijedudev.2021.102460.
8. N. Duwadi, A Systematic Review on Blockchain in Education: Opportunities and challenges, Nepalese Journal of Management Science and Research, 4, Dec. 2021, doi: 10.53056/njmsr-2021.001.2
9. C. W. Bou-Saba and A. Guillen, Using Ethereum platform to securely register students' extracurricular activities, SoutheastCon, pp. 463–470, Apr. 2023, doi: 10.1109/southeastcon51012.2023.10115089
10. J. Yli-Huumo, D. Ko, S. Choi, S. Park, and K. Smolander, Where is current research on blockchain Technology?—A systematic review, PLoS ONE, 11(10), p. e0163477, Oct. 2016, doi: 10.1371/journal.pone.0163477.

3rd International Engineering Research Symposium 2025 (IERS 2025)
Colombo, Sri Lanka

Structural Analysis of Biomimetic Fog Harvesters: Integrating Additive Manufacturing and Electrostatic Concepts

K. S. Dawson[1*], P. C. N. Fernando[1], S. M. U. S. T. J. A. Subasinghe[2], M. S. Kahandawala[1], L. N. Wickramarathna[1]

[1]Department of Mechanical Engineering, Faculty of Engineering, University of Peradeniya, Sri Lanka
[2]Department of Chemical and Process Engineering, Faculty of Engineering, University of Peradeniya, Sri Lanka
e18057@eng.pdn.ac.lk

Abstract. Water scarcity remains a critical global challenge, especially in arid and semi-arid regions where conventional freshwater sources are limited. This research contribution presents an experimentation rig to represent the effects of fog harvesting using electronic injection method which is previously explored by MIT, USA as well as additive manufactured structures which can be easily utilized for biomimetic fog harvesting structures. Fog harvesting is mostly done by passive structures. Though they provide valuable contributions for water preservation and consumption among the arid region's populace. The focus has to shift to novel methods due to the lack of the efficiency in water collection usually resulting in upto 10 $l/m^2/day$ 10% of the efficiency, where it is probably possible with advanced material and coatings. It is said to have an efficiency over 90% for the electrostatic mesh if the conditions are achieved but the validation for various conditions have not been tested where this research provides some insights to the matter at hand while the structure of the 3D printed mesh facilitates a novel mesh implemented using conventional fabrication methods. The double wishbone design is a conceptual model which aims to reduce impacts from wind conditions while in the field. The limitations include scaling the setup for real world application.

Keywords: Biomimicry, Electrostatic, Fog harvesting, Additive manufacturing

1 Introduction

a. Background and overview for sustainable water harvesting

Increasing population, climate change, management issues and altering rainfall patterns amount to water scarcity around 2.3 billion people and further increases by the day. Agriculture usually is more intensive of water consumption annually consuming around 70% of freshwater around the world where food scarcity is also presents a threat to humankind. When the biodiversity is also concerned shrinking wetlands and depleting rivers amount to the peril of the wild life creating problems related to sustainability and eco-consciousness. [1]

b. Biomimetic inspiration for current fog harvesters

Fog harvesting, inspired by nature, offers a sustainable water solution for arid and semi-arid regions. Fog, rich in water content, appears not only in cold climates but also at dawn in coastal deserts and cloud forests, where winds carry moisture across the land, nourishing plants and animals. Biomimicry allows us to replicate such strategies for human use. [2]

- Namib Desert Beetle (*Stenocara gracilipes*): Collects fog by using hydrophilic bumps and hydrophobic troughs on its back to channel water droplets to its mouth. [3]
- Pine Trees (Genus Pinus): Capture fog on their leaves, enabling condensation that either nourishes the tree directly or moistens the soil for root absorption.
- Spiders: Their webs self-repair through hydrophilic knots that absorb water, tightening the silk and restoring damaged structures.

These natural examples highlight how fog harvesting can inspire innovative, sustainable water collection methods. [4–6]

c. Limitations of conventional systems

The fog harvesters currently use passive 3D spaced mesh structures (see Fig.1) fabricated using conventional mechanical methods. Those meshes tend to clog up water but might have a destructive effect when a high wind and turbulence is present if not supported properly. Static structures do present resistance to natural high winds and unpredictable climates etc. but dynamic structures tend to breakdown due to the unpredictable nature of

the conditions presented by high speed winds and extreme conditions [7]. The most pressing matter is with the materials used and the drag forces where the structures tend to tear if not supported sufficiently.

Fig. 1. 3D spacer mesh used in a commercial fog harvester (copyright: *aqualonis*)

If these structures are not properly maintained by a community or a crew, in most remote installments after a certain amount of time they tend to be neglected thus affecting the local fauna and flora creating further issues with biodiversity.

The traditional Raschel mesh is one of the first types of meshes used for fog harvesting (see Fig.2) The drag forces on the model explains how much of a support should conventional systems exert on the mesh. They tend to get broken up during high winds typically without enough support.

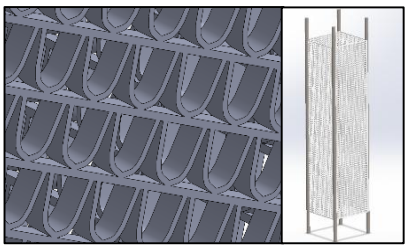

Fig. 2. The Raschel mesh (left) and model (right) used for initial estimations [8, 9]

d. State of the art fog harvesters

Mesh based passive fog harvesters. Most passive fog harvesters have a common structure overall (see Fig. 3.). The structure is usually composed of a mesh fabricated with a

hydrophobic material, a durable structure for the frame and the supporting base and a piping system to collect the water which is collected from the mesh.

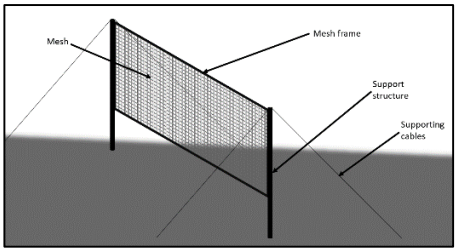

Fig. 3. Typical composition of a fog harvester

Utilizing vertical nets made form hydrophobic materials like PE, PP or nylon. The mesh captures water droplets from fog which then drips down and is collected. The fog harp which developed by Virginia Tech is one of the innovative harvesters where the efficiency has been improved due it's double mesh and higher contact region[10, 11] where dripping is made easier with the vertical cables directed towards the collecting gutter/ pipe. They usually utilize the Raschel mesh (as seen in Fig. 2. which was built for simulations) or a 3D spacer textile mesh (As in Fig. 1.).

Fog fences are large vertical structures which usually use the 3D spacer meshes or something similar to Raschel meshes that act as barriers, capturing water droplets that are carried by the wind and mist. The water runs down the surface into collection systems below. They often are located on top of mountainous areas where clouds and mist tend to pass through creating a humid environment during a certain period of the day. The water collected then seeps through to a collection tank and distributed to remote communities. Large fog collectors also known as LFCs tend to have a larger area thereby subjecting them to a substantial wind load created from the drag of the wind [8, 12–14].

3D printing utilization is one of the most adaptable when it comes to creating structures of fog catchers like in [15]. The creator has used 3D printing to fabricate the whole structure to minimize shorting of the circuit as well as make it appealing and smooth improving functionality and appeal for that version of the fog catcher.

Hybrid fog harvesters. Hybrid fog harvesters can be described as consisting of dynamic structures as well as static structures incorporated to their designs these promise a higher efficiency. Depending on the weather conditions hybrid structures can either perform well or poorly (In rough conditions).

Fig. 4. Wind damage to the Whirly Mk II (left) and to the aluminium drive ring (right)

As seen in Fig.4. "*Whirly*" and "*Whirly MK II*" were innovative fog harvesters used to harvest fog in the African continent. The structures have pivoting mechanisms in high wind forces allowing the mesh to rotate on a bearing. Though being designed with a higher safety factor the dynamic structures tend to perform poorly and the report provides a comprehensive analysis regarding the final outcome of the structures [7]. A proposed design was found related to a manually rotatable dynamic structure which can be directed toward the wind to maximize fog collection by a person manually [16]. The second approach might be better compared to the auto adjusting one giving the advantage of an adjustable structure meanwhile having a certain amount of rigidity when in action presenting a stable static. Despite having a continuously calibrating design in the previous case it is more likely for high wind damages even though the rotating and moving parts were to have higher safety factors. Even the design was to be done with a high strength material it wouldn't be as cost effective.

Electrostatics fog collection systems. A study by Damak and Varanasi at MIT presents an innovative approach to atmospheric water collection by integrating electrostatics with fog harvesting systems. Traditional mesh-based collectors are limited by low efficiency due to aerodynamic drag, capturing only a small fraction of airborne water droplets. To overcome this, the authors introduce an electrostatic method where fog droplets are charged using a corona discharge and then directed toward a grounded collector through an electric field. This technique significantly enhances droplet capture efficiency, with experimental results showing over a 200% improvement compared to passive systems generally while specific efficiencies were not available in the study. With energy consumption lower than conventional desalination methods, this active fog harvesting approach offers a promising, scalable solution for sustainable water sourcing in arid, fog-rich environments.

They have specifically used a single wire of 1.88mm diameter to charge the particles as the positive terminal and the grounded mesh was fixed with a diameter of 1.7mm. Concluding the design at an internal distance between the meshes of 4.2mm where the mesh was selected to be a corrosion resistant 304 type stainless steel wire cloth. While varying the voltage from 7kV (Visible results were obtained from 7kV onwards) the researchers found the best results to be at 15kV. [17]

2 Methodology

a. Mechanical design using biomimicry

Fig. 5. Design and Fabricated small fog collector (600 mm^2) exhibiting the triple mesh and rotatable mesh frame

The initial fabrication was done with standard methods in a workshop using box bars and steel housing a triple nylon mesh for fog catching. The finished prototype can be observed in Fig. 5. Along side with the dimensions of the fog harvester. The mesh design is unique to optimize the water collection without clogging the water droplets and the triple mesh does not increase the wind drag or turbulence. The structure was tested twice in the field and tested for a wind of upto 33m/s using CFD simulations. The structure's safety was

ensured using ANSYS static structural simulation. Inspired by a spider web the design is durable and the selected materials were suitable for long term usage [18].

b. 3D printed components

The modified small-scale model for demonstration was fabricated using additive manufacturing (AM) and the design was altered to have a double wishbone design for both the vertical members (see Fig.6) of the mesh frame to aid in dampening the vibrations and reduce the impact of the drag forces. Curved and joint bodies were either difficult to manufacture or it takes a tremendous amount of work or cost to achieve them. Thereby for biomimetic designs 3D printing/ AM were preferably in these cases.

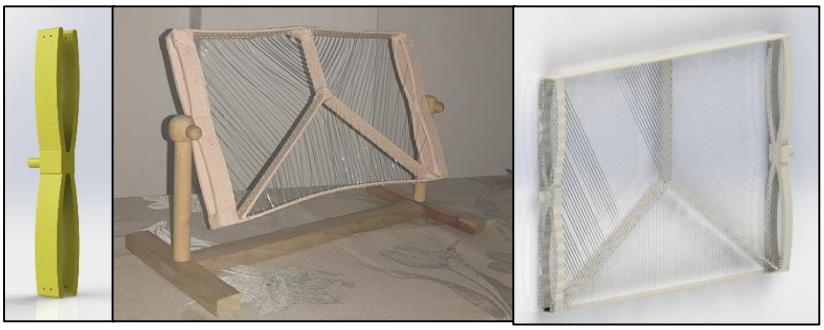

Fig. 6. Fabricated 1:3 model using the double wishbone members (left) and the rendered model (right)

c. Electrostatically charged mesh system

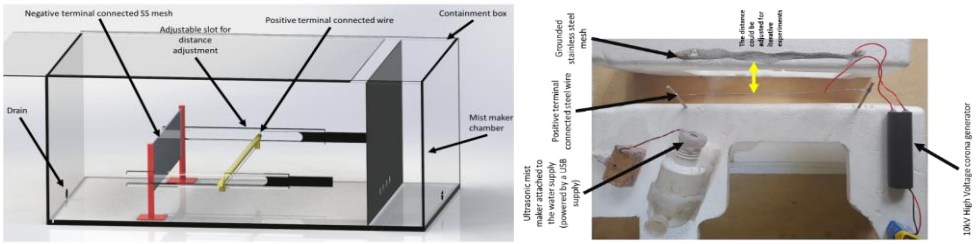

Fig. 7. Experimental rig design /components (left) and initial setup used for 10kV(right)

A corona discharger was attached as a high voltage supplier (around 10kV was the voltage supplied by commonly available commercially available corona discharging unit). The end of the positive terminal was connected to a thin wire to ionize the fog released from the ultrasonic mist maker and the negative terminal was connected to the stainless-steel mesh having 1mm square sections. A pulsed voltage was supplied by connecting and disconnecting the corona discharger. (see Fig. 7 for the experimental rig)

3 Results

$$F_d = \frac{1}{2} C_d \rho_{air} v_{mist}^2 A_f \quad (1)$$

- C_d (Drag coefficient) is constant (typically 1.2 for cylindrical objects in airflow)
- v_{mist} (mist speed) is uniform across the frontal area.
- ρ_{air} (Air density) is a constant (typically 1.225 kg/m^3: standard air density at sea level)
- A_f frontal contact area

$$\eta = 1 - \exp\left(-\frac{d}{d_0}\right) \quad (2)$$

- $d_0 = 0.75$ mm (Based on effective minimum diameter for water collection)

$$\eta_c = \frac{d_{drop}}{d_{string}} . C_s^2 \quad (3)$$

- C_s (Slip coefficient) 0.5 for nylon strings
- d_{string} often 0.75 *mm*
- $d_{drop} = 10\ \mu m$

$$A_{surface} = \pi d_{string} . L \quad (4)$$

- L = 1 *m*: Considering a uniform length

$$F_{detach} = \gamma . \pi d_{string} . cos(\theta) \quad (5)$$

- γ = *0.0728 N/m (Average surface tension*) does not vary
- $70^0 \leq \theta \leq 80^0$ (Contact angle between water and nylon)

$$M_{collected} = \rho_{water} . A_{surface} . \eta_c . v_{mist} \quad (6)$$

- $\rho_{water} = 1000\ kg/m^3$; standard density of water
- $0\ m/s \leq v_{mist} \leq 44\ m/s$

The results obtained from equations (1) – (6) can be observed from Table 1 and the new results for the Ansys model in Fig. 9. Can be observed in Table 2.

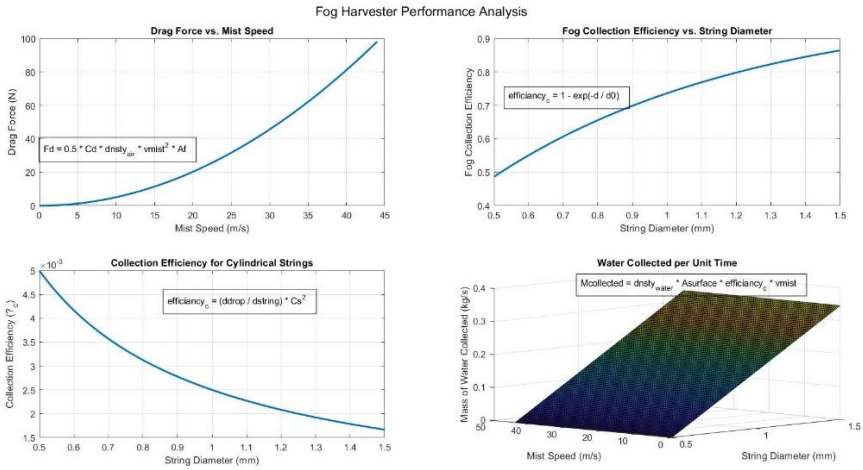

Fig. 8. Variation of Drag force vs Mist speed, Efficiency vs String diameter, Efficiency vs String diameter and Mass of water collected against variable mist speed and string diameter.

Table 1. Obtained MATLAB and CFD results for the full-scale prototype

Property	Result
String Diameter	1.5mm optimum (used 0.75mm)
String spacing (Mesh density)	5mm to 10mm
Wind speed	16 m/s (optimum)
Droplet size	10 µm to 30 µm (10 µm considered for least optimum conditions)

Mesh wettability	70° < Contact angle< 90°
Tested maximum wind with CFD	33 m/s
Maximum pressure drop through 3 layers of the novel mesh's (simulation with SimScape[19])	323Pa

The 10kV low current power supply did not affect the fog collection drastically although tested in normal conditions and room temperature, ionizing did not significantly occur during the practical. There might be valid reasons for this encounter discussed in the sections below.

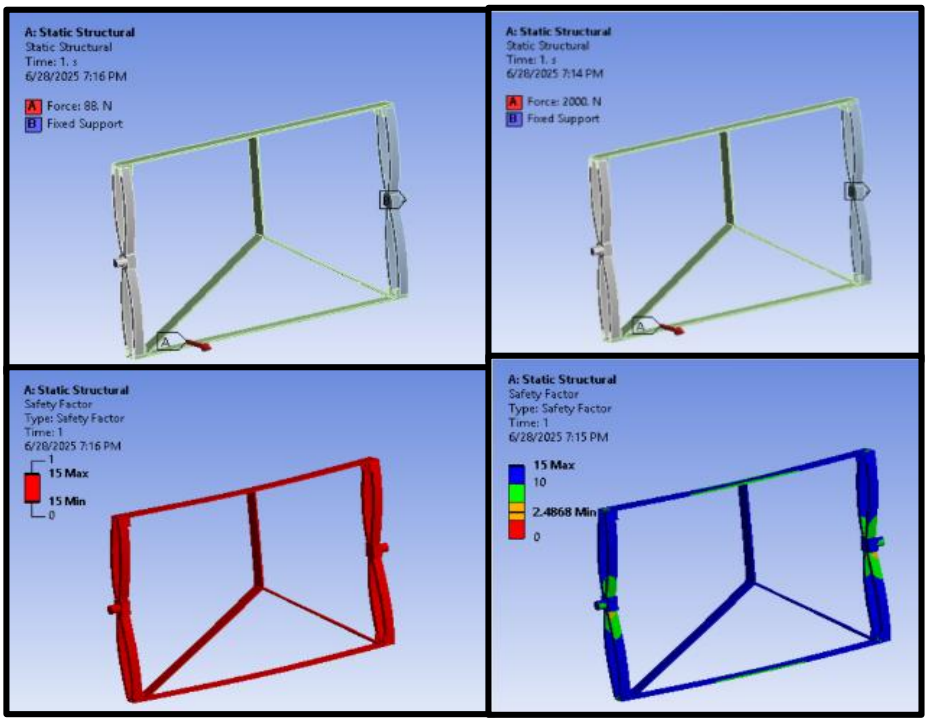

Fig. 9. ANSYS structural simulation for 88 N (left top and bottom - Equivalent for 100 kph) and 2000 N (right top and bottom/ wind forces calculated from equation 1 [18])

Table 2. Obtained results for the full-scale AM model (additional to all the results from Table 1)

Property	Result
Maximum force subjected by a front facing wind	88N (100kph) to 2000N (~200kph)
String spacing (Mesh density)	10mm
Safety factor for the frame at 100kp (88N)	>15
Safety factor for the frame at 259 kph (2000N)	2.4868
Efficiencies	efficiencies could be obtained due to the scalability issue

4 Discussion

The passive fog harvester prototype with its spider-web–inspired single-layer mesh performed as expected in wind simulations. Under a 33 m/s inflow, CFD (k–ω turbulence model) showed local velocity variations of –5 to +13 m/s (18.7–46.6 m/s range) around the mesh, indicating that the design can maintain stability under turbulent conditions. The optimization study further revealed that a 1.5 mm string diameter with 5–10 mm spacing at ~16 m/s wind, with 10–30 µm droplets and a contact angle of 70–90°, provides the highest predicted capture efficiency. However, while this geometry maximizes water yield, practical fabrication and structural concerns (wind drag at larger diameters) must also be considered.

The use of 3D-printed double-wishbone supports was effective in enabling complex, curved geometries that enhance structural stability. Simulation confirmed that the frame could withstand forces equivalent to 259 kph wind without failure, demonstrating that the biomimetic and AM-enabled structure is mechanically viable for harsh conditions.

In contrast, the electrostatic charging experiment did not show measurable improvement in water yield. The corona source was limited to 10 kV, lower than the voltages used in successful demonstrations. The short pulse duration and ambient room conditions (ordinary humidity, still air) further reduced ionization effectiveness. As a result, droplets were unlikely to receive sufficient net charge for enhanced collection. These limitations explain why no significant benefit was observed, suggesting that higher voltage and controlled environmental conditions are essential for future trials.

5 Conclusions

This study demonstrates that integrating biomimetic design with additive manufacturing produces a fog harvester that is both structurally stable and manufacturable. The spider-web–inspired mesh combined with a 3D-printed double-wishbone frame can withstand extreme wind conditions while maintaining effective water capture. Although optimization identified a 1.5 mm string diameter as the most efficient, fabrication and drag constraints highlight the need for a compromise between theoretical optimum and practical durability.

The electrostatic charging component, however, requires further development. At the tested conditions, no improvement in yield was observed, primarily due to insufficient voltage and environmental limitations. Future work should focus on higher-power corona systems and testing under controlled fog environments.

In summary, the biomimetic passive harvester achieved its design goals, whereas the active electrostatic method remains inconclusive and needs refinement before practical application.

References

1. O. Klemm, R. S. Schemenauer, A. Lummerich, P. Cereceda, V. Marzol, D. Corell, J. Van Heerden, D. Reinhard, T. Gherezghiher, J. Olivier, P. Osses, J. Sarsour, E. Frost, M. J. Estrela, J. A. Valiente, G. M. Fessehaye, Fog as a fresh-water resource: Overview and perspectives, (2012). https://doi.org/10.1007/s13280-012-0247-8.
2. G. Pohl, W. Nachtigall, Biomimetics for Architecture & Design. Springer International Publishing (2015). https://doi.org/10.1007/978-3-319-19120-1.
3. J. J. Lee, D. Y. Kim, Investigation of Morphology and Surface Structure of Stenocara eburnea, Namib Desert Beetle: Microscopy and Microanalysis. 25, 1096–1097 (2019). https://doi.org/10.1017/s1431927619006214.
4. H. Venkatesan, J. Chen, H. Liu, W. Liu, J. Hu, A Spider-Capture-Silk-Like Fiber with Extremely High-Volume Directional Water Collection. Adv Funct Mater. 30, (2020). https://doi.org/10.1002/adfm.202002437.
5. Y. Zheng, H. Bai, Z. Huang, X. Tian, F. Q. Nie, Y. Zhao, J. Zhai, L. Jiang, Directional water collection on wetted spider silk. Nature. 463, pp. 640–643 (2010). https://doi.org/10.1038/nature08729.
6. C. Guo, C. Wang, Q. Huang, Z. Wang, X. Gong, S. Ramakrishna, 3D-printed spider-web structures for highly efficient water collection. Heliyon. 8, (2022). https://doi.org/10.1016/j.heliyon.2022.e10007.

7. J. Olivier, J. Van Heerden, H. Rautenbach, E. Pretorius, Optimising fog water harvesting in South Africa. Water Research Commission (2015).
8. IntoAction 5_Fog nets. (2015).
9. J. de D. Rivera, D. Lopez-Garcia, Mechanical characteristics of Raschel mesh and their application to the design of large fog collectors. Atmos Res. 151, pp. 250–258 (2015). https://doi.org/10.1016/j.atmosres.2014.06.011.
10. Virginia Tech, Virginia Tech's fog harp harvests water even in the lightest fog, Virginia Tech News, https://news.vt.edu/articles/2020/04/fogharp_results.html, last accessed 2025/06/24.
11. W. Shi, T. W. van der Sloot, B. J. Hart, B. S. Kennedy, J. B. Boreyko, Harps Enable Water Harvesting under Light Fog Conditions. Adv Sustain Syst. 4, (2020). https://doi.org/10.1002/ADSU.202000040.
12. R. Holmes, J. de D. Rivera, E. de la Jara, Large fog collectors: New strategies for collection efficiency and structural response to wind pressure. Atmos Res. 151, pp. 236–249 (2015). https://doi.org/10.1016/j.atmosres.2014.06.005.
13. J. de D. Rivera, D. Lopez-Garcia, Mechanical characteristics of Raschel mesh and their application to the design of large fog collectors. Atmos Res. 151, pp. 250–258 (2015). https://doi.org/10.1016/j.atmosres.2014.06.011.
14. B. Eric Bank, M. Finance, How to Calculate Wind Loads From Wind Speeds. (2018).
15. Solving Desert Water Shortages Using 20,000 Volts - YouTube, https://www.youtube.com/watch?v=G2brxBRnRH4, last accessed 2025/09/03.
16. S. Swarndeep, Design Optimisation of Fog Collector. (2016).
17. M. Damak, K. K. Varanasi, Electrostatically driven fog collection using space charge injection. Sci Adv. 4, (2018). https://doi.org/10.1126/sciadv.aao5323.
18. K. S. Dawson, L. N. Wickramarathna, Biomimetic Fog Harvester Design: Enhancing Durability and Wind Resistance For Sustainable Water Collection In Harsh Environments, ICRES 2025.
19. SimScale, Computational Fluid Dynamics (CFD) Simulation Software, https://www.simscale.com/product/cfd/, last accessed 2025/06/27.
20. D. Charoensook, S. M. A. Nipu, A. Girish, Q. He, S. Cheng, K. Chapman, N. Xie, C. X. Li, Y. Yang, Three-Dimensional Printing of Bioinspired Hierarchical Structures for Enhanced Fog Collection Efficiency in 3D Space via Vat Photopolymerization. Biomimetics. 9, (2024). https://doi.org/10.3390/biomimetics9120734.
21. S. Lee, H. Choi, J. Kim, Development of 3D-Printed Vibration Absorbers for Noise Control in Material Removal Processes. Machines. 13, (2025). https://doi.org/10.3390/machines13050370.

22. H. Fu, W. Xu, Z. Liu, K. Yan, Fog Droplet Collection by Corona Discharge in a Needle–Cylinder Electrostatic Precipitator with a Water Cooling System. Separations. 9, (2022). https://doi.org/10.3390/separations9070169.
23. D. Li, C. Li, M. Xiao, M. Zhang, J. Li, Z. Yang, Q. Fu, K. Yu, Y. Yang, Y. Pan, Y. Du, X. Zhao, Sustainable solutions for water scarcity: a review of electrostatic fog harvesting technology, (2025). https://doi.org/10.1038/s44172-025-00381-x.

IERS 2025 – Business Partners and Sponsors

With Best Complement


BANK OF CEYLON
BOC
Bankers to the Nation
Dialog 5G Ready
RotaxLimited
BIO
CONSTRUCTION
INSEE
CEMENT
GENEXT PVT LTD
Hayleys
FABRIC
ISS
Islandwide Scientific (Pvt) Ltd
Marlbo
SINCE 1989

Ministry of Science & Technology

IERS 2025

Organized by National Engineering Research and Development Centre of Sri Lanka

ISBN 978-624-5505-05-0